

UNIVERSITY OF OKLAHOMA

GRADUATE COLLEGE

DETECTION THRESHOLDS FOR SPECTRAL MOMENTS AND

POLARIMETRIC VARIABLES

A DISSERTATION

SUBMITTED TO THE GRADUATE FACULTY

in partial fulfillment of the requirements for the

Degree of

DOCTOR OF PHILOSOPHY

By

IGOR RADE IVIĆ

Norman, Oklahoma

December 2008

DETECTION THRESHOLDS FOR SPECTRAL MOMENTS AND
POLARIMETRIC VARIABLES

A DISSERTATION APPROVED FOR THE
SCHOOL OF ELECTRICAL AND COMPUTER ENGINEERING

BY

Dr. Tian-You Yu

Dr. Phillip Chilson

Dr. Murad Ozaydin

Dr. Sebastian Torres

Dr. Mark Yeary

Dr. Dušan Zrníc

©Copyright by IGOR RADE IVIĆ 2008
All Rights Reserved.

Acknowledgements

I would like to express my deepest gratitude to my mentor Dr. Dušan Zrnić for the guidance he provided during the course of this research work. His help and advice were invaluable for the successful completion of this work. My special thanks go to my adviser, Dr. Tian-You Yu whose help, constructive comments and productive insights have made this dissertation clear and understandable to the readers not involved in the narrow field of study this work deals with. I would also like to thank Drs. Phillip Chilson, Murad Ozaydin, Sebastian Torres, and Mark Yeary for their participation on my doctoral committee. My thanks go, as well, to Allen Zahrai at NSSL for allowing flexible work hours. I wish to acknowledge the National Severe Storms Laboratory for providing the equipment necessary to carry this project out. Lastly, I would like to thank my friends and family for their support during my stay at OU.

Table of Contents

1. Introduction.....	1
1.1 Polarimetric Doppler Weather Radar	1
1.2 Weather Signal Characteristics.....	3
1.3 Overview of Spectral Moments and Polarimetric Variables.....	5
2. Problem Statement.....	11
3. Classical Methods for Hypotheses Testing.....	16
4. Coherency Based Methods	28
4.1 Comparison with the Likelihood Ratio Hypothesis Testing	45
5. Optimizing Detection Using Weighted Sum	49
5.1 Importance Sampling Application.....	54
5.2 Distribution Fitting.....	60
5.3 Evaluation of Moments for Noise.....	69
5.4 Control Variates for Moment Estimation	75
5.5 Threshold Calculation.....	78
5.6 Assessment of Weight Optimization	79
5.7 Implementation Issues	97
6. Implementation of Weighted Sum on Real Data.....	102
7. Real-Time Implementation of the Weighted Sum.....	151
8. Summary and Conclusions	159
References.....	164
Appendix A.....	167
Appendix B.....	170
Appendix C.....	176
Appendix D.....	181
Appendix E.....	186
Appendix F.....	190
Appendix G.....	197
Appendix H.....	202
Appendix I.....	215
Appendix J.....	231
Appendix K.....	248
Appendix L.....	252
Appendix M.....	253

List of Tables

Table 3.1 Number of real computations as function of the number of samples M .	26
Table 5.1 The table relating appendices to moment approximations for some forms.	73
Table 5.2 Max. POD weight combination as a function of M for $\sigma_v = 2 \text{ m s}^{-1}$, $Z_{DR} = 1 \text{ dB}$, and $N_v/N_h = 1$.	90
Table 5.3 Max. POD maximizing weight combination as a function of M for $\sigma_v = 2 \text{ m s}^{-1}$, $Z_{DR} = 1 \text{ dB}$, and $N_v/N_h = 0.8269$.	90
Table 5.4 POD maximizing weights for $\sigma_v = 2 \text{ m s}^{-1}$.	92
Table 6.1 POD maximizing weights for $N_v/N_h = 0.8269$.	108
Table 6.2 Real data statistics comparison for various weights in the sum when $N_v/N_h = 0.8269$, and $\text{PFA} = 1.2 \cdot 10^{-6}$.	119
Table 6.3 Real data statistics for the power/weighted sum OR combination when $N_v/N_h = 0.8269$ and $\text{PFA} = 1.2 \cdot 10^{-6}$.	119
Table 6.4 Real data statistics for surveillance scan collected on 03/19/06.	120
Table 6.5 Real data statistics for Doppler scan with $M = 52$, and weights $\alpha = 1.5$, $\beta = 1.5$, $\gamma = 2$.	131
Table 6.6 Statistics for range unfolded Doppler scan collected on 03/19/06.	137
Table 6.7 Real data statistics comparison for various weights in the sum when $M = 17/52$, $N_v/N_h = 1$, and $\text{PFA} = 1.2 \cdot 10^{-6}$.	138
Table 6.8 Real data statistics comparison for various weights in the sum when $M = 17/52$, $N_v/N_h = 0.9$, and $\text{PFA} = 1.2 \cdot 10^{-6}$.	139
Table 6.9 Real data statistics comparison for various weights in the sum when $M = 17/52$, $N_v/N_h = 0.8$, and $\text{PFA} = 1.2 \cdot 10^{-6}$.	139
Table 6.10 Real data statistics comparison for various weights in the sum when $M = 17/52$, $N_v/N_h = 0.7$, and $\text{PFA} = 1.2 \cdot 10^{-6}$.	139
Table 6.11 Real data statistics for surveillance scan collected on 04/24/07.	140
Table 6.12 Statistics for range unfolded Doppler scan collected on 04/24/07.	145
Table 7.1 The estimated drop in uniform sum POD vs. the drop in the ratio of N_v/N_h for threshold set to PFA of $1.2 \cdot 10^{-6}$, for the unity ratio N_v/N_h , and signal parameters $\text{SNR} = 0 \text{ dB}$, $\sigma_v = 2 \text{ m s}^{-1}$, $Z_{DR} = 1 \text{ dB}$, $\rho_{hv} = 0.96$.	154
Table 7.2 The uniform sum detections vs. the difference between the actual ratio of N_v/N_h and the one the threshold was adjusted for, in case of $M = 17$, and PFA of $1.2 \cdot 10^{-6}$.	155
Table 7.3 The uniform sum detections vs. the difference between the actual ratio of N_v/N_h and the one the threshold was adjusted for, in case of $M = 52$, and PFA of $1.2 \cdot 10^{-6}$.	155
Table 7.4 Parameters for the uniform sum threshold calculation as $\text{THR} = \max(N_h, N_v) \cdot (\min(N_h, N_v) / \max(N_h, N_v))^B \cdot \exp(A + C \cdot \min(N_h, N_v) / \max(N_h, N_v))$.	157

Table 7.5 Parameters for threshold calculation as $THR = \max(N_h, N_v) \cdot (\min(N_h, N_v) / \max(N_h, N_v))^B \cdot \exp(A + C \cdot \min(N_h, N_v) / \max(N_h, N_v))$	158
Table 7.6 Parameters for threshold calculation as $THR = \max(N_h, N_v) \cdot (\min(N_h, N_v) / \max(N_h, N_v))^B \cdot \exp(A + C \cdot \min(N_h, N_v) / \max(N_h, N_v))$	158

List of Figures

Figure 1.1 Polarimetric Doppler weather radar block diagram.	3
Figure 1.2 Resolution volume description.	4
Figure 2.1 Ratio of distances in dual and single-pol modes versus the relative echo power, where r_0 is the distance of the phenomena in a single-pole, and r_1 is the distance at which the same phenomena would have to appear in a dual-pol setting in order to be detected given the power-based censoring scheme.	15
Figure 3.1 Assessment of the likelihood-ratio test sensitivity to variation in difference among the input samples parameters and those that the likelihood-ratio is tuned to. The likelihood-ratio is adjusted for $SNR^n = 0.5$ dB, $v^n = 0$ ms ⁻¹ , $\sigma_v^n = 2$ ms ⁻¹ , $Z_{DR}^n = 2$ dB, $\rho_{hv}^n = 0.96$, and $\phi_{dp}^n = 90$ deg. It is also compared to the single-polarization mode power detector. Likelihood-ratio PFA is 10^{-5} and the single-polarization PFA is 1.1749×10^{-6} . The number of samples M is 17.	25
Figure 4.1 PFAs for different approaches.	39
Figure 4.2 POD comparison for several detector functions.	41
Figure 4.3 POD comparison for OR combination.	42
Figure 4.4 POD for varied SNR . For comparison, the uniform sum curve is plotted against the case with no 3 dB loss (single-polarization) with the power threshold set to 2 dB above the noise, and the 3 dB loss (dual-polarization) with the power thresholds of 2 and 1.4 dB.	43
Figure 4.5 POD for varied σ_v . For comparison, the uniform sum curve is plotted against the case with no 3 dB loss (single-polarization) with the power threshold set to 2 dB above the noise, and the 3 dB loss (dual-polarization) with the power thresholds of 2 and 1.4 dB.	44
Figure 4.6 POD of uniform sum for varied Z_{DR}	45
Figure 4.7 ML vs. uniform sum comparison.	48
Figure 5.1 Histogram of the uniform sum pdf for noise only case and signal+noise.	61
Figure 5.2 3-D representation of the POD vs. α and β for the following $\gamma = 2$, $SNR_h = 1.5$ dB, $\sigma_v = 2$ m s ⁻¹ , $Z_{DR} = 1$ dB, $\rho_{hv} = 0.96$, $M = 25$, and $N_v/N_h = 1$	80
Figure 5.3 3-D representation of the POD vs. α and β for the following $\gamma = 2$, $\sigma_v = 2$ m s ⁻¹ , $Z_{DR} = 4$ dB, $\rho_{hv} = 0.96$, $M = 25$, $N_v/N_h = 1$, and $PFA = 10^{-2}$	82
Figure 5.4 3-D representation of the POD vs. α and β for the following $\gamma = 2$, $SNR_h = 0$ dB, $Z_{DR} = 1$ dB, $\rho_{hv} = 0.96$, $M = 25$, $N_v/N_h = 1$, and $PFA = 10^{-2}$	83
Figure 5.5 3-D representation of the POD vs. α and β for the following $\gamma = 2$, $SNR_h = 0$ dB, $\sigma_v = 2$ m s ⁻¹ , $\rho_{hv} = 0.96$, $M = 25$, $N_v/N_h = 1$, and $PFA = 10^{-2}$	84
Figure 5.6 3-D representation of the POD vs. α and β for the following $\gamma = 2$, $SNR_h = 0$ dB, $\sigma_v = 2$ m s ⁻¹ , $Z_{DR} = 1$ dB, $M = 25$, $N_v/N_h = 1$, and $PFA = 10^{-2}$	85

Figure 5.7 3-D representation of the POD vs. α and β for the following $\gamma = 2$, $SNR_h = 0$ dB, $\sigma_v = 2$ m s ⁻¹ , $Z_{DR} = 1$ dB, $M = 25$, $N_v/N_h = 1$, and $PFA = 10^{-2}$.	86
Figure 5.8 3-D representation of the POD vs. α and β for the following $\gamma = 2$, $SNR_h = 0$ dB, $\sigma_v = 2$ m s ⁻¹ , $Z_{DR} = 1$ dB, $M = 25$, $\rho_{hv} = 0.96$, and $PFA = 10^{-2}$.	87
Figure 5.9 3-D representation of the POD vs. α and β for various γ values, and the following $SNR_h = 0$ dB, $\sigma_v = 2$ m s ⁻¹ , $Z_{DR} = 1$ dB, $M = 25$, $\rho_{hv} = 0.96$, $N_v/N_h = 1$, and $PFA = 10^{-2}$.	88
Figure 5.10 3-D representation of the POD vs. α and β for various γ , and the following $SNR_h = 0$ dB, $\sigma_v = 2$ m s ⁻¹ , $Z_{DR} = 1$ dB, $M = 25$, $\rho_{hv} = 0.96$, $N_v/N_h = 1$, and $PFA = 10^{-6}$.	89
Figure 5.11 3-D representation of the POD vs. variation in σ_v and Z_{DR} for $\alpha = 1$, $\beta = 1.5$, $\gamma = 2$, and the following $SNR_h = 0$ dB, $M = 25$, $\rho_{hv} = 0.96$, $N_v/N_h = 1$, and $PFA = 10^{-6}$.	91
Figure 5.12 POD for different weight combinations and several N_v/N_h ratios as a function of varied Z_{DR} , for $SNR = 0$ dB, $M = 17$, $\sigma_v = 2$ m s ⁻¹ , $\rho_{hv} = 0.96$, and $PFA = 1.2 \times 10^{-6}$. Bracketed Z_{DR} value indicates the weight optimization parameter.	94
Figure 5.13 POD for different weight combinations and several N_v/N_h ratios as a function of varied Z_{DR} , for $SNR = 0$ dB, $M = 52$, $\sigma_v = 2$ m s ⁻¹ , $\rho_{hv} = 0.96$, and $PFA = 1.2 \times 10^{-6}$. Bracketed Z_{DR} value indicates the weight optimization parameter.	96
Figure 5.14 POD of the OR combination of power and uniform sum versus the POD of the uniform sum only.	101
Figure 6.1 The original “single-pol” reflectivity field.	103
Figure 6.2 The histogram of the SNR distribution in the horizontal channel before the noise power is doubled.	104
Figure 6.3 Reflectivity field (a) and the classification of detections (b) obtained after doubling the noise power, but not changing the threshold.	106
Figure 6.4 Reflectivity field (a) and the classification of detections (b) obtained after doubling the noise power, and increasing the threshold to 2 dB above the doubled noise power.	107
Figure 6.5 POD for different weight combinations as a function of varied Z_{DR} , and $SNR = 0$ dB, $M = 17$, $\sigma_v = 2$ m s ⁻¹ , $\rho_{hv} = 0.96$, $N_v/N_h = 0.8269$, and $PFA = 1.2 \times 10^{-6}$.	108
Figure 6.6 Reflectivity field (a) and the classification of detections (b) obtained after doubling the noise power, and using the weighted sum for detection.	110
Figure 6.7 Reflectivity field (a) and the classification of detections (b) obtained after doubling the noise power, and using the OR combination of power and weighted sum for detection.	111
Figure 6.8 Reflectivity field (a) and the classification of detections (b) obtained after doubling the noise power, and using the weighted sum for detection.	112
Figure 6.9 Reflectivity field (a) and the classification of detections (b) obtained after doubling the noise power, and using the OR combination of power and weighted sum for detection.	113

Figure 6.10 Reflectivity field (a) and the classification of detections (b) obtained after doubling the noise power, and using the weighted sum for detection.	114
Figure 6.11 Reflectivity field (a) and the classification of detections (b) obtained after doubling the noise power, and using the OR combination of power and weighted sum for detection.	115
Figure 6.12 Reflectivity field (a) and the classification of detections (b) obtained after doubling the noise power, and using the uniform sum for detection.	116
Figure 6.13 Reflectivity field (a) and the classification of detections (b) obtained after doubling the noise power, and using the OR combination of power and uniform sum for detection.	117
Figure 6.14 Reflectivity (a) and mean velocity (b) fields for SNR threshold of 3.5 dB with the number of samples per velocity estimate $M = 52$	122
Figure 6.15 Reflectivity (a) and velocity (b) fields with the classification of detections (c) obtained after doubling the noise power, but not changing the threshold.	123
Figure 6.16 Reflectivity (a) and mean velocity (b) fields with the classification of detections (c) obtained by lowering the threshold to 0.5 dB above the artificially doubled noise.	125
Figure 6.17 Reflectivity (a) and mean velocity (b) fields with the classification of detections (c) obtained after doubling the noise power, and using the weighted sum for detection.	127
Figure 6.18 Reflectivity (a) and mean velocity (b) fields with the classification of detections (c) obtained after doubling the noise power, and using the uniform sum for detection.	128
Figure 6.19 Reflectivity (a) and mean velocity (b) fields with the classification of detections (c) obtained by lowering the power threshold to -1 dB above the artificially doubled noise.	130
Figure 6.20 Original range unfolded velocity field for SNR thresholds of 2 and 3.5 dB in surveillance and Doppler scans, respectively. Sample numbers M are 17, and 52 in surveillance and Doppler scans, respectively.	133
Figure 6.21 Unfolded velocity field obtained after doubling the noise power, but not changing the thresholds.	134
Figure 6.22 Unfolded mean velocity field obtained by lowering the threshold to -1 dB, in surveillance, and to 0.5 dB in Doppler scan, above the artificially doubled noise.	136
Figure 6.23 Unfolded mean velocity field obtained by lowering the threshold to -1 dB, in both the surveillance and Doppler scan, above the artificially doubled noise.	137
Figure 6.24 Unfolded mean velocity field obtained after doubling the noise power, and using the uniform sum for detection.	138
Figure 6.25 The original “single-pol” reflectivity field.	140
Figure 6.26 The histogram of the SNR distribution in the horizontal channel before the noise power is doubled.	141

Figure 6.27 Reflectivity field (a) and the classification of detections (b) obtained after doubling the noise power, but not changing the threshold.	142
Figure 6.28 Reflectivity field obtained after doubling the noise power, and increasing the threshold to 2 dB above the doubled noise power.	143
Figure 6.29 Reflectivity field (a) and classification of detections (b) obtained after doubling the noise power, and using the uniform sum for detection.	144
Figure 6.30 Original range unfolded velocity field for <i>SNR</i> thresholds of 2 and 3.5 dB in surveillance and Doppler cuts, respectively. Sample numbers <i>M</i> are 17, and 52 in surveillance and Doppler scans, respectively.	146
Figure 6.31 Unfolded velocity field obtained after doubling the noise power, but not changing the thresholds.	147
Figure 6.32 Unfolded mean velocity field obtained by lowering the threshold to -1 dB, in surveillance, and to 0.5 dB in Doppler scan, above the artificially doubled noise.	148
Figure 6.33 Unfolded mean velocity field obtained by lowering the threshold to -1 dB, in both the surveillance and Doppler scan, above the artificially doubled noise.	149
Figure 6.34 Unfolded mean velocity field obtained after doubling the noise power, and using the uniform sum for detection.	150
Figure 7.1 Uniform sum PFA sensitivity to change in the ratio N_v/N_h for threshold adjusted for PFA of 1.2×10^{-6} , and the unity ratio N_v/N_h	152
Figure 7.2 Uniform sum POD sensitivity to change in the ratio N_v/N_h for threshold set to PFA of 1.2×10^{-6} , for the unity ratio N_v/N_h , and signal parameters $SNR = 0$ dB, $\sigma_v = 2$ m s ⁻¹ , $Z_{DR} = 1$ dB, $\rho_{hv} = 0.96$	153
Figure 7.3 Least squares approximation using $x^B e^{A+Cx}$ yielding function that takes the N_v/N_h ratio as an input and outputs threshold for PFA = 1.2×10^{-6}	155
Figure F.1 Comparison between moments obtained through simulation and approximation.	196
Figure K.1 3-D plot of a weighted sum approximation errors using generalized gamma distribution for $M = 17$, and $\gamma = 2$	249
Figure K.2 3-D plot of a weighted sum approximation errors using generalized gamma distribution for $M = 25$, and $\gamma = 2$	250
Figure K.3 3-D plot of a weighted sum approximation errors using generalized gamma distribution for $M = 32$, and $\gamma = 2$	251
Figure M.1 False alarm rate dependency on the number of samples M	254
Figure M.2 Reflectivity field (a) and the classification of detections (b) obtained after doubling the noise power, and using the proposed algorithm for detection.	259
Figure M.3 Unfolded velocity field obtained after doubling the noise power, and using the proposed algorithm for detection.	260

Abstract

Presently, the Signal-to-Noise-Ratio (SNR) measurement is used to determine the presence of a weather signal for Weather Surveillance Radar – 1988 Doppler (WSR-88D). Growing popularity of polarimetric radars prompts the need for improved signal detection scheme. Namely, the ongoing upgrade of the WSR-88D network to dual polarization results in a 3 dB reduction of the SNR per channel because the existing transmitter power is split between horizontal (H) and vertical (V) channels. Therefore, the radar sensitivity is degraded and many valid weather signals may be discarded if the current censoring scheme is retained. In this work, statistical techniques of mitigating the impact of the 3 dB SNR loss with the goal of improving data censoring for the dual-polarization system are examined. First, the performance and implementation of a classical likelihood-ratio method is investigated. It is concluded that such a method is not practical for operational systems due to insufficient processing capability of the signal processor. With the system constraint in mind, several efficient methods based on the signal coherency in sample-time and across channels, such as power and autocorrelation measurements in H and V channels, as well as the cross-correlation of signals from the H and V channels, are proposed. Statistical analyses of various combinations of these variables are performed using Monte Carlo simulations. The performance is further demonstrated and verified using time series data collected by the research polarimetric radar (KOUN), operated by the National Severe Storms Laboratory. Both the statistical analysis and the performance comparisons on time series imply that the novel approach has the potential to significantly improve the signal detection on dual-polarization weather radars; thus mitigating the impact of the 3 dB SNR loss in the WSR-88D radars.

1. Introduction

Pulsed-Doppler radars provide the capability to remotely scan weather phenomena which has paramount importance in advancing our understanding of thunderstorms. Networks of such radars are used to provide accurate weather forecast and early warnings of impending severe weather, as well as to improve aviation safety. A recent advancement in weather radar technology is the addition of polarimetric capability. Unlike single polarization radar, a polarimetric radar typically transmits radio waves with both horizontal (H) and vertical (V) polarizations and is also termed as dual-polarization radar. Such arrangement provides additional information which yields an increase in the accuracy of **rainfall estimation**, **precipitation classification**, and **weather hazard detection**, as shown by the JPOLE experiment (Schuur et al. 2003). An overview of polarimetric Doppler weather radar as well as the estimation of spectral moments and polarimetric variables is given in the following section.

1.1 Polarimetric Doppler Weather Radar

A Doppler radar generates a sequence of high-energy pulses, creating a propagating electromagnetic field, while receiving echoes from scatterers (e.g., hydrometeors such as raindrops, snow, hail etc.) in between pulse transmissions. The electric field at scatterers' location is expressed as

$$E(r, \theta, \phi, t) = \frac{A(\theta, \phi)}{r} \exp \left[j2\pi f \left(t - \frac{r}{c} \right) + j\psi_T \right], \quad (1.1)$$

where A depends on angles θ and ϕ which specify azimuth and elevation angles, with respect to the radiation source. Distance from the radar is given by r , and ψ_T is an

unknown but constant transmitter phase. Constant c is the speed of light (i.e., 3×10^8 m s⁻¹) and f is the radar frequency.

Electromagnetic pulses of duration τ are transmitted into space at a predetermined time interval, termed pulse repetition time (PRT) and denoted by T . Microwaves have wavelengths between 10^{-3} and 10^{-1} m and they have the unique ability to penetrate clouds and rain (which is not possible at higher frequencies). Therefore, the weather radar carrier frequency (i.e., f) used to modulate the transmitted pulses is in the microwave frequency band. A simplified block diagram showing the components of the NEXRAD dual-pol testbed (KOUN WSR-88D) located in Norman, OK is given in Figure 1.1. The stabilized local oscillator (STALO) generates a continuous sinusoidal signal of high spectral purity. This signal is then combined with the IF (intermediate frequency) signal from the “COHO” (coherent oscillator) to produce the carrier frequency. The pulse modulator shapes this signal into pulses (turns it on and off). The klystron then amplifies the shaped signal to produce a high-power electromagnetic pulse. This pulse is then split into two halves by the power splitter for transmission in each of the two polarizations. Echoes backscattered by weather targets are received by the antenna in both polarization planes and converted into electrical signals. After passing through the mixer, H and V signals are downconverted to intermediate frequency (IF). Each component is then amplified and passed through a bandpass filter. At this point, analog signals are digitized by A/D converters and turned into video signals by a digital synchronous detector. This removes the IF component, resulting in in-phase (I) and quadrature (Q) components, in each of the H and V channels, that preserve the amplitude and the phase of the signal. These digital

video signals are subsequently passed on to a signal processing subsystem for estimating Doppler spectral moments and polarimetric variables.

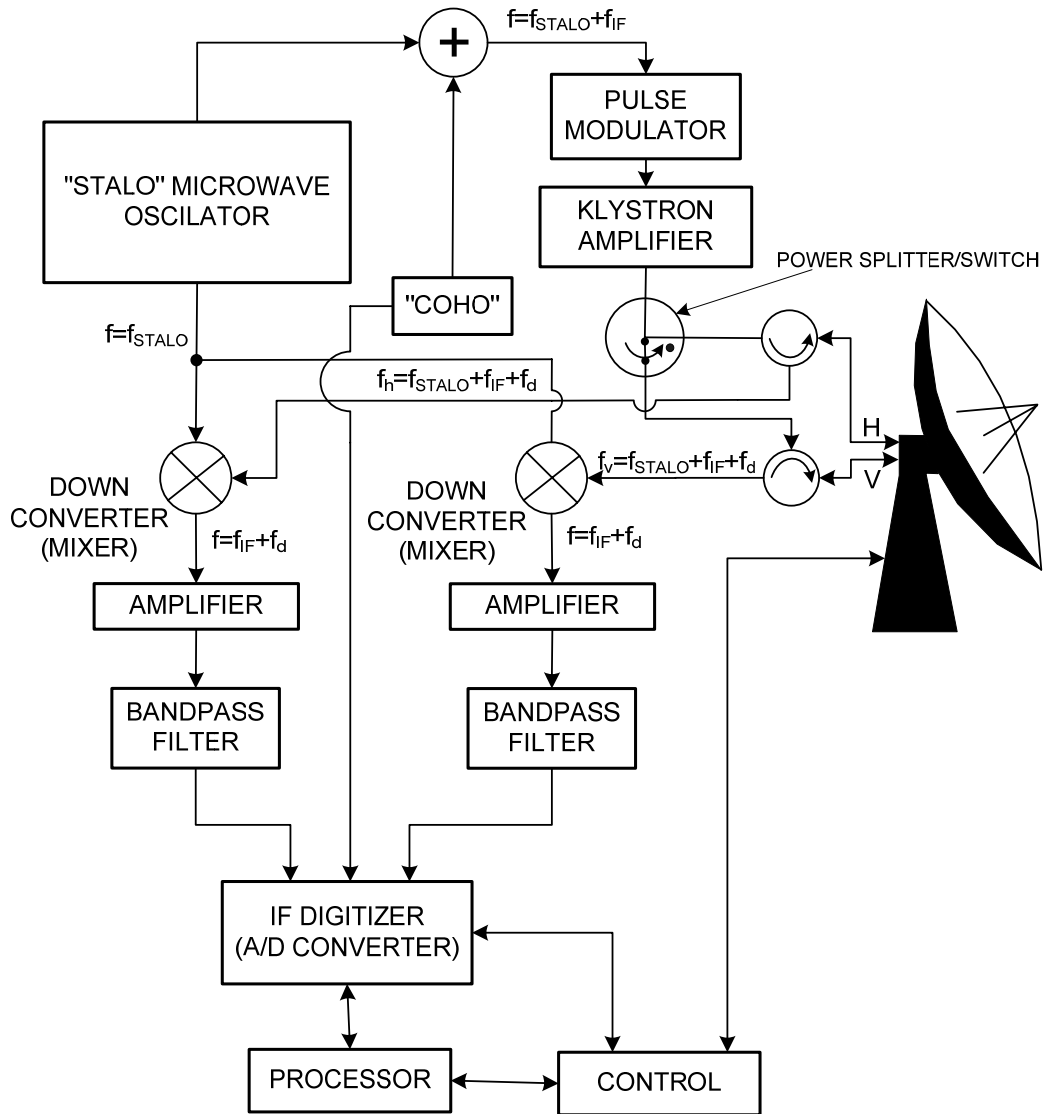


Figure 1.1 Polarimetric Doppler weather radar block diagram.

1.2 Weather Signal Characteristics

Weather radars survey vast areas of space. The central position of a resolution volume in space is determined by range r , azimuth ϕ_0 , and elevation θ_0 , with respect to the radiation source. The size and shape of a radar resolution volume is determined in range by a range-weighting function (given by the convolution of the transmitted pulse

envelope and the receiver impulse response), and by the beamwidth θ_l in azimuth and elevation (Figure 1.2), where the beamwidth is defined as the angle within which the microwave radiation is at least one-half its peak intensity. Note that the pulse depth in range is $c\tau/2$ (where τ is the pulse width and division by two is applied because of the round trip the pulsed wave traveled). The distance between the antenna and the resolution volume is determined by the time delay between the transmitted pulse and the echo scattered from the weather targets ($r = c\tau_s/2$, where τ_s , also called the range time, is the time measured from the beginning of the transmitted pulse to the moment the reflected signal is received; division by two is applied because of the round trip the pulsed wave travels).

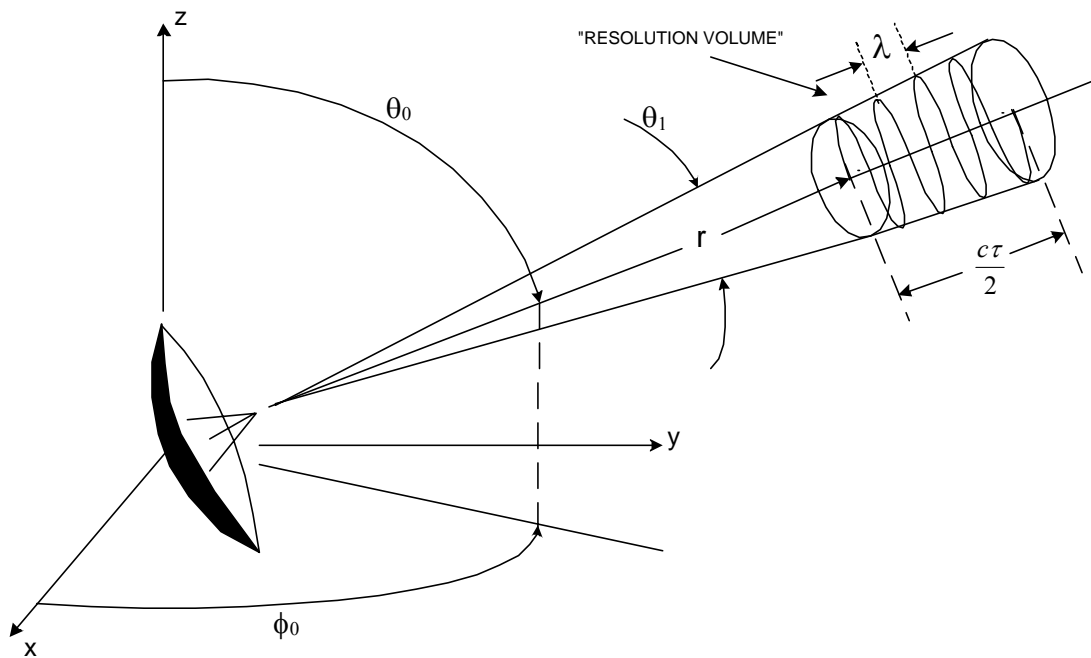


Figure 1.2 Resolution volume description.

The weather signal, at any given time, is a composite of individual echoes from a large number of scatterers within the radar resolution volume. Echoes from different scatterers interfere with each other to produce a complex voltage sample $V(\tau_s) = I(\tau_s) +$

$jQ(\tau_s)$. Because the location and size of scatterers vary randomly in time, the amplitude and phase of the resulting signal $V(\tau_s)$ are random variables. Because the number of scatterers in each resolution volume is large and all are independent (while none being dominant), it is assumed the central limit theorem can be applied to the samples of a weather signal. As a result, both the in-phase component $I(\tau_s)$ and the quadrature phase component $Q(\tau_s)$ have Gaussian probability density functions (*pdf*) with variance σ^2 and zero mean (Zrnić 1975).

A set of signals, originating from the consecutive pulse transmissions, spaced in time by T , and having the same relative time delay measured from the pulse rising edge (i.e., having the same location in range) are referred to as being in the same sample-time domain. These samples exhibit correlation along sample-time provided that the pulse transmission rate is sufficiently high (as is the case for Doppler measurements). The sample-time correlation is described by (Doviak and Zrnić 1993):

$$R(mT) = S e^{-8\left(\frac{\pi\sigma_v mT}{\lambda}\right)^2} e^{-j\frac{4\pi\bar{v}mT}{\lambda}}, \quad (1.2)$$

where m is the autocorrelation lag, and λ is the wavelength of the transmitted electromagnetic wave. S is the average signal power, \bar{v} is the mean radial velocity, and σ_v is the spectrum width, which are the three fundamental radar measurements directly related to meteorological phenomena.

1.3 Overview of Spectral Moments and Polarimetric Variables

A polarimetric weather radar, which simultaneously transmits in the H and V channels, can measure the three spectral moments from each channel and three polarimetric variables. The spectral moments are power, mean radial velocity, and

spectrum width. The polarimetric variables are differential reflectivity, cross-correlation coefficient, and specific differential phase. A description of these variables is presented below.

Doppler spectral moments are:

1. Signal power (S) or the zero moment. It is a measure of liquid water content or precipitation rate in the resolution volume.
2. Mean Doppler velocity (\bar{v}) or the first moment. It is related to components of air-motion toward or away from the radar, within the resolution volume. Radial velocity of the phenomena in each resolution volume is measured using the Doppler effect. This is a phenomenon that occurs if a wave of frequency f is reflected by a moving object having a velocity component v_r in the direction toward the radar. The corresponding frequency shift (of the returned wave) is $f_d = -2v_r/\lambda$.
3. Spectrum width (σ_v), which is the square root of the second moment. This is a measure of velocity dispersion within the resolution volume.

Polarimetric variables are:

1. Differential reflectivity (Z_{DR}) or the ratio of the reflected horizontal and vertical power returns. It is a good indicator of drop shape, which in turn is a good estimate of average drop size.
2. Magnitude of the cross-correlation coefficient (ρ_{hv}), which gives a statistical correlation between the reflected horizontal and vertical power returns. It is a good indicator of regions where there is a mixture of precipitation types, such as rain and snow.

3. Specific Differential Phase (ϕ_{dp}), which is a measure of the phase difference between the returned horizontal and vertical pulses. This phase difference is caused by the difference in the number of wave cycles (or wavelengths) along the propagation path for horizontal and vertically polarized waves. It should not be confused with the Doppler frequency shift, which is caused by the motion of the cloud and precipitation particles. Unlike the differential reflectivity and cross-correlation coefficient, which are all dependent on reflected power, the specific differential phase is a "propagation effect." It is a very good estimator of rainfall rate.

A sample from the m -th radial of data, taken at time instance τ_s , is denoted by $V(m, \tau_s)$. Henceforth, a radial is defined as a set of samples spaced in range-time by τ_s and each originating from the same pulse transmission. Note that two samples having the same range-time τ_s , but different subscripts m_1 and m_2 , are from the same range location (i.e., belong to the same resolution volume located at a distance $r_s = c\tau_s/2$), but are spaced in time by $(m_2 - m_1)T$.

Estimation of the spectral moments is described next.

1. Total power in each channel is estimated using the following formula (Doviak and Zrnić 1993)

$$\hat{P}_h(\tau_s) = \frac{1}{M} \sum_{m=0}^{M-1} |V_h(m, \tau_s)|^2 \quad \text{and} \quad \hat{P}_v(\tau_s) = \frac{1}{M} \sum_{m=0}^{M-1} |V_v(m, \tau_s)|^2, \quad (1.3)$$

where M is the number of samples. Subscripts h and v denote the horizontal and vertical channels, respectively. Note that as the number of samples becomes large the estimated power asymptotically approaches $S+N$, where S is the signal power

and N is the receiver noise power. The signal power in each channel is estimated as:

$$\hat{S}_h(\tau_s) = \hat{P}_h(\tau_s) - N_h \quad \text{and} \quad \hat{S}_v(\tau_s) = \hat{P}_v(\tau_s) - N_v, \quad (1.4)$$

where N_h and N_v are the noise powers in the horizontal and the vertical channels, respectively.

2. Because the radio waves in both H and V polarizations are transmitted simultaneously, the velocity can be found from the argument of the autocorrelation at lag 1 along sample-time either in the horizontal or the vertical channel

$$\begin{aligned} \hat{R}_h(T, \tau_s) &= \frac{1}{M-1} \sum_{m=0}^{M-2} V_h^*(m, \tau_s) V_h(m+1, \tau_s) \\ \hat{R}_v(T, \tau_s) &= \frac{1}{M-1} \sum_{m=0}^{M-2} V_v^*(m, \tau_s) V_v(m+1, \tau_s) \end{aligned}, \quad (1.5)$$

where $V(m, \tau_s)$ and $V(m+1, \tau_s)$ are two successive samples taken at the same range but separated in time by T . Note that the unbiased estimate of the autocorrelation is used. Then, the mean velocity is given by (Doviak and Zrnić 1993)

$$\hat{v}_h(\tau_s) = -\frac{\lambda}{4\pi T} \arg[\hat{R}_h(T, \tau_s)] \quad \text{and} \quad \hat{v}_v(\tau_s) = -\frac{\lambda}{4\pi T} \arg[\hat{R}_v(T, \tau_s)], \quad (1.6)$$

where λ is the wavelength of the transmitted signal. Additionally, because $E\{\hat{v}_h(\tau_s)\} = E\{\hat{v}_v(\tau_s)\}$, the velocity estimate can be improved by combining the two autocorrelation estimates as (Melnikov 2004):

$$\hat{v}(\tau_s) = -\frac{\lambda}{4\pi T} \arg[\hat{R}_h(T, \tau_s) + \hat{R}_v(T, \tau_s)]. \quad (1.7)$$

3. Spectrum width is obtained from measurements in H or V channels (Doviak and Zrnić 1993):

$$\hat{\sigma}_v(\tau_s) = \frac{\lambda}{2\pi T\sqrt{2}} \sqrt{\left| \ln \left(\frac{\hat{S}_p(\tau_s)}{|\hat{R}_p(T, \tau_s)|} \right) \right|} \operatorname{sgn} \left[\ln \left(\frac{\hat{S}_p(\tau_s)}{|\hat{R}_p(T, \tau_s)|} \right) \right], \quad (1.8)$$

where subscript p is either h for the horizontal or v for the vertical channel. Usually, σ_v measurement from H channel is better due to the oblateness of hydrometeors, which results in more power returned in the horizontal polarization.

Polarimetric variable estimates are obtained as

- a) Differential reflectivity

$$\hat{Z}_{DR}(\tau_s) = 10 \log_{10} \left(\frac{\hat{S}_h(\tau_s)}{\hat{S}_v(\tau_s)} \right). \quad (1.9)$$

- b) Cross-correlation coefficient is derived from the cross-correlation estimate between signals in H and V channels

$$\hat{R}_{hv}(0, \tau_s) = \frac{1}{M} \sum_{m=0}^{M-1} V_h^*(m, \tau_s) V_v(m, \tau_s) \quad (1.10)$$

as

$$\hat{\rho}_{hv}(\tau_s) = \frac{|\hat{R}_{hv}(0, \tau_s)|}{\sqrt{\hat{S}_h(\tau_s)\hat{S}_v(\tau_s)}}. \quad (1.11)$$

- c) Specific differential phase is

$$\hat{\phi}_{dp}(\tau_s) = \arg \left[\hat{R}_{hv}(0, \tau_s) \right]. \quad (1.12)$$

This dissertation is organized as follows. First, the problem is defined in Chapter 2. The classical approach is analyzed in Chapter 3. Further, various approaches that take advantage of the signal coherency are compared using simulations and the method

producing the best result is identified in Chapter 4. Subsequently, the tools that allow for extended analysis and practical use of this method are developed in Chapter 5. Performance on real data is assessed in Chapter 6. Finally, the procedure for the operational implementation of the proposed method is developed in Chapter 7.

2. Problem Statement

It is customary practice to display weather radar data after applying thresholds on signal-to-noise ratio (SNR) and/or the magnitude of autocorrelation coefficient at lag one (Keeler 1990, SIGMET 2006). Such thresholds have also been used for censoring questionable (i.e., low SNR) spectral moments. Proper data censoring is essential to operational weather radars such as the Weather Surveillance Radar – 1988 Doppler (WSR-88D) (Crum et al. 1993) to help forecasters’ interpretation of spectral moments (reflectivity, mean radial velocity, and spectrum width) and to minimize detrimental effects on automated feature recognition and hazard detection algorithms (e.g., Stumpf et al. 1998). Presently, spectral moments at each range location are censored (i.e., labeled not useful) if the SNR is insufficient or the echoes from the subsequent trips are overlaid. For example, on the WSR-88D network the default SNR threshold is 2 dB for reflectivity and 3.5 dB for velocity estimates.

Prior to the development of Doppler radar, the censoring rule was a simple threshold test of the estimated SNR. Thus, basic concepts of the detection theory, well developed for non-Doppler radars, can be directly applied to the weather radar signals if only SNR is used for censoring. The probability of false alarms and detection for a square-law detector and point targets with fluctuating power (i.e., sinusoid signals embedded in noise) was derived by Swerling (1954) for fully coherent and fully incoherent signal within the dwell time. In weather radars one deals with innumerable targets (i.e., distributed scatterers) whose radar cross section fluctuates about a mean value as the scatterers trace air motion. When scatterers are illuminated by an electromagnetic wave, each produces a sinusoid signal. The superposition of these signals is received and

sampled by weather radar producing samples that fluctuate both in amplitude and phase. These samples of weather echoes are partially-coherent within the dwell time, and by processing these one obtains estimates of power.

Introduction of Doppler measurements to weather radar brought an additional variable, signal coherency, which is also suitable for censoring. The coherency, expressed either as the Doppler spectrum width or the autocorrelation coefficient at lag one, was and is still used to censor data prior to display of spectral moment fields and/or dual Doppler analysis (Keeler 1990, SIGMET 2006). Nonetheless, no systematic attempt to produce an optimum detection scheme based on both the coherency and SNR has been made. Classical detection theory provides the formalism for such endeavor which, in its essence, consists of maximizing the probability of detection while maintaining the probability of false detections (i.e., false alarms) at or below an acceptable level (Neyman and Pearson 1933). Furthermore, dual-polarization has added new measurements that can be used for the censoring of spectral moments and polarimetric variables (the number of signal parameters pertinent for detection more than doubles). There are two SNRs, two autocorrelation values, and the cross-correlation of the polarization signals (i.e., cross-coherency). In this work, signal detection for such dual-polarization radars is explored.

Prime motivation for this work is the forthcoming upgrade of the network of WSR-88Ds (i.e., NEXRAD systems) to include polarimetric capability starting in about 2009. Simultaneous transmission and reception of horizontally and vertically polarized waves was accepted for implementation (Doviak et al. 2000). Given the same transmitted power, the average received power per channel will be halved (i.e., 3 dB lower) compared to the current single-polarization system. Even though additional SNR may be

gained by upgrading to better low-noise amplifiers and/or improving the system losses, it is unlikely that the 3 dB loss will be fully recovered. The aforementioned SNR loss has two effects on the non-censored spectral moments. First, more data will fall below the processing thresholds and some valid weather signals will be lost. Second, the errors of estimates will inevitably increase. The impact of these effects on operational WSR-88D products and algorithms (using the legacy detector based on a simple threshold test of the estimated SNR) were evaluated by Scharfenberg et al. (2005) who have shown that the 3 dB SNR loss leads to an average drop of 5.5% in detection of weather features. Moreover, in case of “clear-air” events the loss increases to 8.4%. Most of the loss occurs in the areas of low reflectivity such as near the tops of convection and along the edges of a weather system (Scharfenberg et al. 2005). This behooves us to develop a new and practical censoring algorithm which yields an improved detection, thus mitigating the adverse effects caused by the SNR decrease.

To put the 3 dB SNR loss in a more illustrative context, let us consider a well-known fact that the power of electromagnetic wave decreases as the wave propagates through media (known as propagation attenuation). Consequently, if there were two identical phenomena located at different distances from radar, the closer one would have stronger radar return than the one farther away. Consider a radar volume, filled up with scatterers, at a radial distance r_0 from the radar. Let us assume that for a single-pol radar, like the current WSR-88D, the returned power is somewhere between 0 and 3 dB higher than the threshold (THR) used for signal censoring. Evidently, after the dual-pol upgrade, the returned power from the same phenomena will be decreased by 3 dB (i.e., between -3 and 0 dB relative to the THR). If the same censoring scheme is used, the weather signal will

be discarded due to insufficient SNR. In view of the propagation attenuation, it is of interest to determine at which maximum range such phenomenon needs to be located so it is detected after the dual-pol upgrade. To answer this, we examine the weather radar equation (eq. 4.14 in Doviak and Zrnić 1993). This equation shows that the returned power is inversely proportional to the distance square between the phenomenon and the radar as:

$$P(r) = \frac{C}{r^2}, \quad (2.1)$$

where C stands for all other terms in the weather radar equation. Let A denote the power received in a single-pol system relative to the power threshold THR , and $A \in [0, 3]$ dB (since the returned power of such signal falls below THR after the transmitted power is halved). After the dual-pol upgrade, the received power reduces to $A-3$ dB. In other words, additional $3-A$ dB (i.e., $A-3+x = 0 \Rightarrow x = 3-A$) of signal power, on the average, is needed for the power estimate to be above the censoring threshold (assuming no atmospheric attenuation). Hence we write:

$$\frac{C}{r_{\text{dual}}^2} = 10^{\frac{3-A}{10}} \frac{C}{r_{\text{single}}^2} \Rightarrow r_{\text{dual}} = 10^{\frac{A-3}{20}} r_{\text{single}}, \quad (2.2)$$

where r_{dual} is the farthest distance, from the radar, the phenomenon can to be at in order to be detected after the dual-pol upgrade. This is graphically depicted in Figure 2.1. Assuming the power A is uniformly distributed in the interval 0 to 3 dB above THR , the expected value of the ratio $r_{\text{dual}}/r_{\text{single}}$ is calculated as:

$$E \left\{ \frac{r_{\text{dual}}}{r_{\text{single}}} \right\} = \frac{1}{3} \int_0^3 10^{\frac{A-3}{20}} dA = \frac{1}{3} \int_0^3 \exp\left(\frac{A-3}{20} \ln 10\right) dA = \frac{20}{3 \ln 10} 10^{\frac{A-3}{20}} \Big|_0^3 = 0.84558. \quad (2.3)$$

Let us assume a resolution volume, located at 100 km from the radar, filled with scatterers producing the returned power that falls into the bracket $[THR, THR+3]$ dB, when illuminated by a single-pol WSR-88D. Formula (2.3) implies that the same group of scatterers needs to be located at a resolution volume 84.5 km away from the dual-pol WSR-88D in order to be detected (if the current censoring scheme is used). After these considerations it becomes clear that the 3 dB SNR loss has potentially significant impact on the data and it becomes imperative to develop an alternative censoring algorithm that mitigates these adverse effects.

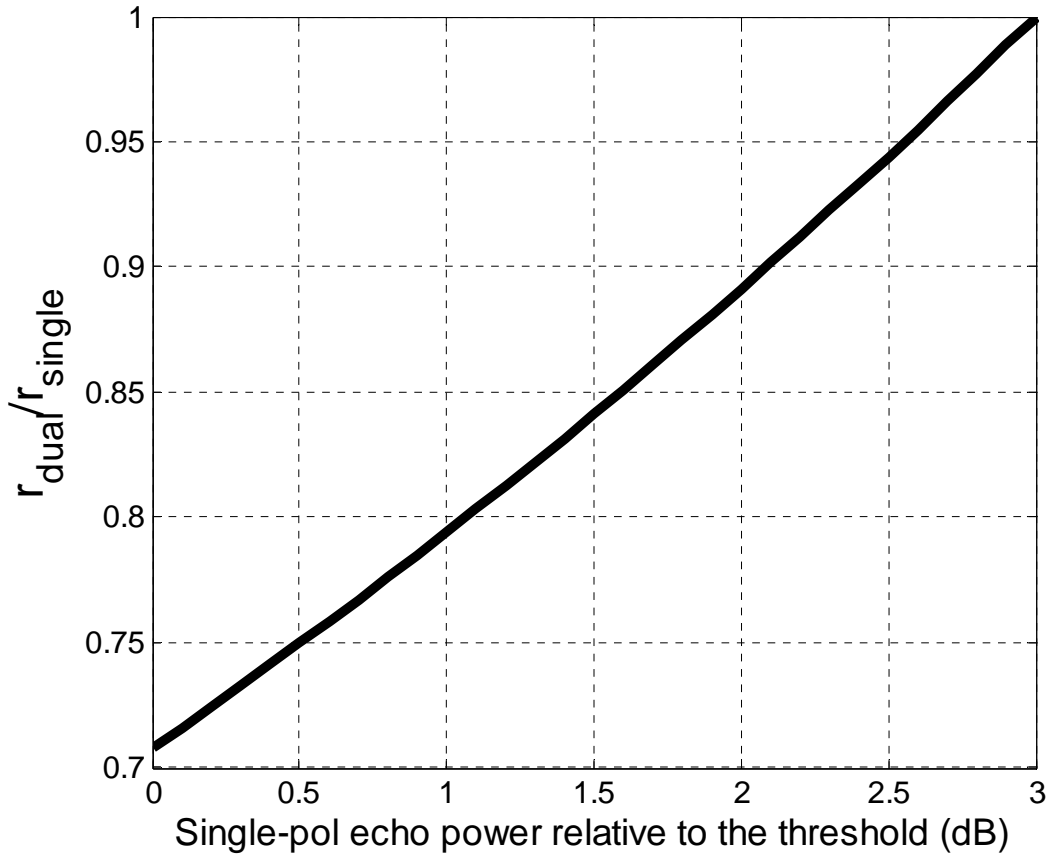


Figure 2.1 Ratio of distances in dual and single-pol modes versus the relative echo power, where r_0 is the distance of the phenomena in a single-pole, and r_1 is the distance at which the same phenomena would have to appear in a dual-pol setting in order to be detected given the power-based censoring scheme.

3. Classical Methods for Hypotheses Testing

One of common approaches applicable to the problem of detection is the likelihood-ratio test. A likelihood-ratio test is a statistical test in which the ratio is computed between the likelihood functions for the null hypothesis and the alternative hypotheses (Neyman and Pearson 1933). This ratio is subsequently compared against a threshold to decide which of the two hypotheses should be accepted. The threshold value is typically selected to satisfy some type of constraint, such as the probability of rejecting the null/alternative hypothesis when the null/alternative hypothesis is true. The general setup is as follows:

- (1) Given n random variables y_i ($i \in [1, \dots, n]$), let $p_{\theta}(y_1, \dots, y_n)$ be their joint probability density function (*pdf*) where $\boldsymbol{\theta} = [\theta_1, \dots, \theta_k]^T \in \Theta$ is a vector of unknown parameters in the distribution. Let us write one realization chosen from the population distributed as $p_{\theta}(y_1, \dots, y_n)$ as the vector $\mathbf{y} = [\hat{y}_1, \dots, \hat{y}_n]^T$ which is defined as the vector of observations.
- (2) Let Ω be a subset of Θ . Then we wish to define a test to determine whether \mathbf{y} came from a distribution with parameters belonging to Ω or to $\Theta \setminus \Omega$ (i.e., Ω^C , the complement of Ω). The hypothesis that \mathbf{y} has a distribution function $p_{\theta}(y_1, \dots, y_n)$ with parameters belonging to Ω is denoted by H_0 , while the alternative hypothesis that \mathbf{y} has the distribution function $p_{\theta}(y_1, \dots, y_n)$ with parameters belonging to $\Theta \setminus \Omega$ is denoted by H_1 .
- (3) The goal is to find the test which will maximize the probability of accepting H_0 , given that $\boldsymbol{\theta} \in \Omega$ (i.e., $P(\text{accept } H_0 | \boldsymbol{\theta} \in \Omega)$), subject to the condition that the

probability of rejecting H_1 , given that $\theta \in \Theta \setminus \Omega$, equals ε (i.e., $P(\text{reject } H_1 | \theta \in \Theta \setminus \Omega) = \varepsilon$).

The likelihood-ratio test criterion for hypotheses testing which satisfies the above is given by Neyman and Pearson (1933). They suggest to find two sets of parameters θ_0' and θ_1' belonging to Ω and $\Theta \setminus \Omega$, respectively. These parameters should satisfy:

$$\begin{aligned} p_{\theta}(\hat{y}_1, \hat{y}_2, \dots, \hat{y}_n | \theta = \theta_0') &\geq p_{\theta}(\hat{y}_1, \hat{y}_2, \dots, \hat{y}_n | \theta \in \Omega) \\ p_{\theta}(\hat{y}_1, \hat{y}_2, \dots, \hat{y}_n | \theta = \theta_1') &\geq p_{\theta}(\hat{y}_1, \hat{y}_2, \dots, \hat{y}_n | \theta \in \Theta \setminus \Omega) \end{aligned} \quad (3.1)$$

The decision rule is then:

$$\frac{p_{\theta}(\hat{y}_1, \hat{y}_2, \dots, \hat{y}_n | \theta = \theta_0')}{p_{\theta}(\hat{y}_1, \hat{y}_2, \dots, \hat{y}_n | \theta = \theta_1')} \geq THR(\theta_0', \theta_1'), \quad (3.2)$$

where the threshold $THR(\theta_0', \theta_1')$ is chosen so it satisfies the condition $P(\text{reject } H_1 | \theta \in \Theta \setminus \Omega) = \varepsilon$. In short we can write:

$$\frac{\sup_{\theta_0 \in \Omega} p_{\theta_0}(\hat{y}_1, \hat{y}_2, \dots, \hat{y}_n | \theta_0 \in \Omega)}{\sup_{\theta_1 \in \Theta \setminus \Omega} p_{\theta_1}(\hat{y}_1, \hat{y}_2, \dots, \hat{y}_n | \theta_1 \in \Theta \setminus \Omega)} \geq THR(\theta_0, \theta_1). \quad (3.3)$$

Notice that the expressions in the numerator and the denominator are the maximum likelihood estimators (MLE) of θ over Ω and $\Theta \setminus \Omega$, respectively.

For the detection of weather radar signals, it is defined that the hypothesis H_0 is true if samples from observations consist of signal plus noise and H_1 is true if only noise is present. Because the noise is assumed to be additive white Gaussian with zero mean, the maximum likelihood-ratio becomes:

$$\frac{\sup_{\theta_{S+N} \in \Theta_{S+N}} p_{\theta_{S+N}}(x_1, x_2, \dots, x_n)}{p_{\theta_N}(x_1, x_2, \dots, x_n)} \geq THR(\theta_{S+N}), \quad (3.4)$$

where Θ_{S+N} is the set of all possible distribution parameters values when signal and noise are present. To apply the likelihood-ratio principle we must know the joint *pdf* of the elements in the vector of complex Gaussian random variables $\mathbf{V} = [V_h(0, \tau_s), \dots, V_h(M-1, \tau_s), V_v(0, \tau_s), \dots, V_v(M-1, \tau_s)]^T$, where each $V_h(m, \tau_s)$, and $V_v(m, \tau_s)$ are obtained by sampling voltage echoes at a range location $\tau_s^{(1)}$ and sample-time mT (T is the Pulse Repetition Time or PRT), in horizontal (subscript h) and vertical polarization (subscript v) channels.

The joint *pdf* is (Miller 1969):

$$pdf(\mathbf{V}) = \pi^{-2M} |\det \mathbf{C}^{-1}| \exp(-\mathbf{V}^H \mathbf{C}^{-1} \mathbf{V}), \quad (3.5)$$

where \mathbf{C} is the covariance matrix of size $2M \times 2M$ defined as (superscript H denotes conjugate transpose):

$$\mathbf{C} = E\{\mathbf{V}\mathbf{V}^H\} = E\left\{\begin{bmatrix} \mathbf{V}_h \\ \mathbf{V}_v \end{bmatrix} \begin{bmatrix} \mathbf{V}_h^H & \mathbf{V}_v^H \end{bmatrix}\right\} = \begin{bmatrix} E\{\mathbf{V}_h \mathbf{V}_h^H\} & E\{\mathbf{V}_h \mathbf{V}_v^H\} \\ E\{\mathbf{V}_v \mathbf{V}_h^H\} & E\{\mathbf{V}_v \mathbf{V}_v^H\} \end{bmatrix} = \begin{bmatrix} \mathbf{C}_h & \mathbf{C}_{vh} \\ \mathbf{C}_{hv} & \mathbf{C}_v \end{bmatrix}. \quad (3.6)$$

where $\mathbf{V}_h = [V_h(0), \dots, V_h(M-1)]^T$ and $\mathbf{V}_v = [V_v(0), \dots, V_v(M-1)]^T$. In case of pure noise \mathbf{C} is:

$$\mathbf{C} = \begin{bmatrix} N_h & 0 & 0 & 0 & \dots & 0 \\ 0 & \ddots & \vdots & \vdots & \dots & 0 \\ 0 & \dots & N_h & 0 & \dots & 0 \\ 0 & \dots & 0 & N_v & \dots & 0 \\ 0 & \dots & 0 & 0 & \ddots & \vdots \\ 0 & \dots & 0 & 0 & \dots & N_v \end{bmatrix}. \quad (3.7)$$

where N_h and N_v are the noise powers in horizontal and vertical channels, respectively.

The *pdf* becomes:

¹ For brevity the designation τ_s is dropped in further text.

$$pdf(\mathbf{V}_N) = (\pi^2 N_h N_v)^{-M} \exp\left(-\frac{1}{N_h} \sum_{m=0}^{M-1} |V_h(m)|^2 - \frac{1}{N_v} \sum_{m=0}^{M-1} |V_v(m)|^2\right) \quad (3.8)$$

In the case of signal plus noise we have:

$$\mathbf{C}_h = \begin{bmatrix} S_h + N_h & R_h^*(1) & \cdots & R_h^*(M-1) \\ R_h(1) & S_h + N_h & \cdots & R_h^*(M-2) \\ \vdots & \vdots & \ddots & \vdots \\ R_h(M-1) & R_h(M-2) & \cdots & S_h + N_h \end{bmatrix}, \quad (3.9)$$

where $R_h(m) = S_h \rho(m)$ and $\rho(m) = \exp\left[-(\pi\sigma_v m/v_a)^2/2\right] \exp(-j\pi v m/v_a)$. Here, S_h is the signal power in horizontal channel, v is the mean radial velocity, v_a is the maximum unambiguous velocity and σ_v is the spectrum width. Obviously, \mathbf{C}_v is obtained from \mathbf{C}_h by replacing the subscript h with v . Further,

$$\mathbf{C}_{hv} = \sqrt{S_h S_v} \rho_{hv} e^{j\phi_{dp}} \begin{bmatrix} 1 & \rho^*(1) & \cdots & \rho^*(M-1) \\ \rho(1) & 1 & \cdots & \rho^*(M-2) \\ \vdots & \vdots & \ddots & \vdots \\ \rho(M-1) & \rho(M-2) & \cdots & 1 \end{bmatrix}, \quad (3.10)$$

where ρ_{hv} is the cross-correlation coefficient (Sachidananda and Zrnić 1985) and ϕ_{dp} the differential phase (Sachidananda and Zrnić 1986). Similarly:

$$\mathbf{C}_{vh} = \sqrt{S_h S_v} \rho_{hv} e^{-j\phi_{dp}} \begin{bmatrix} 1 & \rho^*(1) & \cdots & \rho^*(M-1) \\ \rho(1) & 1 & \cdots & \rho^*(M-2) \\ \vdots & \vdots & \ddots & \vdots \\ \rho(M-1) & \rho(M-2) & \cdots & 1 \end{bmatrix}. \quad (3.11)$$

Note that the only difference between \mathbf{C}_{hv} and \mathbf{C}_{vh} is in the sign of the differential phase.

Now the likelihood-ratio function is obtained as followed:

$$\frac{\sup_{SNR_h, v, \sigma_v, Z_{dr}, \rho_{hv}, \phi_{dp}} \pi^{-2M} |\det \mathbf{C}^{-1}| \exp(-\mathbf{V}^H \mathbf{C}^{-1} \mathbf{V})}{(\pi^2 N_h N_v)^{-M} \exp\left(-\frac{1}{N_h} \sum_{m=0}^{M-1} |V_h(m)|^2 - \frac{1}{N_v} \sum_{m=0}^{M-1} |V_v(m)|^2\right)} \geq THR. \quad (3.12)$$

where SNR_h is the signal-to-noise ratio estimated from the horizontal channel signals, and Z_{dr} is the ratio of signal powers in horizontal and vertical channels (i.e., differential reflectivity $Z_{DR} = 10\log_{10}Z_{dr}$) (Seliga and Bringi 1976). Eq. (3.12) can be simplified to:

$$\frac{1}{N_h} \sum_{m=0}^{M-1} |V_h(m)|^2 + \frac{1}{N_v} \sum_{m=0}^{M-1} |V_v(m)|^2 + \max_{SNR_h, \nu, \sigma_v, Z_{dr}, \rho_{hv}, \phi_{dp}} \left(\ln |\det \mathbf{C}^{-1}| - \mathbf{V}^H \mathbf{C}^{-1} \mathbf{V} \right) \geq THR', \quad (3.13)$$

where $THR' = \ln(THR/(N_h N_v)^M)$. Unfortunately, the set of parameter values producing the maximum of the second term in (3.13) cannot be found analytically due to the complexity of the expression in the brackets (i.e., $\ln |\det \mathbf{C}^{-1}| - \mathbf{V}^H \mathbf{C}^{-1} \mathbf{V}$). Alternatively, it can be found using a search technique by varying these six parameters (listed in the subscript of the second term) through a discrete list of predetermined values, and choosing the combination for which $\ln |\det \mathbf{C}^{-1}| - \mathbf{V}^H \mathbf{C}^{-1} \mathbf{V}$ has a maximum value. Note that by doing this, an actual maximum likelihood estimation of signal parameters is performed. Once this is done, the threshold THR' must be determined so that:

$$P \left(\sum_{m=0}^{M-1} \frac{|V_h(m)|^2}{N_h} + \sum_{m=0}^{M-1} \frac{|V_v(m)|^2}{N_v} + \ln |\det \mathbf{C}^{-1}| - \mathbf{V}^H \mathbf{C}^{-1} \mathbf{V} \geq THR' \mid \text{only noise present} \right) = \varepsilon. \quad (3.14)$$

In (3.14), ε denotes the probability of rejecting the hypothesis that only noise is present when this hypothesis is actually true (i.e., the probability of false signal detection). In weather radar applications it is desired that the probability of false detection is fairly small. In the remainder of the text, the probability of the false detection is referred to as the Probability of False Alarm (PFA). Next, we discuss the brute force search for the maximum likelihood solution.

Assume that the list of predetermined values for each of the six parameters is of length N_p (where subscript p denotes one of the six parameters and takes values of

1, ..., 6). Then the maximum of $\ln|\det\mathbf{C}^{-1}|-\mathbf{V}^H\mathbf{C}^{-1}\mathbf{V}$ in (3.13) is determined by evaluating all possible combinations of parameter values (i.e., through multiple trials). This requires a total of $N_1N_2\dots N_6$ trials. Evidently, for larger values of N_p more computations of $\ln|\det\mathbf{C}^{-1}|-\mathbf{V}^H\mathbf{C}^{-1}\mathbf{V}$ are needed. Alternatively, to decrease the computational intensity of the process, one could estimate the six parameters prior to detection (e.g., using sub-optimum processing like autocovariance (Doviak and Zrnić 1993) for velocity and spectrum width), and attempt to locate the maximum by searching in the vicinity of these estimates. Note that in every trial, the matrix \mathbf{C} in the expression (3.13) is calculated for predetermined (or nominal) values of parameters $SNR^{(2)}$, v , σ_v , Z_{DR} , ρ_{hv} , and ϕ_{dp} , and the resulting likelihood-ratio is adjusted (tuned) for detection of a signal with exactly these parameter values. Hence, it detects such a signal with the highest possible Probability Of Detection (POD) subject to the constraint that PFA is less than or equal to ε (as stated by the Neyman-Pearson lemma). But, if any parameter of the signal to be detected changes from the one the expression (3.13) is adjusted for, the POD will inevitably decline; for example, if the difference between the nominal velocity value (i.e., the one used to calculate the matrix \mathbf{C}) and the mean velocity of input samples in \mathbf{V} is not 0 m s^{-1} , the likelihood-ratio test does not produce the highest possible POD. Consequently, the intensity (i.e., coarseness) of the search for the maximum of $\ln|\det\mathbf{C}^{-1}|-\mathbf{V}^H\mathbf{C}^{-1}\mathbf{V}$ depends on the sensitivity of the maximum likelihood (ML) detector (whose matrix \mathbf{C} is calculated for nominal parameter values) to the change in the parameters of input samples in \mathbf{V} . In addition, the amount of the variation in POD can be a function of the signal parameters (i.e., the amount of decline in POD may depend on the signal parameter type,

² For brevity the subscript h is dropped from further text. By default the parameter SNR stands for SNR in horizontal channel.

as it departs from its nominal value). Therefore, the granularity/steps (i.e., spacing between each two consecutive values in the discrete list for each of the six signal parameters), with which we search through values of each parameter, ought to be set so that the changes in POD per step increment are about equal. The sensitivity of the ML expression to the variation in signal parameters is investigated using Monte Carlo simulations for the case where the detector is tuned to the following nominal signal parameters, $SNR = 0.5$ dB, $v = 0$ m s⁻¹ ($v_a = 8.9$ m s⁻¹), $\sigma_v = 2$ m s⁻¹, $Z_{DR} = 2$ dB, $\rho_{hv} = 0.96$, $\phi_{dp} = 90$ deg, and THR' is chosen so that the PFA is 10^{-5} (i.e., $\varepsilon = 10^{-5}$). Additionally, the performance of the likelihood-ratio test is plotted against that of the single-polarization system for the SNR threshold set to 2 dB above the noise level. In both cases the number of samples M is chosen to be 17. The 2 dB power threshold and M of 17 are used because these are the standard settings for the surveillance scan in the WSR-88D system. The results are shown in Figure 3.1. Notice that the PFA for the likelihood-ratio is 10^{-5} as opposed to the 1.1749×10^{-6} for the single-polarization system (Appendix A). The empirical criterion for choosing 10^{-5} for PFA is that it produces only 3.6 false detections (on the average) in the Planar Position Indicator (PPI) of a weather field with $360 \times 1000 = 360000$ data points. In Figure 3.1 (a) the POD is directly proportional to the change in SNR difference. This is expected because the higher the SNR the stronger the signal power is, which makes it more discernible from noise. Figure 3.1 (b) shows the POD behavior vs. the difference between the input samples velocity and the velocity for which the ML detector is adjusted for (i.e., nominal velocity). As expected, the local maximum occurs at 0 m s⁻¹ difference. At the same time, notice that the POD declines rapidly as the velocity difference departs from 0 m s⁻¹. Note that the

curve presented in Figure 3.1 (b) does not change regardless of the choice of the velocity to which the detector is tuned to. The reason is that the phase of the $E\{\mathbf{V}^H\mathbf{C}^{-1}\mathbf{V}\}$ depends on the difference between the input samples mean velocity and the nominal velocity. In Figure 3.1 (c) the spectrum width difference is varied from -1.5 to 4 m s^{-1} to show that the POD significantly deteriorates as the signal σ_v changes further from the value the ML detector is tuned to (i.e., 2 m s^{-1} in this case). Assessment of Z_{DR} difference behavior in Figure 3.1 (d) reveals that the POD is inversely proportional to Z_{DR} . Such behavior is logical because the higher Z_{DR} indicates the lower SNR in V channel, which adversely affects the detection. The Figure 3.1 (e) indicates that in the case of weather signal, the variation in ρ_{hv} bears no significant impact on detection. Finally, in Figure 3.1 (f) the ϕ_{dp} difference is varied from -90 to 270 deg to show that the ML detector performance rapidly degrades as the input samples ϕ_{dp} departs from the value for which the detector is adjusted for. Similar to velocity, the phase of the $E\{\mathbf{V}^H\mathbf{C}^{-1}\mathbf{V}\}$ is influenced by the difference between the input samples differential phase and the ϕ_{dp} that the detector is tuned to (i.e., nominal ϕ_{dp}). Consequently, the curve in Figure 3.1 (f) remains the same regardless of the nominal ϕ_{dp} choice. Clearly, the assessment of the ML detector's sensitivity to the variation in signal parameters verifies the need for multiple trials. Note that if the likelihood-ratio with the given PFA (i.e., 10^{-5}) is used, the actual POD at and near the nominal parameter values improves compared to the POD produced by the power-threshold-based detector in single-polarization (despite the loss in SNR, but at the cost of higher PFA). In addition, when samples are selected from the population with nominal parameters values, the likelihood-ratio test achieves the maximum POD subject to the constraint that PFA is less than or equal to ε . This is known as the venerable

Neyman-Pearson lemma and is stated as follows (within the framework given at the beginning of the chapter):

Neyman-Pearson Lemma: Let us define the decision rule represented through function $\phi(\mathbf{x})$ as

$$\phi(\mathbf{x}) = \begin{cases} 1, & \frac{p_{\theta}(\mathbf{x}|\theta = \theta_0)}{p_{\theta}(\mathbf{x}|\theta = \theta_1)} \geq T(\theta_0, \theta_1) \\ 0, & \frac{p_{\theta}(\mathbf{x}|\theta = \theta_0)}{p_{\theta}(\mathbf{x}|\theta = \theta_1)} < T(\theta_0, \theta_1) \end{cases}, \quad (3.15)$$

where ϕ takes value of one if we choose that samples belong to population with parameters θ_0 and zero if the test outcome is $\theta = \theta_1$. Then we can represent the PFA and the POD as:

$$\begin{aligned} PFA(\phi) &= \int \phi(\mathbf{x}) p_{\theta}(\mathbf{x}|\theta = \theta_1) d\mathbf{x} = E\{\phi(x)|\theta = \theta_1\} \\ POD(\phi) &= \int \phi(\mathbf{x}) p_{\theta}(\mathbf{x}|\theta = \theta_0) d\mathbf{x} = E\{\phi(x)|\theta = \theta_0\} \end{aligned} \quad (3.16)$$

Given the decision rule (3.15) with $T(\theta_0, \theta_1)$ chosen to give $PFA(\phi) = \varepsilon$, there is no other decision rule ϕ' such that $PFA(\phi') \leq \varepsilon$ and $POD(\phi') > POD(\phi)$.

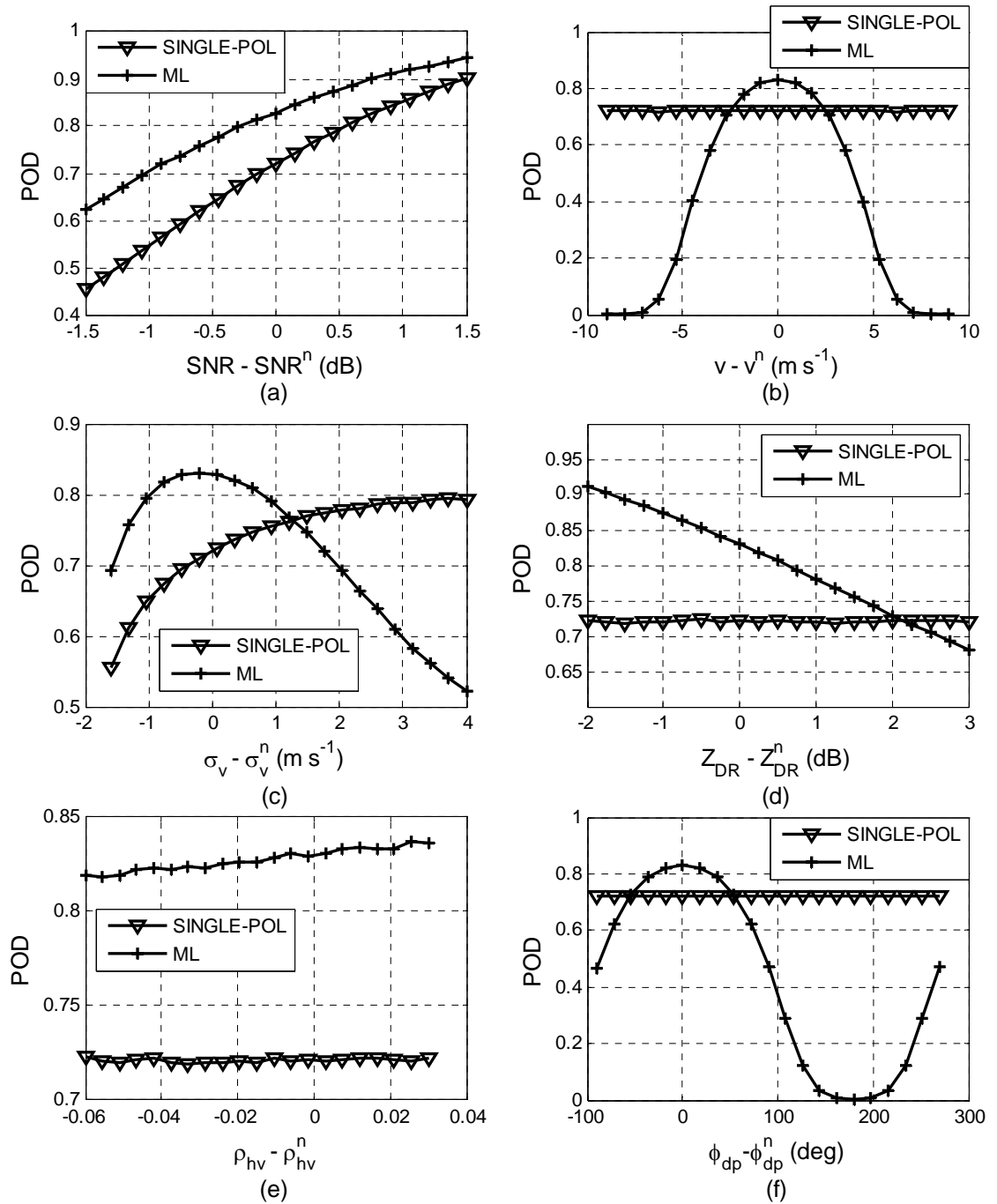


Figure 3.1 Assessment of the likelihood-ratio test sensitivity to variation in difference among the input samples parameters and those that the likelihood-ratio is tuned to. The likelihood-ratio is adjusted for $SNR^n = 0.5$ dB, $v^n = 0$ ms^{-1} , $\sigma_v^n = 2$ ms^{-1} , $Z_{DR}^n = 2$ dB, $\rho_{hv}^n = 0.96$, and $\phi_{dp}^n = 90$ deg. It is also compared to the single-polarization mode power detector. Likelihood-ratio PFA is 10^{-5} and the single-polarization PFA is 1.1749×10^{-6} . The number of samples M is 17.

Apparently, the likelihood-ratio presents a quite appealing candidate for signal detection on the WSR-88Ds. The important aspect however, is the computational intensity of this scheme (exemplified by the need for multiple trials). Let us quantify the amount of computational load each trial puts on a processor in terms of GFLOPS (i.e., 10^9 floating point operations per second) for the case of $M = 17$. We start by first analyzing the calculation of the first two terms in (3.14). Each sum requires $2M$ real multiplications and $2M-1$ real additions. In total, it takes $4M$ real multiplications, $4M-1$ real additions and two divisions to calculate and add the first two terms. To calculate $\mathbf{V}^H \mathbf{C}^{-1}$ it takes $(2M)^2$ complex multiplications and $2M(2M-1)$ complex additions. Taking that each complex multiplication requires 4 real multiplications and 2 additions we get $16M^2$ real multiplications and $16M^2-4M$ real additions. To get $(\mathbf{V}^H \mathbf{C}^{-1})\mathbf{V}$ we note that the final result is always real, hence the complex part of the vector multiplication need not be calculated as it always amounts to zero. The total number of basic real computations is given in Table 3.1.

	Additions No.	Multiplications No.	Divisions No.
Current method	$2M-1$	$2M$	1
Likelihood-ratio	$16M^2+4M-1$	$8M(2M+1)$	2

Table 3.1 Number of real computations as function of the number of samples M .

We immediately notice that the likelihood-ratio, compared to the current method, requires (in the limit) a factor of $8M$ more additions and multiplications (with multiplications being more important as they require more processing time) for each trial. To put this in terms of GFLOPS we calculate the computational workload of the surveillance scan in VCP-11 ($M = 17$) per each trial as the ratio of the total number of the

required real operations versus the allowed processing time frame. To get the time frame allowed for processing we take the range resolution to be 250 m (e.g., the range resolution of the WSR-88D system), which can be written as a function of the speed of light c and the time between contiguous samples τ_R (i.e., $c\tau_R/2 = 250\text{m}$). The processing time is then $M\tau_R$. As a result, the computational workload is given by the following formula (based on the total number of basic computations):

$$\frac{32M^2 + 12M + 1}{M * 2 * 250/c * 10^9} = \frac{32 * 17^2 + 12 * 17 + 1}{17 * 500 * 10/3} = 0.33364 \text{ GFLOPS/trial}. \quad (3.17)$$

Current NEXRAD signal processor is based on the Simgnet RVP8 which features “Dual SMP Pentium processors easily upgradeable as faster processors become available” (RVP8 specifications). To be on the safe side, let us assume these two processors run at 4 GHz each. Assuming the peak performance (1 FLOP per each cycle) this processor would deliver total of 8 GFLOPS of computing power, which would permit 24 trials to be performed. In reality, though, no system can sustain the processor peak performance continuously. In addition, it also must perform the operating system tasks, as well as to generate Doppler moments and polarimetric variables, which further tapers off performance. In addition, when M increases to 32 and 52 the expression (3.17) shows the workload to increase to about 0.6 and 1 GFLOPS per trial, respectively. We can readily see that the likelihood-ratio approach would be extremely demanding on computing resources to the point that its applicability would not be feasible. Consequently, we proceed by pursuing alternative (i.e., computationally less demanding) approaches based partly on our knowledge of the signal features and partly on intuition. This is achieved by having in mind the constraints imposed by the current NEXRAD signal processing capabilities.

4. Coherency Based Methods

The main idea of the proposed approach is to exploit the coherency of weather signals in sample-time and/or across channels to improve detection. This is achieved by comparing the value of a function $f[V_h(0, \tau_s), \dots, V_h(M-1, \tau_s), V_v(0, \tau_s), \dots, V_v(M-1, \tau_s)]$ against a threshold to decide whether or not the signal is present at the range location τ_s , where $V_h(m, \tau_s)$, and $V_v(m, \tau_s)$ are complex random variables obtained by sampling signals in the horizontal and vertical channels. Clearly, these samples can be combined in many ways to obtain the function f . However, a good combination is the one that can emphasize known signal features in white Gaussian noise. For example, the total power in horizontal and vertical channels is the sum of signal and noise powers, thus the total power reflects the notion that the estimated total power is higher when a signal is present. Moreover, the autocorrelation function of white noise at lags other than zero is zero but increases if signal is present. Hence, the autocorrelation coefficients estimates in each channel are a measure of the coherency in sample-time. Finally, because weather signals from horizontal and vertical channels are highly correlated, the cross-correlation has much higher value when signal is present. The estimators of powers and autocorrelations at the first lag in horizontal and vertical channels, as well as the cross-correlation are⁽³⁾:

$$\begin{aligned} \hat{P}_h &= \frac{1}{M} \sum_{m=0}^{M-1} |V_h(m)|^2 & \hat{P}_v &= \frac{1}{M} \sum_{m=0}^{M-1} |V_v(m)|^2 \\ \hat{R}_h(T) &= \frac{1}{M-1} \sum_{m=0}^{M-2} V_h^*(m) V_h(m+1) & \hat{R}_v(T) &= \frac{1}{M-1} \sum_{m=0}^{M-2} V_v^*(m) V_v(m+1) \\ \hat{R}_{hv}(0) &= \frac{1}{M} \sum_{m=0}^{M-1} V_h^*(m) V_v(m). \end{aligned} \quad (4.1)$$

³ Note that the range designation τ_s has been dropped as it is understood that the same procedure is repeated for each set of $2M$ samples at all range locations

We refer to these estimators as the core functions. Consequently, various signal detection schemes can be devised by building a function f as a combination of several core functions which would, presumably, yield different POD given the same desired PFA. Note that extra computations added to the existing processor are minimized because these core functions are already used for the fundamental spectral moment and polarimetric variables calculation. The previous discussion showed that the POD of the maximum-likelihood detector rapidly declines when signal's velocity and differential phase change from those that the detector is adjusted for. In addition, if the complex values of the auto and cross-correlation estimates were to be used for detection, the function f would be complex as well, which would significantly complicate the analysis. To avoid these problems, the absolute values of autocorrelations and cross-correlation are used. By doing so, the amount of information used for signal detection is decreased; consequently the performance is not expected to achieve that of the ML detector. Thus, performance is traded for simplicity.

Performance is assessed for 10 functions (i.e., combinations) listed below:

1. $|\hat{R}_h(T)| \geq THR_1$
2. $\left(|\hat{R}_h(T) + \hat{R}_v(T)|\right) \geq THR_2$
3. $\left(|\hat{R}_h(T)| + |\hat{R}_v(T)|\right) \geq THR_3$
4. $|\hat{R}_{hv}(0)| \geq THR_4$
5. $\left(|\hat{R}_h(T) + \hat{R}_v(T)| + |\hat{R}_{hv}(0)|\right) \geq THR_5$ (4.2)
6. $\left(|\hat{R}_h(T)| + |\hat{R}_v(T)| + |\hat{R}_{hv}(0)|\right) \geq THR_6$

7. $\left(\hat{P}_h + \hat{P}_v + \left|\hat{R}_h(T) + \hat{R}_v(T)\right| + \left|\hat{R}_{hv}(0)\right|\right) \geq THR_7$
8. $\left(\hat{P}_h + \hat{P}_v + \left|\hat{R}_h(T)\right| + \left|\hat{R}_v(T)\right| + \left|\hat{R}_{hv}(0)\right|\right) \geq THR_8$
9. $\left|\hat{R}_h(T)\right| \geq THR_9$ OR $\left(\left|\hat{R}_h(T) + \hat{R}_v(T)\right|\right) \geq THR_{10}$ OR $\left|\hat{R}_{hv}(0)\right| \geq THR_{11}$
10. $\left|\hat{R}_h(T)\right| \geq THR_{13}$ OR $\left(\left|\hat{R}_h(T)\right| + \left|\hat{R}_v(T)\right|\right) \geq THR_{14}$ OR $\left|\hat{R}_{hv}(0)\right| \geq THR_{15}$

The threshold for each function is chosen so that the PFA of the corresponding function is the same. Clearly, false detections should not significantly clutter the radar product display. Consequently, the values of PFA around 10^{-5} are taken as a reference for comparisons among the 10 listed functions.

From a set of real data collected by the KOUN radar, the noise powers were measured (in the internal processor power units) for both the horizontal and the vertical channels.

- $N_h = 3.4174 \times 10^{-6}$ for the horizontal channel
- $N_v = 2.8259 \times 10^{-6}$ for the vertical channel.

Notice that noise powers in H and V channels are not the same and in this particular case the noise is higher in the horizontal channel. In practice, the amount of noise power is particular to each radar and may vary over time even in the same system. Let us now examine how the noise powers affect the corresponding threshold of each detection scheme. For a single-pol system, it is clear that a threshold determined for the unit value of the noise power can be appropriately scaled to work in any system by simply multiplying it by the actual measured noise power value. When the samples from both the H and V channels are used, it is obvious that a simple scaling by the measured noises does not produce the desired result. To investigate such a case it is illustrative to examine

the censoring scheme listed under number 7 due to its generality. This function can be written as

$$\hat{P}_h + \hat{P}_v + \left| \hat{R}_h(T) + \hat{R}_v(T) \right| + \left| \hat{R}_{hv}(0) \right| = N_h \left(\frac{\hat{P}_h}{N_h} + \frac{N_v}{N_h} \frac{\hat{P}_v}{N_v} + \left| \frac{\hat{R}_h(T)}{N_h} + \frac{N_v}{N_h} \frac{\hat{R}_v(T)}{N_v} \right| + \sqrt{\frac{N_v}{N_h}} \frac{\left| \hat{R}_{hv}(0) \right|}{\sqrt{N_h N_v}} \right). \quad (4.3)$$

When only noise is present it reduces to

$$\begin{aligned} \hat{P}_h + \hat{P}_v + \left| \hat{R}_h(T) + \hat{R}_v(T) \right| + \left| \hat{R}_{hv}(0) \right| = N_h & \left(\frac{1}{M} \sum_{m=0}^{M-1} \left| V_U(m) \right| + \frac{N_v}{N_h} \frac{1}{M} \sum_{m=M}^{2M-1} \left| V_U(m) \right| + \right. \\ & \left. \frac{1}{M-1} \left| \sum_{m=0}^{M-2} V_U^*(m) V_U(m+1) + \frac{N_v}{N_h} \sum_{m=M}^{2M-2} V_U^*(m) V_U(m+1) \right| + \right. \\ & \left. \sqrt{\frac{N_v}{N_h}} \frac{1}{M} \sum_{m=0}^{M-1} \left| V_U^*(m) V_U(m+M) \right| \right), \end{aligned} \quad (4.4)$$

where $V_U(m)$ ($m = 0, \dots, 2M$) are samples of white Gaussian noise with unit power (i.e., variance). The expression (4.4) shows that in this case, the threshold can be expressed as a function of noise power in the H (or V) channel and the ratio of noise powers in V (or H) and H (or V) channel. Thus, when the threshold is determined for the unit noise power in H channel and some ratio of noise powers in V and H channels, such threshold can be scaled to any actual noise power value in H channel as long as the ratio of noise powers remains the same. This gives us assurance that a comparison of detection schemes carried out for a certain values of noise powers holds exactly for any other case as long as the ratio of noise powers is the same (or at least similar). The actual ratio N_v/N_h of the measured noise powers is 0.8269. Because it is closely half way between 0.5 and one, this appears like a good ratio value to carry out the comparisons for; namely, it seems highly unlikely that the noise power in H channel would ever be more than twice higher than in V channel, or vice versa. Additionally, the expression on the right side of (4.4)

shows that the output of the sample detection scheme for the unity N_h and some value x of the ratio N_v/N_h is the same as when N_v is one and N_h/N_v equals x . Thus, the comparison carried out for N_v/N_h ratio value of $1-\Delta$ holds for the N_v/N_h ratio value of $(1-\Delta)^{-1}$ as well. To simulate the 3 dB reduction of the SNR, the noise power values of the investigated detection functions were multiplied by two and used for the threshold calculation. This way the same noise samples can be used for comparison to the legacy detector (i.e., by keeping the noise power in H channel unchanged). Consequently, for comparison purposes all calculations are performed for the following effective noise powers:

- $N_h = 2 \times 3.4174 \times 10^{-6}$ for the horizontal channel
- $N_v = 2 \times 2.8259 \times 10^{-6}$ for the vertical channel.

The threshold for each function with a desired PFA (e.g., 10^{-5}) can be obtained using the following equation

$$\int_{THR}^{\infty} pdf(x) dx = \text{Desired PFA}, \quad (4.5)$$

where $pdf(x)$ is the probability density of the function for which we seek the threshold. Because $pdf(x)$ is unknown, the simple Hit or Miss Monte Carlo method of integration (Rubinstein 1981) was used to calculate the PFA for each THR value. It is based on the fact that:

$$\int_{THR}^{\infty} f(x) dx = \lim_{n \rightarrow \infty} \frac{1}{n} \sum_{i=0}^{n-1} X_i, \quad (4.6)$$

where n is the number of trials, and X_0, \dots, X_{n-1} are independent identically distributed Bernoulli random variables such that:

$$X_i = \begin{cases} 1 & \text{if } X_i \geq THR \\ 0 & \text{if } X_i < THR \end{cases} \quad i = 0, \dots, n-1. \quad (4.7)$$

Proof: We have $P(X_i = 1) = \int_{THR}^{\infty} f(x)dx$, and $P(X_i = 0) = 1 - \int_{THR}^{\infty} f(x)dx = \int_0^{THR} f(x)dx$.

Then:

$$\begin{aligned}
 E\left\{\frac{1}{n}\sum_{i=0}^{n-1}X_i\right\} &= \frac{1}{n}\sum_{i=0}^{n-1}E\{X_i\} \\
 &= \frac{1}{n}\sum_{i=0}^{n-1}[1 \cdot P(X_i = 1) + 0 \cdot P(X_i = 0)] \\
 &= P(X_i = 1) \\
 &= \int_{THR}^{\infty} f(x)dx.
 \end{aligned} \tag{4.8}$$

Using values for noise power, the noise samples were generated in MATLAB as:

```

randn('state',sum(100*clock));
IQNh = sqrt(Nh/2)*(randn(M,K) + j*randn(M,K));
IQNv = sqrt(Nv/2)*(randn(M,K) + j*randn(M,K));

```

To estimate how many trials are required to achieve the desired level of accuracy, the variance of the estimate is calculated as follows. Let us introduce the random variable X as:

$$X = \frac{1}{n}\sum_{i=0}^{n-1}X_i. \tag{4.9}$$

Then, $E\{X\} = \int_{THR}^{\infty} f(x)dx = p$. To obtain the variance we calculate the second moment

$$\begin{aligned}
 E\{X^2\} &= \frac{1}{n^2}\sum_{i=0}^{n-1}\sum_{j=0}^{n-1}E\{X_iX_j\} \\
 &= \frac{1}{n^2}\left[\sum_{i=0}^{n-1}E\{X_i^2\} + \sum_{i \neq j}E\{X_i\}E\{X_j\}\right] \\
 &= \frac{1}{n^2}\left[\sum_{i=0}^{n-1}(1^2 \cdot p + 0^2 \cdot (1-p)) + \sum_{i \neq j}p^2\right] \\
 &= \frac{1}{n^2}[np + (n^2 - n)p^2] \\
 &= \frac{p(1-p)}{n} + p^2.
 \end{aligned} \tag{4.10}$$

The variance is then

$$\text{Var}\{X\} = E\{X^2\} - E^2\{X\} = \frac{p(1-p)}{n} \quad (4.11)$$

Let us now calculate the probability that the estimate lies within a certain error limit ε .

That is

$$P(p - \varepsilon < X < p + \varepsilon) = P(-\varepsilon < X - p < \varepsilon) = P(|X - p| < \varepsilon). \quad (4.12)$$

Clearly, the Chebyshev's inequality provides the upper bound as:

$$P(|X - p| < \varepsilon) \geq 1 - \frac{\text{Var}\{X\}}{\varepsilon^2} = 1 - \frac{p(1-p)}{n\varepsilon^2}. \quad (4.13)$$

For instance, when $n = 10^8$, $p = 10^{-5}$, and $\varepsilon = 10^{-6}$ we get a confidence level of at least 90%.

A different approach can be taken using the *DeMoivre-Laplace limit theorem* which says that for each random binomial variable Y defined on n independent trials for which $p = P(\text{success})$ the following holds

$$\lim_{n \rightarrow \infty} P\left(a \leq \frac{Y - np}{\sqrt{np(1-p)}} \leq b\right) = \lim_{n \rightarrow \infty} P\left(a \leq \frac{Y/n - p}{\sqrt{p(1-p)/n}} \leq b\right) = \frac{1}{\sqrt{2\pi}} \int_a^b e^{-\frac{z^2}{2}} dz. \quad (4.14)$$

This can be used as:

$$\begin{aligned} P(-\varepsilon \leq X - p \leq \varepsilon) &= P\left(\frac{-\varepsilon}{\sqrt{p(1-p)/n}} \leq \frac{X - p}{\sqrt{p(1-p)/n}} \leq \frac{\varepsilon}{\sqrt{p(1-p)/n}}\right) \\ &= \frac{2}{\sqrt{2\pi}} \int_0^{\frac{\varepsilon}{\sqrt{p(1-p)/n}}} e^{-\frac{z^2}{2}} dz \\ &= \frac{2}{\sqrt{\pi}} \int_0^{\frac{\varepsilon}{\sqrt{2p(1-p)/n}}} e^{-t^2} dt \\ &= \text{erf}\left(\frac{\varepsilon}{\sqrt{2p(1-p)/n}}\right). \end{aligned} \quad (4.15)$$

Thus, the PFA estimator distribution is approximated by a Gaussian. Using this approach for $n = 10^8$, $p = 10^{-5}$, and $\varepsilon = 10^{-6}$ we get the confidence level of 99.843%.

In our analysis we use a large number of trials (well in excess of 10^6), which implies that the random variable X is normally distributed in the limit. Also, as shown by an earlier study (Erchard 1991), the *pdf* of a PFA estimator is approximately Gaussian if $n \geq 10/p$. Consequently, we can confidently rely on the error estimate using the *DeMoivre-Laplace limit theorem*.

A total of 10^8 trials were used to calculate the PFAs. The PFAs as a function of thresholds for the first 8 functions listed in (4.2) are shown in Figure 4.1 for the case of $M = 17$. In addition, the relationship between the PFAs and POD for these approaches is shown in Figure 4.2. It is apparent that the function

$$\left(\hat{P}_h + \hat{P}_v + \left| \hat{R}_h(T) + \hat{R}_v(T) \right| + \left| \hat{R}_{hv}(0) \right| \right) \geq THR_7, \quad (4.16)$$

produces the highest detection rate. This outcome is intuitively expected because this sum captures all signal features that discern it from the noise. In the remainder of the text this approach will be referred to as the *uniform sum*.

To evaluate the OR combinations (i.e., the last two functions in (4.2)) a range of thresholds were used. For each threshold, the OR combination PFA was calculated. Subsequently, POD was calculated for each combination. The results are shown in Figure 4.3. For comparison, the results from the uniform sum are included as a reference. It is apparent that the uniform sum performs significantly better than these two approaches.

Let us now examine how the uniform sum behaves in terms of the POD for the preset PFA of 10^{-5} and an M that equals 17. The threshold was obtained by linear interpolation of the values shown in Figure 4.1 based on the two nearest neighboring values of 10^{-5} .

For POD evaluation, a total of 50,000 trials were used. For example, using Chebyshev's inequality, a confidence levels of 98.2% and 95% are obtained for $\varepsilon = 10^{-2}$ and p values of 0.1 and 0.5, respectively (note that when $p = 0.9$ the confidence level is the same as when $p = 0.1$). If a normal approximation is used, the resulting confidence level is 100% for all practical purposes. In Figure 4.4, SNR varies from -1 to 2 dB and 2 to 5 dB in dual-polarization and single-polarization cases, respectively. The POD for the power-threshold-based detector in single-polarization is presented as the standard so that the performance of all other detectors can be compared to it. In dual-polarization, the thresholds of 2 and 1.4 dB are applied to the power-threshold-based detectors. The POD for the first is presented to show how much the detection rate deteriorates if the legacy detection scheme is retained after the 3 dB SNR loss. The POD for the second is shown for fair comparison against the uniform sum because the threshold of 1.4 dB yields the PFA of 10^{-5} . For given signal parameters in Figure 4.4 (a), the power-threshold-based detection in a single-polarization system slightly outperforms the detection using the uniform sum in the dual-polarization case. Nevertheless, the latter offers substantial improvement over both the power-threshold-based legacy detection in the dual-polarization system, and the square-law detector with the same PFA. In Figure 4.4 (b), the Z_{DR} is decreased by 2 dB in which case the performance of the uniform sum surpasses that of the single-polarization legacy detector. Figure 4.5 shows similar comparisons of PODs but as a function of σ_v . In Figure 4.5 (a) similar trend is observed as the uniform sum approaches (but does not exceed) the single-polarization performance at lower spectrum widths, while yielding significant increase in POD with respect to the square law detector in dual-polarization. It is interesting to note that the POD of uniform sum

appears approximately constant up to spectrum width of 2 m s^{-1} but decreases with increasing spectrum width afterwards. This is because the uniform sum takes advantage of signal correlation for detection. Thus, as correlation of signals decreases at larger spectrum widths, the detection gain diminishes. In Figure 4.5 (b) the POD behavior vs. σ_v is examined but for the Z_{DR} that is decreased by 2 dB. In such case, it shows the POD for uniform sum to be less sensitive to the change in σ_v than the power based detector. This is because both powers and autocorrelations are used for detection by the uniform sum. For highly correlated signals the power estimates have higher statistical uncertainties that cause the spreading of the power estimator probability density function. Because the mean value of the power estimator is fixed (for constant signal power), more of the probability mass is shifted below the threshold degrading the performance for the case where only the power estimate is used for detection. The uniform sum, however, mitigates this effect through the inclusion of the autocorrelation whose mathematical expectation is directly proportional to signal coherency resulting in the larger expected value of the uniform sum for highly correlated signals. Larger expected value of the uniform sum can effectively shift more of the cumulative probability mass above the threshold level thus offsetting negative effects caused by spreading of the *pdf*. On the other hand, in the case of high spectrum widths, the autocorrelation estimates decrease and the mean of the uniform sum is closer to the threshold. Nonetheless, because the samples are less correlated the uniform sum estimate is more stable (i.e., *pdf* has less spread) resulting in the reduced amount of probability mass that falls below the threshold. Overall, this produces more balanced and improved detection rates (i.e., POD) for varied σ_v . Figure 4.6 demonstrates that the POD of the uniform sum is inversely proportional to

Z_{DR} . This is expected because the variance of the cross-correlation estimates is directly proportional to Z_{DR} (Melnikov 2004). At the same time, the POD of the power-threshold-based detector does not depend on Z_{DR} because only power in horizontal channel is used for detection. The uniform sum contains the modulus of the cross-correlation and the autocorrelation sum for detection; hence its performance is insensitive to variation in the velocity and differential phase. Typically, the weather signals from the horizontal and the vertical channels are highly correlated. Sachidananda and Zrnić (1985) indicate the theoretical value of $|\rho_{hv}(0)|$ is larger than 0.99 for rain drops with negligible canting. Additionally, the measured values in precipitation other than hail and melting snow are between 0.96 and 0.99 (Doviak and Zrnić 1993). This implies that the variations in the cross-correlation coefficient are fairly small and bear no significant impact on the uniform sum performance.

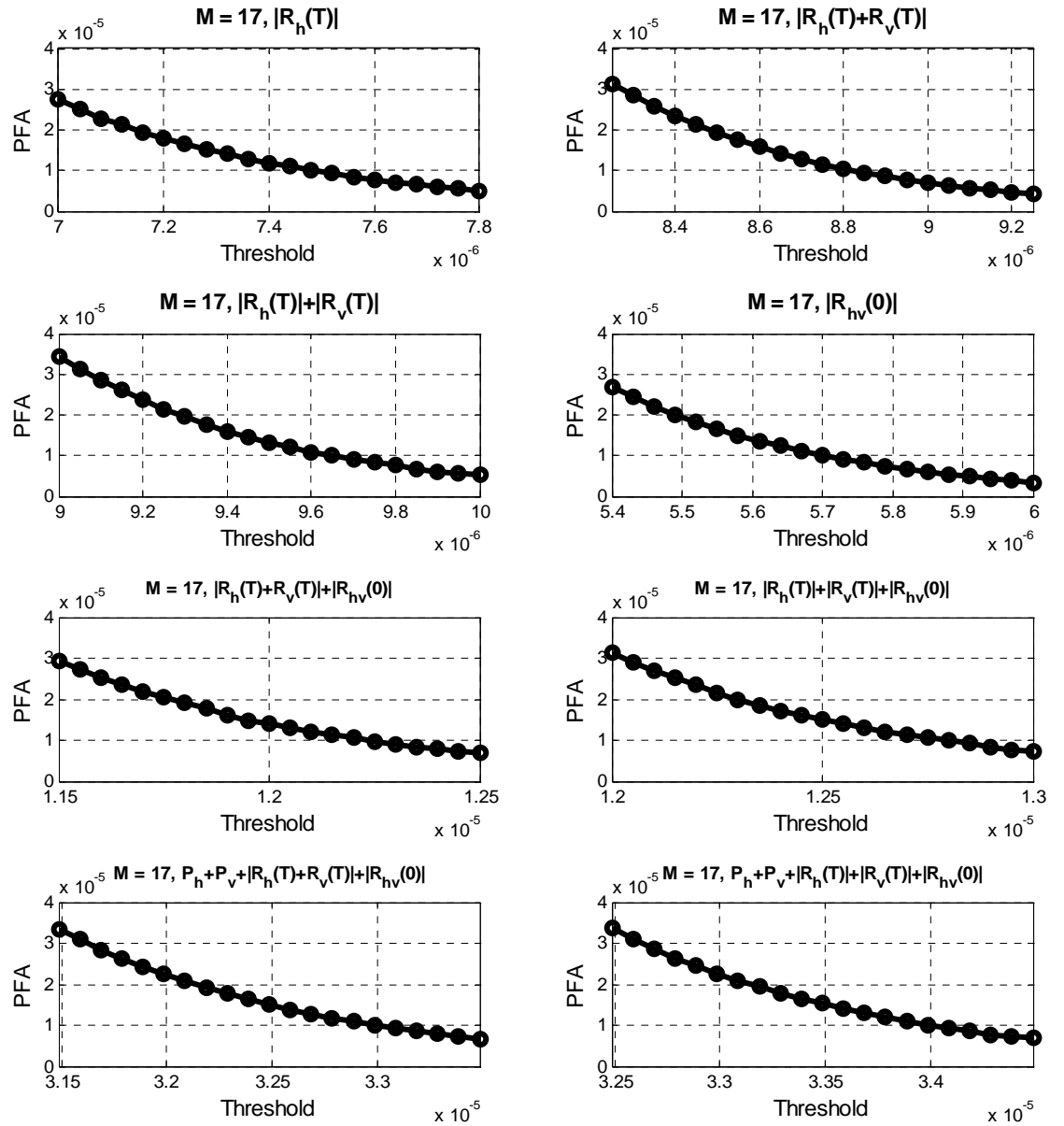
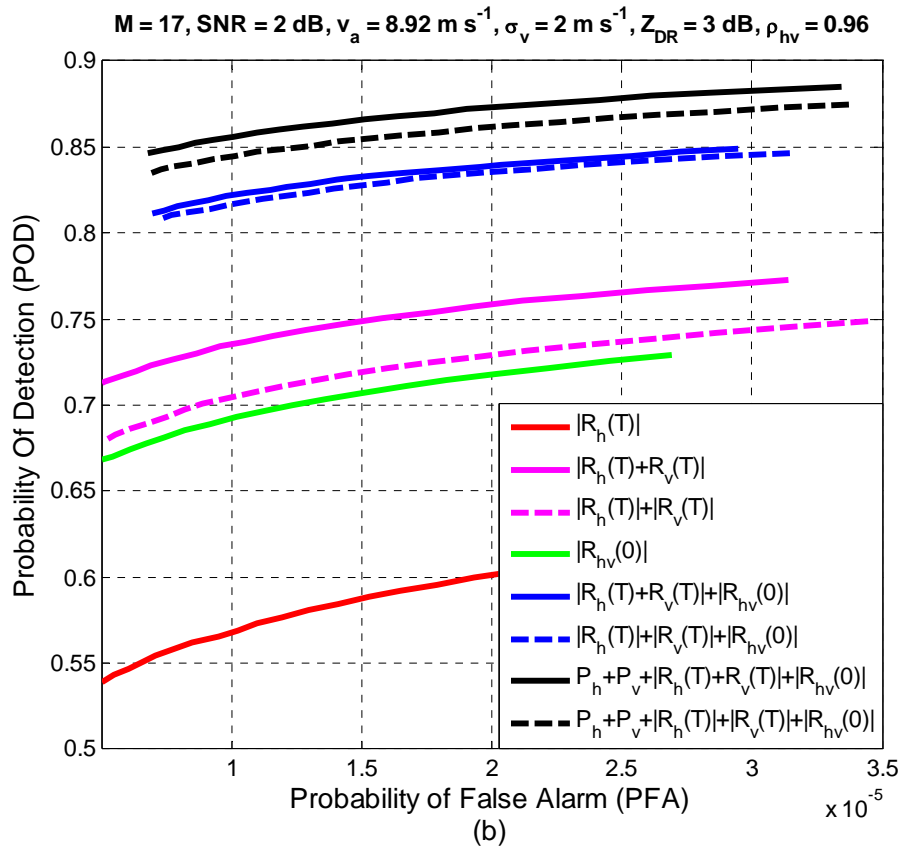
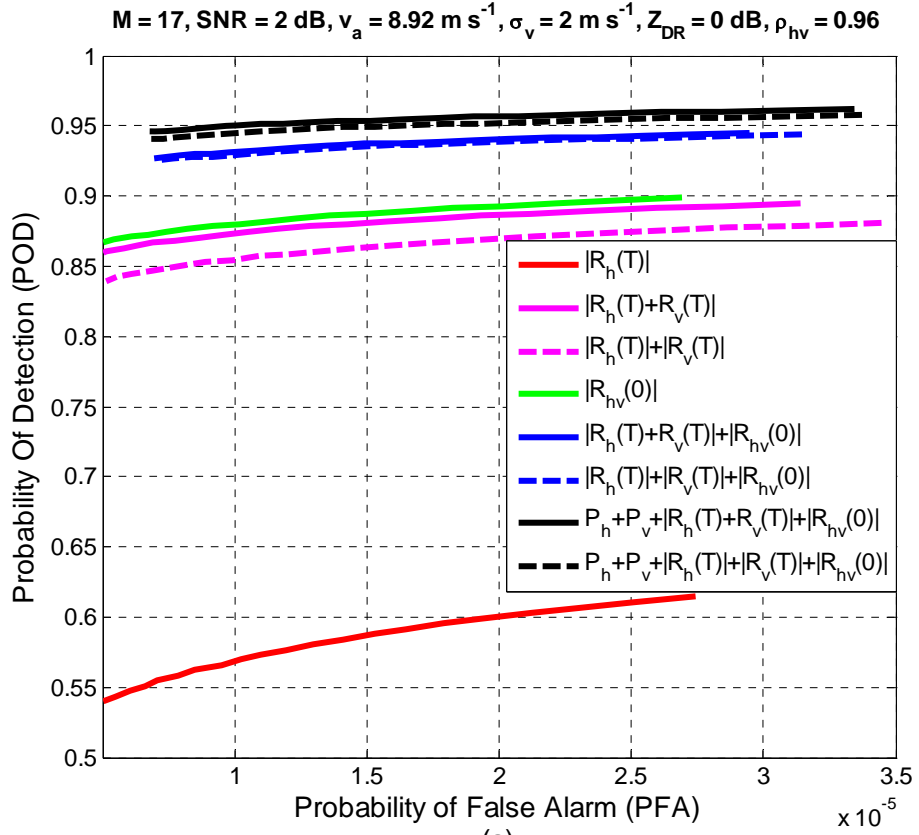
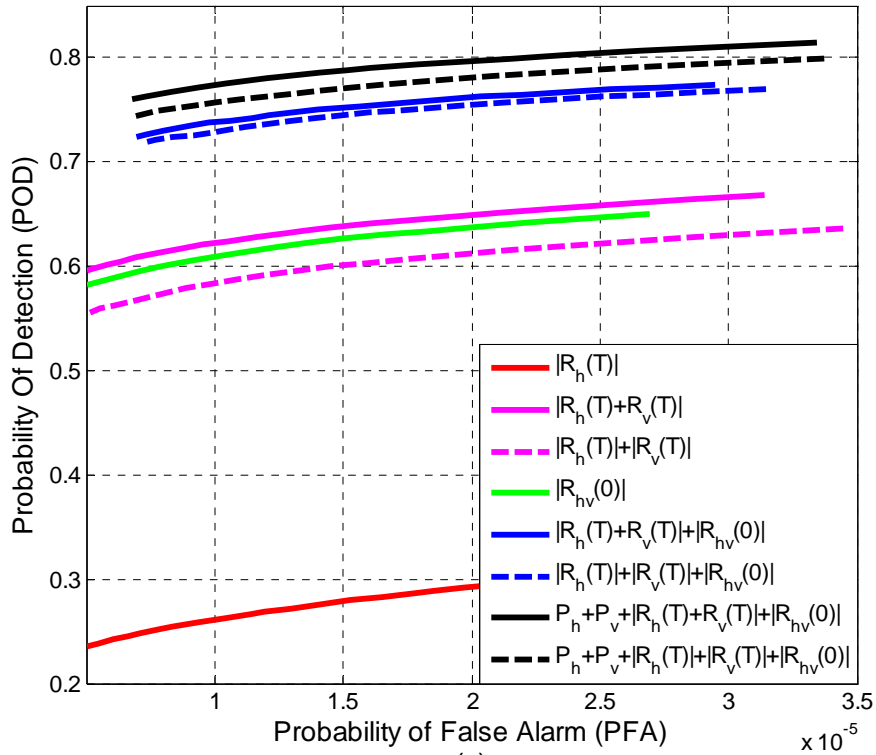


Figure 4.1 PFAs for different approaches.



$M = 17, \text{SNR} = 0 \text{ dB}, v_a = 8.92 \text{ m s}^{-1}, \sigma_v = 2 \text{ m s}^{-1}, Z_{\text{DR}} = 0 \text{ dB}, \rho_{\text{hv}} = 0.96$



$M = 17, \text{SNR} = 0 \text{ dB}, v_a = 8.92 \text{ m s}^{-1}, \sigma_v = 2 \text{ m s}^{-1}, Z_{\text{DR}} = 3 \text{ dB}, \rho_{\text{hv}} = 0.96$

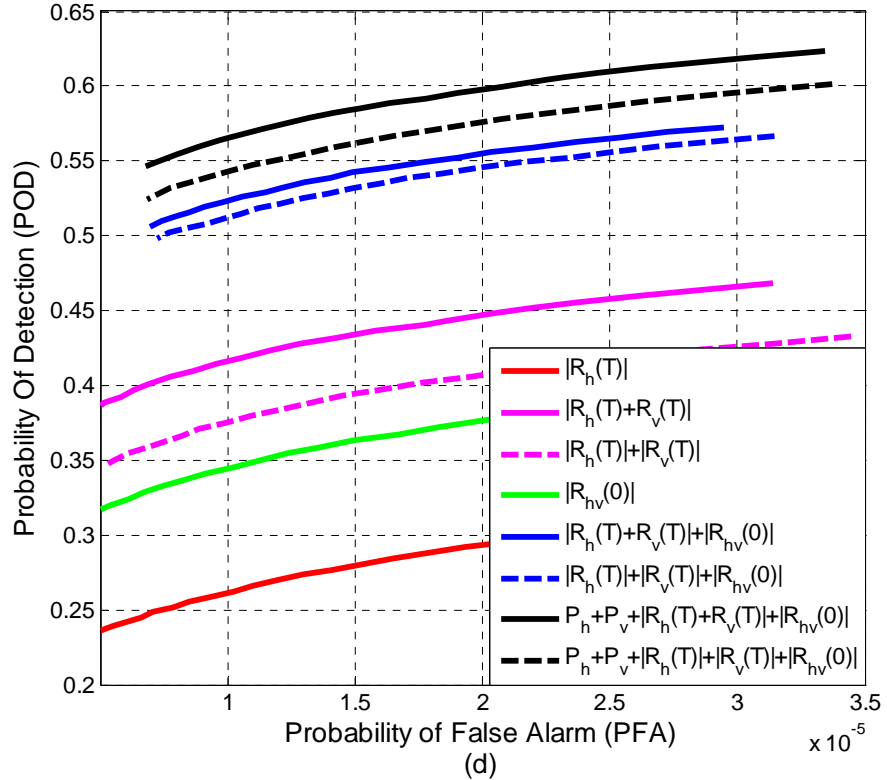


Figure 4.2 POD comparison for several detector functions.

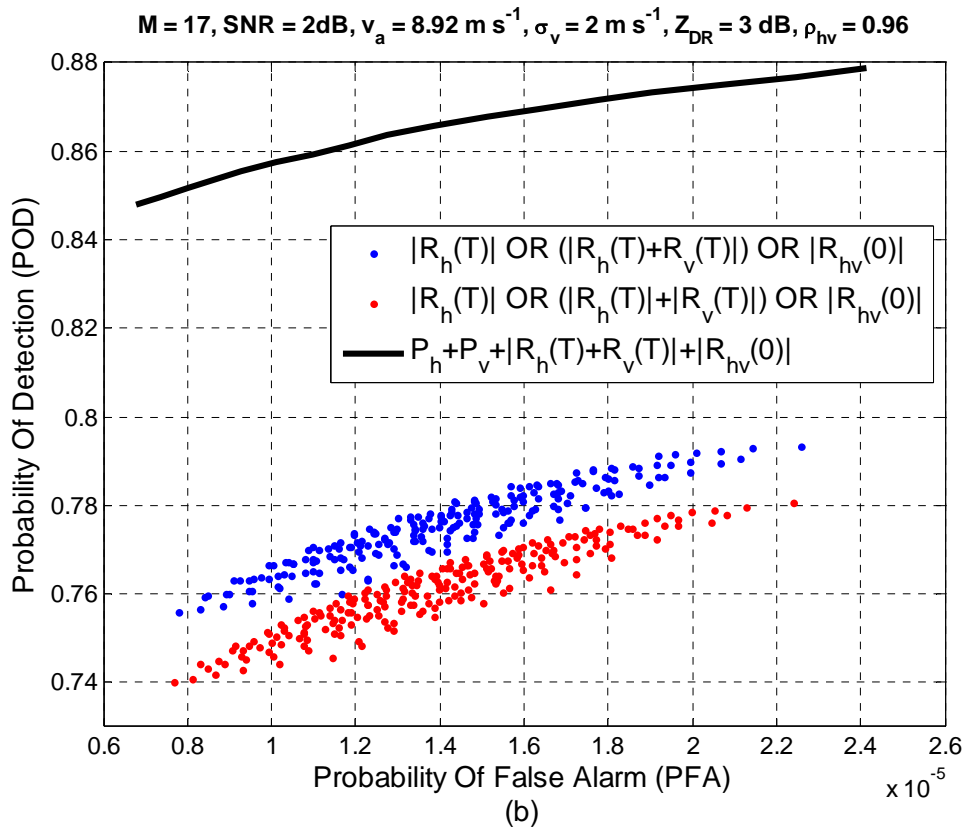
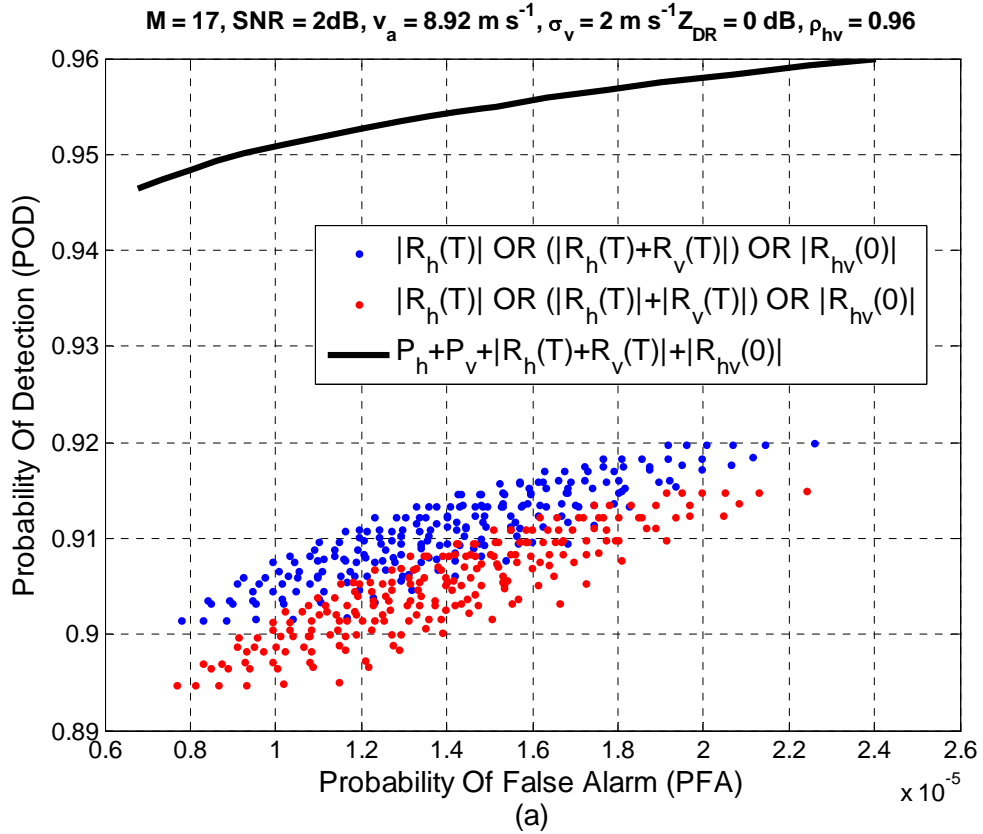


Figure 4.3 POD comparison for OR combination.

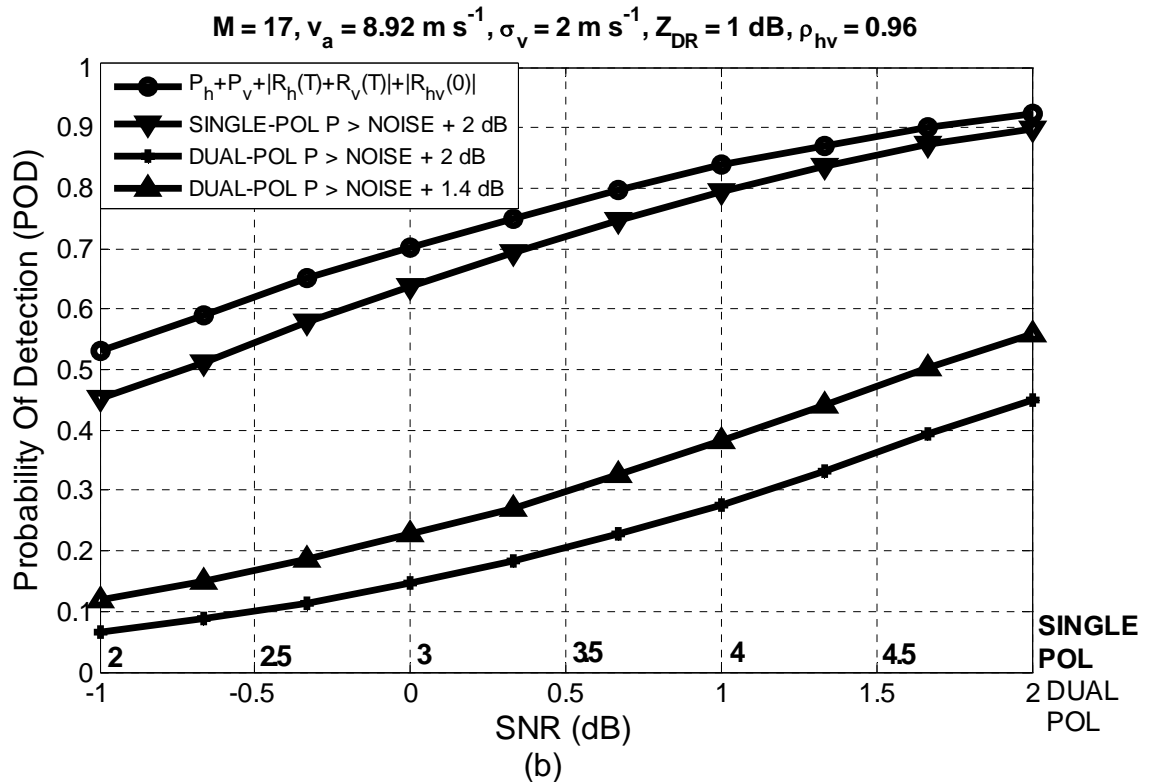
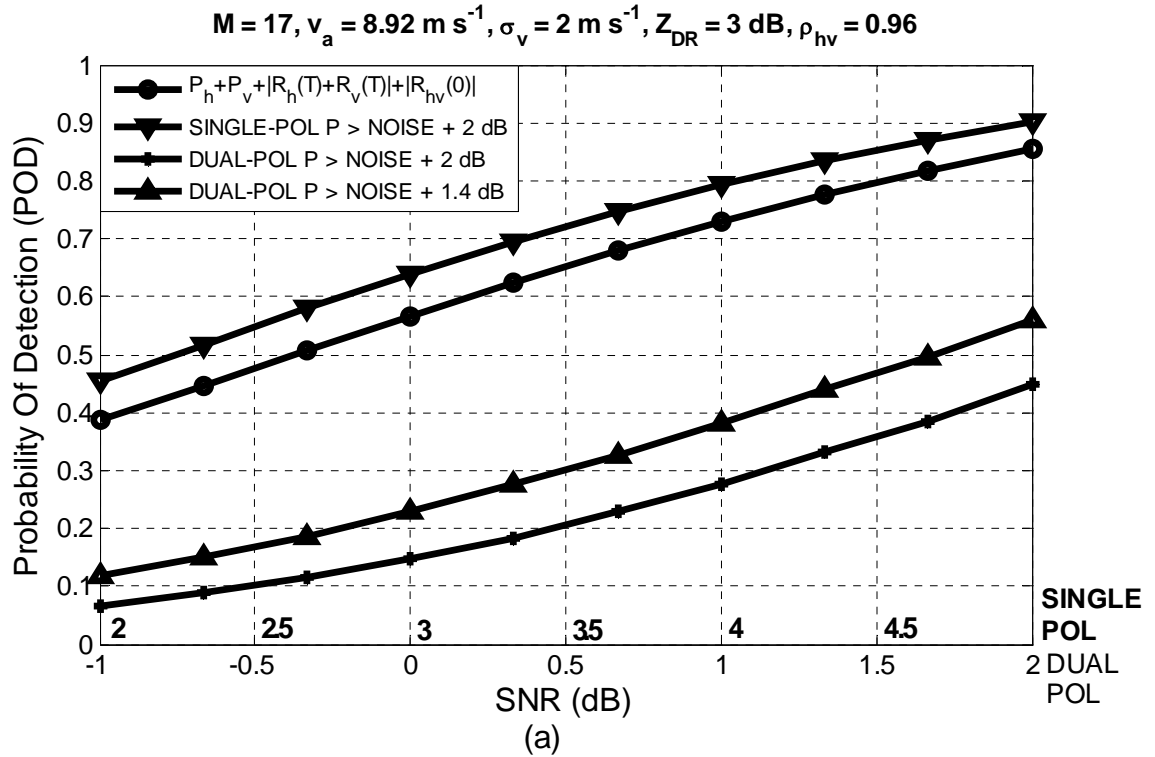


Figure 4.4 POD for varied SNR . For comparison, the uniform sum curve is plotted against the case with no 3 dB loss (single-polarization) with the power threshold set to 2 dB above the noise, and the 3 dB loss (dual-polarization) with the power thresholds of 2 and 1.4 dB.

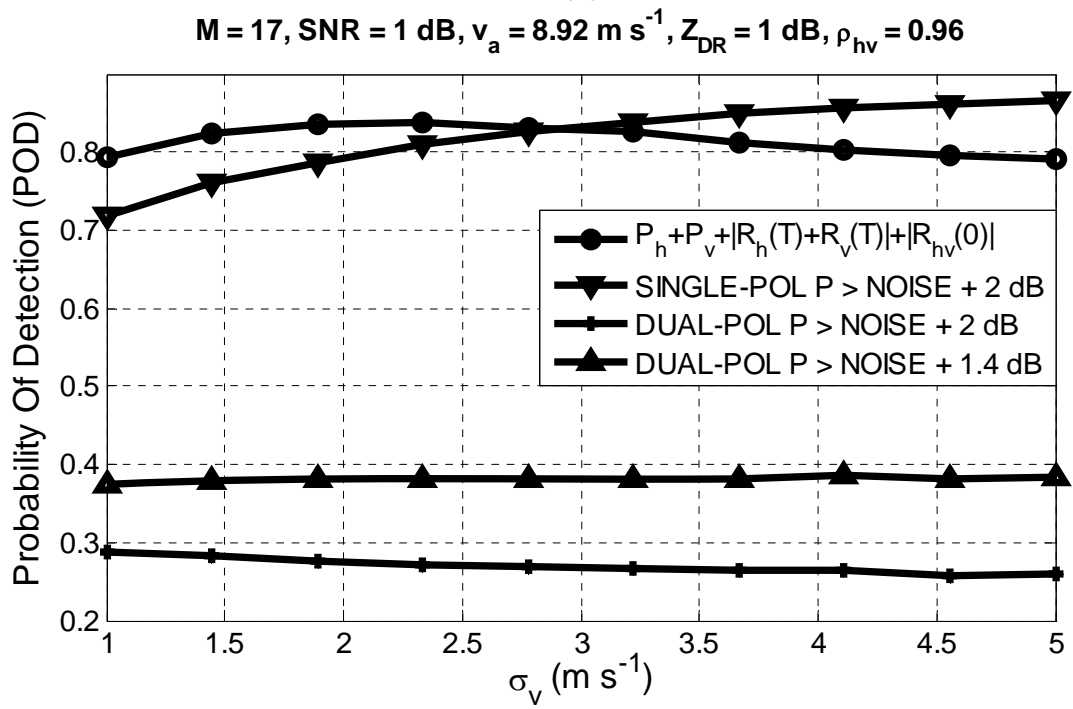
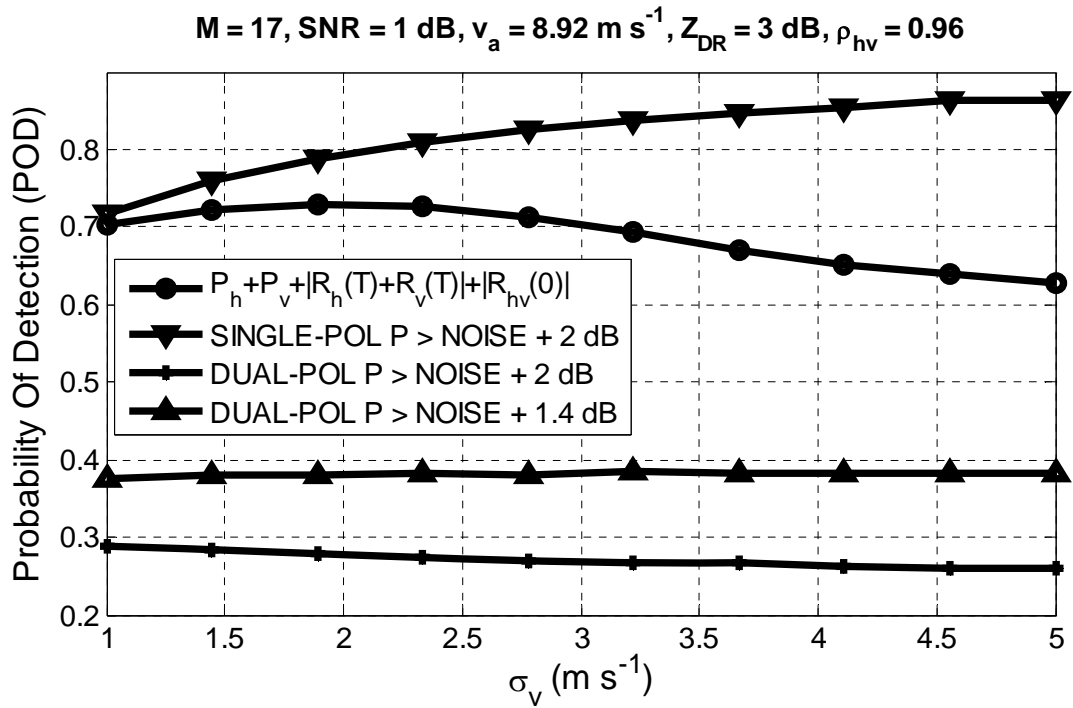


Figure 4.5 POD for varied σ_v . For comparison, the uniform sum curve is plotted against the case with no 3 dB loss (single-polarization) with the power threshold set to 2 dB above the noise, and the 3 dB loss (dual-polarization) with the power thresholds of 2 and 1.4 dB.

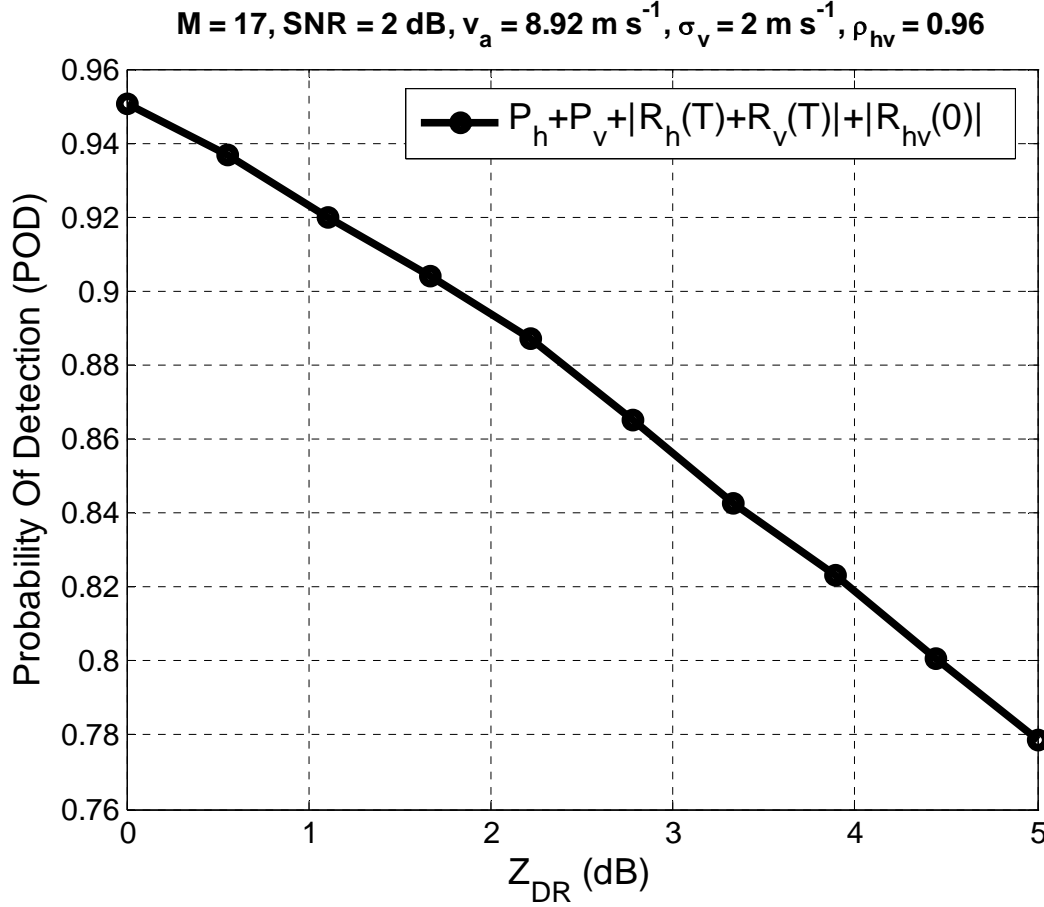


Figure 4.6 POD of uniform sum for varied Z_{DR} .

4.1 Comparison with the Likelihood Ratio Hypothesis Testing

So far, it has been established that the uniform sum yields significant improvement in signal detection compared to the standard power-threshold-based approach. The next objective is to find the maximum POD that can be achieved subject to the condition of the predetermined PFA.

Hypothesis testing using the likelihood-ratio, in case when the distribution parameters are known, provides the most powerful detection (as shown in Chapter 2). In this particular setting, Eq. (3.13) becomes:

$$\frac{1}{N_h} \sum_{m=0}^{M-1} |V_h(m)|^2 + \frac{1}{N_v} \sum_{m=0}^{M-1} |V_v(m)|^2 + \ln |\det \mathbf{C}^{-1}| - \mathbf{V}^H \mathbf{C}^{-1} \mathbf{V} \geq THR', \quad (4.17)$$

where THR' is set so that

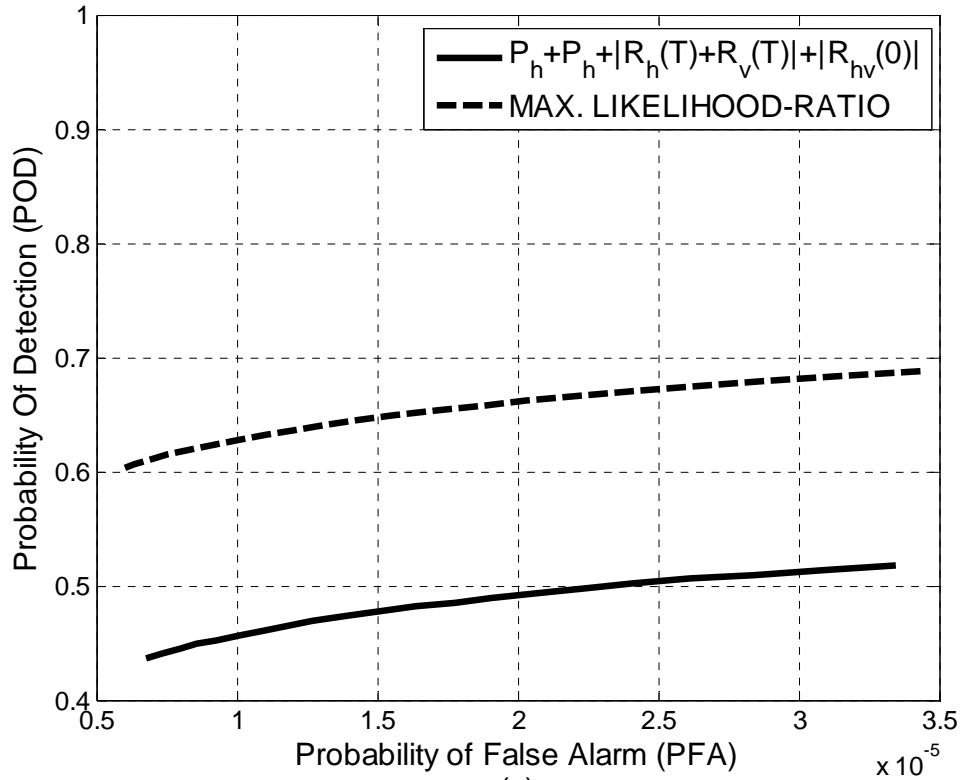
$$P \left(\sum_{m=0}^{M-1} \frac{|V_h(m)|^2}{N_h} + \sum_{m=0}^{M-1} \frac{|V_v(m)|^2}{N_v} + \ln |\det \mathbf{C}^{-1}| - \mathbf{V}^H \mathbf{C}^{-1} \mathbf{V} \geq THR' \mid \text{only noise present} \right) = \varepsilon, \quad (4.18)$$

and \mathbf{C} is calculated assuming known distribution parameters. In the Figure 4.7 the Maximum-Likelihood-ratio (ML) and the uniform sum are compared for several sets of signal parameters. The comparison shows that the difference between these two methods is inversely proportional to the SNR . For example, the difference in POD is approximately 0.04, 0.11 and 0.17 for $SNR = 2$ dB, 0.5 dB and -1 dB, for the PFA of 10^{-5} . In all cases, the ML approach performs better than the uniform sum. This result is expected as the uniform sum utilizes less information about the signal than the ML detector. Nonetheless, the significant difference in performance may imply that further improvements to the uniform sum could be possible. We speculate that a *weighted sum*, such as

$$\hat{P}_h + \alpha \hat{P}_v + \beta \left| \hat{R}_h(T) + \hat{R}_v(T) \right| + \gamma \left| \hat{R}_{hv}(0) \right| \quad (4.19)$$

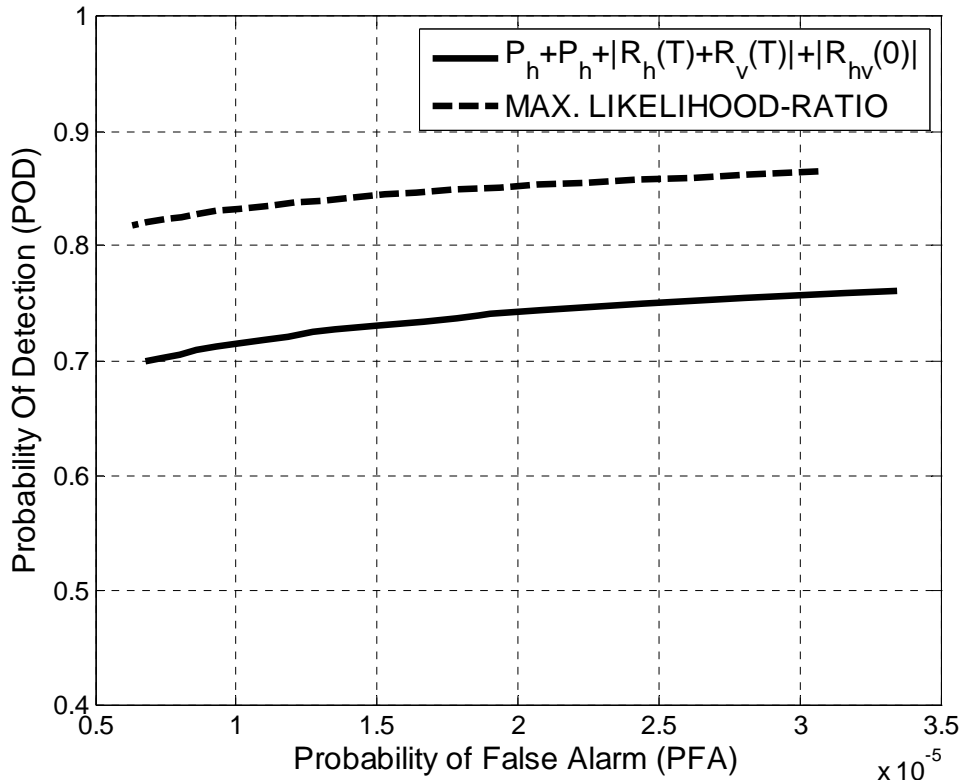
might provide a better performance than the uniform sum. This will be discussed in the next chapter.

$M = 17, SNR = -1dB, v_a = 8.92 \text{ m s}^{-1}, \sigma_v = 2 \text{ m s}^{-1}, Z_{DR} = 2 \text{ dB}, \rho_{hv} = 0.96$



(a)

$PRT 1, M = 17, Z_{DR} = 2 \text{ dB}, \rho_{hv} = 0.96, SNR = 0.5dB, \sigma_v = 2 \text{ m s}^{-1}$



(b)

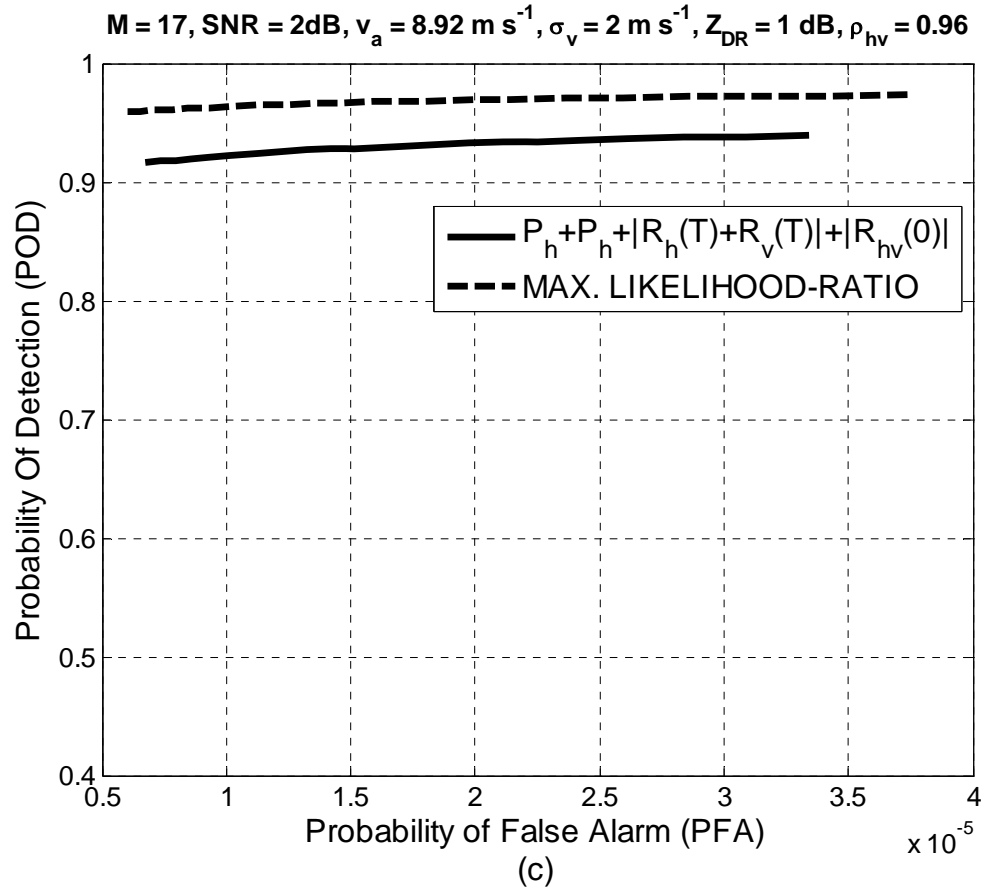


Figure 4.7 ML vs. uniform sum comparison.

5. Optimizing Detection Using Weighted Sum

In an attempt to improve the performance of the uniform sum, different weights are introduced to each term in the sum to produce a *weighted sum*. We speculate that the weights can be appropriately selected to maximize the rate of detection (i.e., POD) given specific values of SNR , σ_v , Z_{DR} , and ρ_{hv} . Inevitably, the performance of the weighted sum degrades as the difference between the mean parameters of samples in \mathbf{V} and the ones that the sum is optimized for grows larger. We can, however, attempt to find a set of values for SNR , σ_v , Z_{DR} , and ρ_{hv} , that the weighted sum is optimized for, which would minimize the performance degradation. We speculate that for each parameter such value is its median. For example, it can be assumed that 2 m s^{-1} is the median of σ_v for most weather events of interest (Fang et al. 2004) and we would like to adjust the weights accordingly. Similar approach can be applied for other parameters. Nonetheless, what the proper median values are for these parameters remains an open question. Another possible approach would be to find such a combination of weights that would produce relatively balanced detection rate for a wide range of signal parameters of interest.

Let us now analyze the approach in which the weights are adjusted for a given set of median values, as well as the desired PFA. An idealized way to achieve this is to find the *pdf* of the weighted sum in a closed form (which is a function of signal parameters and their weights). If we could do this, we would essentially have two functions. One is the *pdf* of the weighted sum for noise only, and the other one is for the case where both signal and noise are present. The former is denoted as $f(W_{S_N})$ and the latter one is denoted as $f(W_{S_{S+N}})$, where the W_{S_N} and $W_{S_{S+N}}$ are the random variables that represent the weighted sum outputs when noise and signal+noise are present. Note that both functions

have similar notation except for the subscripts, which stand for the function input (i.e., N for noise only and $N+S$ for signal and noise). This is done purposely because these two functions have the same form except that if only noise is present, we set $SNR = -\infty$ dB, $\sigma_v = \infty$ m s⁻¹ (i.e., $\rho = 0$), $\rho_{hv} = 0$, and Z_{DR} to the known value which can be obtained by measuring the noise powers in both H and V channels. Now we can define the problem as follows:

We want to find values for weights α , β , and γ such that:

$$\begin{aligned}
 P(WS_{S+N} \geq THR | \alpha, \beta, \gamma) &\geq P(WS_{S+N} \geq THR | \alpha', \beta', \gamma') \\
 &\text{OR} \qquad \qquad \qquad \text{for } \forall \alpha', \beta', \gamma' \in \mathbb{R}, \\
 \int_{THR}^{\infty} f(WS_{S+N}; \alpha, \beta, \gamma) dWS_{S+N} &\geq \int_{THR}^{\infty} f(WS_{S+N}; \alpha', \beta', \gamma') dWS_{S+N}
 \end{aligned}$$

under the condition that

$$P(WS_N > THR | \alpha, \beta, \gamma) = \int_{THR}^{\infty} f(WS_N; \alpha, \beta, \gamma) dWS_N \leq \varepsilon \tag{5.1}$$

where ε is the desired PFA, and THR is the threshold.

Clearly, both WS_N and WS_{S+N} are functions of the observation vector $\mathbf{V} = [V_h(0), \dots, V_h(M-1), V_v(0), \dots, V_v(M-1)]^T$. Note that each element in the vector is a random variable and therefore, WS_N and WS_{S+N} are transformations of random variables in \mathbf{V} . Thus, to derive f , we naturally start with the joint *pdf* (look at eq. (3.5)) for all the elements in \mathbf{V} . Nonetheless, a brief examination of the problem indicates that finding the *pdf* of either WS_N or WS_{S+N} is not feasible in an analytical form. All is not lost however, let us state the goal using formulas in Chapter 3 (i.e., (3.5) and (3.8)) which give us the exact expression for joint *pdf*'s as:

We want to find values for weights α , β , and γ such that:

$$\int_{WS_{S+N}^{\alpha, \beta, \gamma} \geq THR} \pi^{-2M} |\det \mathbf{C}^{-1}| \exp(-\mathbf{V}^H \mathbf{C}^{-1} \mathbf{V}) d\mathbf{V} \geq \int_{WS_{S+N}^{\alpha', \beta', \gamma'} \geq THR} \pi^{-2M} |\det \mathbf{C}^{-1}| \exp(-\mathbf{V}^H \mathbf{C}^{-1} \mathbf{V}) d\mathbf{V}$$

for $\forall \alpha', \beta', \gamma' \in \mathbb{R}$,

under the condition that

$$\int_{WS_N^{\alpha, \beta, \gamma} \geq THR} (\pi^2 N_h N_v)^{-M} \exp\left(-\frac{1}{N_h} \sum_{m=0}^{M-1} |V_h(m)|^2 - \frac{1}{N_v} \sum_{m=0}^{M-1} |V_v(m)|^2\right) d\mathbf{V} \leq \varepsilon, \quad (5.2)$$

where ε is the desired PFA, and THR is the threshold.

Because there are $2M$ random variables, each integral in (5.2) represents a volume in a $2M$ multidimensional space. Thus, the condition $WS_{N+S}^{\alpha, \beta, \gamma} \geq THR$ specifies the region in a $2M$ dimensional sample space where the weighted sum is greater than, or equal to, the threshold, for the case when both signal and noise are present. The condition $WS_N^{\alpha, \beta, \gamma} \geq THR$ stands for the region in $2M$ dimensional sample space in which the weighted sum is greater than, or equal to, the threshold, in case only noise is present. These two regions can be viewed as sets of all possible values of observation vector for which the weighted sum exceeds the threshold for some values of α , β , and γ . Because in both cases noise present or signal+noise present, an observation vector can take any value (but with different probability), these two regions are the same. Thus, by changing the values of the weights, this region is shaped in the $2M$ dimensional space. Consequently, given the set of signal parameter values for which we want to optimize detection, the goal is to find such set of the values of α , β , and γ that shape this region so that the integration over it, when signal and noise are present, is maximized, while maintaining the same integration value in the presence of noise only. Because it is not feasible to derive the *pdf* analytically, an efficient method of evaluating integrals in (5.2) is needed.

The plain (i.e., conventional) Hit or Miss Monte Carlo integration method is one of the candidates. Given the set of values of α , β , and γ and the threshold value THR , the resulting PFA can be evaluated, using this method, as

$$PFA = \frac{1}{K} \sum_{k=0}^{K-1} D(WS_N^{\alpha,\beta,\gamma}), \quad (5.3)$$

where K is the number of trials and

$$D(WS_N^{\alpha,\beta,\gamma}) = \begin{cases} 1 & \text{if } \hat{P}_h + \alpha \hat{P}_v + \beta |\hat{R}_h(T) + \hat{R}_v(T)| + \gamma |\hat{R}_{hv}(0)| \geq THR \\ 0 & \text{if } \hat{P}_h + \alpha \hat{P}_v + \beta |\hat{R}_h(T) + \hat{R}_v(T)| + \gamma |\hat{R}_{hv}(0)| < THR \end{cases}. \quad (5.4)$$

Elements of the observation vector \mathbf{V} are generated from the distribution given in (3.8); thus, the observation vector elements can be generated directly using a Gaussian random number generator. The POD is evaluated as

$$POD = \frac{1}{K} \sum_{k=0}^{K-1} D(WS_{S+N}^{\alpha,\beta,\gamma}), \quad (5.5)$$

where K is the number of trials and

$$D(WS_{S+N}^{\alpha,\beta,\gamma}) = \begin{cases} 1 & \text{if } \hat{P}_h + \alpha \hat{P}_v + \beta |\hat{R}_h(T) + \hat{R}_v(T)| + \gamma |\hat{R}_{hv}(0)| \geq THR \\ 0 & \text{if } \hat{P}_h + \alpha \hat{P}_v + \beta |\hat{R}_h(T) + \hat{R}_v(T)| + \gamma |\hat{R}_{hv}(0)| < THR \end{cases}. \quad (5.6)$$

Elements of the observation vector \mathbf{V} are generated from the distribution given in (3.5). Note that when both signal and noise are present the covariance matrix \mathbf{C} is not necessarily diagonal and the observation vector elements can not be generated directly using a Gaussian random number generator, but rather using methods given in Zrnić (1975) and Torres (2001).

Clearly, the optimal set of weights is the one producing the largest POD among all possible weight combinations. To find such set, a large number of weight evaluations needs to be performed. Based on the simulations carried out previously, estimating POD

for a known set of weights and a given threshold does not require exorbitant number of trials to achieve the desired accuracy; hence this can be done relatively fast. Yet, before estimating the POD, an appropriate threshold value that preserves the desired PFA must be obtained. So far, the only tool we have at our disposal is the plain Monte Carlo. Due to the low values of the desired PFA (on the order of $10^{-5} \div 10^{-6}$), evaluating each candidate threshold requires a large number of trials (as shown in Chapter 4). This makes the plain Monte Carlo approach computationally impractical when evaluation of numerous thresholds is required. Additionally, if the weighted sum is to be used for detection operationally, an efficient method for threshold calculation needs to be devised. Consequently, it becomes imperative to introduce an optimization that will reduce the number of trials required to achieve the desired accuracy of Monte Carlo integration in case when only noise is present. Having done so, an appropriate threshold could be found by starting with an arbitrary value and varying it (i.e., increasing or decreasing it) until the one that yields the desired PFA is located. Unfortunately, every change in the *THR* value requires a corresponding PFA evaluation and, even with the optimizations, the entire process is still likely to prove time consuming. Consequently, it would be extremely helpful if the *pdf* of the weighted sum could be roughly approximated with a closed form. Such approximation can be used for better selection of the initial threshold, (i.e., the one closer to the desired result) in the iterative process, in order to reduce the number of PFA evaluations using the Monte Carlo integration.

The tools for the threshold computation are developed in this chapter, which is laid out as follows. First, a variance reduction technique, aimed at decreasing the number of trials needed for Monte Carlo integration, is presented in section 5.1. An approach for

approximating weighted sum *pdf* with a generalized gamma distribution is described in section 5.2. Because it is based on matching the first three moments of the weighted sum, an approach to moment evaluation is given in sections 5.3 and 5.4. An iterative method, that uses tools developed in previous sections, to calculate the threshold, given the desired PFA, is described in section 5.5. Using this method and the plain Monte Carlo integration for POD evaluation, as in (5.5), the effects of weighting are assessed in section 5.6. Finally, some implementation issues are discussed in section 5.7.

5.1 Importance Sampling Application

When simulating the occurrence of random rare events (as this is clearly the case), it has been shown that the Importance Sampling (IS) technique has the potential to dramatically reduce the number of trials needed to meet the accuracy requirements (Mitchell 1981). The principle of Importance Sampling (IS) is to select samples from a population different from the original one, so that the occurrence rate of initially rare event increases. Subsequently, the occurrence of each event is scaled by the ratio of the joint probabilities of the original and the biased population in order to compensate the skew in PFA. In other words, different importance is placed on each sample; depending on how likely such a sample would be, if it were generated by the original distribution (e.g., distribution p), rather than the bias sampling distribution (e.g., distribution q). To formulate this approach mathematically, let the original joint *pdf* be denoted as $p(y_1, \dots, y_n)$ and the biased one as $g(y_1, \dots, y_n)$, where y_1, \dots, y_n are n random variables. The result can be represented in an integral form as:

$$I = \int_{-\infty}^{\infty} \cdots \int_{-\infty}^{\infty} D[f(y_1, \dots, y_n)] p(y_1, \dots, y_n) dy_1 \cdots dy_n, \quad (5.7)$$

where $D[f(y_1, \dots, y_n)]$ denotes the decision criterion which is defined by the function f of random variables y_1, \dots, y_n . Naturally:

$$D[f(y_1, \dots, y_n)] = \begin{cases} 1 & \text{if criterion satisfied} \\ 0 & \text{if criterion NOT satisfied} \end{cases} \quad (5.8)$$

We use the biased distribution to re-write I as:

$$I = \int_{-\infty}^{\infty} \dots \int_{-\infty}^{\infty} \frac{p(y_1, \dots, y_n)}{g(y_1, \dots, y_n)} D[f(y_1, \dots, y_n)] g(y_1, \dots, y_n) dy_1 \dots dy_n. \quad (5.9)$$

This result can now be estimated as:

$$\hat{I} = \frac{1}{K} \sum_{k=0}^{K-1} \frac{p(\hat{y}_1(k), \dots, \hat{y}_n(k))}{g(\hat{y}_1(k), \dots, \hat{y}_n(k))} D[f(\hat{y}_1(k), \dots, \hat{y}_n(k))], \quad (5.10)$$

where $\hat{y}_1(k), \dots, \hat{y}_n(k)$ is k -th occurrence of the set generated from the joint *pdf* $g(y_1, \dots, y_n)$.

The IS algorithm is now (Denny 2001):

1. Sample $\hat{y}_1(k), \dots, \hat{y}_n(k)$ from $g(y_1, \dots, y_n)$.
2. Apply decision criteria $D[f(y_1, \dots, y_n)]$. If it is true set $I_k = p(\hat{y}_1(k), \dots, \hat{y}_n(k))/g(\hat{y}_1(k), \dots, \hat{y}_n(k))$ else set $I_k = 0$.
3. Estimate the integral as $\hat{I} = \frac{1}{K} \sum_{k=0}^{K-1} I_k$.

What remains is the proper choice of the bias distribution. It is our goal to choose the bias function that will minimize the variance, defined in the following form

$$\text{Var}(\hat{I}) = E\{\hat{I}^2\} - E^2\{\hat{I}\}. \quad (5.11)$$

The value of the second term cannot be influenced by the choice of function g , which leaves us with:

$$\begin{aligned}
E\{\hat{I}^2\} &= E\left\{\frac{1}{K}\sum_{k=0}^{K-1}\frac{p(\hat{y}_1(k),\dots,\hat{y}_n(k))}{g(\hat{y}_1(k),\dots,\hat{y}_n(k))}D[f(\hat{y}_1(k),\dots,\hat{y}_n(k))]\right. \\
&\quad \left.\frac{1}{K}\sum_{l=0}^{K-1}\frac{p(\hat{y}_1(l),\dots,\hat{y}_n(l))}{g(\hat{y}_1(l),\dots,\hat{y}_n(l))}D[f(\hat{y}_1(l),\dots,\hat{y}_n(l))]\right\} \\
&= E\left\{\frac{1}{K^2}\sum_{k=0}^{K-1}\frac{p^2(\hat{y}_1(k),\dots,\hat{y}_n(k))}{g^2(\hat{y}_1(k),\dots,\hat{y}_n(k))}D[f(\hat{y}_1(k),\dots,\hat{y}_n(k))]\right\} + \frac{K-1}{K}I^2
\end{aligned} \tag{5.12}$$

Hence, the variance is:

$$Var(\hat{I}) = E\left\{\frac{1}{K^2}\sum_{k=0}^{K-1}\frac{p^2(\hat{y}_1(k),\dots,\hat{y}_n(k))}{g^2(\hat{y}_1(k),\dots,\hat{y}_n(k))}D[f(\hat{y}_1(k),\dots,\hat{y}_n(k))]\right\} - \frac{1}{K}I^2. \tag{5.13}$$

It also can be written:

$$Var(\hat{I}) = E\left\{\frac{1}{K^2}\sum_{k=0}^{K-1}D[f(\hat{y}'_1(k),\dots,\hat{y}'_n(k))]\right\} - \frac{1}{K}I^2, \tag{5.14}$$

where each set $\hat{y}'_1(k),\dots,\hat{y}'_n(k)$ is chosen from a population distributed as $p^2(\hat{y}'_1(k),\dots,\hat{y}'_n(k))/g(\hat{y}'_1(k),\dots,\hat{y}'_n(k))$.

Let us investigate how to apply IS to the case when only noise is present given the joint *pdf* p in eq. (3.5). The main question is how to choose the biased *pdf* (i.e., g) in order to maximize improvement in the estimate performance. Among many biasing methods, scaling technique has been widely used (Srinivasan 2002). The objective is to shift the probability mass toward the region of desired event in order to effectively increase the occurrence (i.e., probability) of the rare event. If the scaling technique is used, a biasing distribution is obtained as $g(x) = 1/a:f(x/a)$, whereas parameter a is chosen to minimize the estimate variance. The implementation of the scaling method is described now.

It is convenient to choose g in the following form:

$$g(\mathbf{V}) = \left(\pi^{2M} \prod_{m=0}^{2M-1} N(m) \right)^{-1} \exp \left(- \sum_{m=0}^{2M-1} \frac{|V(m)|^2}{N(m)} \right). \quad (5.15)$$

In order to select the values of $N(m)$, the Cross-Entropy method (de Boer et al. 2005) was used. The general stochastic equation, as given by (22) in de Boer et al. (2005), is as follows

$$\begin{aligned} \max_{\mathbf{N}} \frac{1}{K} \sum_{k=0}^{K-1} D \left[WS(\mathbf{V}_k) > \hat{T}_t \right] & \frac{\prod_{l=0}^{2M-1} \hat{N}_{t-1}(l0)}{(N_h N_v)^M} \exp \left(- \sum_{l=0}^{M-1} \left(\frac{1}{N_h} - \frac{1}{\hat{N}_{t-1}(l1)} \right) |V(l1, k)|^2 - \right. \\ & \left. \sum_{l=2=M}^{2M-1} \left(\frac{1}{N_v} - \frac{1}{\hat{N}_{t-1}(l2)} \right) |V(l2, k)|^2 \right) \ln \left(\frac{\left(\prod_{m=0}^{2M-1} N(m) \right)^{-1}}{\pi^{2M}} \exp \left(- \sum_{m=0}^{2M-1} \frac{|V(m, k)|^2}{N(m)} \right) \right). \end{aligned} \quad (5.16)$$

For each value $N(m)$ we have

$$\frac{\partial}{\partial N(m)} \ln \left(\frac{\left(\prod_{m=0}^{2M-1} N(m) \right)^{-1}}{\pi^{2M}} \exp \left(- \sum_{m=0}^{2M-1} \frac{|V(m, k)|^2}{N(m)} \right) \right) = \frac{|V(m, k)|^2}{N^2(m)} - \frac{1}{N(m)} \quad (5.17)$$

yielding:

$$\begin{aligned} \frac{1}{K} \sum_{k=0}^{K-1} D \left[WS(\mathbf{V}_k) > \hat{T}_t \right] & \frac{\prod_{l=0}^{2M-1} \hat{N}_{t-1}(l0)}{(N_h N_v)^M} \exp \left(- \sum_{l=0}^{M-1} \left(\frac{1}{N_h} - \frac{1}{\hat{N}_{t-1}(l1)} \right) |V(l1, k)|^2 - \right. \\ & \left. \sum_{l=2=M}^{2M-1} \left(\frac{1}{N_v} - \frac{1}{\hat{N}_{t-1}(l2)} \right) |V(l2, k)|^2 \right) \left(\frac{|V(m, k)|^2}{N^2(m)} - \frac{1}{N(m)} \right) = 0, \end{aligned} \quad (5.18)$$

from which we get:

$$\begin{aligned}
N(m) = & \frac{\sum_{k=0}^{K-1} D[WS(\mathbf{V}_k) > \hat{T}_t] \exp\left(-\sum_{l=0}^{M-1} \left(\frac{1}{N_h} - \frac{1}{\hat{N}_{t-1}(l1)}\right) |V(l1, k)|^2 - \dots}{\sum_{k=0}^{K-1} D[WS(\mathbf{V}_k) > \hat{T}_t] \exp\left(-\sum_{l=0}^{M-1} \left(\frac{1}{N_h} - \frac{1}{\hat{N}_{t-1}(l1)}\right) |V(l1, k)|^2 - \dots \right.} \\
& \left. \frac{\sum_{l2=M}^{2M-1} \left(\frac{1}{N_v} - \frac{1}{\hat{N}_{t-1}(l2)}\right) |V(l2, k)|^2 |V(m, k)|^2}{\sum_{l2=M}^{2M-1} \left(\frac{1}{N_v} - \frac{1}{\hat{N}_{t-1}(l2)}\right) |V(l2, k)|^2}\right). \tag{5.19}
\end{aligned}$$

The algorithm for estimating the PFA is summarized as (de Boer et al. 2005):

- (1) Define $\hat{N}_0(m) = N_h$ and $\hat{N}_0(m+M) = N_v$ for $m = 1, \dots, M$. Set $t = 1$ (iteration = level counter)
- (2) Generate a sample V_1, \dots, V_K from the density:

$$g(\mathbf{V}) = \left(\pi^{2M} \prod_{m=0}^{2M-1} \hat{N}_{t-1}(m) \right)^{-1} \exp\left(-\sum_{m=0}^{2M-1} \frac{|V(m)|^2}{\hat{N}_{t-1}(m)}\right). \tag{5.20}$$

Calculate $WS(V(i))$ for all and sort them in ascending order. Compute the sample $(1-\rho)$ -quantile \hat{T}_t of the performance according to $\hat{T}_t = WS(\lceil (1-\rho)K \rceil)$, provided \hat{T}_t is less than THR. Otherwise set $\hat{T}_t = THR$.

- (3) Use the same sample $V(1), \dots, V(K)$ to solve the stochastic equation as given by (5.19). Denote the solution by \hat{N}_t .
- (4) If $\hat{T}_t < THR$, set $t = t+1$ and reiterate from step 2. Else proceed with step 5
- (6) Estimate the PFA using:

$$PFA = \frac{1}{K} \sum_{k=0}^{K-1} D[WS(\mathbf{V}_k) > \hat{T}_t] \frac{\prod_{l=0}^{2M-1} \hat{N}_t(l)}{(N_h N_v)^M} \exp\left(-\sum_{l=0}^{M-1} \left(\frac{1}{N_h} - \frac{1}{\hat{N}_t(l)}\right) |V(l, k)|^2 - \sum_{l=M}^{2M-1} \left(\frac{1}{N_v} - \frac{1}{\hat{N}_t(l)}\right) |V(l, k)|^2\right) \quad (5.21)$$

The above algorithm provides an efficient avenue for obtaining the PFA for a given threshold. However, our problem is that given a desired PFA we need to determine the corresponding threshold. The process for threshold finding is proposed as follows.

1. Choose initial threshold arbitrarily.
2. Estimate the corresponding PFA.
3. If the estimated PFA is within an acceptable range of the desired one, accept the threshold. If the estimated PFA is greater than the desired one, increase the threshold by some small value Δ , and go back to step 2. If the estimated PFA is smaller than the desired one, decrease the threshold by some small value Δ , and go back to step 2.

The above algorithm would work reliably, but even with the optimization techniques introduced, the process could still prove very time consuming, because the further the initial threshold is from the solution, the longer it takes for the process to converge. Thus, we proceed by finding an approximation to the *pdf* of the weighted sum with an analytical function. Such function is used to calculate the threshold given a desired PFA. Hopefully, this threshold is close enough to the one that produces the desired PFA, and when used as the initial threshold in the iterative process reduces the numbers of steps needed to reach the final result. Consequently, the following section is devoted to finding

an acceptable approximation to the *pdf* of the weighted sum by fitting it to some distribution function model.

5.2 Distribution Fitting

The goal of distribution fitting is to select the model of statistical distribution that fits best to the data generated by a random process. In this work, the moments of the distribution are used as the criteria for fitting. Let's consider the n -th moment of the weighted sum

$$m_n = E \left\{ \left(\hat{P}_h + \alpha \hat{P}_v + \beta \left| \hat{R}_h(T) + \hat{R}_v(T) \right| + \gamma \left| \hat{R}_{hv}(0) \right| \right)^n \right\}. \quad (5.22)$$

Using the multinomial theorem we can write:

$$\begin{aligned} m_n &= \sum_{k_1, k_2, k_3, k_4} \frac{n!}{k_1! k_2! k_3! k_4!} E \left\{ \left(\hat{P}_h \right)^{k_1} \left(\alpha \hat{P}_v \right)^{k_2} \left(\beta \left| \hat{R}_h(T) + \hat{R}_v(T) \right| \right)^{k_3} \left(\gamma \left| \hat{R}_{hv}(0) \right| \right)^{k_4} \right\} \\ &= \sum_{k_1, k_2, k_3, k_4} \frac{N_h^{k_1+k_2+k_3+k_4} n!}{k_1! k_2! k_3! k_4!} E \left\{ \left(\frac{\hat{P}_h}{N_h} \right)^{k_1} \left(\alpha \frac{N_v}{N_h} \frac{\hat{P}_v}{N_v} \right)^{k_2} \left(\beta \left| \frac{\hat{R}_h(T)}{N_h} + \frac{N_v}{N_h} \frac{\hat{R}_v(T)}{N_v} \right| \right)^{k_3} \right. \\ &\quad \left. \left(\gamma \sqrt{\frac{N_v}{N_h}} \frac{\left| \hat{R}_{hv}(0) \right|}{\sqrt{N_h N_v}} \right)^{k_4} \right\}. \end{aligned} \quad (5.23)$$

Note that if we have moments evaluated for unit N_h power and the ratio N_v/N_h , we can scale the moments to any power value in the H channel as long as the ratio N_v/N_h remains the same. Similarly, the threshold found for the unity power can be scaled to fit any power in H channel (as long as the ratio N_v/N_h is similar) by simply multiplying it by the measured N_h .

Now, how can one select a proper model for the fitting algorithm? In order to address the question, the histograms of the uniform sum are shown in Figure 5.1 for both cases of noise and signal+noise.

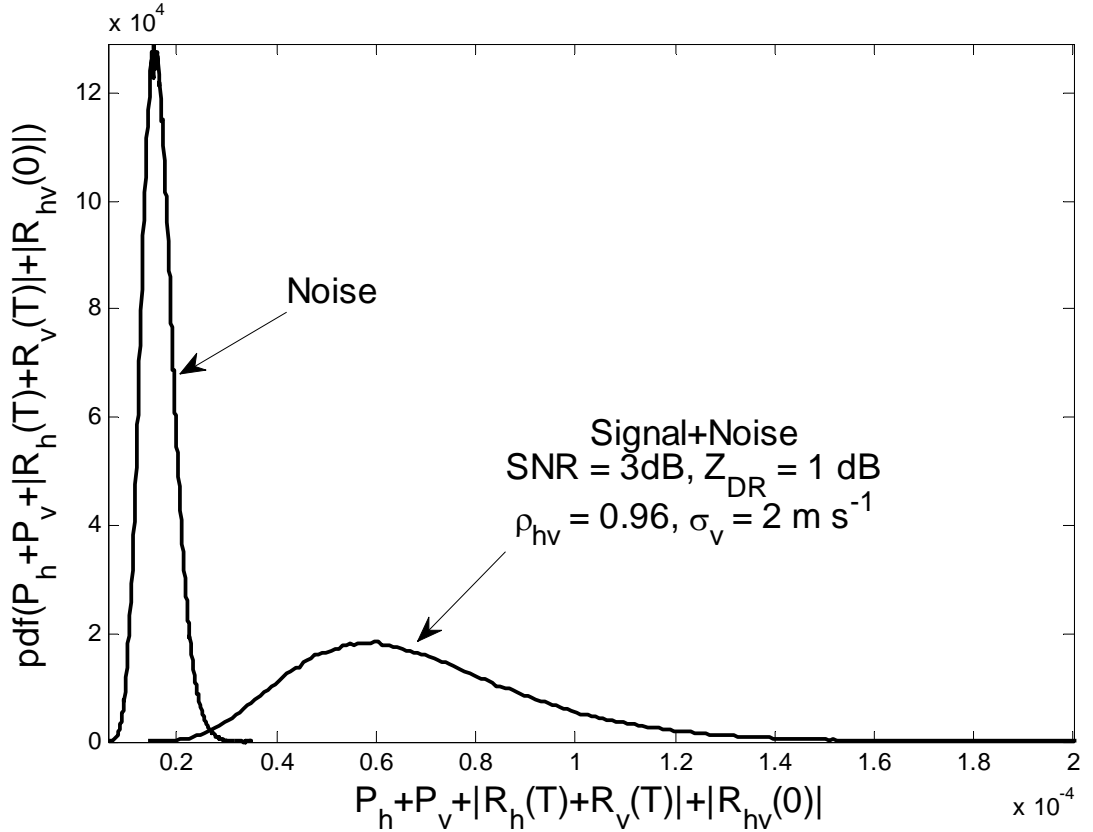


Figure 5.1 Histogram of the uniform sum *pdf* for noise only case and signal+noise.

There are several known distributions that follow the shapes similar to the ones given in Figure 5.1. The best known among those is gamma distribution which is defined as:

$$f(x) = \begin{cases} \frac{x^\alpha e^{-x/\theta}}{\theta^{\alpha+1} \Gamma(\alpha+1)} & \text{if } x > 0 \\ 0 & \text{if } x < 0 \end{cases} \quad (5.24)$$

It is known that the mean and the variance of the distribution are:

$$\begin{aligned} m &= (\alpha+1)\theta \\ \sigma^2 &= (\alpha+1)\theta^2. \end{aligned} \quad (5.25)$$

In addition, the parameters α and θ can be presented in terms of m and σ^2 as:

$$\begin{aligned} \alpha + 1 &= m^2 / \sigma^2 \\ \theta &= \sigma^2 / m. \end{aligned} \quad (5.26)$$

In other words, the gamma distribution function is determined by the first two moments. Therefore, the fitting using the gamma distribution function is performed by only fitting the first two moments. However, this approach does not guarantee matching of any moments higher than the second. If matching to higher moments is desired, the procedure of error correction (Papoulis and Pillai 2002) can be applied. It uses polynomials orthogonal with respect to the probability function⁽⁴⁾ to correct its n -th moment. In case of gamma distribution, there is a family of polynomials that are orthogonal with respect to it. These are known as Laguerre polynomials. A more detailed description is given in Appendix B. Intuitively, polynomial moment correction can be perceived graphically as slightly changing the shape of the gamma distribution function so it better matches the shape of the *pdf* that is being modeled. Thus, it should work fine as long as the shape of the distribution being modeled is reasonably similar to the gamma distribution. In many cases, though, even after setting the first two moments of the gamma distribution to those of the unknown *pdf*, the shape of the gamma distribution is so dissimilar from the target one that even the polynomial moment matching is unable to tweak it into the desired shape. In such cases, it is desirable to find a more general model which is flexible enough to accommodate various distribution shapes more closely. Such a model is likely to have more degrees of freedom so higher moments can be matched. Therefore, a generalized gamma distribution (Stacy 1962) is proposed, which accommodates for matching up to the third moment. This model function is listed below:

⁴ Two polynomials p_0 and p_1 are orthogonal with respect to a function $w(x)$ if $\int_0^{\infty} p_0 \cdot p_1 \cdot w(x) dx = 0$.

$$f(x) = \begin{cases} \frac{x^{p-1} e^{-\left(\frac{x}{a}\right)^{\frac{1}{q}}}}{qa^p \Gamma(qp)} & \text{if } x \geq 0 \\ 0 & \text{if } x < 0. \end{cases} \quad (5.27)$$

The n -th moment of the distribution is given by:

$$m_n = \frac{1}{qa^p \Gamma(qp)} \int_0^{\infty} x^{p+n-1} e^{-\left(\frac{x}{a}\right)^{\frac{1}{q}}} dx = a^n \frac{\Gamma(qp + qn)}{\Gamma(qp)}. \quad (5.28)$$

Let's assume the values of the first three moments as m_1 , m_2 , and m_3 are known. The problem becomes how to find values of a , q , and p so that:

$$\begin{aligned} m_1 &= a \frac{\Gamma(qp + q)}{\Gamma(qp)}, \\ m_2 &= a^2 \frac{\Gamma(qp + 2q)}{\Gamma(qp)}, \\ m_3 &= a^3 \frac{\Gamma(qp + 3q)}{\Gamma(qp)}. \end{aligned} \quad (5.29)$$

This is a non-linear system of three equations with three unknowns, and clearly a closed-form solution for an arbitrary values of a , q , and p cannot be obtained. Therefore, an iterative numerical method is used, which is described now.

Let us consider the case when q is a positive integer. Then we have:

$$\begin{aligned} m_1 &= a \prod_{i=0}^{q-1} (qp + i), \\ m_2 &= a^2 \prod_{i=0}^{2q-1} (qp + i), \\ m_3 &= a^3 \prod_{i=0}^{3q-1} (qp + i). \end{aligned} \quad (5.30)$$

Apparently, when q is an integer this new system of equations may not have the solution that will match all three moments. Instead, it is possible to find a and p for a given integer

q so the first two moments are matched. This can be achieved using the following equation

$$\prod_{i=0}^{q-1} (qp+i)m_2 = m_1^2 \prod_{i=q}^{2q-1} (qp+i) \Leftrightarrow m_1^2 \prod_{i=q}^{2q-1} (qp+i) - \prod_{i=0}^{q-1} (qp+i)m_2 = 0. \quad (5.31)$$

Then, possible solutions for p are the zeroes of the polynomial. We choose only positive real zeroes and discard the complex conjugate and negative ones. For each real p the corresponding a can be found as:

$$a = \frac{m_1}{\prod_{i=0}^{q-1} (qp+i)}. \quad (5.32)$$

Each pair (p,a) produces the corresponding third moment that is different from the desired value of m_3 . We select that pair (p,a) which yields the third moment closest to the desired value of m_3 . This can be performed over an arbitrary number of integer values of q until the third moment closest to m_3 is obtained. Subsequently, the q value can be fine tuned by varying it by some small amount. After this change q is not an integer any more. Therefore, the Newton's iterative method (Ypma 1995) is applied to solve for a and p . In this method, an initial guess, reasonably close to the true root, is selected. Then, the function is approximated by its tangent line (which can be computed using the tools of calculus), and one computes the x -intercept of this tangent line (which is easily done with elementary algebra). This x -intercept will typically be a better approximation to the function's root than the original guess, and the method can be iterated. An update formula is:

$$p_{n+1} = p_n - \frac{f(p_n)}{f'(p_n)}. \quad (5.33)$$

To apply Newton's method we setup the following:

$$m_1^2 \frac{\Gamma(qp+2q)}{\Gamma^2(qp+q)} \Gamma(qp) - m_2 = 0. \quad (5.34)$$

Hence:

$$f(p_n) = m_1^2 \frac{\Gamma(qp_n+2q)}{\Gamma^2(qp_n+q)} \Gamma(qp_n) - m_2. \quad (5.35)$$

We now find the derivative:

$$\begin{aligned} \frac{df(p_n)}{dp_n} &= m_1^2 \frac{\Gamma'(qp_n+2q)\Gamma(qp_n) + \Gamma(qp_n+2q)\Gamma'(qp_n)}{\Gamma^2(qp_n+q)} - \\ &\quad 2m_1^2 \frac{\Gamma(qp_n+2q)\Gamma(qp_n)}{\Gamma^3(qp_n+q)} \Gamma'(qp_n+q) \\ &= m_1^2 \frac{\psi(qp_n+2q)\Gamma(qp_n+2q)\Gamma(qp_n) + \Gamma(qp_n+2q)\psi(qp_n)\Gamma(qp_n)}{\Gamma^2(qp_n+q)} q - \\ &\quad 2m_1^2 \frac{\Gamma(qp_n+2q)\Gamma(qp_n)}{\Gamma^2(qp_n+q)} \psi(qp_n+q) q \\ &= m_1^2 q \Gamma(qp_n+2q)\Gamma(qp_n) \frac{\psi(qp_n+2q) + \psi(qp_n) - 2\psi(qp_n+q)}{\Gamma^2(qp_n+q)}, \end{aligned} \quad (5.36)$$

where ψ is digamma function (Abramowitz and Stegun 1964). We now devise an algorithm to fine tune q after the integer value of q , that yields the third moment closest to m_3 , is obtained.

(1) Set the desired errors $\varepsilon m_2 = |m_2'/m_2 - 1|$ and $\varepsilon m_3 = |m_3'/m_3 - 1|$, where m_2' and m_3' are the second and third moments obtained from the (a,p) pair at the end of iteration process. Set the initial value for p_0 to be the value obtained from the chosen integer value of q_0 . Then we need to decide on the initial step for q (i.e., Δq). We choose:

$$\text{if} \left(m_3 - a^3 \prod_{i=0}^{3q-1} (qp+i) \right) > 0 \quad \Delta q = 0.1 \quad \text{else} \quad \Delta q = -0.1, \quad (5.37)$$

where q is an integer value that yields the third moment closest to the true one, and a, p are the corresponding values. Set $n = 0$ and $p_n = p$.

(2) Update $q_{n+1} = q_n + \Delta q$

(3) Set $pp_0 = p_n, k = 0$.

(4) Start Newton's iteration:

$$pp_{k+1} = pp_k - \frac{m_1^2 T_k - m_2}{m_1^2 q_{n+1} T_k (\psi(q_{n+1} pp_k + 2q_{n+1}) + \psi(q_{n+1} pp_k) - 2\psi(q_{n+1} pp_k + q_{n+1}))}, \quad (5.38)$$

$$\text{where } T_k = \frac{\Gamma(q_{n+1} pp_k + 2q_{n+1}) \Gamma(q_{n+1} pp_k)}{\Gamma^2(q_{n+1} pp_k + q_{n+1})}.$$

Note: In cases when argument is too large (e.g., in excess of 200) gamma function may overflow and yield ∞ as output. To avoid this T_k can be calculated using formula (3) in Raff (1970).

(5) if $\left| \frac{m_1^2}{m_2} \frac{\Gamma(q_{n+1} pp_{k+1} + 2q_{n+1})}{\Gamma^2(q_{n+1} p_{k+1} + q_{n+1})} \Gamma(q_{n+1} pp_{k+1}) - 1 \right| < \epsilon m_2$ go to step 6, otherwise set $k = k$

+ 1 and go back to step 4.

(6) Set $p_{n+1} = pp_{k+1}$, set $m_3' = m_1^3 \Gamma^2(q_{n+1} p_{n+1}) \Gamma(q_{n+1} p_{n+1} + 3q_{n+1}) / \Gamma^3(q_{n+1} p_{n+1} + q_{n+1})$.

If $|m_3' / m_3 - 1| < \epsilon m_3$ go to step 7. If $\text{sgn}(m_3 - m_3') \neq \text{sgn}(\Delta q)$ set $q_n = q_n - \Delta q, \Delta q = \Delta q / 10$, else $n = n + 1$. Go to step 2.

(7) Set $q = q_{n+1}, p = p_{n+1}, a = m_1 \Gamma(qp_n) / \Gamma(qp_n + q)$.

This process is terminated when the result matches the third moment up to the desired accuracy. Once the first three moments are matched, the PFA approximation can be determined using

$$PFA \approx \frac{1}{qa^p \Gamma(qp)} \int_{THR}^{\infty} x^{p-1} e^{-\left(\frac{x}{a}\right)^q} dx = \Gamma_{inc} \left(\left(\frac{THR}{a} \right)^{\frac{1}{q}}, qp \right), \quad (5.39)$$

where $\Gamma_{inc}(x, \alpha)$ is an incomplete gamma function that is defined in Appendix A.

If matching to moments higher than the third order is desired, one needs to consider the polynomial moment matching. In the case of generalized gamma distribution, there is no family of polynomials that are orthogonal with respect to it. Nevertheless, it is still possible to perform the moment matching but each polynomial must be algebraically obtained. A general process is presented next.

It is known that any orthogonal sequence has a recurrence formula that relates any three consecutive polynomials in the following form:

$$p_{n+1} = (x - b_{n+1}) p_n - c_{n+1} p_{n-1}, \quad (5.40)$$

where b_n and c_n are some constants and p 's are polynomials defined by:

$$p_n = x^n + \sum_{i=0}^{n-1} k_{n,i} x^i \quad k_{n,i} \in \mathbb{R}. \quad (5.41)$$

Thus, if we know two polynomials in a row, we can calculate the third in a row. In order to describe the procedure for calculating p_{n+1} we shall use the inner product

$$\langle f(x), g(x) \rangle = \int_0^{\infty} f(x) g(x) w(x) dx, \quad (5.42)$$

where $f(x)$, $g(x)$ are some arbitrary functions and $w(x)$ is a weight function. If we are dealing with polynomials orthogonal with respect to some function, we take $w(x)$ to be exactly it. Hence, the approach is general. In this particular case, the choice of function is generalized gamma distribution. Now we can establish formulas based on the fact that p_{n+1} is orthogonal to both p_n and p_{n-1} . This gives us:

$$\begin{aligned}\langle p_{n+1}, p_n \rangle = 0 &\Leftrightarrow \langle xp_n, p_n \rangle - b_{n+1} \langle p_n, p_n \rangle = 0 \Rightarrow b_{n+1} = \frac{\langle xp_n, p_n \rangle}{\langle p_n, p_n \rangle}, \\ \langle p_{n+1}, p_{n-1} \rangle = 0 &\Leftrightarrow \langle xp_n, p_{n-1} \rangle - c_{n+1} \langle p_{n-1}, p_{n-1} \rangle = 0 \Rightarrow c_{n+1} = \frac{\langle xp_n, p_{n-1} \rangle}{\langle p_{n-1}, p_{n-1} \rangle}.\end{aligned}\tag{5.43}$$

The next step is to choose the first two polynomials. It is common that we choose the zeroth polynomial to be unity. As for the first one we choose it as:

$$p_1 = (x - b_0) p_0 \wedge \langle p_1, p_0 \rangle = 0 \Rightarrow b_0 = \frac{\langle xp_0, p_0 \rangle}{\langle p_0, p_0 \rangle} = \int_0^\infty xw(x) dx = m_1,$$
(5.44)

where m_1 is the first moment. For the first two moments we now have:

$$\begin{aligned}p_0 &= 1, \\ p_1 &= x - m_1.\end{aligned}\tag{5.45}$$

Once we have all polynomials, perform correction as:

$$pdf(x) \approx w(x) \left(1 + \sum_{n=i}^j C_n p_n \right),$$
(5.46)

where i and j are the first and the last moment that we want to correct for, respectively.

The next step is to find coefficient C_n values. Let us find C_k ($k \in [i, j]$) using

$$m_k = \int_0^\infty x^k w(x) \left(1 + \sum_{n=i}^j C_n p_n \right) dx = \left\langle x^k, 1 + \sum_{n=i}^j C_n p_n \right\rangle.$$
(5.47)

It is apparent that x^k can be written as a linear combination of polynomials up to and including the k -th polynomial as:

$$x^k = \sum_{n=0}^k A_n p_n.$$
(5.48)

Then we can write:

$$\left\langle x^k, \sum_{n=i}^j C_n p_n \right\rangle = \left\langle \sum_{l=0}^k A_l p_l, \sum_{n=i}^j C_n p_n \right\rangle.$$
(5.49)

Due to the orthogonality of polynomials we have:

$$\left\langle x^k, \sum_{n=i}^j C_n p_n \right\rangle = \left\langle \sum_{l=0}^k A_l p_l, \sum_{n=i}^k C_n p_n \right\rangle = \left\langle x^k, \sum_{n=i}^k C_n p_n \right\rangle = \sum_{n=i}^k C_n \langle x^k, p_n \rangle. \quad (5.50)$$

This results in:

$$m_k = \int_0^{\infty} x^k w(x) dx + \sum_{n=i}^k C_n \langle x^k, p_n \rangle. \quad (5.51)$$

Thus, assuming coefficients up to the $(k-1)$ -st have been calculated, we have:

$$C_k = \frac{m_k - \int_0^{\infty} x^k w(x) dx - \sum_{n=i}^{k-1} C_n \langle x^k, p_n \rangle}{\langle x^k, p_k \rangle}. \quad (5.52)$$

After we have a *pdf* approximation corrected up to the j -th moment, we can obtain PFA approximation using

$$PFA \approx \int_{THR}^{\infty} w(x) \left(1 + \sum_{n=i}^j C_n p_n \right) dx. \quad (5.53)$$

In case of a generalized gamma distribution and a correction up to the 4-th moment:

$$\begin{aligned} PFA &\approx \frac{1}{qa^p \Gamma(qp)} \int_{THR}^{\infty} x^{p-1} e^{-\left(\frac{x}{a}\right)^q} \left(1 + C_4 \sum_{n=0}^4 z_n x^n \right) dx \\ &\approx \Gamma_{inc} \left(\left(\frac{THR}{a} \right)^{\frac{1}{q}}, qp \right) + C_4 \sum_{n=0}^4 z_n \Gamma_{inc} \left(\left(\frac{THR}{a} \right)^{\frac{1}{q}}, q(p+n) \right), \end{aligned} \quad (5.54)$$

where z_n are the coefficients of the polynomial p_4 . Having the tools presented so far, we now turn to methods for evaluating noise moments.

5.3 Evaluation of Moments for Noise

In the previous chapter it was shown that the unknown *pdf* can be approximated by its first few moments. The accuracy of the approximation depends on the number of moments used, the moment accuracy, as well as the degree of similarity between the

model function and the unknown *pdf* (i.e., the one being modeled). This is important for PFA calculation because we are trying to determine the area below the *pdf* curve at the tail. Nonetheless, if the model for fitting is not appropriate, the approximation can be significantly biased even if the moments are evaluated with high accuracy. Because the weighted sum is a function of random variables, the n -th moment is defined as in (5.22). Certainly, the n -th moment can be estimated from simulated data as:

$$\hat{m}_n = \frac{1}{K} \sum_{k=0}^{K-1} \left(\hat{P}_h^{(k)} + \alpha \hat{P}_v^{(k)} + \beta \left| \hat{R}_h^{(k)}(T) + \hat{R}_v^{(k)}(T) \right| + \gamma \left| \hat{R}_{hv}^{(k)}(0) \right| \right)^n, \quad (5.55)$$

where k is the trial number, and K is the total number of trials. To validate the moment estimator, we examine its *bias* and *consistency*. Mathematical expectation of the moment estimator is

$$\begin{aligned} E\{\hat{m}_n\} &= \frac{1}{K} \sum_{k=0}^{K-1} E \left\{ \left(\hat{P}_h^{(k)} + \alpha \hat{P}_v^{(k)} + \beta \left| \hat{R}_h^{(k)}(T) + \hat{R}_v^{(k)}(T) \right| + \gamma \left| \hat{R}_{hv}^{(k)}(0) \right| \right)^n \right\} \\ &= E \left\{ \left(\hat{P}_h + \alpha \hat{P}_v + \beta \left| \hat{R}_h(T) + \hat{R}_v(T) \right| + \gamma \left| \hat{R}_{hv}(0) \right| \right)^n \right\} \\ &= m_n. \end{aligned} \quad (5.56)$$

Equation (5.56) shows that the moment estimator is *unbiased*. In addition, the variance of the estimator can be written in the following form

$$\begin{aligned} Var\{\hat{m}_n\} &= E\{\hat{m}_n^2\} - E^2\{\hat{m}_n\} \\ &= E \left\{ \frac{1}{K} \sum_{k=0}^{K-1} \left(\hat{P}_h^{(k)} + \alpha \hat{P}_v^{(k)} + \beta \left| \hat{R}_h^{(k)}(T) + \hat{R}_v^{(k)}(T) \right| + \gamma \left| \hat{R}_{hv}^{(k)}(0) \right| \right)^n \times \right. \\ &\quad \left. \frac{1}{K} \sum_{l=0}^{K-1} \left(\hat{P}_h^{(l)} + \alpha \hat{P}_v^{(l)} + \beta \left| \hat{R}_h^{(l)}(T) + \hat{R}_v^{(l)}(T) \right| + \gamma \left| \hat{R}_{hv}^{(l)}(0) \right| \right)^n \right\} - \\ &\quad E^2 \left\{ \left(\hat{P}_h + \alpha \hat{P}_v + \beta \left| \hat{R}_h(T) + \hat{R}_v(T) \right| + \gamma \left| \hat{R}_{hv}(0) \right| \right)^n \right\}. \end{aligned} \quad (5.57)$$

Because all trials are independent we have:

$$\begin{aligned}
E\{\hat{m}_n^2\} &= \frac{1}{K^2} \sum_{k=0}^{K-1} E \left\{ \left[\left(\hat{P}_h^{(k)} + \alpha \hat{P}_v^{(k)} + \beta \left| \hat{R}_h^{(k)}(T) + \hat{R}_v^{(k)}(T) \right| + \gamma \left| \hat{R}_{hv}^{(k)}(0) \right| \right)^n \right]^2 \right\} + \\
&\quad \frac{1}{K^2} \sum_{\substack{k,l \\ k \neq l}}^{K-1} E \left\{ \left(\hat{P}_h^{(k)} + \alpha \hat{P}_v^{(k)} + \beta \left| \hat{R}_h^{(k)}(T) + \hat{R}_v^{(k)}(T) \right| + \gamma \left| \hat{R}_{hv}^{(k)}(0) \right| \right)^n \times \right. \\
&\quad \left. E \left\{ \left(\hat{P}_h^{(l)} + \alpha \hat{P}_v^{(l)} + \beta \left| \hat{R}_h^{(l)}(T) + \hat{R}_v^{(l)}(T) \right| + \gamma \left| \hat{R}_{hv}^{(l)}(0) \right| \right)^n \right\} \right\} \\
&= \frac{1}{K} E\{m_n^2\} + \frac{K-1}{K} E^2\{m_n\}.
\end{aligned} \tag{5.58}$$

Finally:

$$\lim_{K \rightarrow \infty} \text{Var}\{\hat{m}_n^2\} = \lim_{K \rightarrow \infty} \frac{1}{K} \left(E\{m_n^2\} - E^2\{m_n\} \right) = \lim_{K \rightarrow \infty} \frac{\text{Var}\{m_n\}}{K} = 0. \tag{5.59}$$

Hence, the moment estimator (5.55) is *consistent*.

Recall that the plain Monte Carlo requires a large number of iterations for estimating moments in order to achieve high accuracy. Moreover, fitting *pdf* to model functions does not lend itself to a reliable variance analysis (like the one given in Chapter 2) and offers no guarantee that the result will be unbiased. Regardless of these drawbacks, this approach still has the potential to provide an approximation that is reasonably close to the true result. More importantly, as shown at the beginning of Chapter 5, the results of moment evaluation apply to a wide range of power values in H and V channels, as well as various weights. However, to achieve this, a moment needs to be broken into terms as given by the multinomial theorem (eq. (5.23)). Then, once evaluated, each term can be re-used with different powers and weights. In addition, some of the terms in the above sum can be evaluated analytically, while others need to be estimated. Because we are using this approach for the noise case, we can concentrate on moment evaluation in such case only.

We shall analyze each moment separately, starting with the first one. It is given by

$$m_1 = E\{\hat{P}_h\} + \alpha E\{\hat{P}_v\} + \beta E\left\{\left|\hat{R}_h(T) + \hat{R}_v(T)\right|\right\} + \gamma E\left\{\left|\hat{R}_{hv}(0)\right|\right\}. \quad (5.60)$$

Obviously, the first two terms of expected values are the noise powers in the horizontal and vertical channels respectively. The third expected value cannot be determined analytically and must be estimated. Finally, the last term can be calculated using formula (E.4) given in Appendix E.

The second moment is represented by the following formula

$$\begin{aligned} m_2 &= \sum_{k_1, k_2, k_3, k_4} \frac{2}{k_1! k_2! k_3! k_4!} E\left\{\hat{P}_h^{k_1} (\alpha \hat{P}_v)^{k_2} \left(\beta \left|\hat{R}_h(T) + \hat{R}_v(T)\right|\right)^{k_3} \left(\gamma \left|\hat{R}_{hv}(0)\right|\right)^{k_4}\right\} \\ &= E\left\{\hat{P}_h^2 + \alpha^2 \hat{P}_v^2 + \beta^2 \left|\hat{R}_h(T) + \hat{R}_v(T)\right|^2 + \gamma^2 \left|\hat{R}_{hv}(0)\right|^2 + 2\left(\alpha \hat{P}_h \hat{P}_v\right.\right. \\ &\quad \left.\left.+ \beta \hat{P}_h \left|\hat{R}_h(T) + \hat{R}_v(T)\right| + \gamma \hat{P}_h \left|\hat{R}_{hv}(0)\right| + \alpha \beta \hat{P}_v \left|\hat{R}_h(T) + \hat{R}_v(T)\right| +\right. \\ &\quad \left.\alpha \gamma \hat{P}_v \left|\hat{R}_{hv}(0)\right| + \beta \gamma \left|\hat{R}_h(T) + \hat{R}_v(T)\right| \left|\hat{R}_{hv}(0)\right|\right\}. \end{aligned} \quad (5.61)$$

Terms $E\{\hat{P}_h^2\}$, $E\{\hat{P}_v^2\}$, and $E\left\{\left|\hat{R}_{hv}(0)\right|^2\right\}$ can be determined using formulas given in Appendix A, and E, while $E\{\hat{P}_h \hat{P}_v\} = N_h N_v$. The second term can be calculated as given in Appendix F as

$$E\left\{\left|\hat{R}_h(T) + \hat{R}_v(T)\right|^2\right\} = \frac{N_h^2 + N_v^2}{M-1}. \quad (5.62)$$

The rest of the terms are to be estimated. The estimator of the second moment is now

$$\begin{aligned} \hat{m}_2 &= \left(\frac{M+1}{M} + \frac{\beta^2}{M-1}\right) N_h^2 + \left(\alpha^2 \frac{M+1}{M} + \frac{\beta^2}{M-1}\right) N_v^2 + \left(2\alpha + \frac{\gamma^2}{M}\right) N_h N_v + \\ &\quad \frac{2}{K} \sum_{k=0}^{K-1} \left(\beta \hat{P}_h^{(k)} \left|\hat{R}_h^{(k)}(T) + \hat{R}_v^{(k)}(T)\right| + \gamma \hat{P}_h^{(k)} \left|\hat{R}_{hv}^{(k)}(0)\right| + \alpha \beta \hat{P}_v^{(k)} \left|\hat{R}_h^{(k)}(T) + \hat{R}_v^{(k)}(T)\right| + \right. \\ &\quad \left. \alpha \gamma \hat{P}_v^{(k)} \left|\hat{R}_{hv}^{(k)}(0)\right| + \beta \gamma \left|\hat{R}_h^{(k)}(T) + \hat{R}_v^{(k)}(T)\right| \left|\hat{R}_{hv}^{(k)}(0)\right|\right). \end{aligned} \quad (5.63)$$

The third moment is expressed as:

$$\begin{aligned}
m_3 &= \sum_{k_1, k_2, k_3, k_4} \frac{6}{k_1! k_2! k_3! k_4!} E \left\{ \hat{P}_h^{k_1} (\alpha \hat{P}_v)^{k_2} \left(\beta \left| \hat{R}_h(T) + \hat{R}_v(T) \right| \right)^{k_3} \left(\gamma \left| \hat{R}_{hv}(0) \right| \right)^{k_4} \right\} \\
&= E \left\{ \hat{P}_h^3 + \alpha^3 \hat{P}_v^3 + \beta^3 \left| \hat{R}_h(T) + \hat{R}_v(T) \right|^3 + \gamma^3 \left| \hat{R}_{hv}(0) \right|^3 + 3 \left(\alpha \hat{P}_h^2 \hat{P}_v + \alpha^2 \hat{P}_h \hat{P}_v^2 + \right. \right. \\
&\quad \left. \beta \hat{P}_h^2 \left| \hat{R}_h(T) + \hat{R}_v(T) \right| + \beta^2 \hat{P}_h \left| \hat{R}_h(T) + \hat{R}_v(T) \right|^2 + \gamma \hat{P}_h^2 \left| \hat{R}_{hv}(0) \right| + \right. \\
&\quad \left. \gamma^2 \hat{P}_h \left| \hat{R}_{hv}(0) \right|^2 + \alpha^2 \beta \hat{P}_v^2 \left| \hat{R}_h(T) + \hat{R}_v(T) \right| + \alpha \beta^2 \hat{P}_v \left| \hat{R}_h(T) + \hat{R}_v(T) \right|^2 + \right. \\
&\quad \left. \alpha^2 \gamma \hat{P}_v^2 \left| \hat{R}_{hv}(0) \right| + \alpha \gamma^2 \hat{P}_v \left| \hat{R}_{hv}(0) \right|^2 + \beta^2 \gamma \left| \hat{R}_h(T) + \hat{R}_v(T) \right|^2 \left| \hat{R}_{hv}(0) \right| + \right. \\
&\quad \left. \beta \gamma^2 \left| \hat{R}_h(T) + \hat{R}_v(T) \right| \left| \hat{R}_{hv}(0) \right|^2 \right) + 6 \left(\alpha \beta \hat{P}_h \hat{P}_v \left| \hat{R}_h(T) + \hat{R}_v(T) \right| + \alpha \gamma \hat{P}_h \hat{P}_v \left| \hat{R}_{hv}(0) \right| + \right. \\
&\quad \left. \beta \gamma \hat{P}_h \left| \hat{R}_h(T) + \hat{R}_v(T) \right| \left| \hat{R}_{hv}(0) \right| + \alpha \beta \gamma \hat{P}_v \left| \hat{R}_h(T) + \hat{R}_v(T) \right| \left| \hat{R}_{hv}(0) \right| \right) \left. \right\}. \tag{5.64}
\end{aligned}$$

\hat{P}_h^n and \hat{P}_v^k	Appendix A
$\left \hat{R}_{hv}(0) \right ^{2m}$	Appendix E
$\left \hat{R}_h(T) + \hat{R}_v(T) \right ^{2l}$	Appendix F
$\hat{P}_h^n \hat{P}_v^k \left \hat{R}_{hv}(0) \right ^{2m}$	Appendix G
$\hat{P}_h^n \hat{P}_v^k \left \hat{R}_h(T) + \hat{R}_v(T) \right ^{2l}$	Appendix H

Table 5.1 The table relating appendices to moment approximations for some forms.

The terms which can be evaluated analytically are of the form $\hat{P}_h^n \hat{P}_v^k \left| \hat{R}_h(T) + \hat{R}_v(T) \right|^{2l} \left| \hat{R}_{hv}(0) \right|^{2m}$ where $n, k, l, m \in \{0, 1, \dots\}$. The formulas for these are derived in Appendices. The Table 5.1 relates several forms to the appendices in which their expected values are derived. The third moment can now be evaluated using the following form

$$\begin{aligned}
\hat{m}_3 = & \frac{(M+1)(M+2)}{M^2} (N_h^3 + \alpha^3 N_v^3) + 3 \left(\frac{M+1}{M} (\alpha N_h^2 N_v + \alpha^2 N_h N_v^2) + \right. \\
& \beta^2 \left(\frac{(M+2)(M+3)}{M(M-1)} N_h^3 + \frac{1}{M-1} N_h N_v^2 \right) + \gamma^2 \frac{M+1}{M^2} N_v N_h^2 + \\
& \alpha \beta^2 \left(\frac{(M+2)(M+3)}{M(M-1)} N_v^3 + \frac{1}{M-1} N_v N_h^2 \right) + \alpha \gamma^2 \frac{M+1}{M^2} N_h N_v^2 + \\
& \frac{1}{K} \sum_{k=0}^{K-1} \left(\beta^3 \left| \hat{R}_h^{(k)}(T) + \hat{R}_v^{(k)}(T) \right|^3 + \gamma^3 \left| \hat{R}_{hv}^{(k)}(0) \right|^3 + 3 \left(\beta \left(\hat{P}_h^{(k)} \right)^2 \left| \hat{R}_h^{(k)}(T) + \hat{R}_v^{(k)}(T) \right| + \right. \\
& \gamma \hat{P}_h^2 \left| \hat{R}_{hv}^{(k)}(0) \right| + \alpha^2 \beta \hat{P}_v^2 \left| \hat{R}_h^{(k)}(T) + \hat{R}_v^{(k)}(T) \right| + \alpha^2 \gamma \hat{P}_v^2 \left| \hat{R}_{hv}^{(k)}(0) \right| + \\
& \beta^2 \gamma \left| \hat{R}_h^{(k)}(T) + \hat{R}_v^{(k)}(T) \right|^2 \left| \hat{R}_{hv}^{(k)}(0) \right| + \beta \gamma^2 \left| \hat{R}_h^{(k)}(T) + \hat{R}_v^{(k)}(T) \right| \left| \hat{R}_{hv}^{(k)}(0) \right|^2 \left. \right) + \\
& 6 \left(\alpha \beta \hat{P}_h \hat{P}_v \left| \hat{R}_h^{(k)}(T) + \hat{R}_v^{(k)}(T) \right| + \alpha \gamma \hat{P}_h \hat{P}_v \left| \hat{R}_{hv}^{(k)}(0) \right| + \right. \\
& \left. \beta \gamma \hat{P}_h \left| \hat{R}_h^{(k)}(T) + \hat{R}_v^{(k)}(T) \right| \left| \hat{R}_{hv}^{(k)}(0) \right| + \alpha \beta \gamma \hat{P}_v \left| \hat{R}_h^{(k)}(T) + \hat{R}_v^{(k)}(T) \right| \left| \hat{R}_{hv}^{(k)}(0) \right| \right). \quad (5.65)
\end{aligned}$$

Thus, the terms in each of the three moments can be divided into the ones that can be expressed in a closed form and the ones that are estimated. It is possible to use the plain Monte Carlo to estimate these moments. Naturally, it is desirable that the moments are evaluated as accurately as possible. The use of the plain Monte Carlo, however, may require large number of trials to achieve this. Hence, the question now is whether we can improve the accuracy of moment estimates by using some types of the variance reduction techniques (Rubinstein 1981). In this particular case, the control variates technique has the potential to improve the estimates errors. The main idea is that one or more control variates can be employed to achieve variance reduction by exploiting the correlation among the control random variables and the one being estimated. The application of this technique is discussed in the next section.

5.4 Control Variates for Moment Estimation

The method of control variates can be used when a random vector $\mathbf{C} = (C_1, \dots, C_q)$ with a known mean vector $\boldsymbol{\mu}_C = (\mu_1, \dots, \mu_q)$ is correlated with the random variable X to be estimated. The vector of control variates \mathbf{C} can be used to construct an unbiased estimator of the mean value μ_X as:

$$\hat{\mu}_X(\boldsymbol{\beta}) = \frac{1}{K} \sum_{k=0}^{K-1} (X_k - \boldsymbol{\beta}^T (\mathbf{C}_k - \boldsymbol{\mu}_C)) = \bar{X} - \boldsymbol{\beta}^T (\bar{\mathbf{C}} - \boldsymbol{\mu}_C). \quad (5.66)$$

The variance of such estimator is:

$$\begin{aligned} \text{Var}(\hat{\mu}_X(\boldsymbol{\beta})) &= E \left\{ \left[\bar{X} - \boldsymbol{\beta}^T (\bar{\mathbf{C}} - \boldsymbol{\mu}_C) - \mu_X \right] \left[\bar{X} - \boldsymbol{\beta}^T (\bar{\mathbf{C}} - \boldsymbol{\mu}_C) - \mu_X \right]^T \right\} \\ &= E \left\{ (\bar{X} - \mu_X)^2 \right\} - E \left\{ (\bar{X} - \mu_X) (\bar{\mathbf{C}} - \boldsymbol{\mu}_C)^T \boldsymbol{\beta} \right\} - \\ &\quad E \left\{ (\bar{X} - \mu_X) \boldsymbol{\beta}^T (\bar{\mathbf{C}} - \boldsymbol{\mu}_C) \right\} + E \left\{ \boldsymbol{\beta}^T (\bar{\mathbf{C}} - \boldsymbol{\mu}_C) (\bar{\mathbf{C}} - \boldsymbol{\mu}_C)^T \boldsymbol{\beta} \right\}. \end{aligned} \quad (5.67)$$

Hence, to determine vector $\boldsymbol{\beta}$ that minimizes the variance we set up the following equation.

$$\begin{aligned} \frac{\partial \text{Var}(\hat{\mu}_X(\boldsymbol{\beta}))}{\partial \boldsymbol{\beta}} &= -2E \left\{ (\bar{X} - \mu_X) (\bar{\mathbf{C}} - \boldsymbol{\mu}_C) \right\} + 2E \left\{ (\bar{\mathbf{C}} - \boldsymbol{\mu}_C) (\bar{\mathbf{C}} - \boldsymbol{\mu}_C)^T \boldsymbol{\beta} \right\} \\ &= 0, \end{aligned} \quad (5.68)$$

which gives us:

$$\begin{aligned} \boldsymbol{\beta} &= E \left\{ (\bar{\mathbf{C}} - \boldsymbol{\mu}_C) (\bar{\mathbf{C}} - \boldsymbol{\mu}_C)^T \right\}^{-1} E \left\{ (\bar{X} - \mu_X) (\bar{\mathbf{C}} - \boldsymbol{\mu}_C) \right\} \\ &= \boldsymbol{\Sigma}_C^{-1} \boldsymbol{\sigma}_{XC}, \end{aligned} \quad (5.69)$$

where $\boldsymbol{\sigma}_{XC}$ is a q -dimensional vector whose components are the covariances between X and C_q 's and $\boldsymbol{\Sigma}_C^{-1}$ is the covariance matrix of \mathbf{C} . The resulting variance reduction of such estimator is

$$\frac{Var(\hat{\mu}_X(\boldsymbol{\beta}))}{Var(\hat{\mu}_X)} = 1 - \frac{\boldsymbol{\sigma}_{XC}^T \boldsymbol{\Sigma}_C^{-1} \boldsymbol{\sigma}_{XC}}{Var(\hat{\mu}_X)}. \quad (5.70)$$

Let's discuss how this approach can improve the moment estimates. Let us assume that a random variable P is the product of an arbitrary number of jointly normal random variables. The expected value of any such product can be evaluated in a closed form (Appendix C). Nonetheless, the mathematical expectation of P raised to the fractional power cannot be obtained analytically. Instead, P raised to an integer power is used as a control variate. For example, let the product to be estimated be $E\{P^{m/n}\}$, where m and n are relatively prime (i.e., their greatest common divisor is 1), and $m, n \in N$. Then, we can use P^k and P^l as control variates; as a result, we have $\mathbf{C} = (P^k, P^l)$, where $k \neq l$, and $k, l \in N$. Let us now examine the structure of the covariance vector $\boldsymbol{\sigma}_{XC}$ and matrix $\boldsymbol{\Sigma}_C^{-1}$, which are used to determine the vector $\boldsymbol{\beta}$. We have:

$$\boldsymbol{\sigma}_{PC} = \begin{bmatrix} E\{P^{k+m/n}\} - E\{P^{m/n}\}E\{P^k\} \\ E\{P^{l+m/n}\} - E\{P^{m/n}\}E\{P^l\} \end{bmatrix}, \quad (5.71)$$

$$\boldsymbol{\Sigma}_C^{-1} = \begin{bmatrix} E\{P^{2k}\} - E^2\{P^k\} & E\{P^{k+l}\} - E\{P^k\}E\{P^l\} \\ E\{P^{k+l}\} - E\{P^k\}E\{P^l\} & E\{P^{2l}\} - E^2\{P^l\} \end{bmatrix}.$$

It is apparent that the covariance matrix $\boldsymbol{\Sigma}_C^{-1}$ can be determined exactly, while the covariance vector $\boldsymbol{\sigma}_{XC}$ cannot, as it contains the very expression that we desire to estimate. Let us assume that we know the *pdf* of $X = P^n$ (i.e., $f_X(x)$). In such case we can obtain the *pdf* of $Y = P^{m/n}$ by taking the substitution $Y = X^{1/n}$:

$$P(a < Y < b) = P(a^n < X < b^n) = \int_{a^n}^{b^n} f_X(x) dx = \int_a^b ny^{n-1} f_X(y^n) dy. \quad (5.72)$$

Thus:

$$f_{P^{m/n}}(y) = ny^{n-1} f_{P^m}(y^n). \quad (5.73)$$

Now we can find any moment as:

$$E \left\{ P^{\frac{m}{n}k} \right\} = \int_0^{\infty} ny^{n-1+k} f_{P^m}(y^n) dy. \quad (5.74)$$

The problem is, of course, that we do not know the distribution of P^m . We can, however, approximate this distribution using the moment fitting as described previously, and obtain the following result

$$pdf(P^m) \approx w(y^n) \left(1 + \sum_{n=i}^j C_n p_n \right), \quad (5.75)$$

where p_n is a polynomial of y^n , and $w(y^n)$ is a weighting function which is in most cases the generalized gamma distribution function. This gives us an approximate formula:

$$E \left\{ P^{\frac{m}{n}k} \right\} \approx \int_0^{\infty} ny^{n-1+k} w(y^n) \left(1 + \sum_{n=i}^j C_n p_n \right) dy. \quad (5.76)$$

Using this formula we can obtain approximations of odd moments of P and use those to get vector σ_{XC} . Moreover, the formula can also be used for calculation of all moments, in which case it produces the exact values for even moments used for obtaining the formula. With these tools in hand, we obtain an accurate estimation of the terms in the moment expressions. Approximations are given in Appendices that are listed in Table 5.1. We proceed now with developing procedure for evaluation of the threshold for a given PFA.

5.5 Threshold Calculation

The threshold calculation is based on the *pdf* approximation by fitting moments to the generalized gamma distribution. Once the parameters of the functions are adjusted so the first three moments are matched, the threshold needs to be found such that:

$$PFA = \frac{1}{qa^p \Gamma(qp)} \int_{THR}^{\infty} x^{p-1} e^{-\left(\frac{x}{a}\right)^q} dx = \Gamma_{inc} \left(\left(\frac{THR}{a} \right)^{\frac{1}{q}}, qp \right). \quad (5.77)$$

Clearly, the *THR* value cannot be directly determined. Hence an iterative method is proposed. We start with an arbitrary *THR* value and decrease or increase it, in pre-determined steps, as long as the absolute difference between the obtained and the desired PFA is decreasing. Once the difference starts increasing, we deem to be close enough to the solution so we can continue using the Newton's method as:

$$THR(n+1) = THR(n) - \frac{\Gamma_{inc} \left(\left(\frac{THR(n)}{a} \right)^{\frac{1}{q}}, qp \right) - PFA_d}{\Gamma'_{inc} \left(\left(\frac{THR(n)}{a} \right)^{\frac{1}{q}}, qp \right)}. \quad (5.78)$$

The derivative in the denominator cannot be found using tables, hence we resort to the definition. It is

$$\Gamma'_{inc} \left(\left(\frac{THR(n)}{a} \right)^{\frac{1}{q}}, qp \right) = \lim_{\Delta \rightarrow 0} \frac{\Gamma_{inc} \left(\left(\frac{THR(n) + \Delta}{a} \right)^{\frac{1}{q}}, qp \right) - \Gamma_{inc} \left(\left(\frac{THR(n)}{a} \right)^{\frac{1}{q}}, qp \right)}{\Delta}. \quad (5.79)$$

The derivative is found by decreasing Δ until the limit expression reaches the desired accuracy.

After the threshold is obtained, the corresponding PFA is evaluated using the importance sampling technique. If the difference between the estimated value and the desired PFA is larger than a pre-determined accuracy, a correction is needed. The corrected threshold is obtained using the modified Newton's approach presented below

$$THR(n+1) = THR(n) - \frac{E\{f(WS_N) \geq THR(n)\} - PFA_d}{\Gamma'_{inc} \left(\left(\frac{THR(n)}{a} \right)^{\frac{1}{q}}, qp \right)}. \quad (5.80)$$

The term $E\{f(WS_N) \geq THR(n)\}$ is estimated using the CE technique, and the derivative in the denominator is calculated as given in (5.79). Apparently, the slope of a tangent at a given threshold value obtained from an approximation is assumed to be close to the tangent slope of the true *pdf*. This assumption may fail, however. The failure of the assumption is detected when

$$\frac{E\{f(WS_N) \geq THR(n)\} - PFA_d}{E\{f(WS_N) \geq THR(n-1)\} - PFA_d} < 0. \quad (5.81)$$

When this occurs, the new threshold is found using the straight line approximation as:

$$THR(n+1) = \frac{PFA_d - E\{f(WS_N) \geq THR(n)\}}{E\{f(WS_N) \geq THR(n)\} - E\{f(WS_N) \geq THR(n-1)\}} \times (THR(n) - THR(n-1)) + THR(n). \quad (5.82)$$

Several iterations may be needed to determine the threshold that produces the PFA with sufficient accuracy.

5.6 Assessment of Weight Optimization

The optimal weights, in the weighted sum, for given parameters of SNR , σ_v , Z_{DR} and ρ_{hv} are defined by those that maximize POD for a desired PFA. To illustrate how the

weighted sum behaves, weights α and β are ranged through a set of values while γ is kept constant. This allows for graphical representation as shown in Figure 5.2.

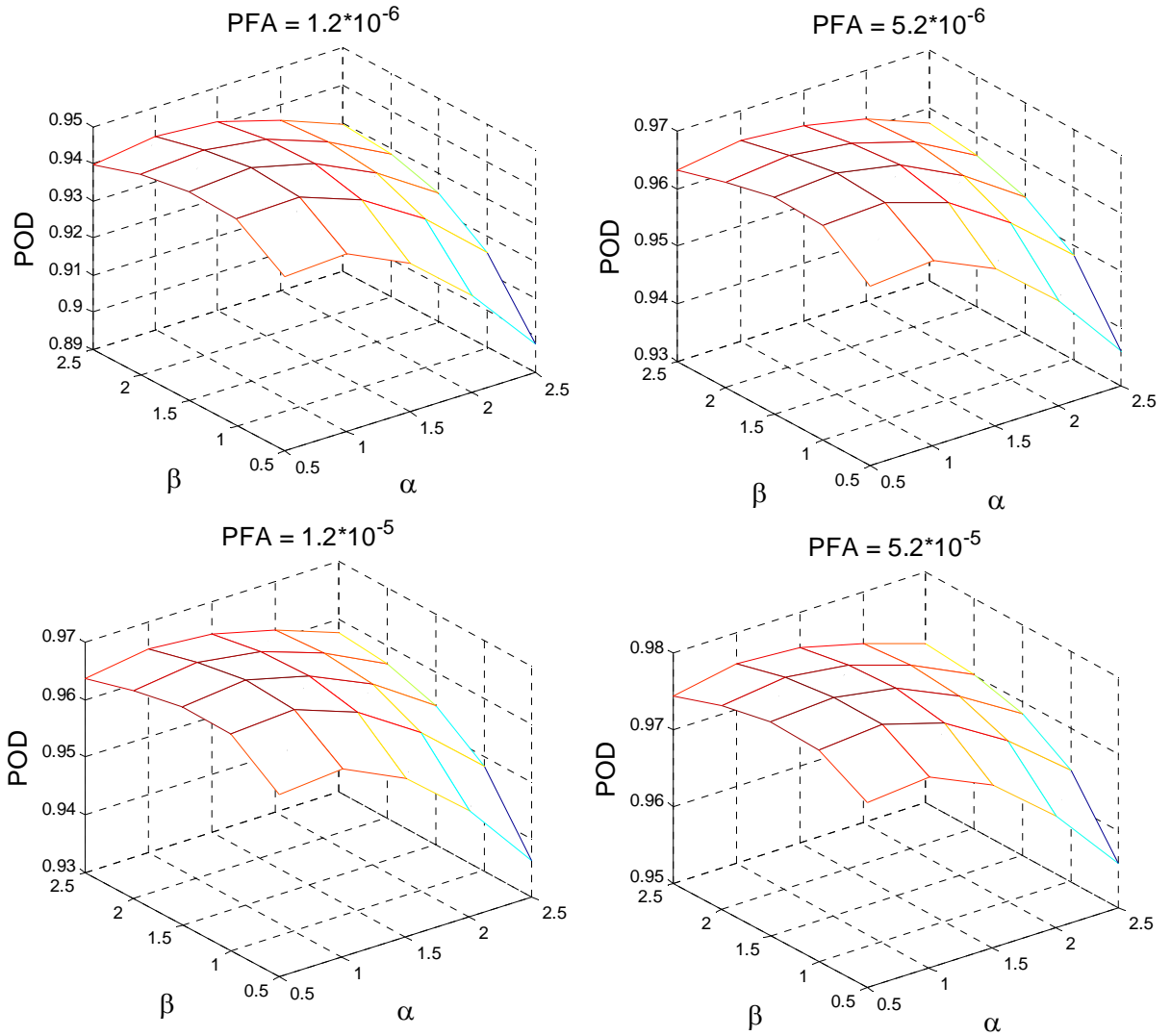


Figure 5.2 3-D representation of the POD vs. α and β for the following $\gamma = 2$, $SNR_h = 1.5$ dB, $\sigma_v = 2$ m s⁻¹, $Z_{DR} = 1$ dB, $\rho_{hv} = 0.96$, $M = 25$, and $N_v/N_h = 1$.

Note that in Figure 5.2 the results are almost the same for all PFAs, except that they are shifted in the POD value. Consequently, the maximum POD is achieved for the same weights in all four cases presented in Figure 5.2. This result indicates that for the given parameters, the combination of the weights for the best POD is always the same. The only difference is that the maximum value of POD changes and is higher for higher PFA.

In this particular case the values $\alpha = 1.5$ and $\beta = 1$ yield the highest PODs which are: 0.947, 0.968, 0.969, 0.979 for PFAs of 1.2×10^{-6} , 5.2×10^{-6} , 1.2×10^{-5} , 5.2×10^{-5} , respectively. In other words, this implies that PFA has no impact on the choice of weights. This conclusion is extremely important because it allows us to analyze how POD changes for different combinations of weights without performing expensive simulations to determine the thresholds for PFA on the order of 10^{-5} or lower. Simply, we can establish the best weights for a higher PFA value (e.g., 10^{-3} or higher) because these weights produce the highest POD for any PFA. The threshold for the desired PFA can then be calculated using the iterative process described earlier. Furthermore, depending on the accuracy of the approximation, one may even be able to circumvent the simulation part and determine the best combination of weights just using the approximation. Such an approach would clearly require much less time to execute as it leaves out the simulation steps. The accuracy of the approximation is discussed in Appendix K. This assessment shows the approximation error to be within 2.9% for $M = 25$, and PFA of 10^{-2} . Consequently, all further analysis will be done using the approximation.

Next we shall investigate how the choice of weights is affected by the *SNR* (i.e., SNR in H channel). It is shown in Figure 5.3 that the shapes are the same and the maximum of POD is reached for the same weight combination for all four different SNRs. This indicates that the same weight combination produces the best POD for all SNRs. Thus, the *SNR* need not be taken into account when determining the optimal weights.

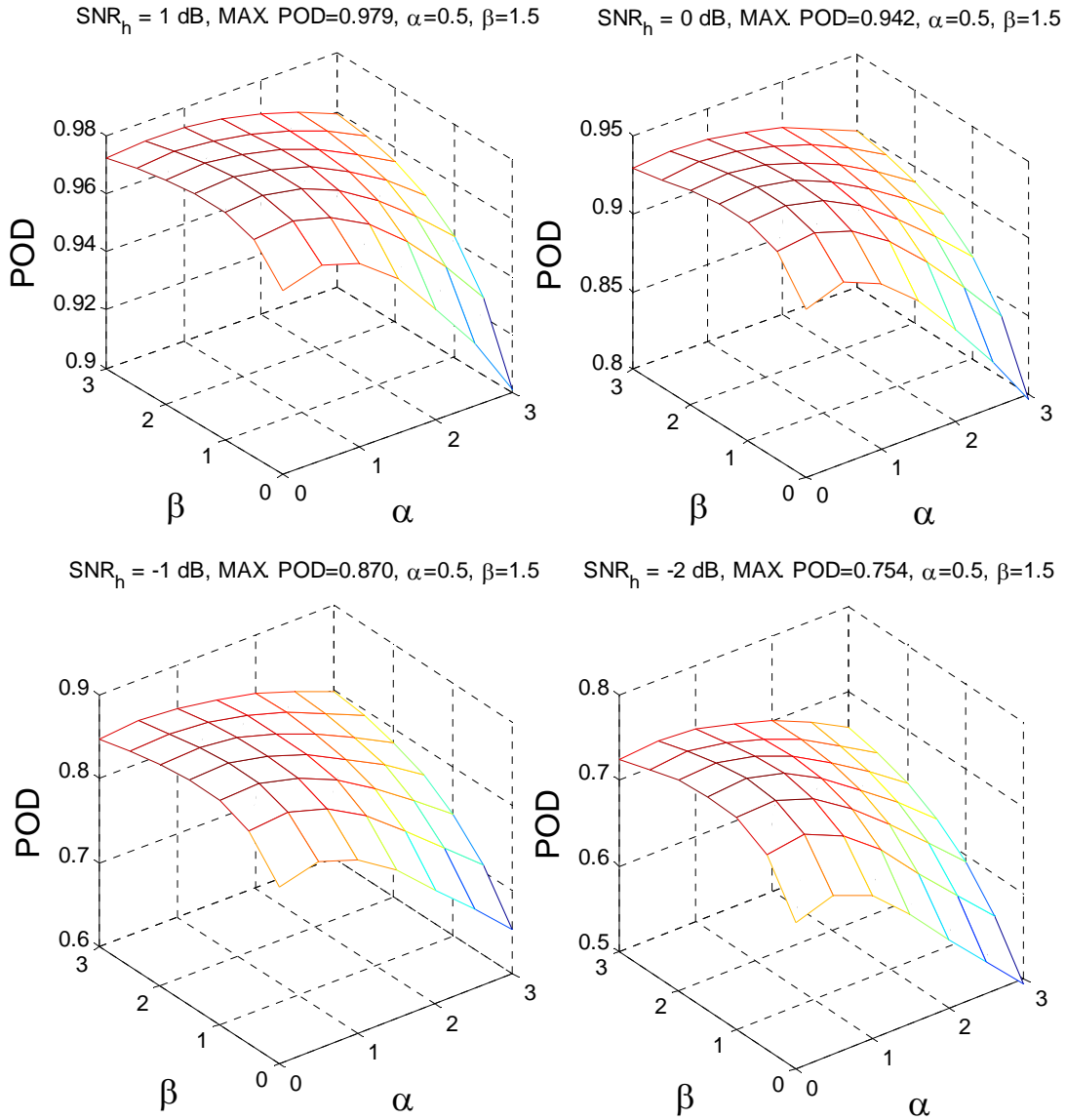


Figure 5.3 3-D representation of the POD vs. α and β for the following $\gamma=2$, $\sigma_v = 2 \text{ m s}^{-1}$, $Z_{DR} = 4 \text{ dB}$, $\rho_{hv} = 0.96$, $M = 25$, $N_v/N_h = 1$, and $\text{PFA} = 10^{-2}$.

Next, let us examine how the spectrum width affects the weights. This is shown in Figure 5.4 for the fixed value of $\gamma = 2$. The (α, β) weight pairs producing maximum POD are $(1, 2)$, $(1, 1.5)$, $(1, 0.5)$, $(1, 0.5)$ for spectrum widths $1, 2, 3, 4 \text{ m s}^{-1}$, respectively. Thus, the weights are sensitive to the variation of spectrum width less than 3 m s^{-1} . For higher σ_v (i.e., larger than 3 m s^{-1}), on the other hand, the weights do not appear to be affected by the spectrum widths.

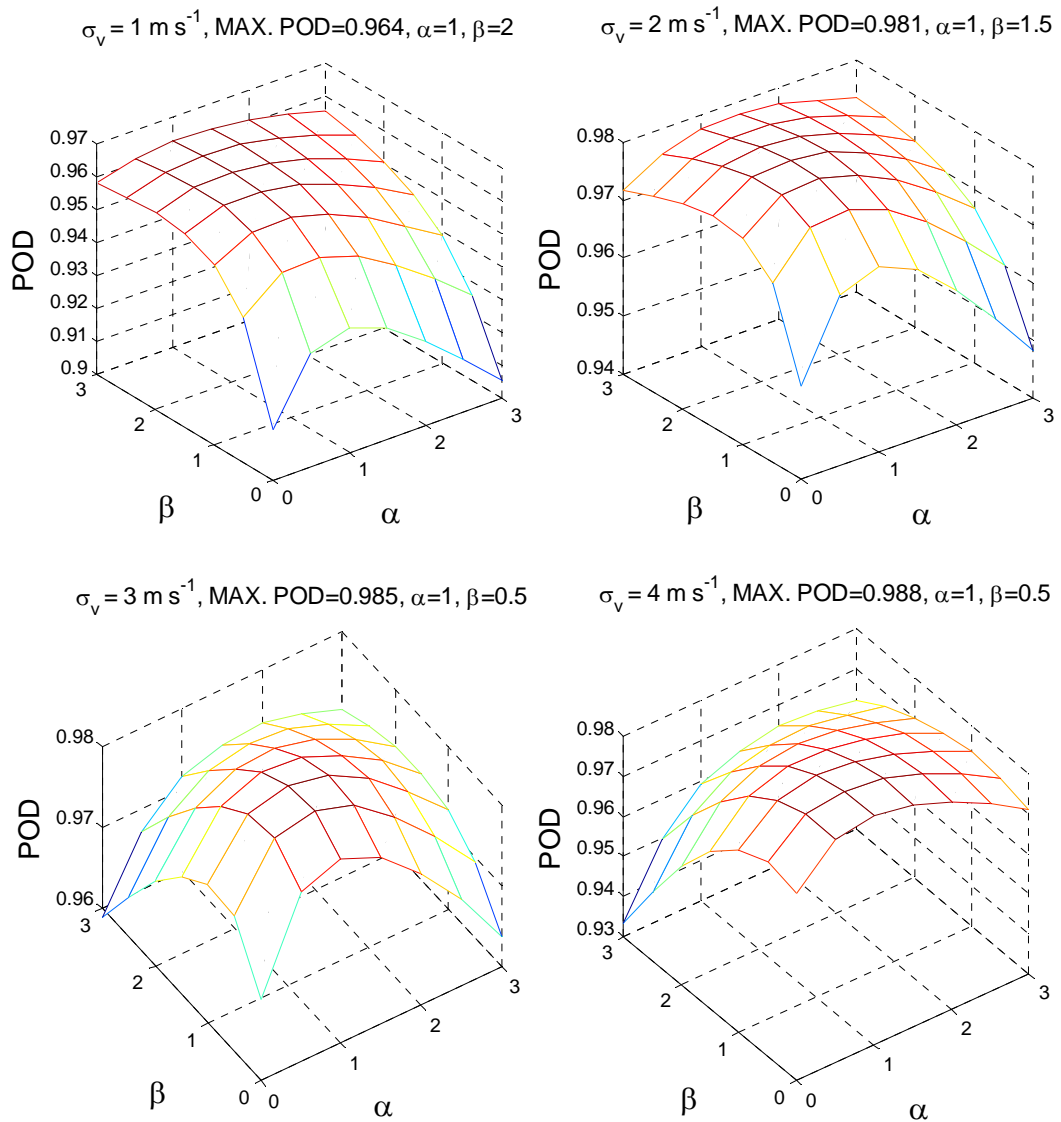


Figure 5.4 3-D representation of the POD vs. α and β for the following $\gamma=2$, $SNR_h = 0 \text{ dB}$, $Z_{DR} = 1 \text{ dB}$, $\rho_{hv} = 0.96$, $M = 25$, $N_v/N_h = 1$, and $PFA = 10^{-2}$.

The impact of Z_{DR} on the choice of weights is shown in Figure 5.5. It shows that different weight choice produces maximum POD at different Z_{DR} values. If possible, a set of weights should be chosen so the weighted sum yields balanced results for weather returns having a wide range of Z_{DR} values. Alternatively, weights that maximize detection of signals with Z_{DR} values that are of most interest can be used.

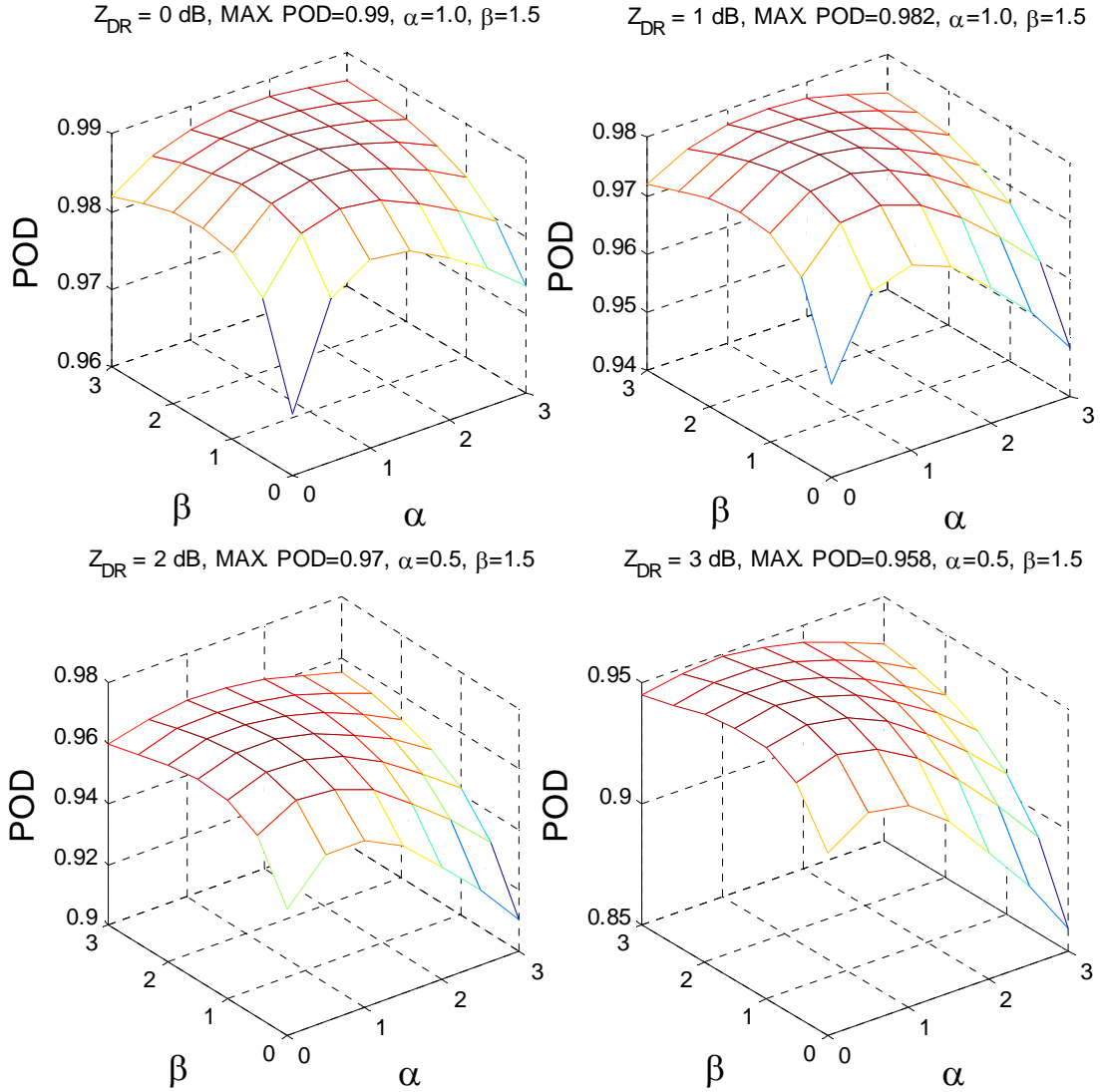


Figure 5.5 3-D representation of the POD vs. α and β for the following $\gamma=2$, $SNR_h = 0$ dB, $\sigma_v = 2$ m s⁻¹, $\rho_{hv} = 0.96$, $M = 25$, $N_v/N_h = 1$, and $PFA = 10^{-2}$.

The sensitivity of the weights to ρ_{hv} is inspected in Figure 5.6. Because weather signals from H and V channels are highly correlated, the plots are shown for ρ_{hv} of 0.99, 0.98, 0.97, and 0.96. In all four cases the maximum POD is achieved for $\alpha = 1$ and $\beta = 1.5$ with the estimated detection rate of 95.431%, 95.367%, 95.388%, 95.383% for ρ_{hv} values of 0.99, 0.98, 0.97, 0.96, respectively. This implies that for weather signal the cross-correlation coefficient has miniscule impact on the choice of weights. There are

other signals of interest, however, which do not exhibit high correlation between H and V. For example, the returns from biological scatterers (i.e., birds and insects), can exhibit cross-correlation as low as 0.4. The analysis for such a case is exemplified in Figure 5.7. The POD maxima for $\rho_{hv} = 0.4$ is achieved for $\alpha = 1.5$ and $\beta = 2$. Thus, if the detection of biological scatterers is of interest, the effect of the cross-correlation needs to be considered.

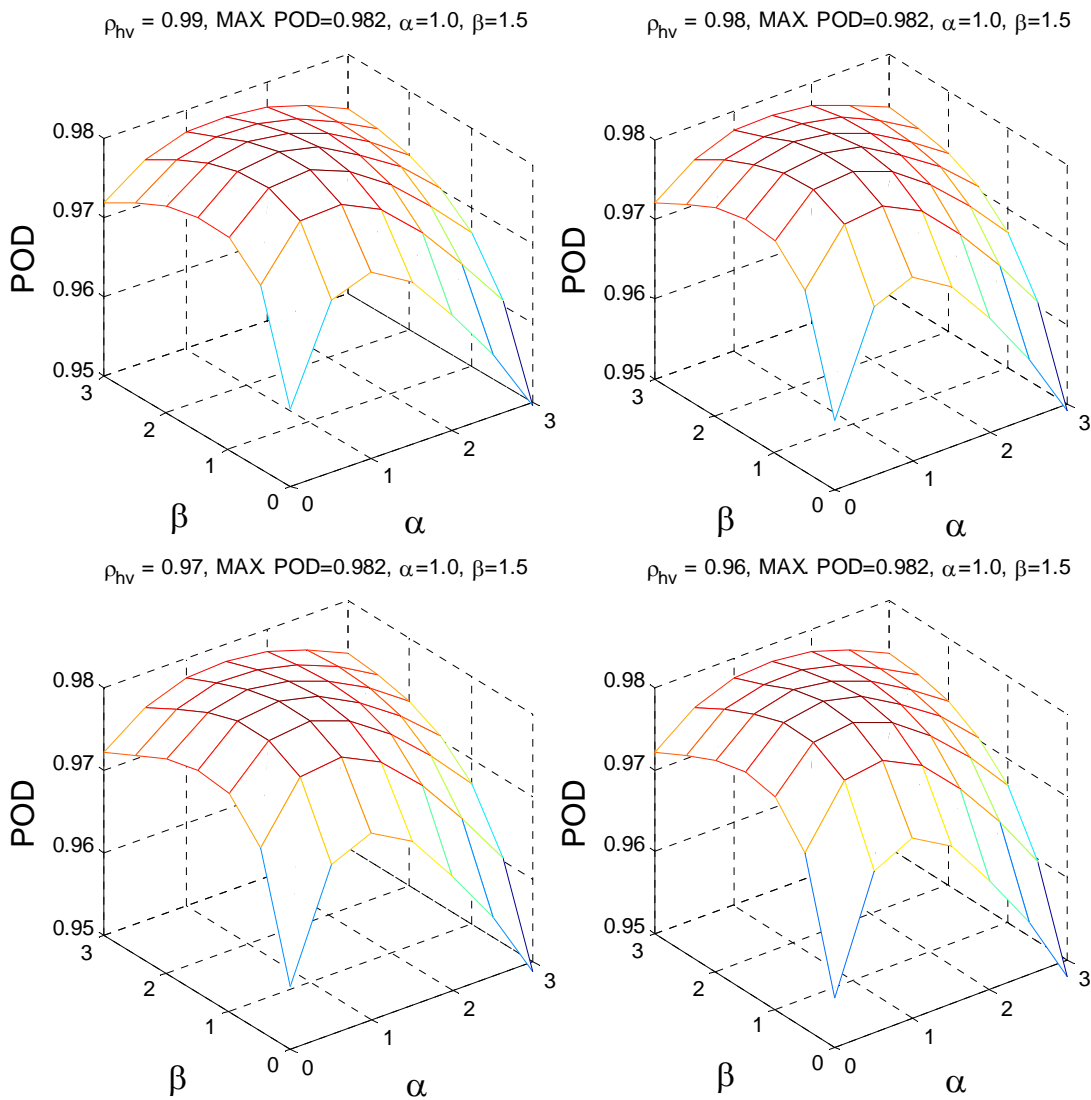


Figure 5.6 3-D representation of the POD vs. α and β for the following $\gamma=2$, $SNR_h = 0$ dB, $\sigma_v = 2$ m s⁻¹, $Z_{DR} = 1$ dB, $M = 25$, $N_v/N_h = 1$, and $PFA = 10^{-2}$.

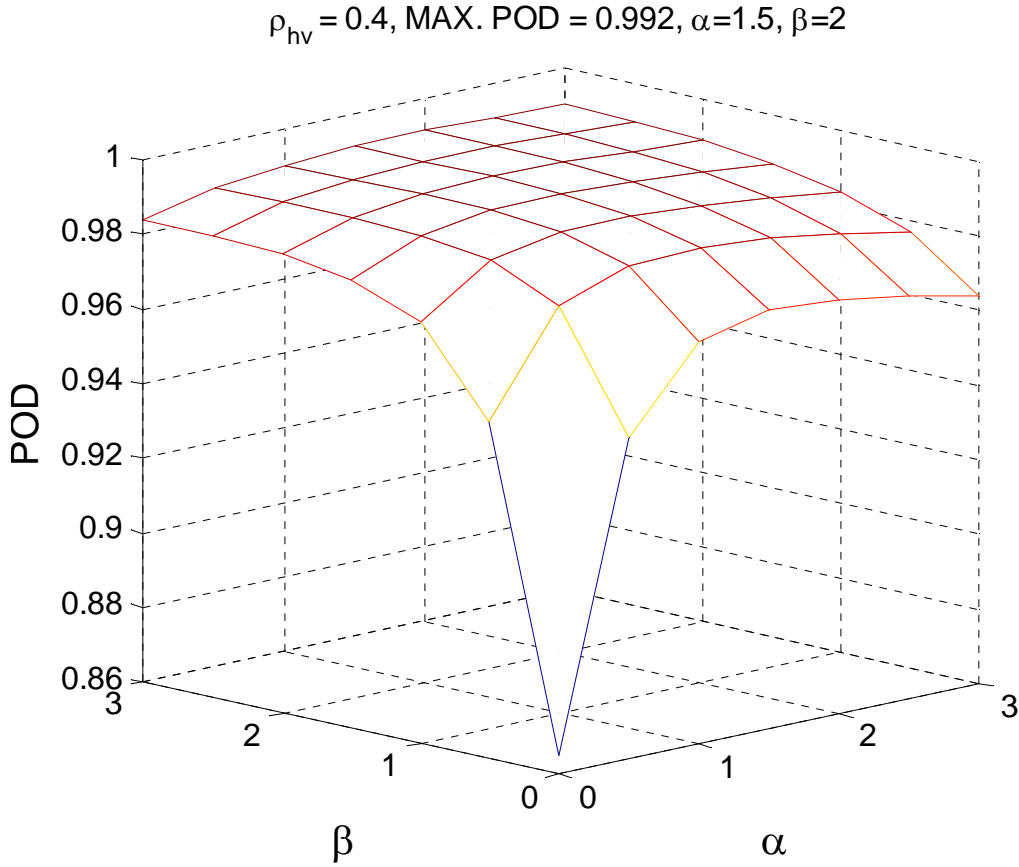


Figure 5.7 3-D representation of the POD vs. α and β for the following $\gamma=2$, $SNR_h = 0$ dB, $\sigma_v = 2$ m s⁻¹, $Z_{DR} = 1$ dB, $M = 25$, $N_v/N_h = 1$, and $PFA = 10^{-2}$.

The effect of the ratio of the noise powers in H and V channels is demonstrated in Figure 5.8. The maximum POD is achieved for $\alpha = 1, \beta = 1.5$ for N_v/N_h of 0.9, 1, and 1.1. For N_v/N_h of 1.2, the maximum POD is obtained for $\alpha = 0.5, \beta = 1$, but compared to the case when $\alpha = 1, \beta = 1.5$ the difference in POD is extremely small (97.265% compared to 97.126%). It is evident that the optimal weights depend on the N_v/N_h ratio.

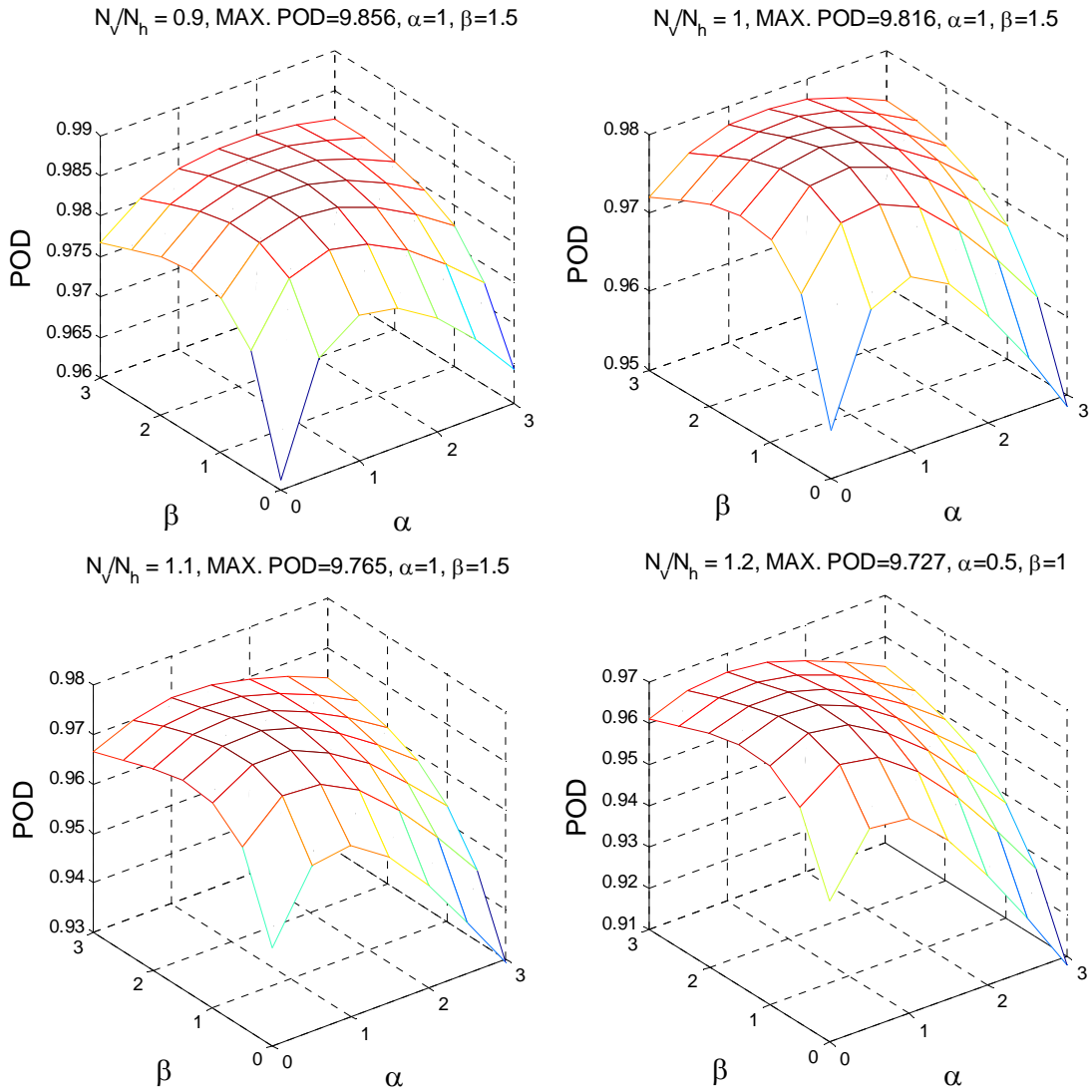


Figure 5.8 3-D representation of the POD vs. α and β for the following $\gamma=2$, $SNR_h = 0$ dB, $\sigma_v = 2$ m s⁻¹, $Z_{DR} = 1$ dB, $M = 25$, $\rho_{hv} = 0.96$, and $PFA = 10^{-2}$.

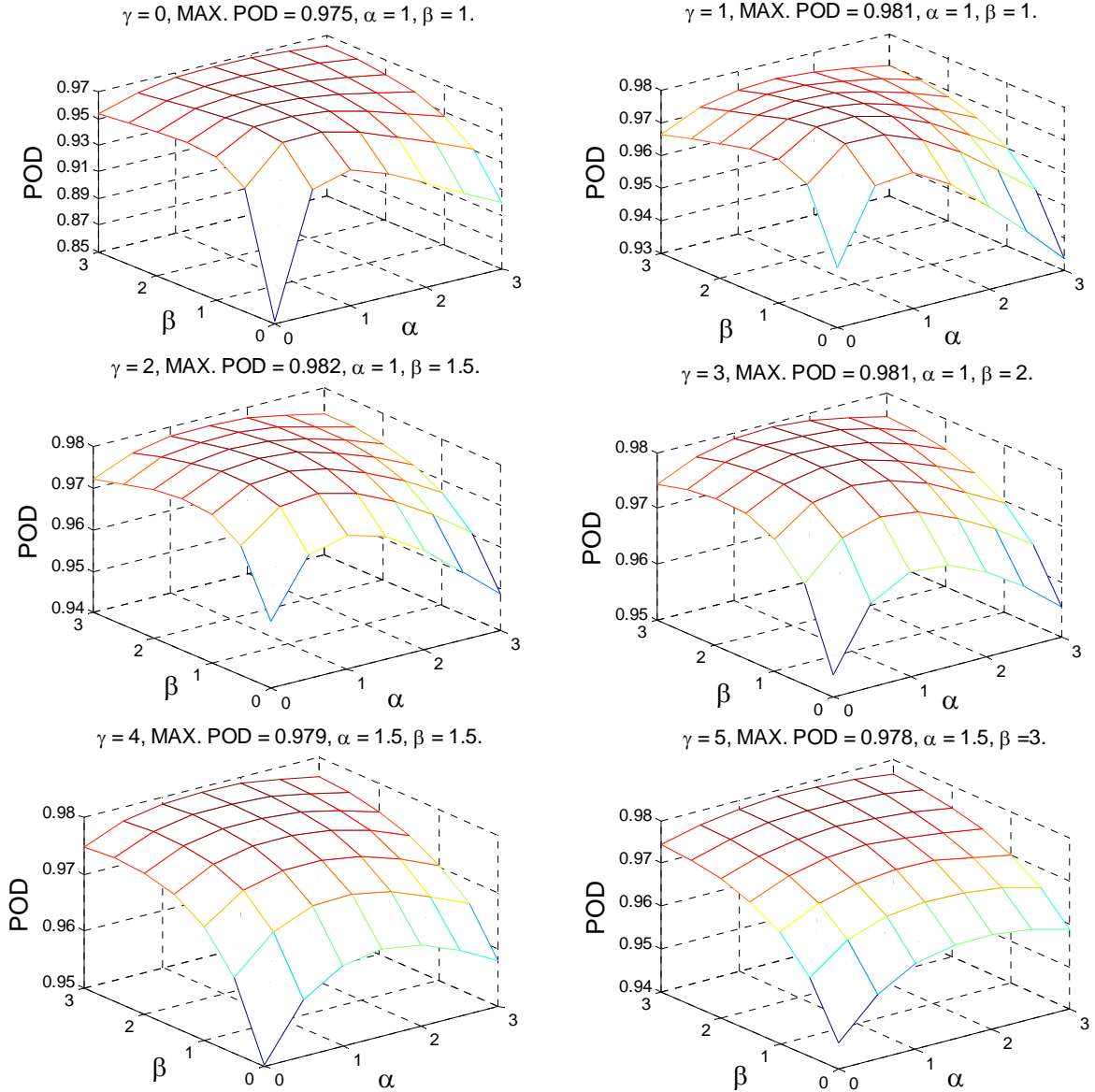


Figure 5.9 3-D representation of the POD vs. α and β for various γ values, and the following $SNR_h = 0$ dB, $\sigma_v = 2$ m s⁻¹, $Z_{DR} = 1$ dB, $M = 25$, $\rho_{hv} = 0.96$, $N_v/N_h = 1$, and $PFA = 10^{-2}$.

Next we examine how the POD is varied by different γ values in Figure 5.9. The maximum POD is achieved for $\alpha = 1$, $\beta = 1.5$, and $\gamma = 2$. The difference in POD, compared to other weight combinations, appears to be miniscule, however. This may be attributed to the fact that the maximum POD is obtained for the PFA of 10^{-2} . For lower PFA the difference may be more significant. To validate this assumption, a similar plot

for PFA of 10^{-6} and γ of 1 and 2 is given in Figure 5.10. It shows that the weights $\alpha = 1$, $\beta = 1.5$, and $\gamma = 2$ yield maximum POD 0.8% higher than the uniform sum. This moderate improvement may not be sufficient to show advantage of applying weights. Nonetheless, if we compare the two plots in Figure 5.10, the overall POD is higher for $\gamma = 2$ and is in general more balanced for a wide range of α and β weights. Because the maximum POD producing weight values depend on signal parameters (i.e., σ_v and Z_{DR}), this could imply that setting the weight γ to 2 might produce better cumulative detection rate for various mean values of input samples parameters in \mathbf{V} .

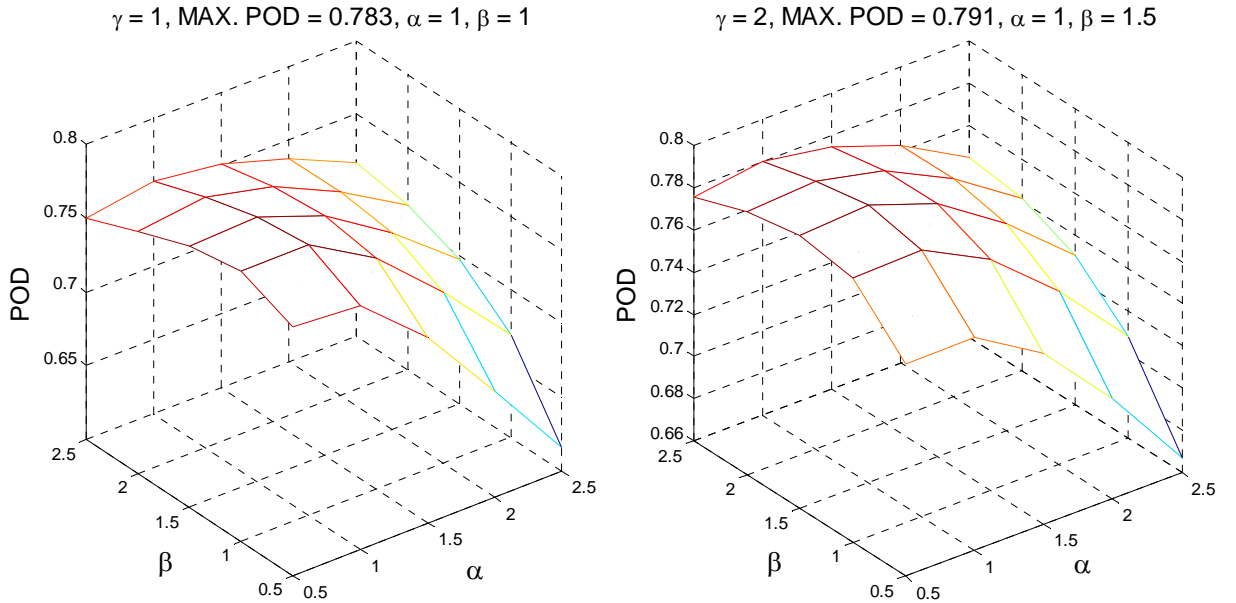


Figure 5.10 3-D representation of the POD vs. α and β for various γ , and the following $SNR_h = 0$ dB, $\sigma_v = 2$ m s $^{-1}$, $Z_{DR} = 1$ dB, $M = 25$, $\rho_{hv} = 0.96$, $N_v/N_h = 1$, and PFA = 10^{-6} .

Now we investigate how the number of samples affects the weights. The results are summarized in Table 5.2. It shows that the choice of optimal weights is not dependent on the number of samples. To further verify the result, the same is shown for $N_v/N_h = 0.8269$ in Table 5.3. As expected, the weights do not vary with M . Nonetheless, because the ratio N_v/N_h is different, the weights changed accordingly (i.e., α changed from 1 to 1.5).

From the 3-D plots a sort of a plateau around the optimal weight combination can be observed, where the POD does not depart significantly from the maximum when the weights change slightly. This could be significant because, if the max. POD producing weights for a wide range of weather parameters are all concentrated within a relatively small volume, one set of weights could prove, for all practical purposes, to yield detection rate close to maximum over various signal parameters and for a wide range of N_v/N_h values.

M	α	β	γ
17	1	1.5	2
27	1	1.5	2
37	1	1.5	2
47	1	1.5	2

Table 5.2 Max. POD weight combination as a function of M for $\sigma_v = 2 \text{ m s}^{-1}$, $Z_{DR} = 1 \text{ dB}$, and $N_v/N_h = 1$.

M	α	β	γ
17	1.5	1.5	2
27	1.5	1.5	2
37	1.5	1.5	2
47	1.5	1.5	2

Table 5.3 Max. POD maximizing weight combination as a function of M for $\sigma_v = 2 \text{ m s}^{-1}$, $Z_{DR} = 1 \text{ dB}$, and $N_v/N_h = 0.8269$.

So far, we have established that the choice of weights depends on the parameters of σ_v , Z_{DR} and the N_v/N_h . For a radar system, the ratio of powers in H and V channels is slow varying and can be considered as a constant over the period of at least one volume scan. Consequently, for a given ratio of N_v/N_h , we would like to find the set of weights that would produce the best overall detection rate over a wide range of values of σ_v and Z_{DR} . In Figure 5.11 a plot showing how POD changes as σ_v and Z_{DR} vary is shown. The POD is considerably more sensitive to Z_{DR} than to σ_v variations, which agrees with the conclusions drawn from Figure 4.5, and Figure 4.6. The weights used to generate the plot

were adjusted for $Z_{DR} = 1$ dB and $N_v/N_h = 1$; hence we would like to examine if adjusting weights for other Z_{DR} values can improve the overall POD behavior over a wide range of differential reflectivity values.

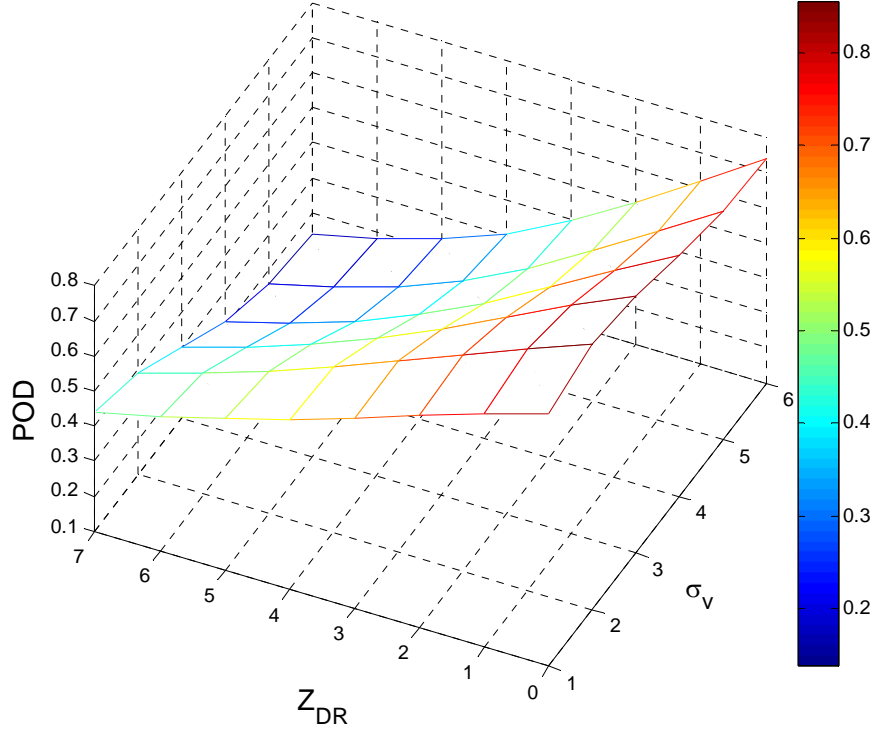


Figure 5.11 3-D representation of the POD vs. variation in σ_v and Z_{DR} for $\alpha = 1$, $\beta = 1.5$, $\gamma = 2$, and the following $SNR_h = 0$ dB, $M = 25$, $\rho_{hv} = 0.96$, $N_v/N_h = 1$, and $PFA = 10^{-6}$.

The weight settings for various Z_{DR} values and for a range of N_v/N_h ratios are given in Table 5.4. Listed values for α indicate that the weights for the vertical channel power are directly proportional to the SNR in this channel (i.e., lower N_v/N_h ratio indicates higher SNR in V channel). This is expected because the weighted sum puts more emphasis on the terms with higher SNR to enhance the detection. The weights associated with the cross-correlation also appear to be inversely proportional to the N_v/N_h ratio. This can be explained by the fact that the weighting scheme attempts to put more accent on this term when the overall noise in both channels is smaller. The weight of the term

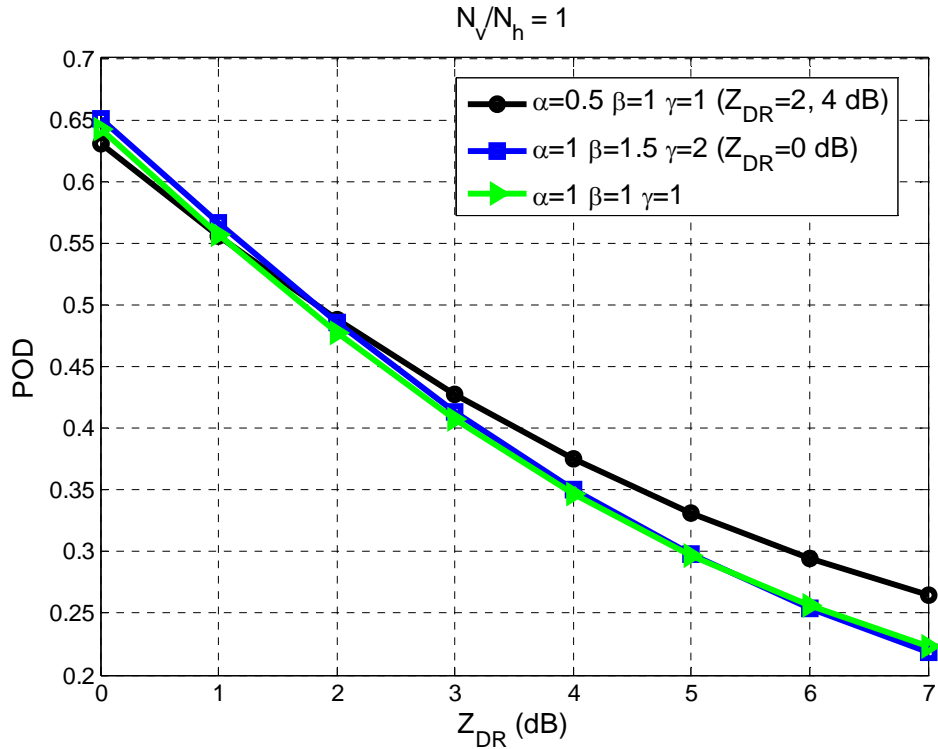
$|\hat{R}_h(T) + \hat{R}_v(T)|$ exhibits less variation but generally appears to be declining with the decrease of the vertical channel SNR. This may be the case because this term is the sum of estimates from both H and V channels. When the SNR of V channel is higher, a larger weight is applied and vice versa.

N_v/N_h	$Z_{DR} = 0$ dB			$Z_{DR} = 2$ dB			$Z_{DR} = 4$ dB		
	α	β	γ	α	β	γ	α	β	γ
0.5	5	2	4	3	1.5	3	2	1.5	2
0.55	4.5	2	4	2.5	1.5	3	1.5	1	2
0.6	3	1.5	3	2.5	1.5	3	1.5	1	2
0.65	3	2	3	2	1.5	2	1	1	2
0.7	3	2	3	1.5	1.5	2	1	1	2
0.75	2	1.5	2	1.5	1.5	2	1	1	1
0.8	1.5	1.5	2	1	1.5	2	0.5	1	1
0.85	1.5	1.5	2	1	1.5	2	0.5	1	1
0.9	1.5	1.5	2	1	1.5	2	0.5	1	1
0.95	1.5	1.5	2	0.5	1	1	0.5	1	1
1	1	1.5	2	0.5	1	1	0.5	1	1

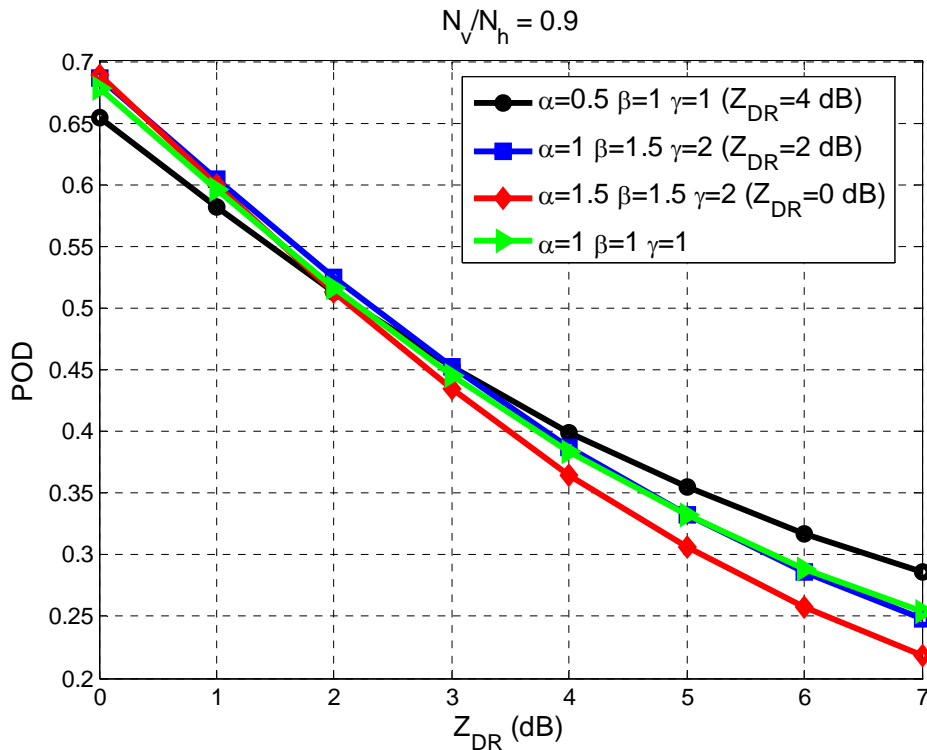
Table 5.4 POD maximizing weights for $\sigma_v = 2 \text{ m s}^{-1}$.

It has been established that Z_{DR} has much more impact on the resulting POD than the signal coherency. Thus, to examine how various optimal weight combinations (from Table 5.4) perform over the range of differential reflectivities, the resulting POD is estimated for different N_v/N_h ratios of 1, 0.9, 0.8, and 0.7 in Figure 5.12, and Figure 5.13 for M of 17 and 52. For comparison, the detection rate of uniform sum is also included. Figure 5.12 shows that the uniform sum has balanced performance for all cases, except possibly when N_v/N_h is unity. In this case, as shown in Figure 5.12 (a), the weights for Z_{DR} of 4 dB may result in significantly better detection when the power in V channel is more than 3 dB smaller than that in the H channel, while producing closely the same POD for Z_{DR} greater than 3 dB. Figure 5.13 shows the similar trend for the increased number of samples (i.e. M is 52). In this case the curves show the performances of all

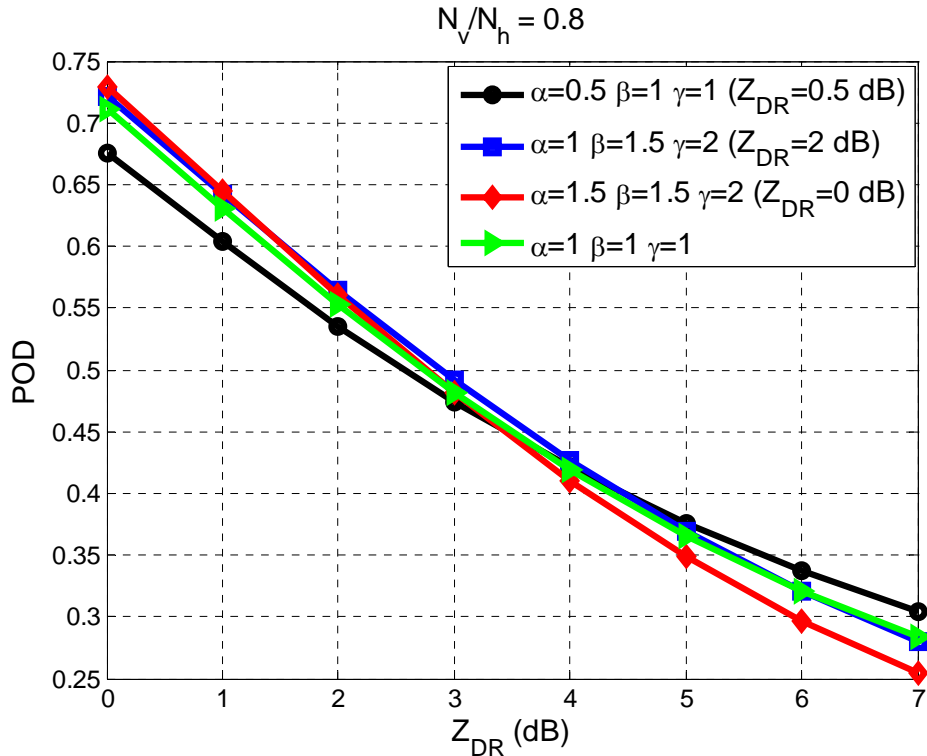
weighted sums to be quite similar up to Z_{DR} of 3 dB, while the difference in PODs increases for higher Z_{DR} values.



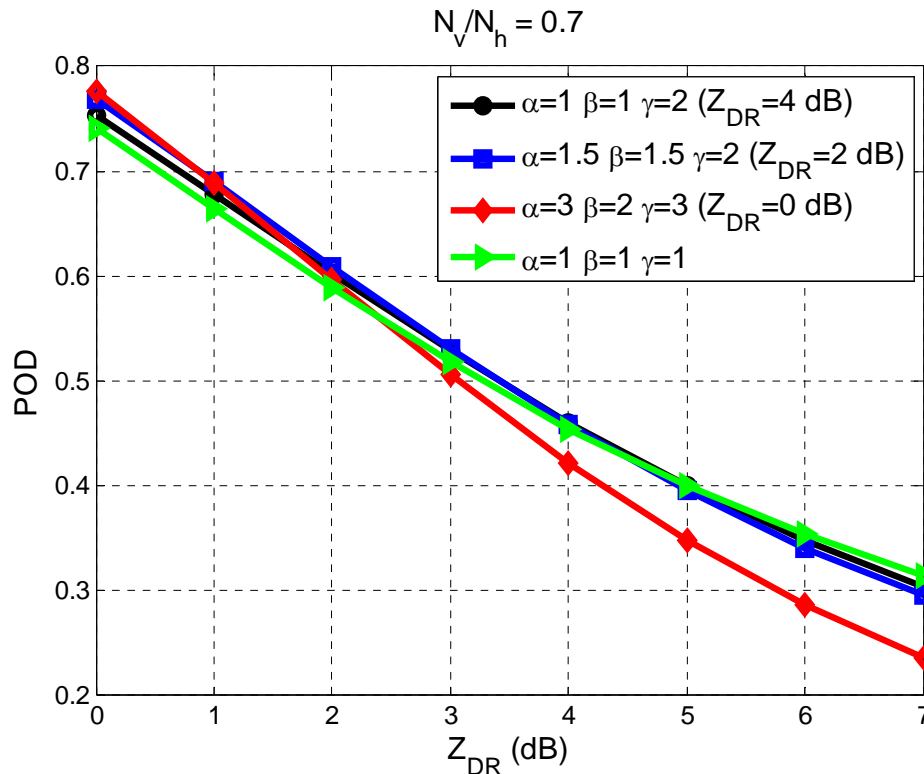
(a)



(b)

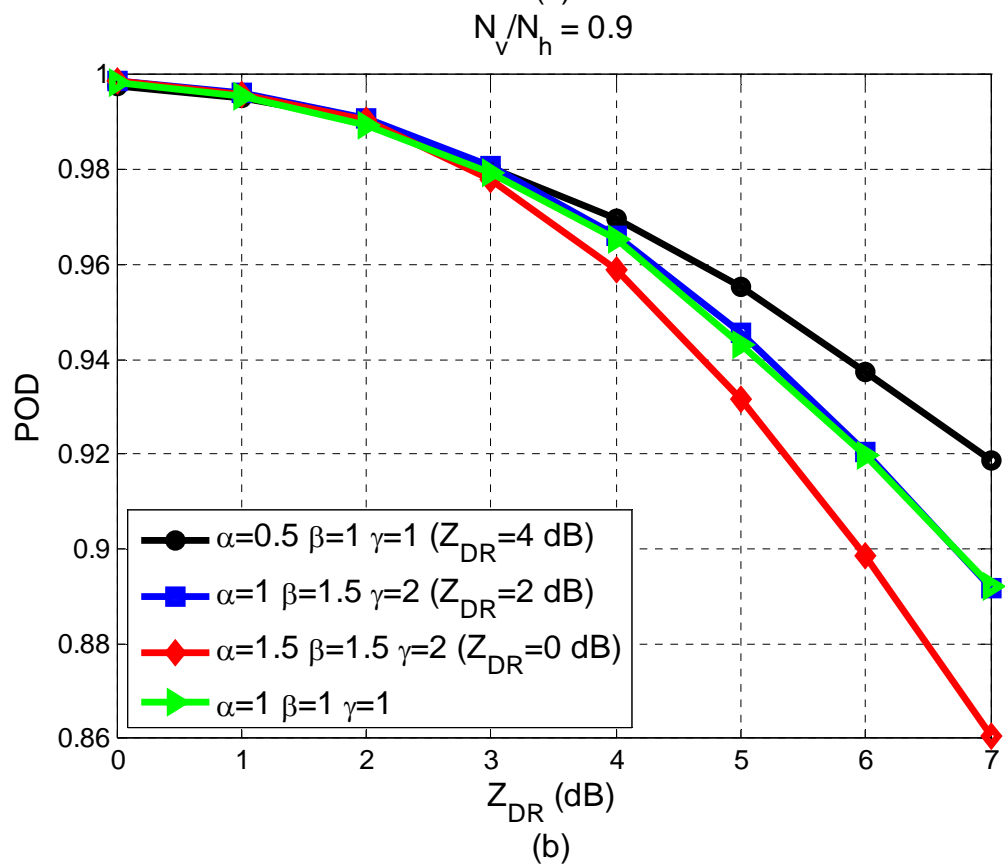
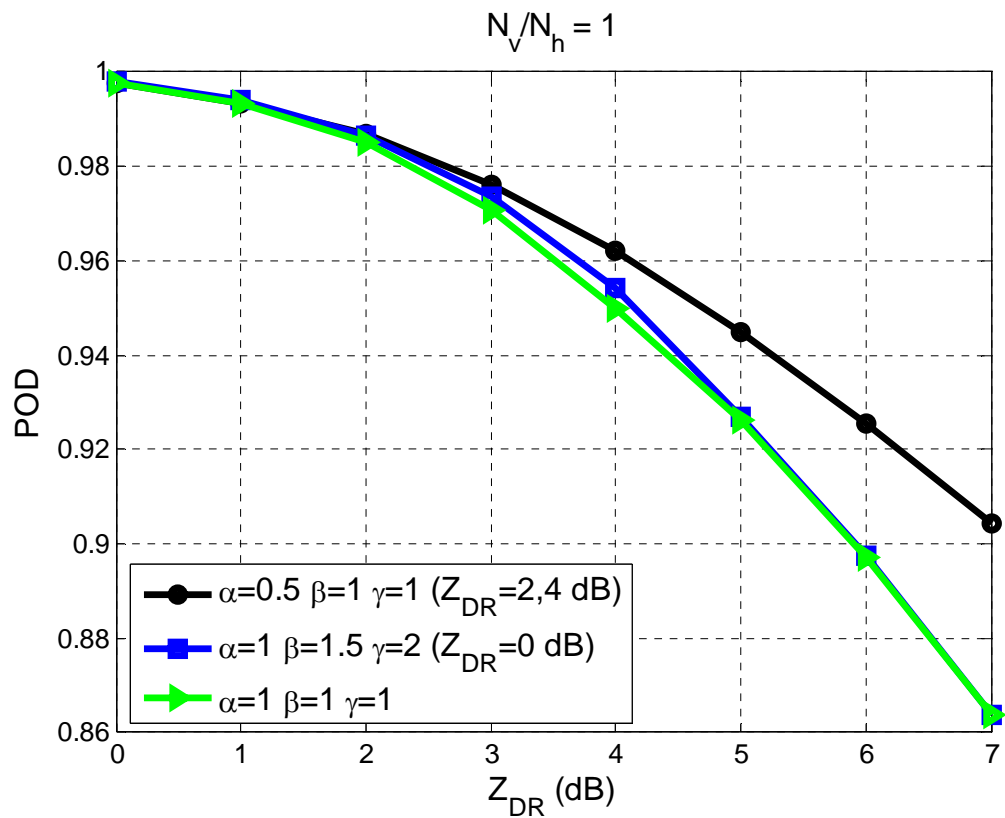


(c)



(d)

Figure 5.12 POD for different weight combinations and several N_v/N_h ratios as a function of varied Z_{DR} , for $SNR = 0$ dB, $M = 17$, $\sigma_v = 2$ m s⁻¹, $\rho_{hv} = 0.96$, and $PFA = 1.2 \times 10^{-6}$. Bracketed Z_{DR} value indicates the weight optimization parameter.



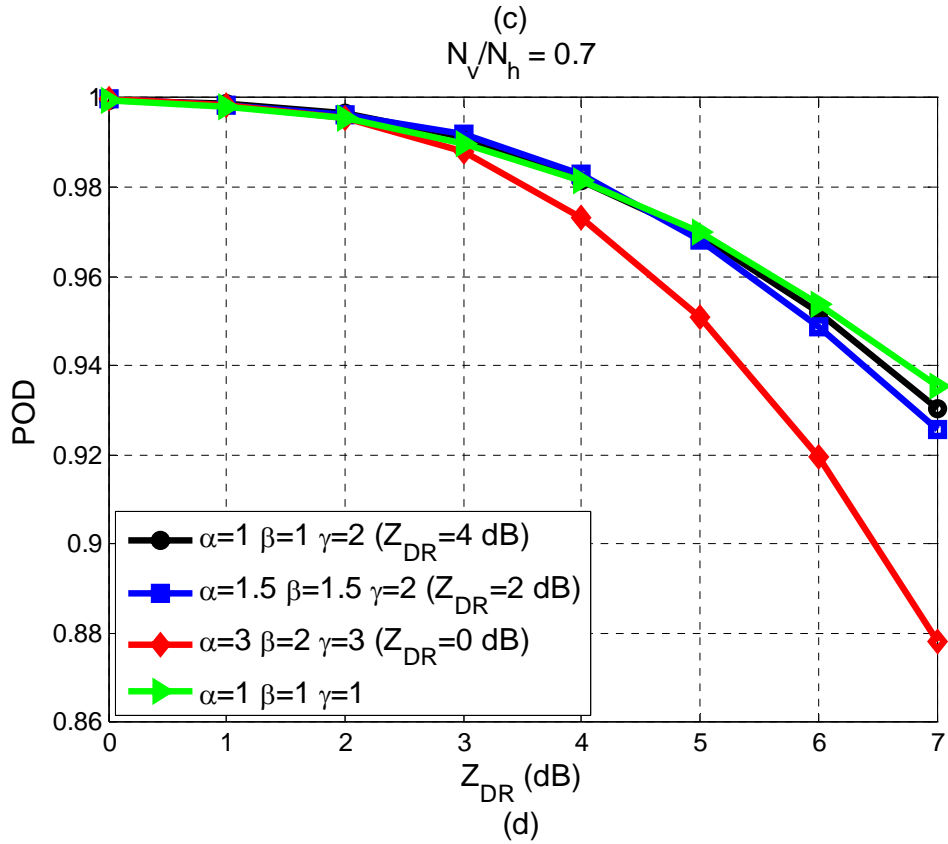
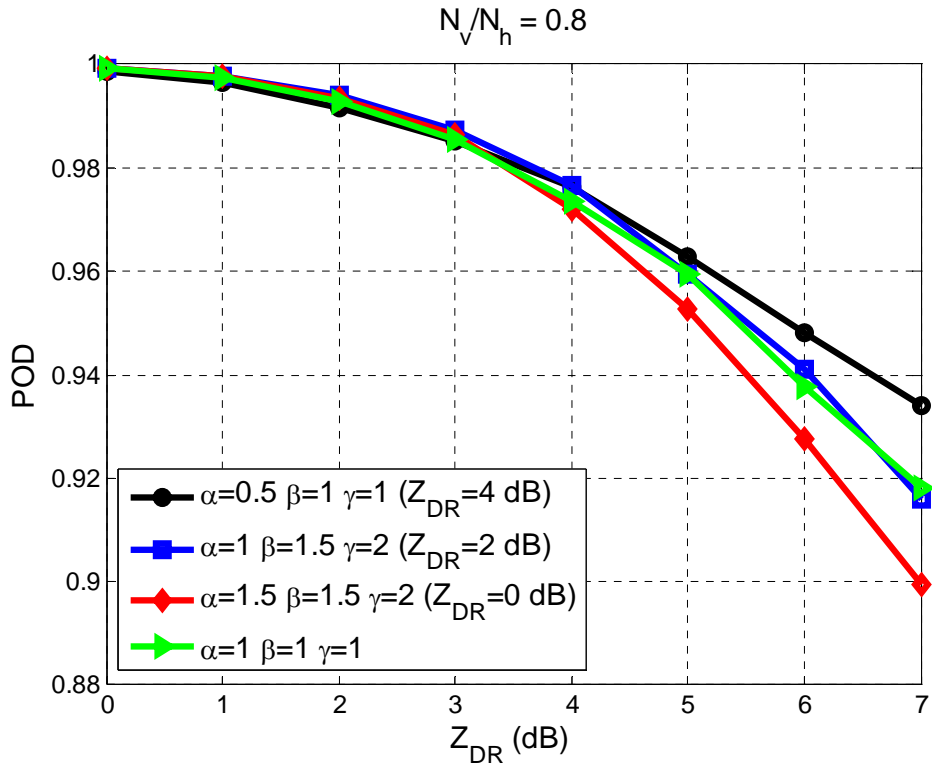


Figure 5.13 POD for different weight combinations and several N_v/N_h ratios as a function of varied Z_{DR} , for $SNR = 0$ dB, $M = 52$, $\sigma_v = 2$ m s⁻¹, $\rho_{hv} = 0.96$, and $PFA = 1.2 \times 10^{-6}$. Bracketed Z_{DR} value indicates the weight optimization parameter.

5.7 Implementation Issues

The weighted sum approach was designed to improve the detection by exploiting the fact that the signals are coherent, while the noise is not. Nonetheless, if the measured power is substantially higher than the known noise, we can accurately classify it as a signal. For example, if only 17 samples are used for estimation, and the measured power is 2 dB above noise, the probability of a false detection (i.e., PFA) is only $\approx 1.2 \times 10^{-6}$ (see Appendix A). Therefore, for practical implementation, we may want to combine both the power and uniform sum based approaches. The apparent arrangement is:

$$\begin{aligned} & \left(\hat{P}_h \geq THR_1 \right) OR \\ & \left[\left(\hat{P}_h < THR_1 \right) AND \left(\hat{P}_h + \alpha \hat{P}_v + \beta \left| \hat{R}_h(T) + \hat{R}_v(T) \right| + \gamma \left| \hat{R}_{hv}(0) \right| \geq THR_2 \right) \right], \end{aligned} \quad (5.83)$$

where a signal is present if the above Boolean combination is true. To give a formal description, we use again the Bernoulli random variable. Let us define:

$$\begin{aligned} X = & \left(\hat{P}_h \geq THR_1 \right) OR \\ & \left[\left(\hat{P}_h < THR_1 \right) AND \left(\hat{P}_h + \alpha \hat{P}_v + \beta \left| \hat{R}_h(T) + \hat{R}_v(T) \right| + \gamma \left| \hat{R}_{hv}(0) \right| \geq THR_2 \right) \right], \end{aligned} \quad (5.84)$$

where

$$X = \begin{cases} 1 & \Rightarrow \text{signal present} \\ 0 & \Rightarrow \text{signal NOT present} \end{cases} \quad (5.85)$$

Clearly, $PFA = P(X = 1 \mid \text{only noise is present})$, and $POD = P(X=1 \mid \text{both signal and noise are present})$. Note that the POD will vary for different values of signal parameters (i.e., $SNR, Z_{DR}, \sigma_v, \rho_{hv}$).

Typically the values of THR_1 , and THR_2 are determined by the desired PFA. Thus, we would like to express the $P(X)$ in terms of numerical operators as opposed to Boolean ones. To do this we use:

$$\begin{aligned}
P(A) \text{ OR } P(B) &= P(A) + P(B) - P(A \text{ AND } B) \\
P(A \text{ AND } B) &= P(B | A)P(A).
\end{aligned} \tag{5.86}$$

Let us denote the events as:

$$\begin{aligned}
A &= P(\hat{P}_h \geq THR_1) \\
\bar{A} &= NOT A = P(\hat{P}_h < THR_1) \\
B &= P(\hat{P}_h + \hat{P}_v + |\hat{R}_h(T) + \hat{R}_v(T)| + |\hat{R}_{mv}(0)| \geq THR_2).
\end{aligned} \tag{5.87}$$

Then,

$$P(X) = P(A \text{ OR } (\bar{A} \text{ AND } B)) = P(A) + P(\bar{A} \text{ AND } B) - P(A \text{ AND } \bar{A} \text{ AND } B). \tag{5.88}$$

Obviously, events A and \bar{A} are mutually exclusive and we have:

$$P(X) = P(A) + P(\bar{A} \text{ AND } B) = P(A) + P(B | \bar{A})P(\bar{A}), \tag{5.89}$$

which yields:

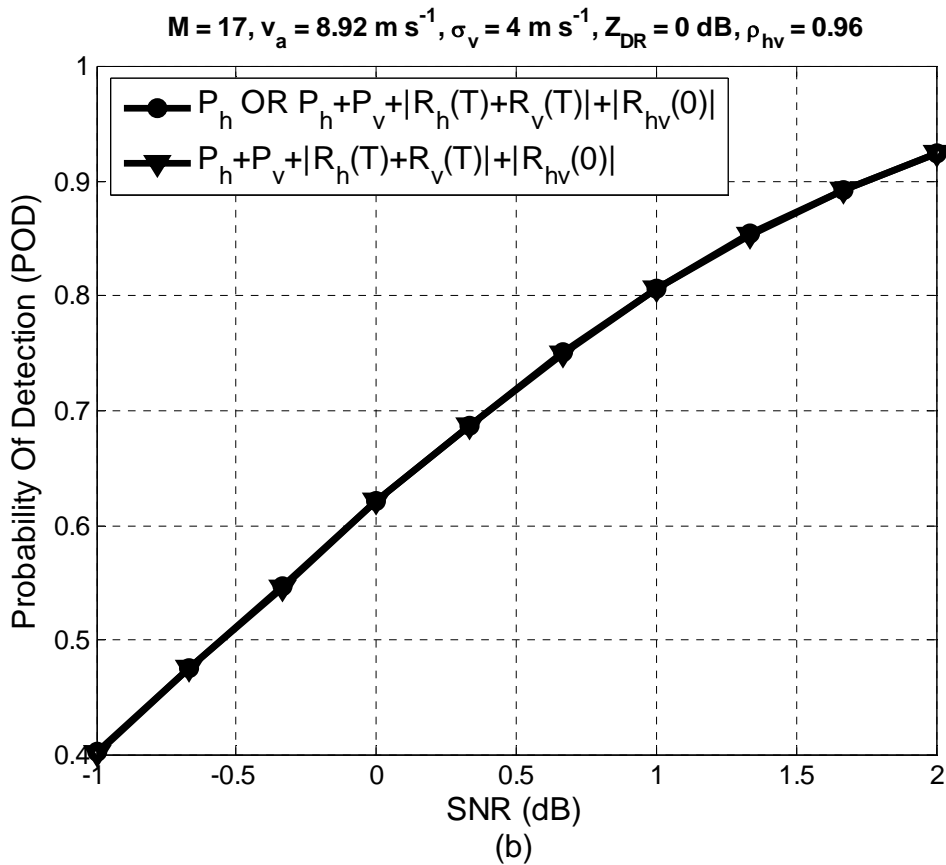
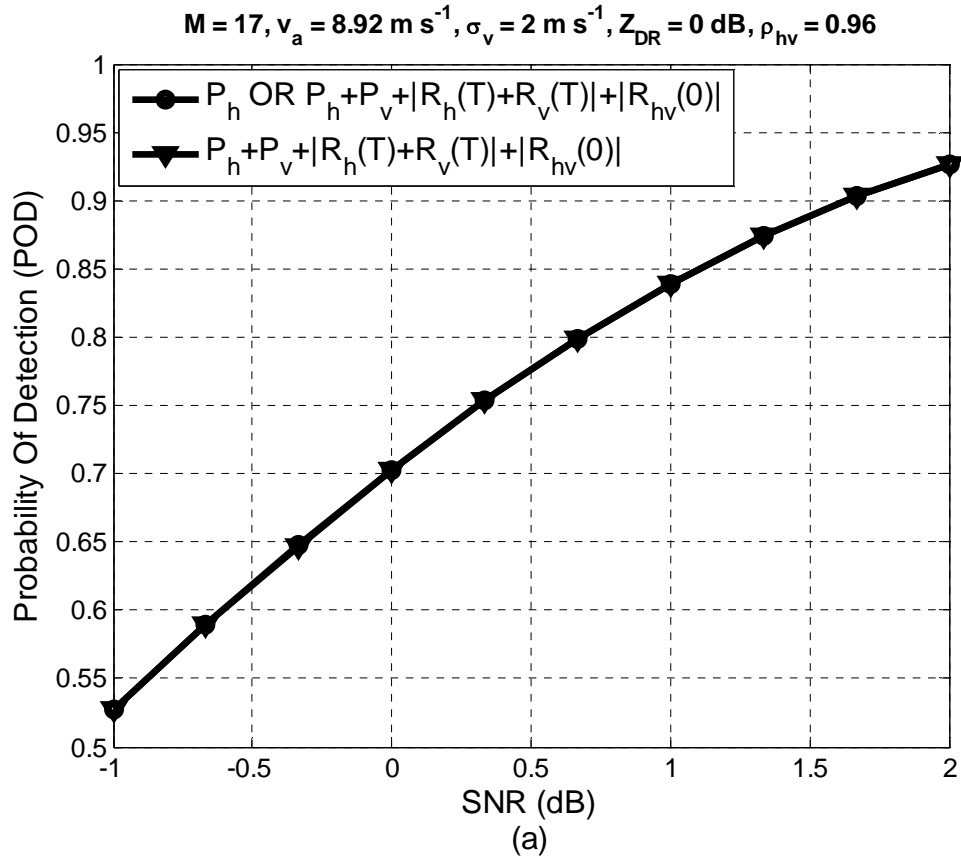
$$\begin{aligned}
P(X=1) &= P(\hat{P}_h \geq THR_1) + \\
&P(\hat{P}_h + \alpha \hat{P}_v + \beta |\hat{R}_h(T) + \hat{R}_v(T)| + \gamma |\hat{R}_{mv}(0)| \geq THR_2 | \hat{P}_h < THR_1) \times \\
&P(\hat{P}_h < THR_1).
\end{aligned} \tag{5.90}$$

If $P(\hat{P}_h < THR_1) \approx 1$ we can write:

$$\begin{aligned}
P(X=1) &\approx P(\hat{P}_h \geq THR_1) + \\
&P(\hat{P}_h + \alpha \hat{P}_v + \beta |\hat{R}_h(T) + \hat{R}_v(T)| + \gamma |\hat{R}_{mv}(0)| \geq THR_2 | \hat{P}_h < THR_1).
\end{aligned} \tag{5.91}$$

This is valid if the power threshold is set at 2 dB above noise (i.e., only ≈ 1.2 power estimates out of million are larger than $N + 2\text{dB}$). Consequently, if (5.83) is used with the THR_2 set so that $P(\hat{P}_h + \alpha \hat{P}_v + \beta |\hat{R}_h(T) + \hat{R}_v(T)| + \gamma |\hat{R}_{mv}(0)| \geq THR_2 | \text{noise only}) = 10^{-5}$ the resultant PFA cannot be greater than 1.12×10^{-5} (i.e., $10^{-5} + 0.11749 \times 10^{-5} < 1.12 \times 10^{-5}$).

Moreover, the structure of the weighted sum implies that in the case of noise samples, it is dominated by the power estimates (as autocorrelations in sample-time and cross-correlation between H and V channels are very small). Thus, the statistics of the weighted sum for independent samples is similar to the case where only power estimates are used. In practice, this implies that the cumulative false alarm rate of this combination is practically the same as the larger of the two. This was verified experimentally using 10^9 trials and the PFA of 1.0519×10^{-5} was obtained. Apparently, not much difference as opposed to when only the weighted sum is used. The same analysis is done when the false alarm rates for both the power threshold and the weighted sum are comparable and the outcome was the same (i.e., no significant difference in PFA). In addition, the comparisons of PODs are shown in Figure 5.14. It is apparent that for all practical purposes there is no difference. Hence, we conclude that these two approaches are **effectively the same**. From the computational point of view, though, using just the weighted sum may be more effective.



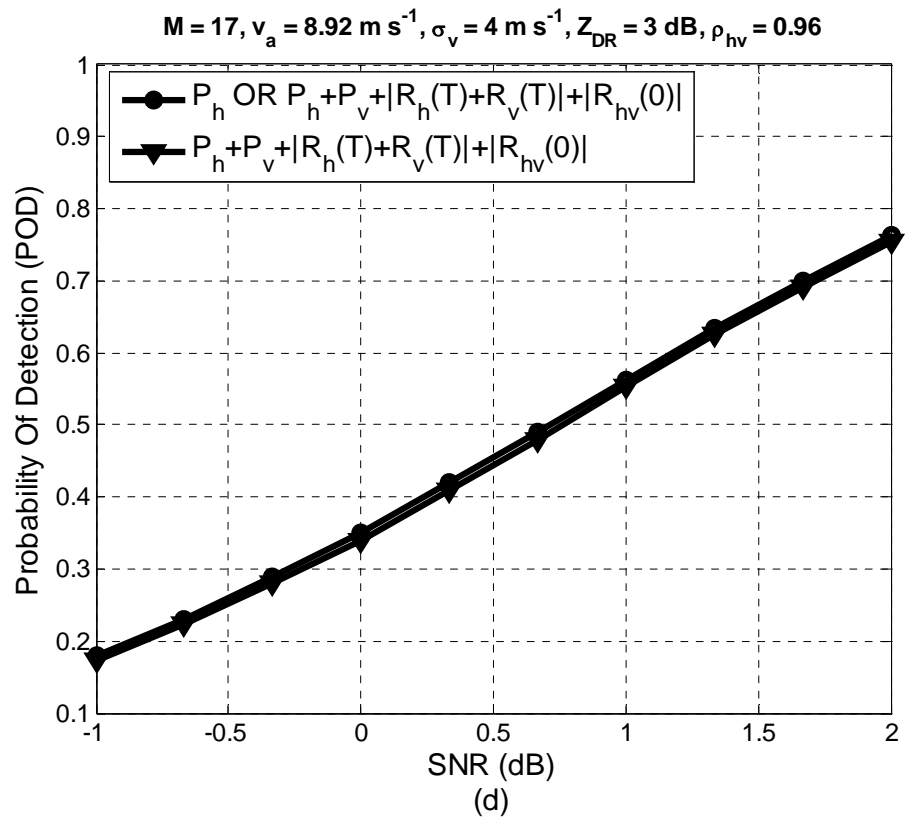
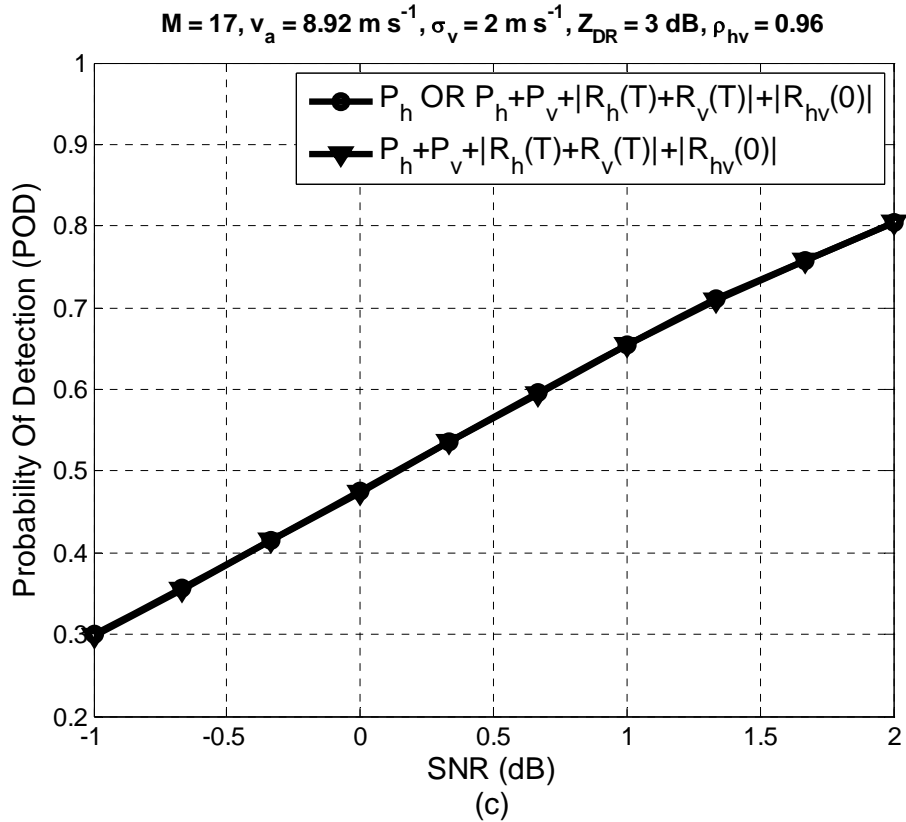


Figure 5.14 POD of the OR combination of power and uniform sum versus the POD of the uniform sum only.

6. Implementation of Weighted Sum on Real Data

To demonstrate and assess the performance of the weighted sum, a set of dual-pol time series data collected by the KOUN radar is used. This data set was collected on 03/19/06 using the long PRT with unambiguous range of 466 km, with $M = 17$, and at elevation of 0.48 deg. In a standard operation, this corresponds to the surveillance scan with the threshold set to 2 dB above noise power. This threshold will be used in subsequent analysis. To simulate the effect of the 3 dB power loss, the noise power was doubled in each channel by simply adding the noise samples as:

$$V_h(n) = V_h(n) + N_h(n) \text{ and } V_v(n) = V_v(n) + N_v(n), \quad (6.1)$$

where each noise sample is generated in MATLAB as:

$$\begin{aligned} N_h(n) &= \text{sqrt}(N_h/2) * (\text{randn}(1,1) + j * \text{randn}(1,1)); \\ N_v(n) &= \text{sqrt}(N_v/2) * (\text{randn}(1,1) + j * \text{randn}(1,1)); \end{aligned}$$

Threshold for each of the investigated weighted sum is set so that the PFA is 1.2×10^{-6} (i.e., the same as for the 2 dB power threshold and $M = 17$). The original “single-pol” reflectivity field is presented in Figure 6.1, and the histogram of the SNR distribution in the horizontal channel is given in Figure 6.2. Each bar in the histogram is roughly 1 dB wide and the first shows the percentage of data with signal power between 2 and 3 dB. Hence, the first three bars represent data with power between 2 and 5 dB. These are critical because after the transmitted power is halved their returned power falls below the legacy 2 dB censoring threshold and thus are lost. The histogram shows that, for the given case, out of all detections these data amount to about 8.4%. Adding the additional noise (i.e., doubling the noise power), without changing the threshold, yields the reflectivity field in Figure 6.3 (a). All detections for this case are classified with respect to the “single-pol” case and presented in Figure 6.3 (b). Missed detections are highlighted

in red. Data that are detected in both the “single” and the “dual-pol” case are given in green. Those that are classified as “significant returns” after doubling the noise, but not before, are shown in white (i.e., additional detections). This is equivalent to setting the threshold to -1 dB above the noise power in the original case. It is apparent that the number of spurious speckles has significantly increased due to the fact that the PFA has increased from $\approx 1.2 \times 10^{-6}$ to 0.003. The result when the threshold is elevated to 2 dB above the noise level is shown in Figure 6.4. It can be observed that a significant portion of the features on the periphery of the phenomena is lost compared to the original reflectivity field in Figure 6.1. It is expected that these features will be recovered if the weighted sum approach is used.

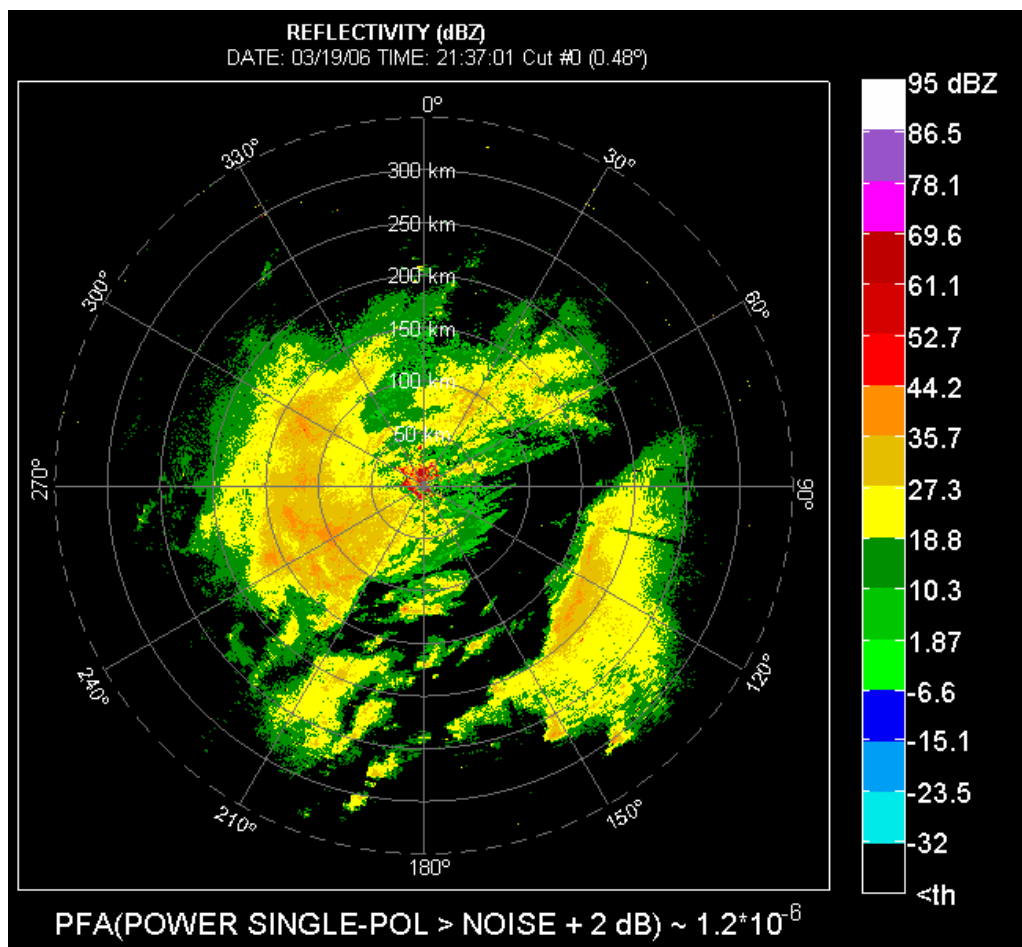


Figure 6.1 The original “single-pol” reflectivity field.

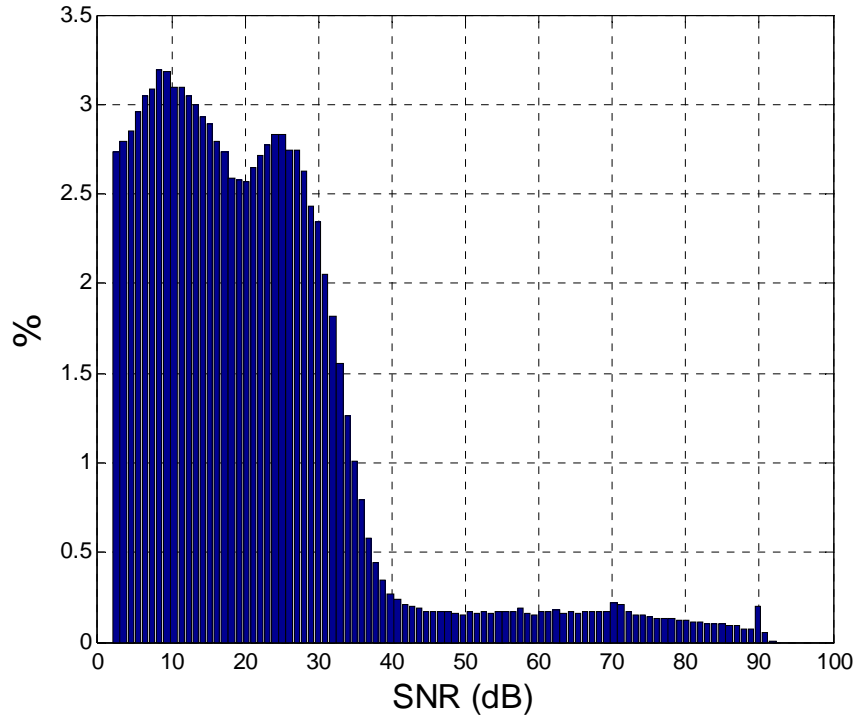
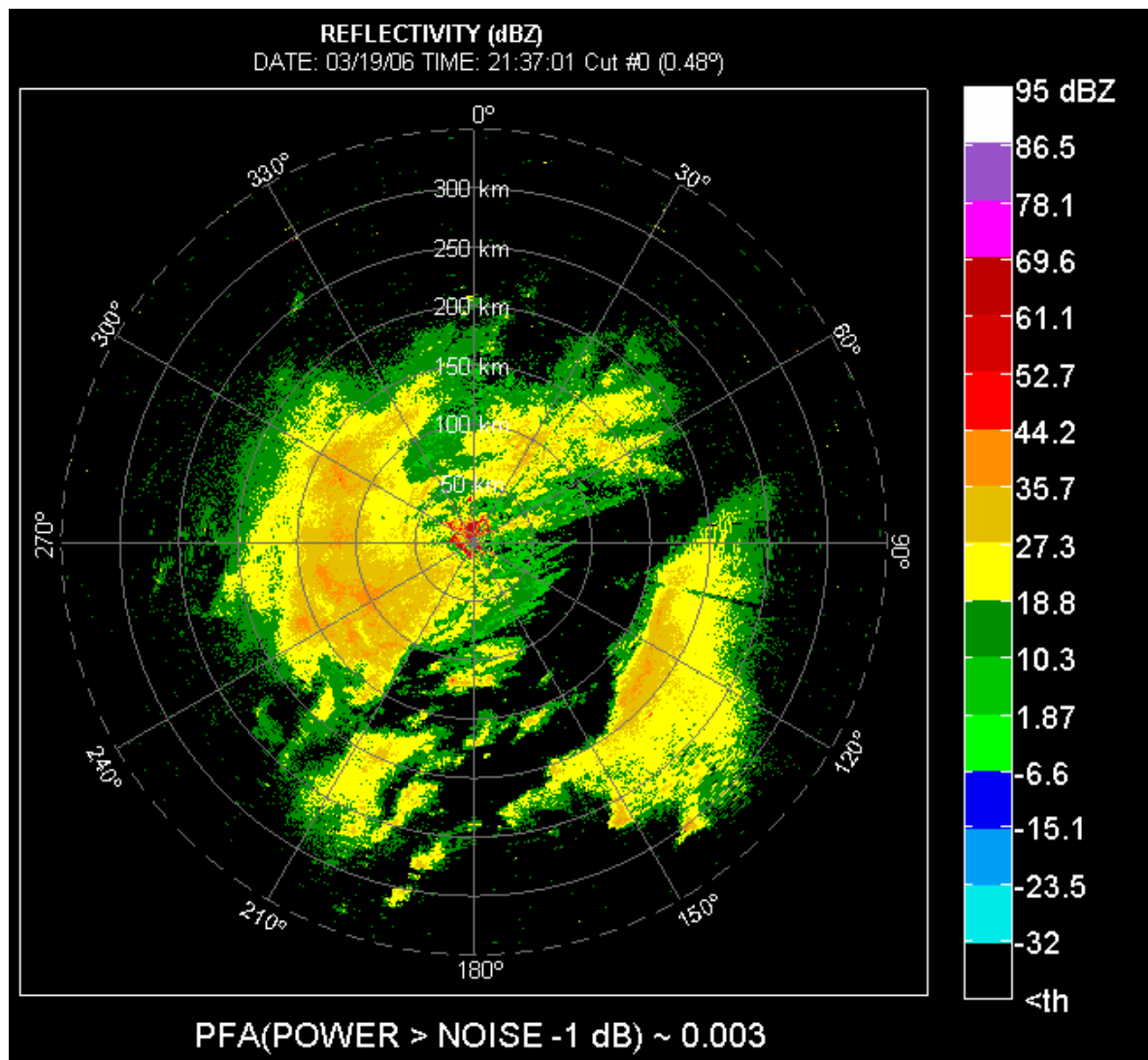


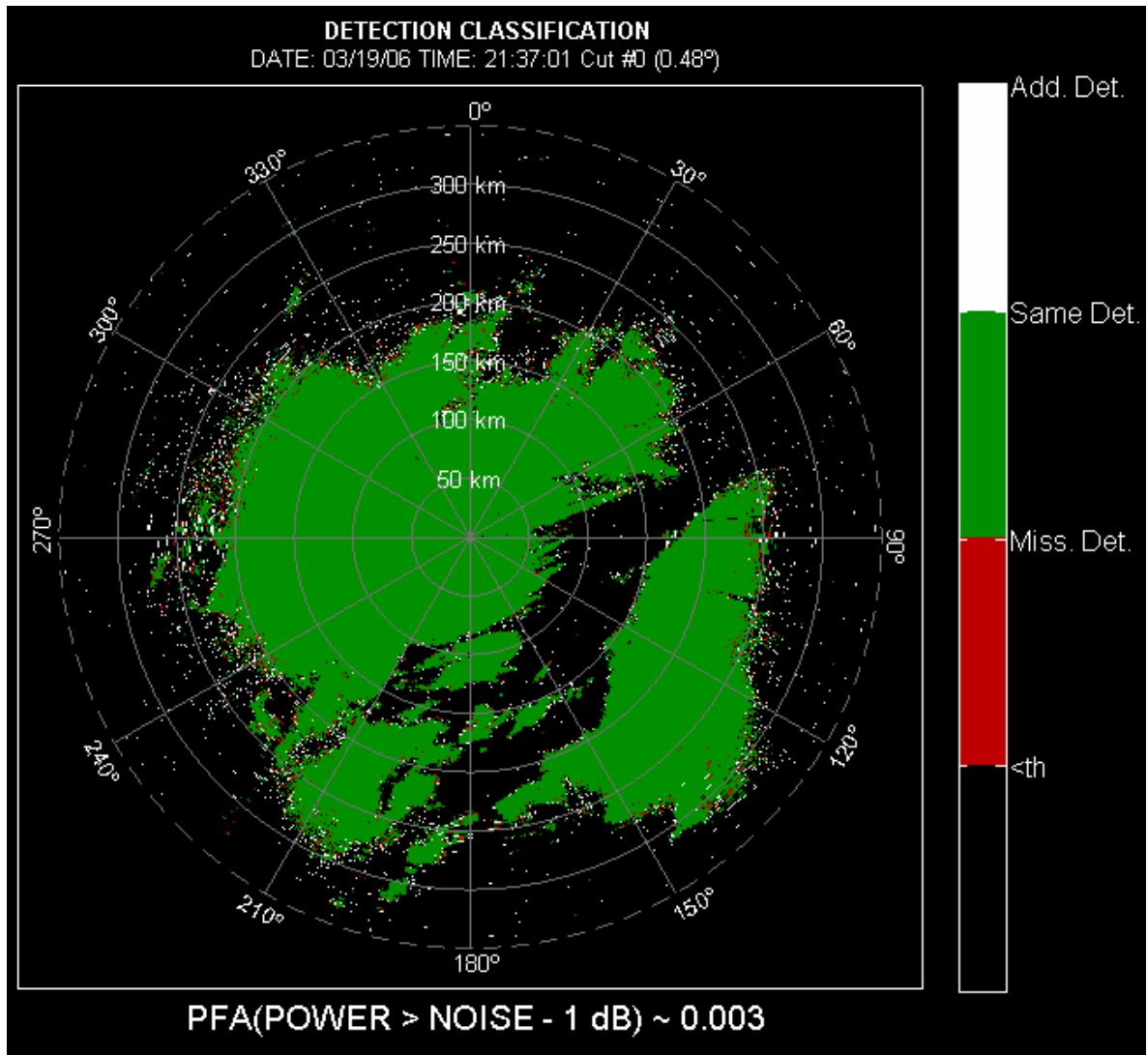
Figure 6.2 The histogram of the SNR distribution in the horizontal channel before the noise power is doubled.

The ratio of H and V noise powers for this data set is $N_v/N_h = 0.8269$. Thus, for implementation, optimal weights (i.e., which produce maximum POD) were found for Z_{DR} ranging from 0 to 6 dB. These are shown in Table 6.1. The resulting PODs as a function of Z_{DR} for these and the unity weights are evaluated using simulation and are in Figure 6.5. As shown at the end of section 5.6, the results are similar for most of the weight combinations except for the case of differential reflectivity of ≥ 4 dB. Most of our concern is for detection of signals with H power smaller than 2 to 3.5 dB above the noise level. At such SNR, noise influences the estimates significantly. Consequently, it seems logical that more emphasis ought to be put on detection of signals with lower differential reflectivities, simply because the cumulative SNR ratio for such signals is higher; thus resulting in more detections and better estimates. Following this rationale, it appears

more beneficial to choose weight arrangements that produce better results for lower Z_{DR} values than those that put more emphasis on detection of signals with higher Z_{DR} .

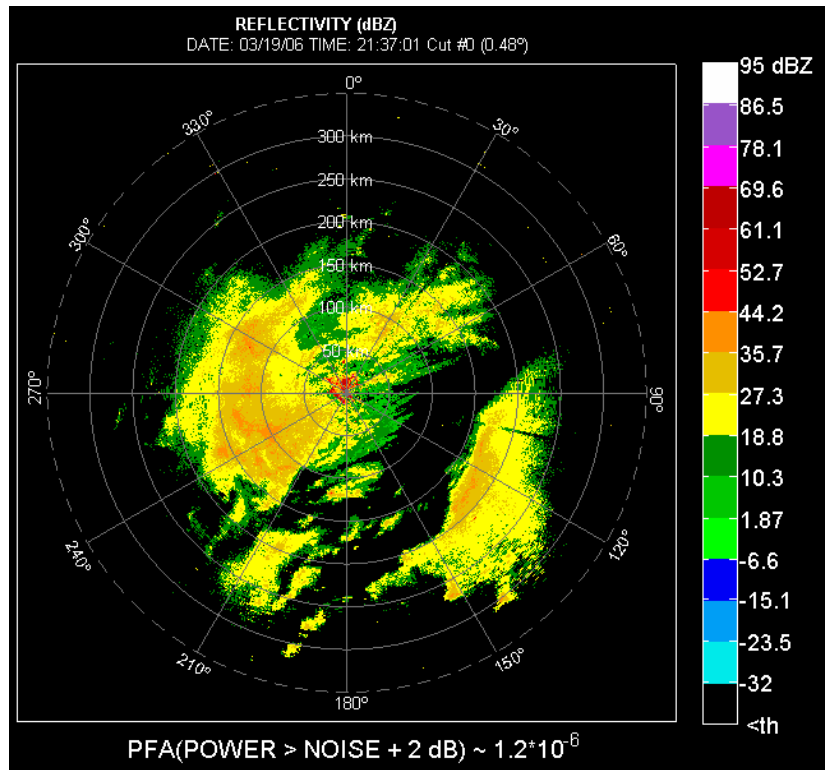


(a)

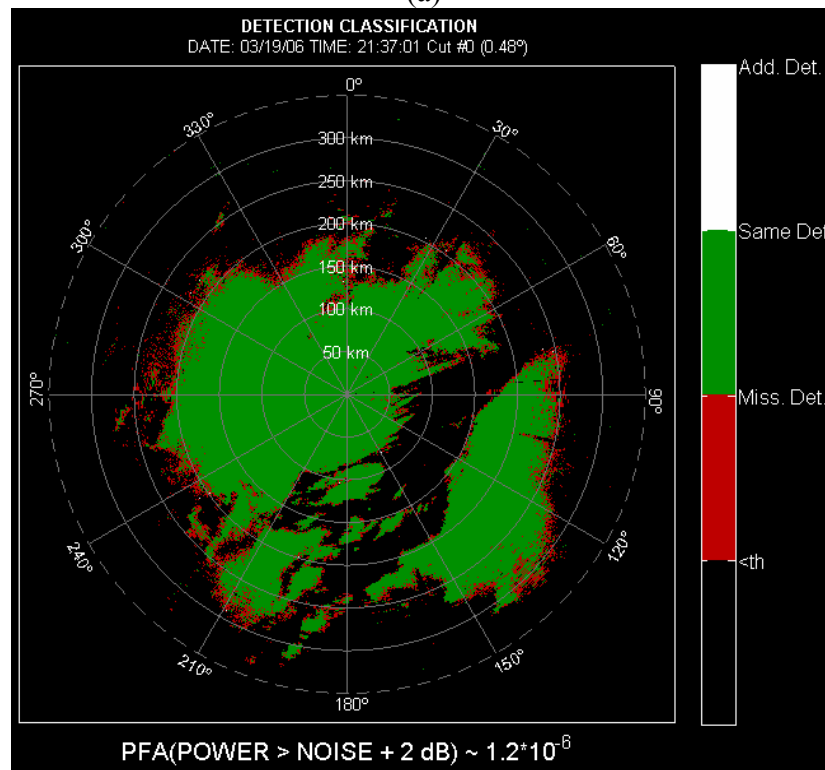


(b)

Figure 6.3 Reflectivity field (a) and the classification of detections (b) obtained after doubling the noise power, but not changing the threshold.



(a)



(b)

Figure 6.4 Reflectivity field (a) and the classification of detections (b) obtained after doubling the noise power, and increasing the threshold to 2 dB above the doubled noise power.

Z_{DR}	α	β	γ
0	1.5	1.5	2
1	1.5	1.5	2
2	1	1.5	2
3	1	1.5	2
4	0.5	1	1
5	0.5	1	1
6	0.5	1	1

Table 6.1 POD maximizing weights for $N_v/N_h = 0.8269$.

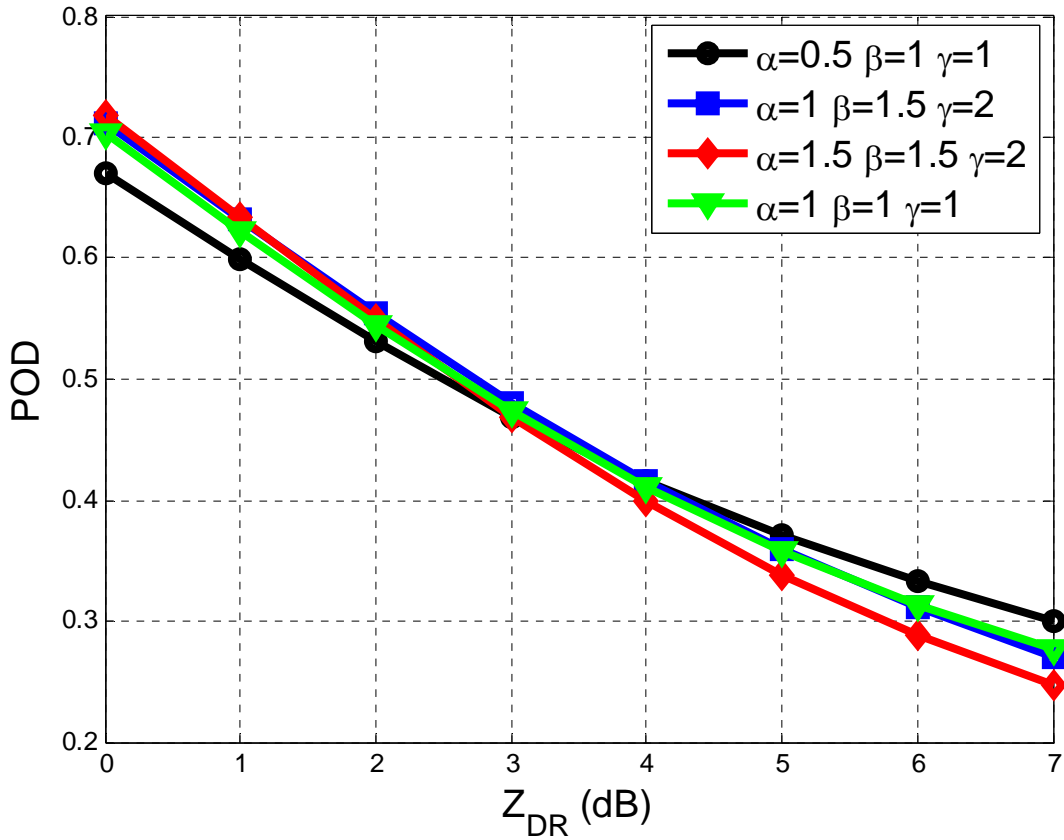
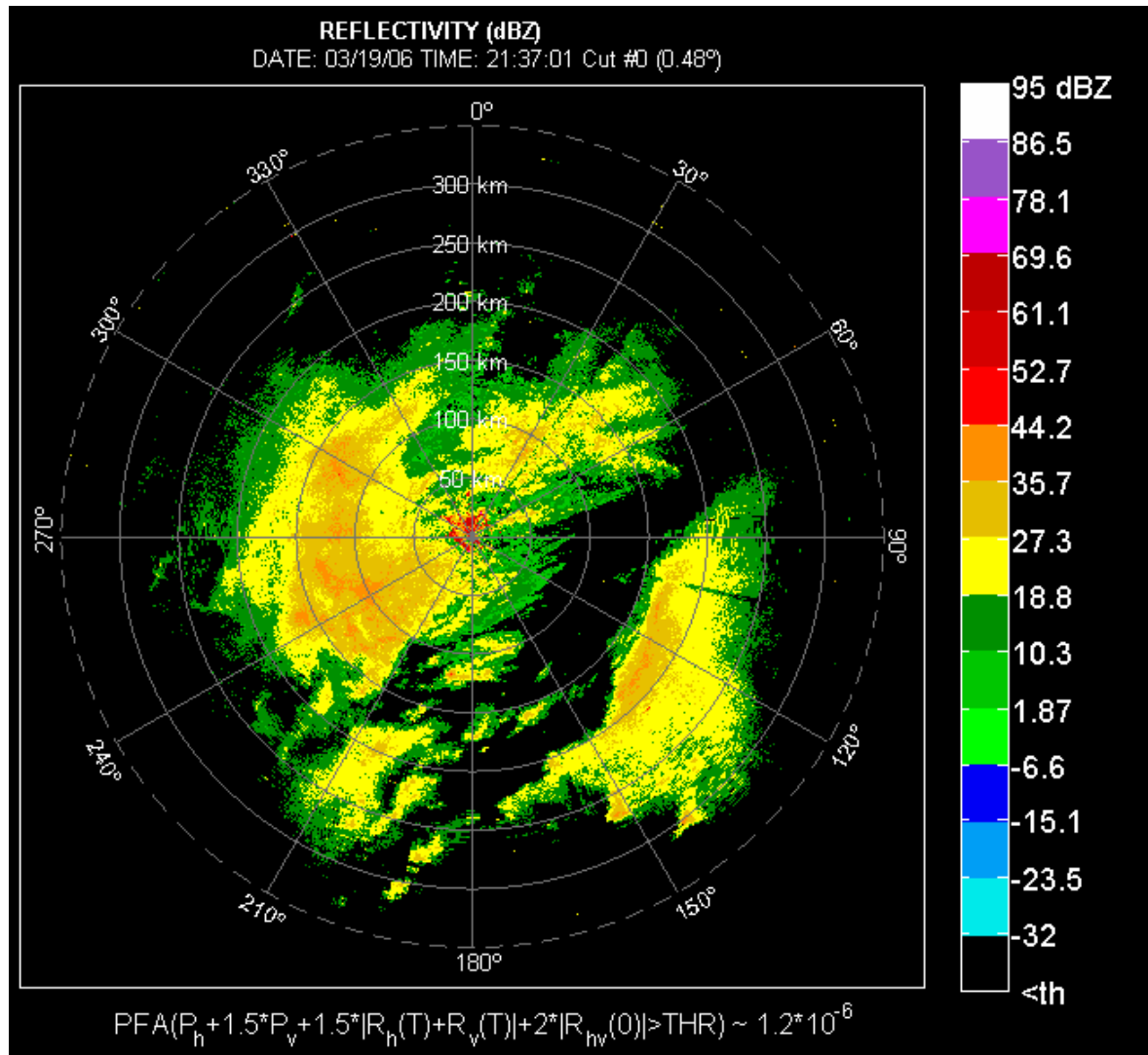


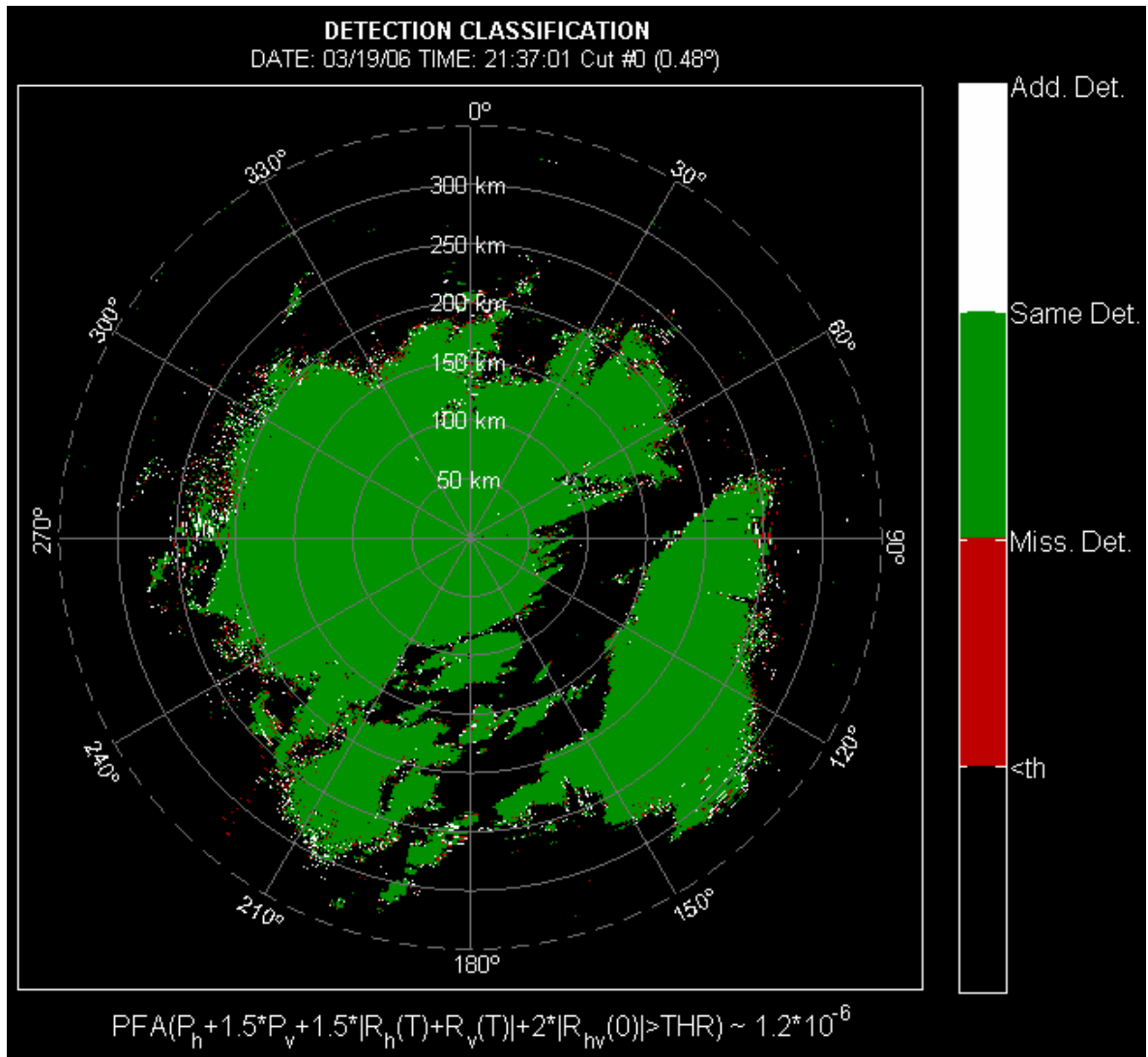
Figure 6.5 POD for different weight combinations as a function of varied Z_{DR} , and $SNR = 0$ dB, $M = 17$, $\sigma_v = 2$ m s⁻¹, $\rho_{hv} = 0.96$, $N_v/N_h = 0.8269$, and $PFA = 1.2 \times 10^{-6}$.

Results for the case of $\alpha = 1.5$, $\beta = 1.5$, and $\gamma = 2$ are shown in Figure 6.6. In addition, the results using the OR combination are shown in Figure 6.7. To assess how change in weights influences the performance on real data, the resultant reflectivity fields, and detections classifications, are shown in Figure 6.8, to Figure 6.11 for weight values of $\alpha = 1$, $\beta = 1.5$, $\gamma = 2$, $\alpha = 0.5$, $\beta = 1$, $\gamma = 1$, and the uniform weights (i.e., $\alpha = 1$, $\beta = 1$,

$\gamma = 1$), respectively. Notice that the choice of weight combinations is the same as in Figure 6.5.

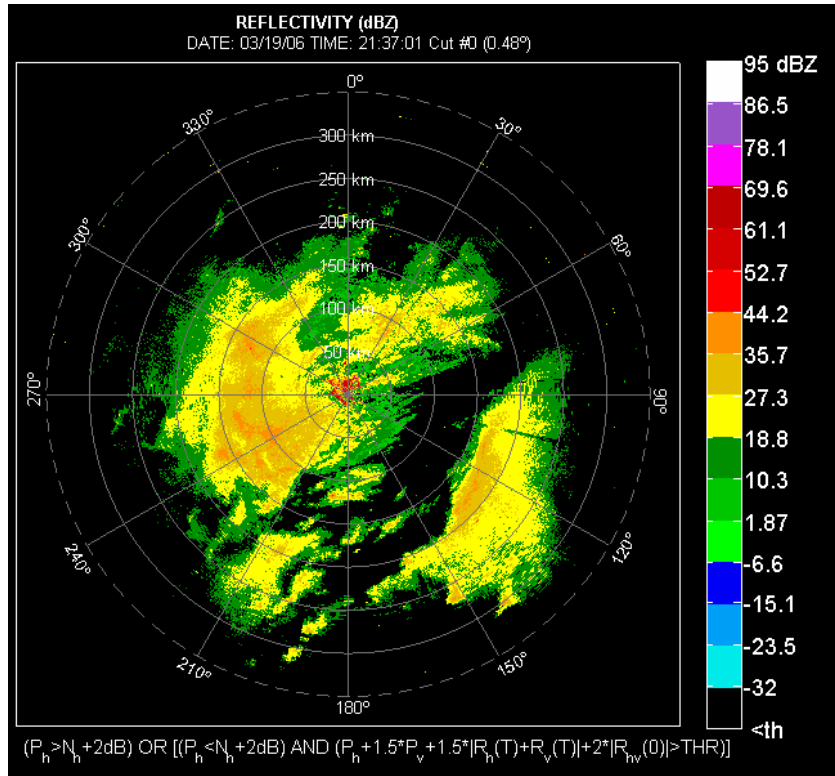


(a)

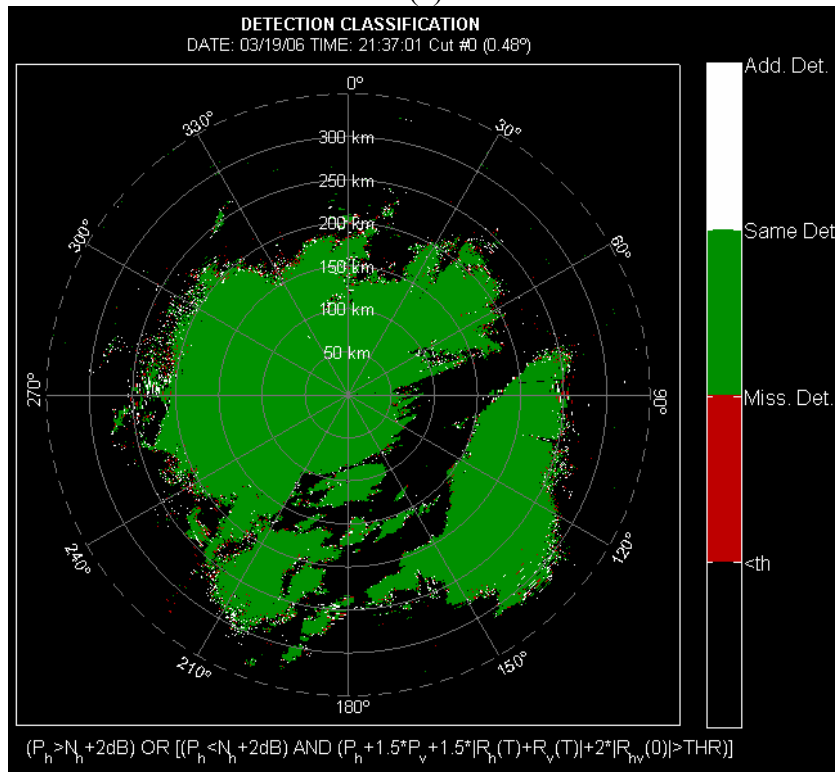


(b)

Figure 6.6 Reflectivity field (a) and the classification of detections (b) obtained after doubling the noise power, and using the weighted sum for detection.

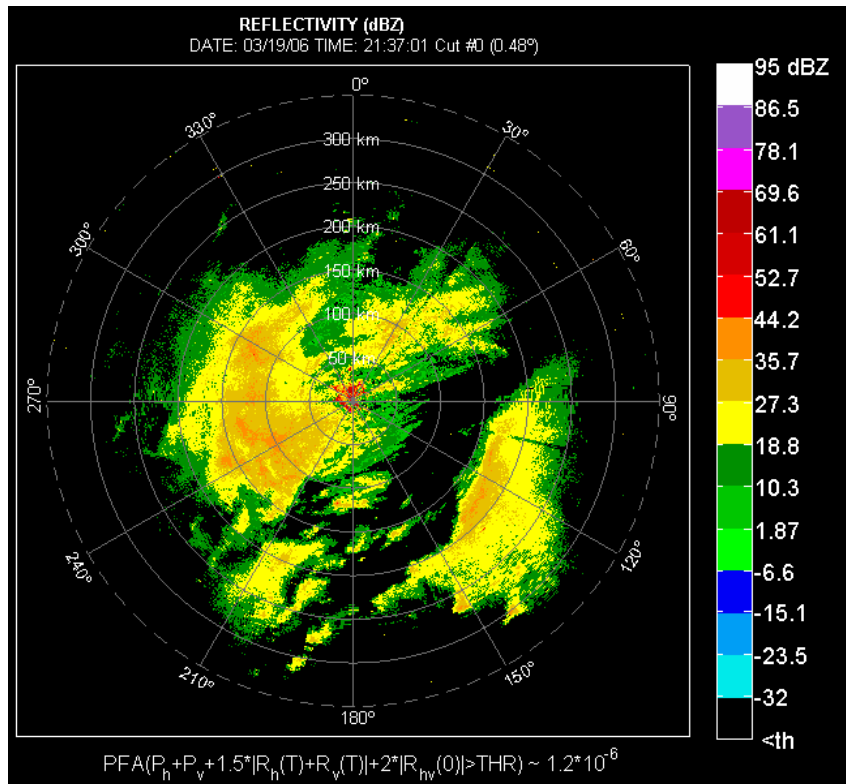


(a)

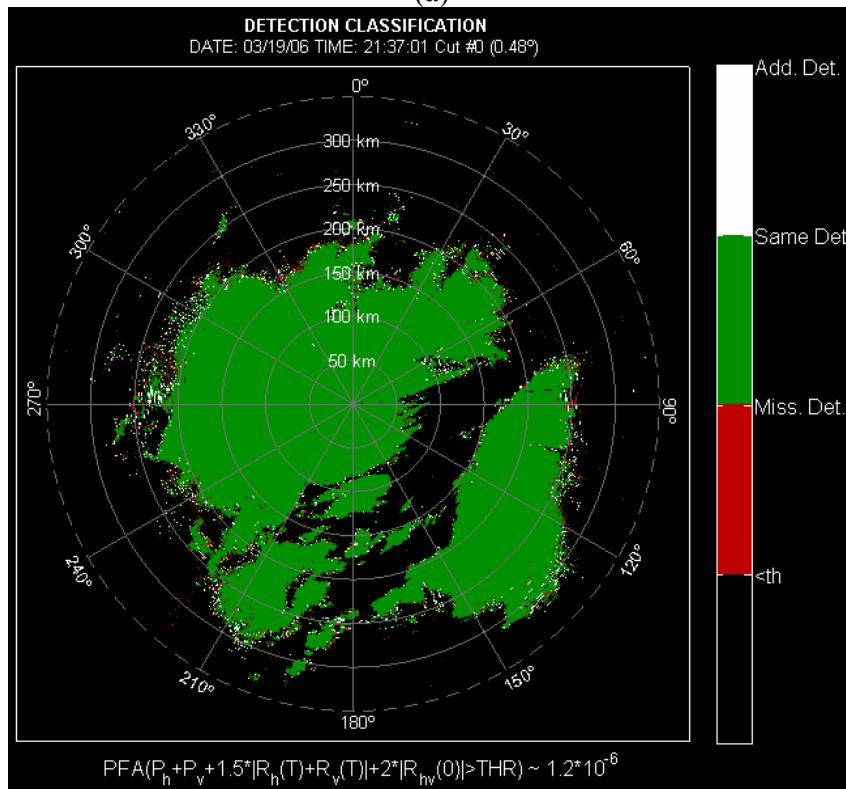


(b)

Figure 6.7 Reflectivity field (a) and the classification of detections (b) obtained after doubling the noise power, and using the OR combination of power and weighted sum for detection.

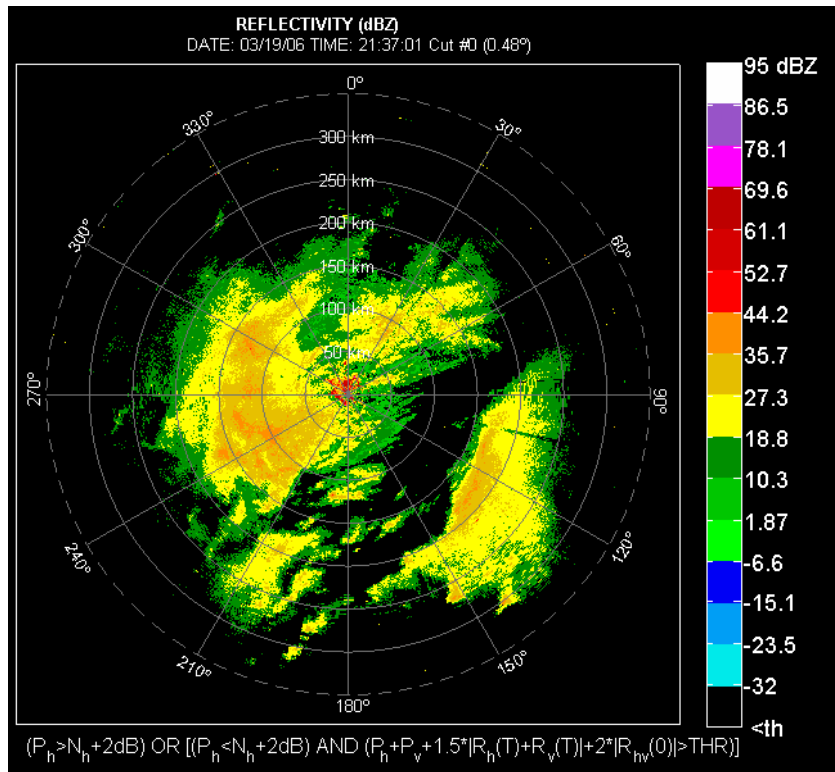


(a)

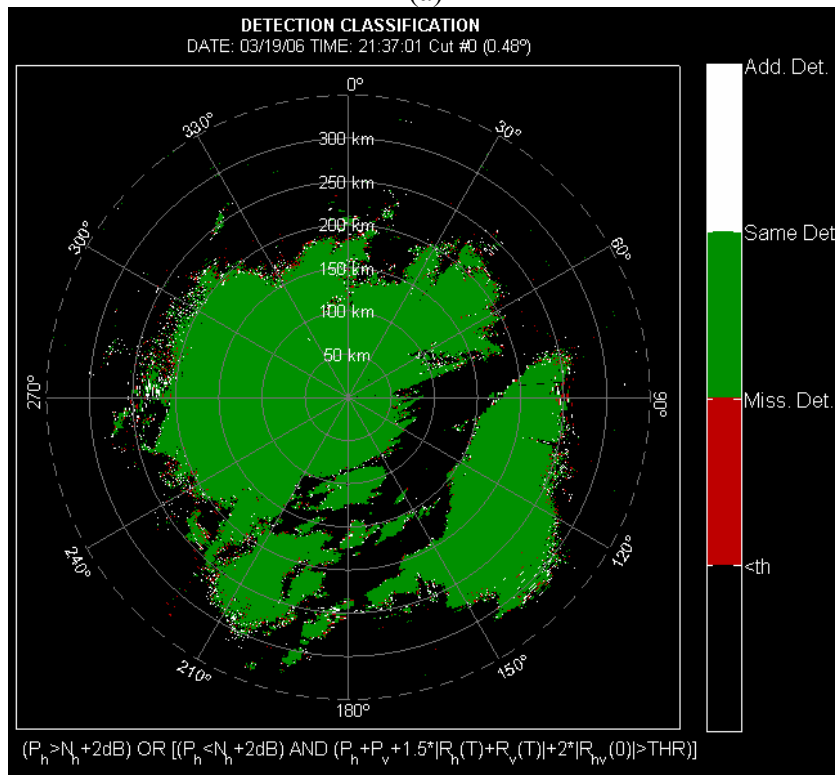


(b)

Figure 6.8 Reflectivity field (a) and the classification of detections (b) obtained after doubling the noise power, and using the weighted sum for detection.

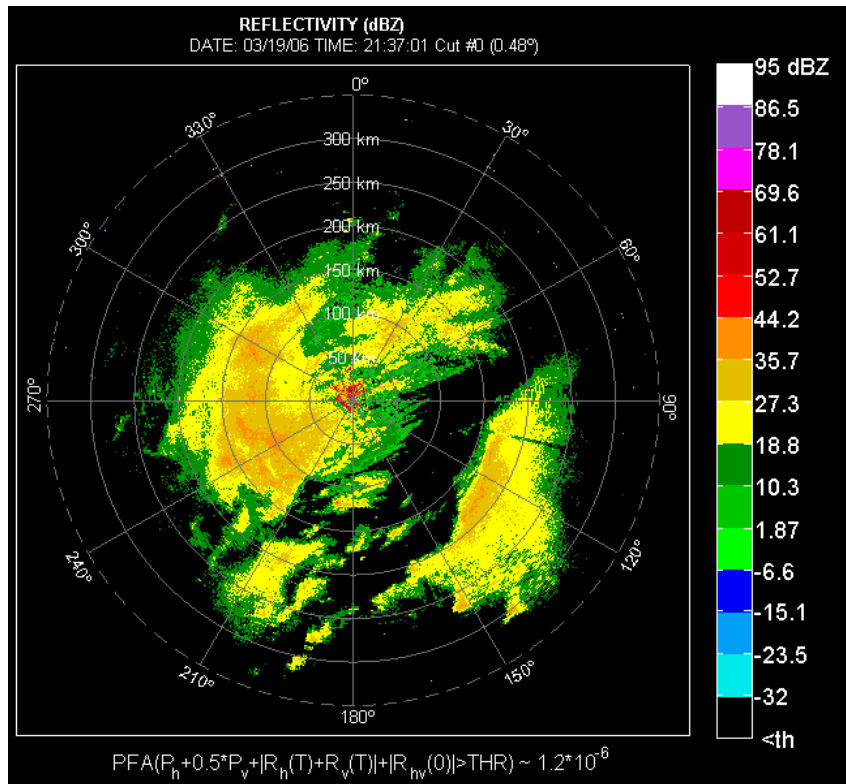


(a)

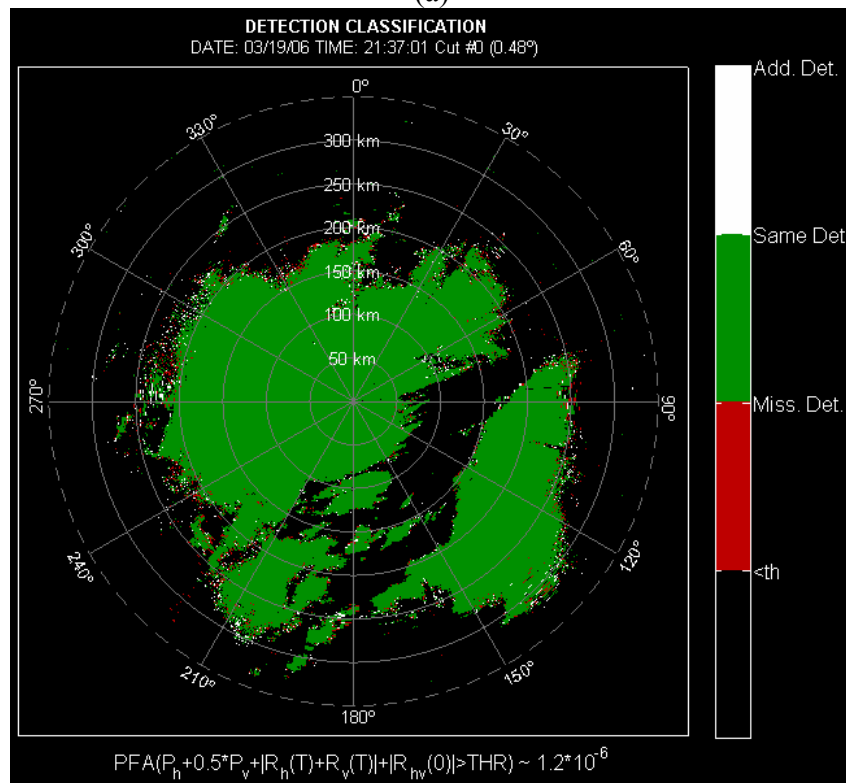


(b)

Figure 6.9 Reflectivity field (a) and the classification of detections (b) obtained after doubling the noise power, and using the OR combination of power and weighted sum for detection.

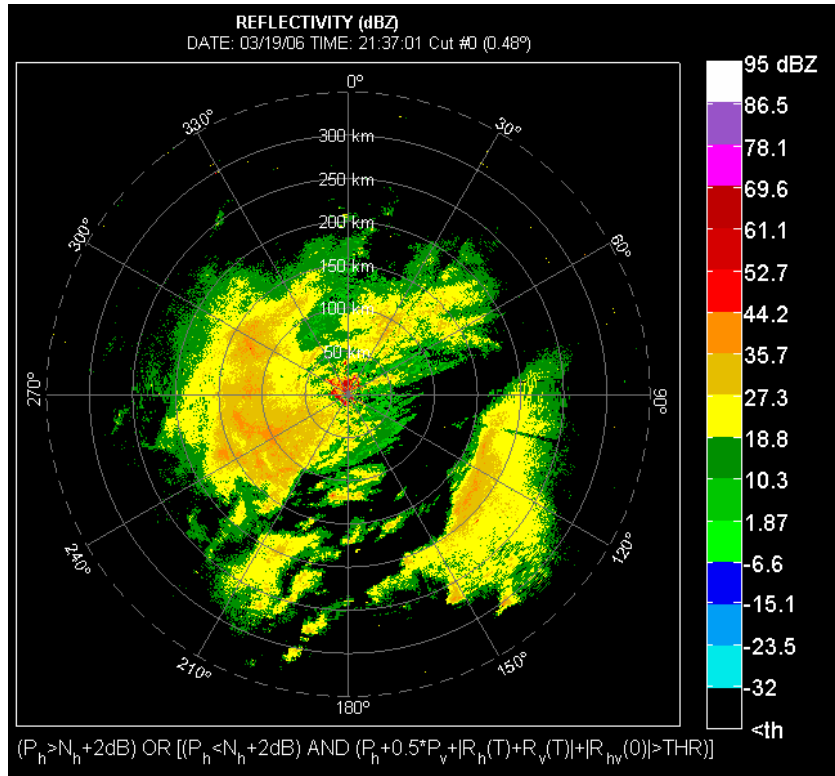


(a)

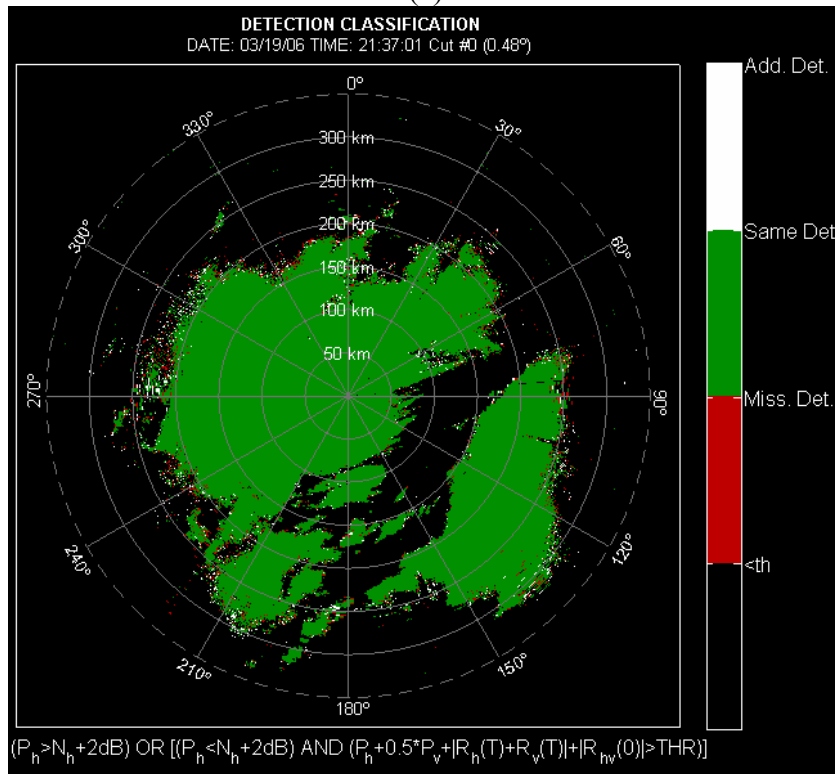


(b)

Figure 6.10 Reflectivity field (a) and the classification of detections (b) obtained after doubling the noise power, and using the weighted sum for detection.

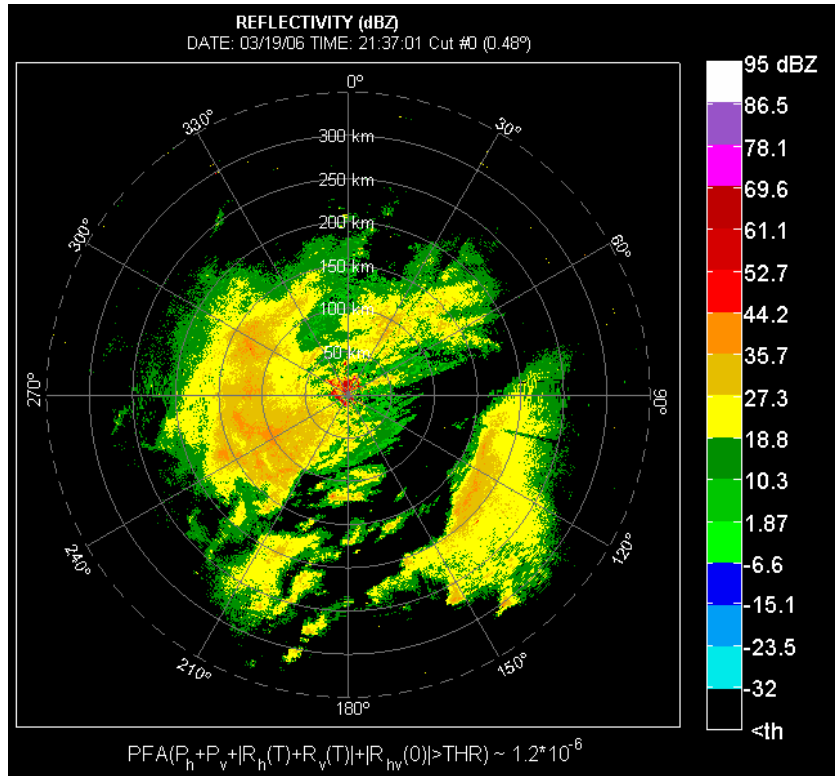


(a)

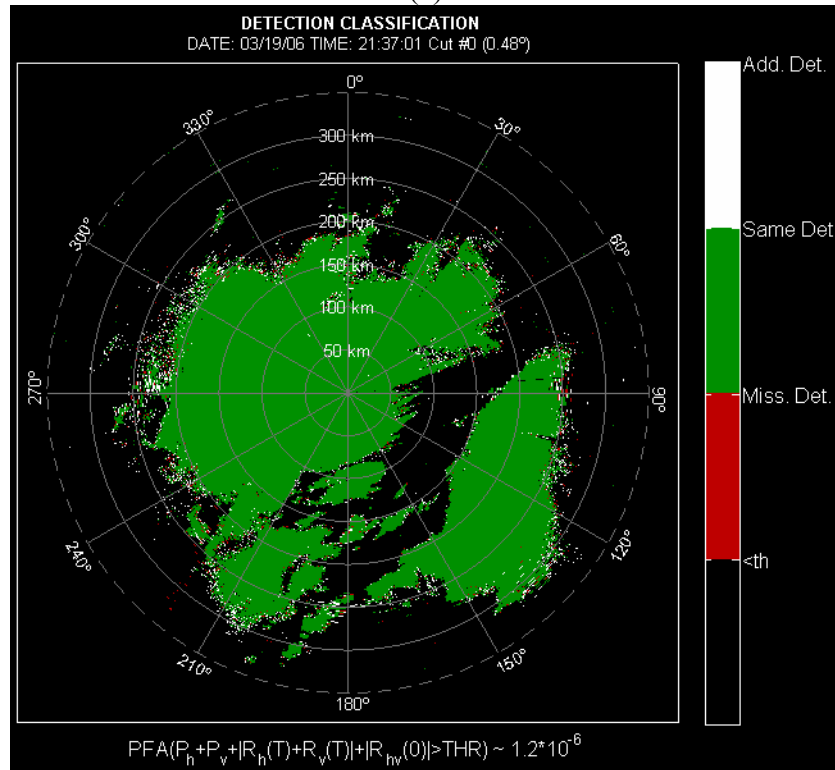


(b)

Figure 6.11 Reflectivity field (a) and the classification of detections (b) obtained after doubling the noise power, and using the OR combination of power and weighted sum for detection.



(a)



(b)

Figure 6.12 Reflectivity field (a) and the classification of detections (b) obtained after doubling the noise power, and using the uniform sum for detection.

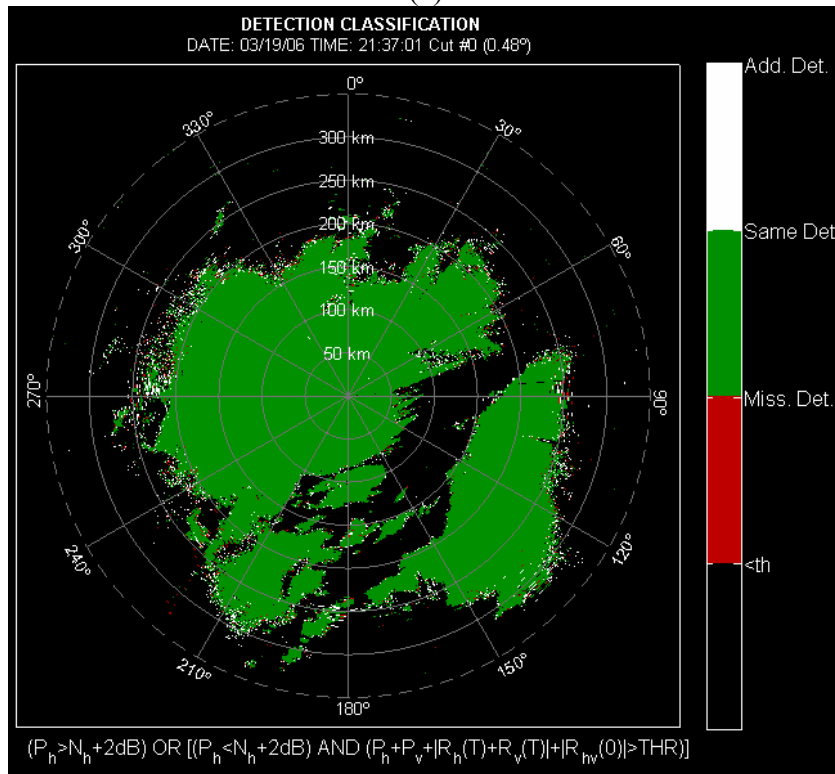
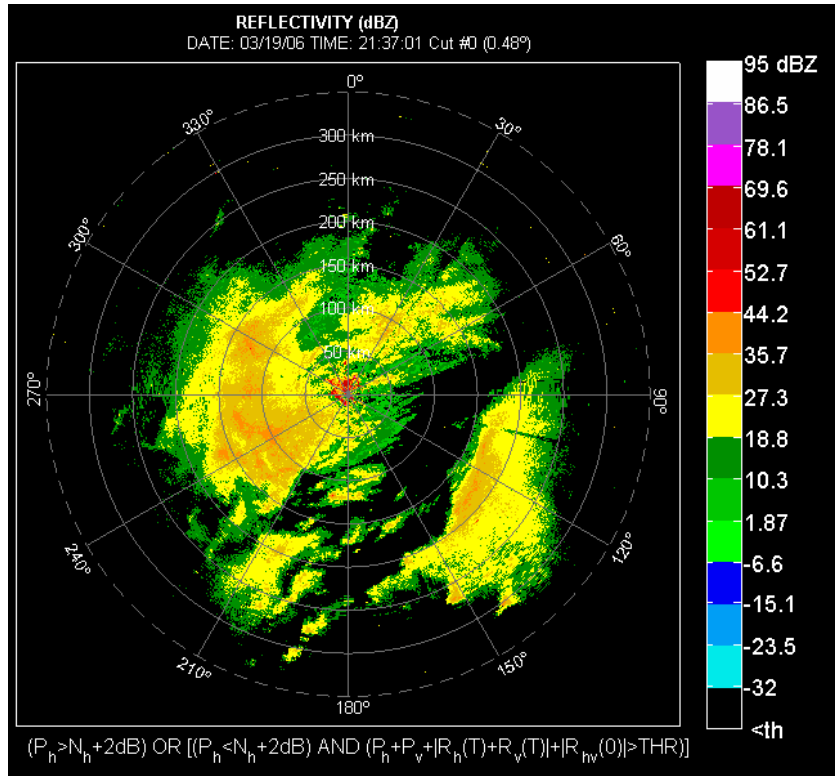


Figure 6.13 Reflectivity field (a) and the classification of detections (b) obtained after doubling the noise power, and using the OR combination of power and uniform sum for detection.

A visual comparison of reflectivity fields for various weights indicates that the differences are subtle. It can be observed that most of the features on the perimeter (i.e., of low reflectivity) have been recovered in all cases. To quantify the performance, the ratio of detections is introduced. Let us consider the PPI image as a matrix of size $360 \times NRB$, where NRB stands for the *Number of Range Bins*. Let W denote the original reflectivity PPI matrix where each element is the power value, in H channel, at the given PPI location. Let $MN(D)$ denote the matrix for the case of reflectivity with doubled noise power and each element is either 1 or 0 depending on the decision that signal is present at a given PPI location or not. D in the brackets denotes the decision test used in determining the matrix entries. Then the values in the row termed as the *Ratio of total detections* are calculated as:

$$\frac{\text{num}([W \geq NOISE + 2dB].*MN(D))}{\text{num}([W \geq NOISE + 2dB])} \quad (6.2)$$

The *Greater than* operator is binary (1 if true, and 0 if false) and is applied to each element in the matrix to produce a new matrix with values of 0 and 1. The operator $.*$ acts as an element-wise matrix multiplication (same as in MATLAB). The *num* operator determines the total number of 1s in the matrix. The *Ratio of bounded detections* is obtained as:

$$\frac{\text{num}([NOISE + 5dB \geq W \geq NOISE + 2dB].*MN(D))}{\text{num}(NOISE + 5dB \geq W \geq NOISE + 2dB)} \quad (6.3)$$

This ratio essentially gives the number of range bins that fall below the 2 dB threshold due to the 3 dB loss in power, but are still detected using the approach being evaluated. The *Ratio of additional detections* is:

$$\frac{\text{num}([W < \text{NOISE} + 2\text{dB}] \cdot \text{MN}(D))}{\text{num}(W \geq \text{NOISE} + 2\text{dB})} \quad (6.4)$$

This ratio gives the number of bins that are originally censored, but are detected as signals using the evaluated detector function.

The described statistics is summarized in Table 6.2 and Table 6.3, for the weighted sum and the OR combination, respectively, as defined in (6.2), (6.3), and (6.4). According to the statistics, the best detection of the signals with power smaller than 2 dB above noise, was achieved for weights $\alpha = 1.5$, $\beta = 1.5$, and $\gamma = 2$ (i.e., 83%), and the worst for $\alpha = 0.5$, $\beta = 1$, and $\gamma = 1$ (i.e., 79%). The performance for $\alpha = 1$, $\beta = 1.5$, and $\gamma = 2$ and the uniform sum was practically identical and only $\sim 0.7\%$ worse than the best recovery rate. The results in the tables are in agreement with the simulation results and both imply that the benefits of the weighted sum are minimal. They also verify that the uniform sum produces detection rates almost equal to the maximum ones obtained by non-uniform weighting.

α, β, γ	1.5, 1.5, 2	1, 1.5, 2	0.5, 1, 1	1, 1, 1
<i>Ratio of total detections</i>	0.985014	0.984376	0.981211	0.984358
<i>Ratio of bounded detections</i>	0.827755	0.821095	0.786889	0.820519
<i>Ratio of additional detections</i>	0.021214	0.019522	0.014455	0.018693

Table 6.2 Real data statistics comparison for various weights in the sum when $N_v/N_h = 0.8269$, and $\text{PFA} = 1.2 \cdot 10^{-6}$.

α, β, γ	1.5, 1.5, 2	1, 1.5, 2	0.5, 1, 1	1, 1, 1
<i>Ratio of total detections</i>	0.985215	0.984565	0.981314	0.984482
<i>Ratio of bounded detections</i>	0.829621	0.822791	0.787786	0.821720
<i>Ratio of additional detections</i>	0.021233	0.019541	0.014469	0.018707

Table 6.3 Real data statistics for the power/weighted sum OR combination when $N_v/N_h = 0.8269$ and $\text{PFA} = 1.2 \cdot 10^{-6}$.

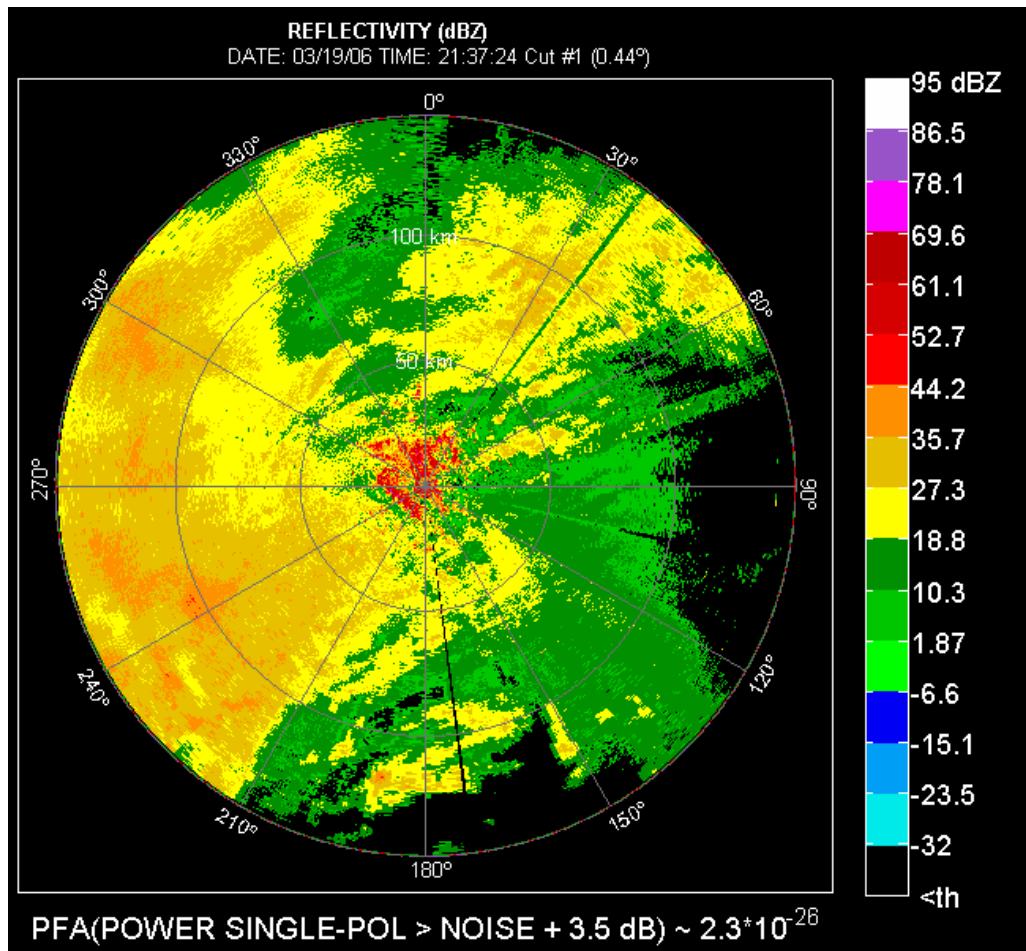
The statistics for power thresholds and uniform sum is given in Table 6.4. Note that when the power threshold is -1 dB below noise as well as when power & uniform sum or uniform sum only is used, approximately 2.6% and 1.9%, respectively, of the bins that initially were censored are detected as signals. In Figure 6.3, Figure 6.12, and Figure 6.13, these *additional detections* are highlighted for all three cases. It can be observed that the *additional detections* gained by the uniform sum (as well as those gained by the weighted sum) are predominantly located at the perimeter of the weather phenomena. This reinforces the hypothesis that the majority of these detections are indeed valid weather returns.

D	$P \geq N_h - 1 \text{ dB}$	$P \geq N_h + 2 \text{ dB}$	P&UNIFORM SUM	UNIFORM SUM
<i>Ratio of total detections</i>	0.982318	0.912253	0.984482	0.984358
<i>Ratio of bounded detections</i>	0.801132	0.141260	0.821720	0.820519
<i>Ratio of additional detections</i>	0.026012	0.000166	0.018707	0.018693

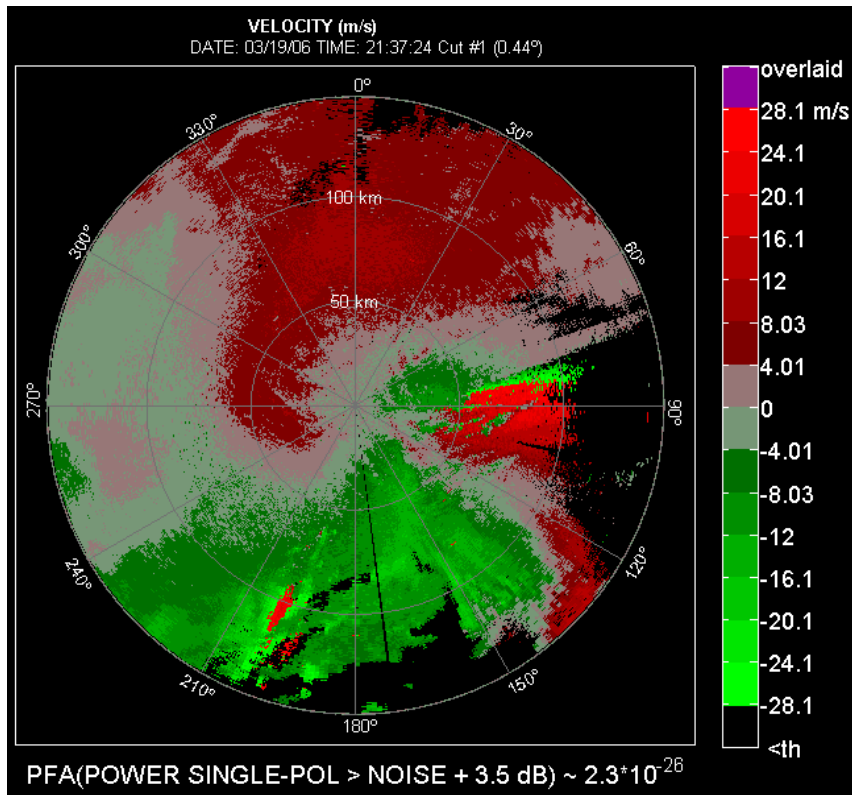
Table 6.4 Real data statistics for surveillance scan collected on 03/19/06.

The next case is the scan of the same weather system, where data were collected with $M = 52$, right after the collection with $M = 17$ (i.e., as part of the same volume coverage pattern). Because this is a Doppler scan, both reflectivity and velocity fields are presented in Figure 6.14. For Doppler scans the default threshold on all WSR-88Ds is $SNR > 3.5$ dB, so it is used as standard for comparisons. After adding noise to the time series data in both H and V channels, the reflectivity/velocity field in Figure 6.15 is obtained, as well as the corresponding detection classification image. As expected there is apparent loss of data compared to the “single-pol” case. To recuperate this lost data, a lower SNR threshold of 0.5 dB is applied, and the result is in Figure 6.16. By visual comparison the reflectivity/velocity fields in Figure 6.14 and Figure 6.16 appear the same. This is also

supported by the lack of missed detections in Figure 6.16 (c). One would, however, expect the velocity field to be more cluttered by speckles after lowering the threshold (as in the case of the surveillance scan). This, however, does not happen; after lowering the threshold to 0.5 dB, the image is still very similar to the one in “single-pol” with the 3.5 dB threshold. The lack of cluttering from speckles can be explained by examining the false alarm rates for 3.5 and 0.5 dB thresholds. These are very low, 2.3368×10^{-26} and 2.1429×10^{-10} , respectively. Lowering the threshold to 0.5 dB (with $M = 52$) significantly increases the rate of false alarms compared to the case where 3.5 dB threshold is applied. Nonetheless, the probability of false detections still remains so low and therefore, no significant speckling in the reflectivity or the velocity fields is apparent.

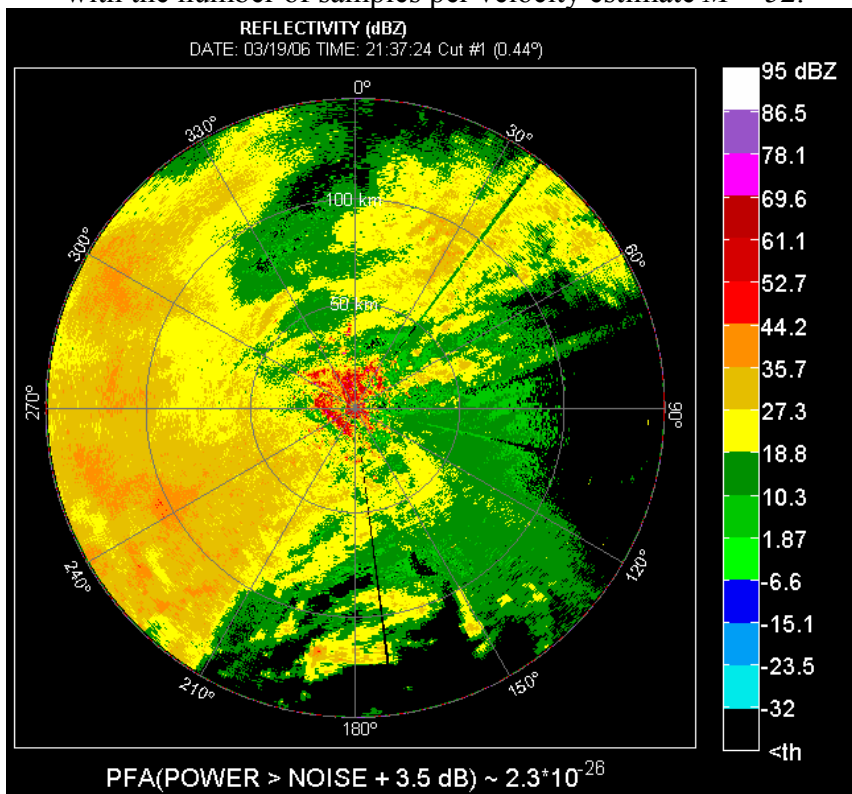


(a)

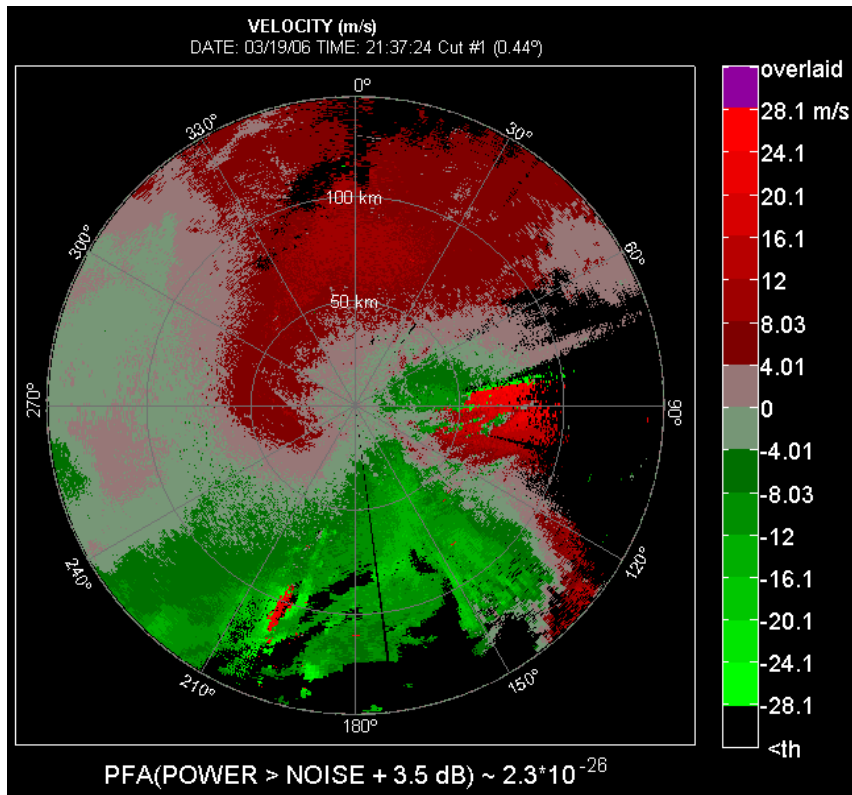


(b)

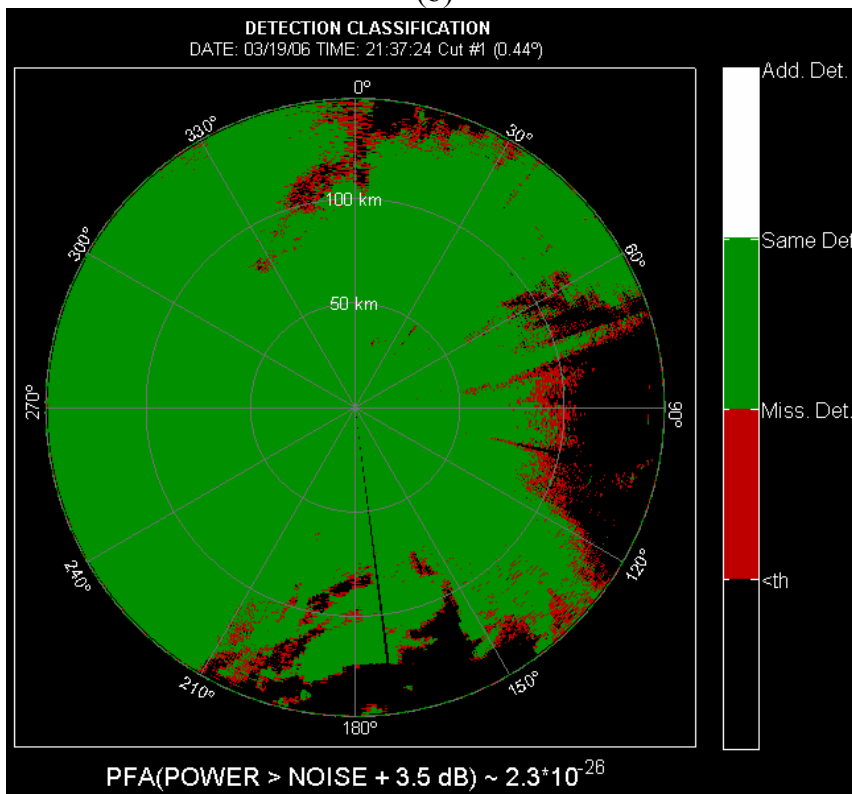
Figure 6.14 Reflectivity (a) and mean velocity (b) fields for SNR threshold of 3.5 dB with the number of samples per velocity estimate $M = 52$.



(a)



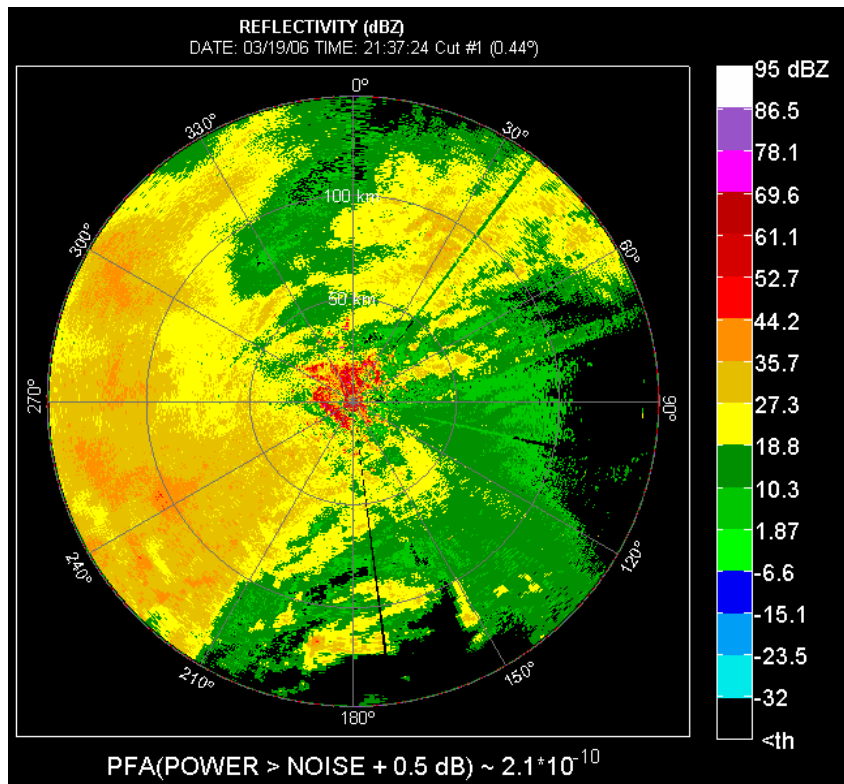
(b)



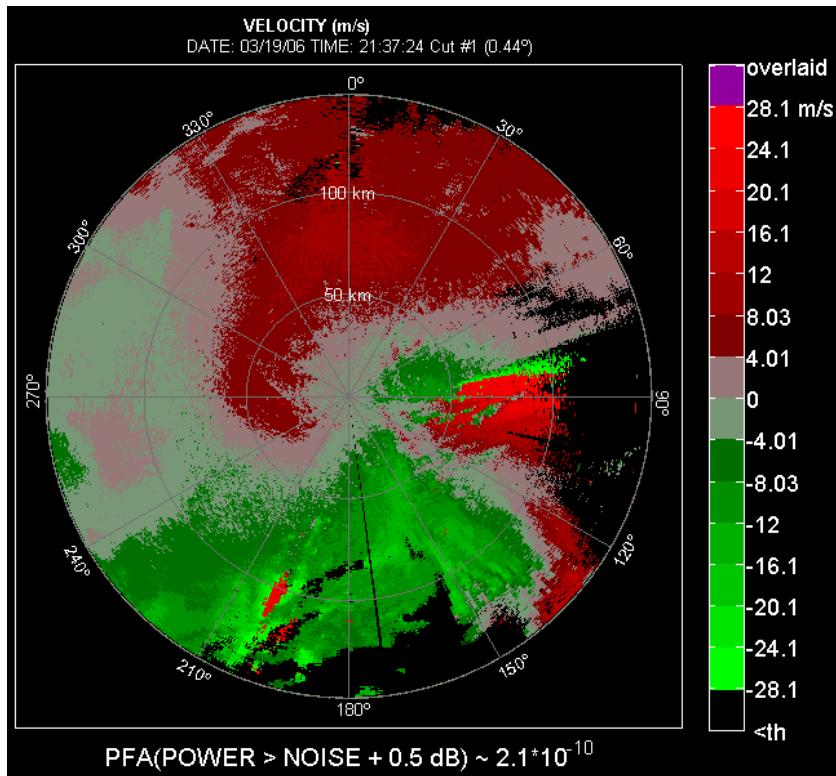
(c)

Figure 6.15 Reflectivity (a) and velocity (b) fields with the classification of detections (c) obtained after doubling the noise power, but not changing the threshold.

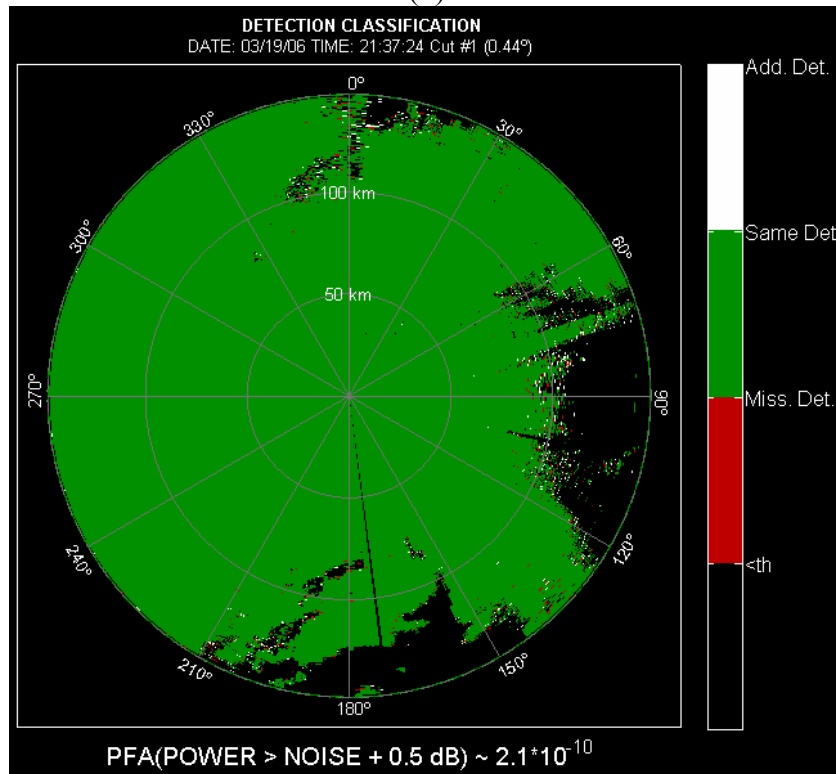
The field obtained after application of threshold based on the weighted sum, with $\alpha = 1.5$, $\beta = 1.5$, and $\gamma = 2$ is now discussed. The velocity field obtained is shown in Figure 6.17. Obviously the area of “useful” data is noticeably larger than in the cases where power thresholds were applied. This is not surprising because the false alarm rate for the “best” sum is 1.2×10^{-6} which is much higher than the false alarm rate for any of the power thresholds. Consequently, the probability of detecting the signal is also relatively high compared to the probability of detection for the cases based on power thresholds. For comparison, the same is done when the uniform sum is used, and the results are shown in Figure 6.18. Moreover, the performance of the power threshold approach for PFA of 1.2×10^{-6} (using eq. (A.11) in Appendix A we get power threshold to be -1 dB) is demonstrated in Figure 6.19. The statistical comparison between the power thresholds with weighted and uniform sum is given in Table 6.5.



(a)

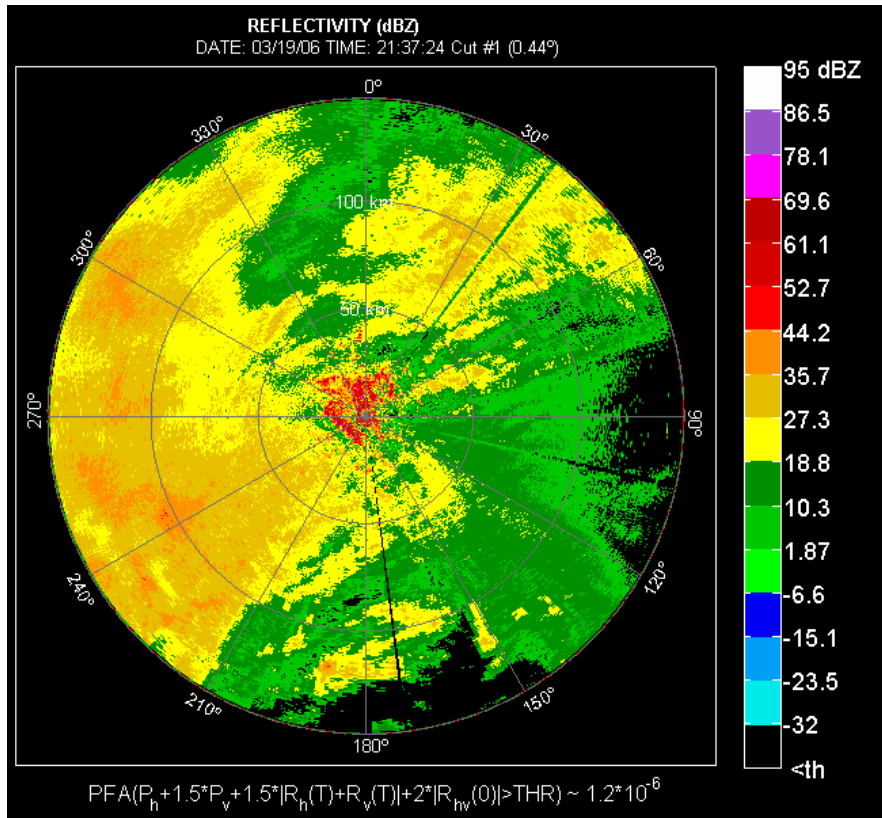


(b)

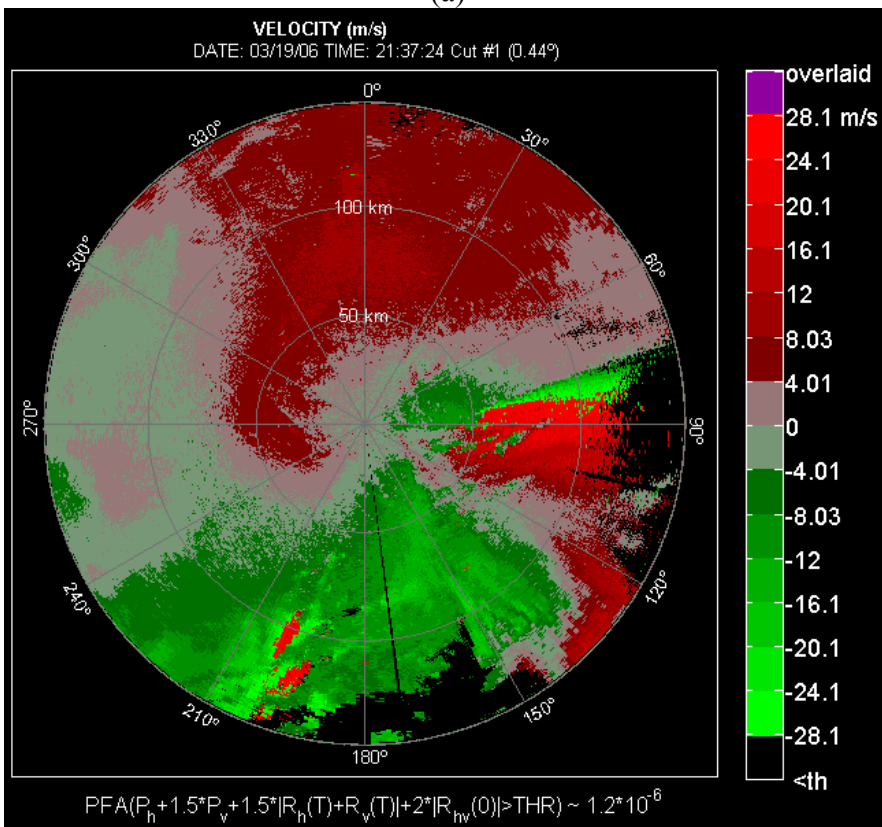


(c)

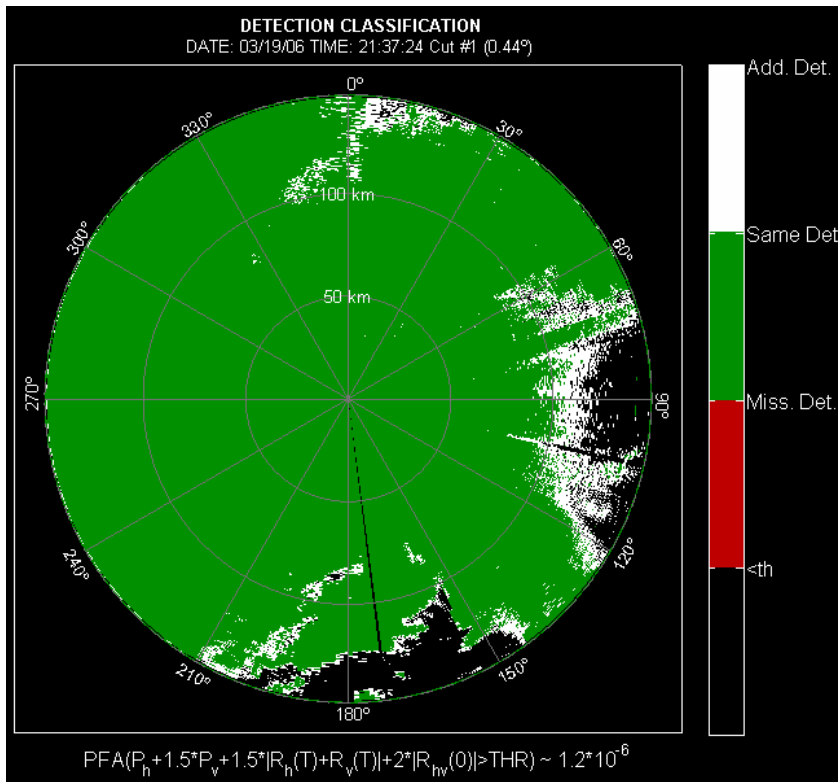
Figure 6.16 Reflectivity (a) and mean velocity (b) fields with the classification of detections (c) obtained by lowering the threshold to 0.5 dB above the artificially doubled noise.



(a)

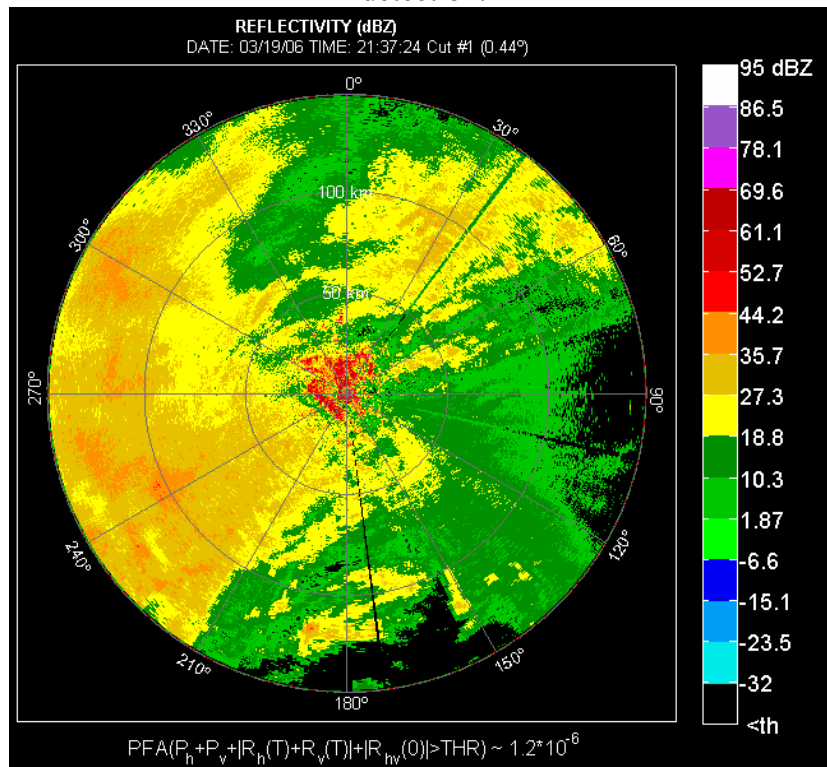


(b)

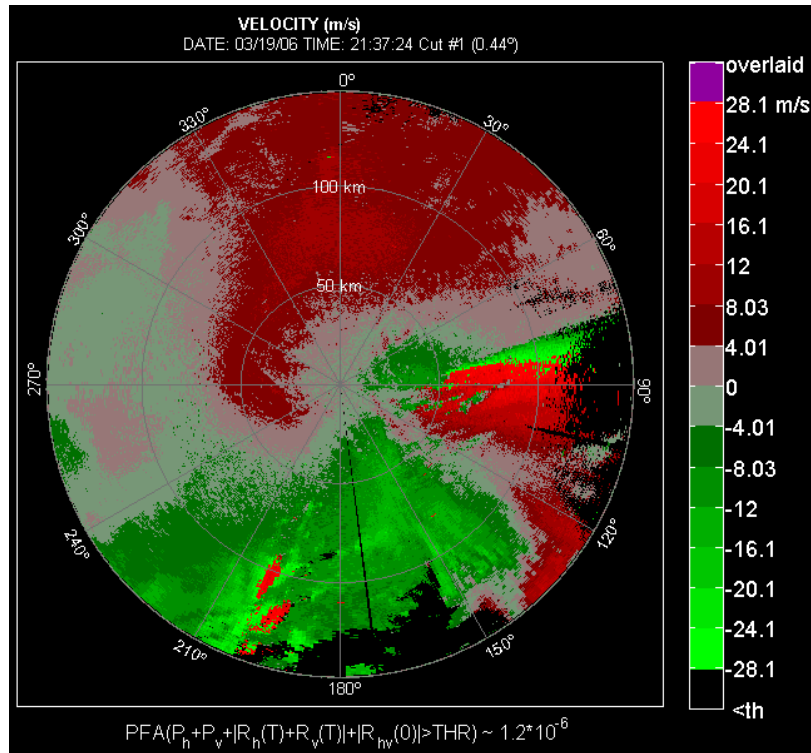


(c)

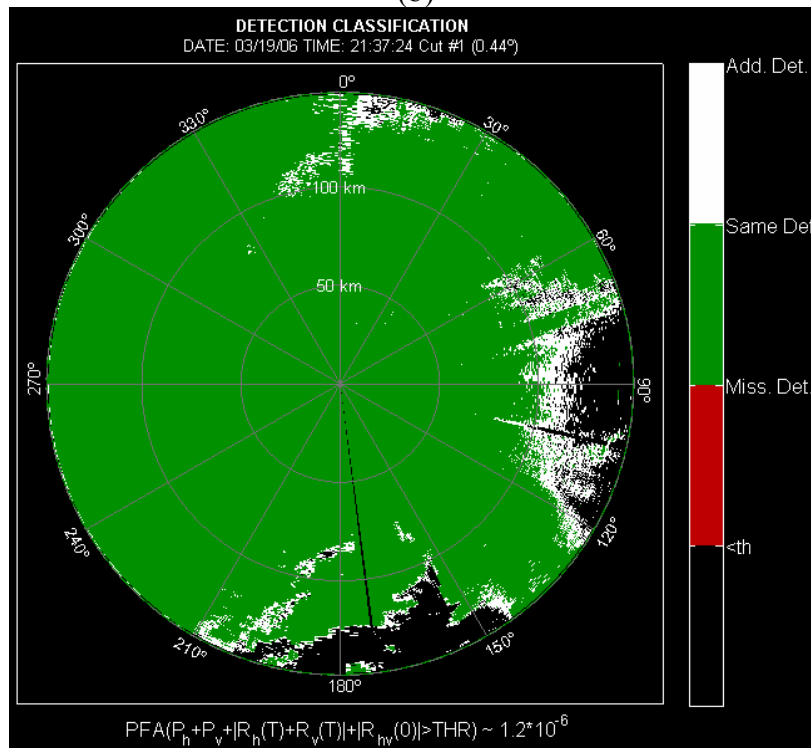
Figure 6.17 Reflectivity (a) and mean velocity (b) fields with the classification of detections (c) obtained after doubling the noise power, and using the weighted sum for detection.



(a)



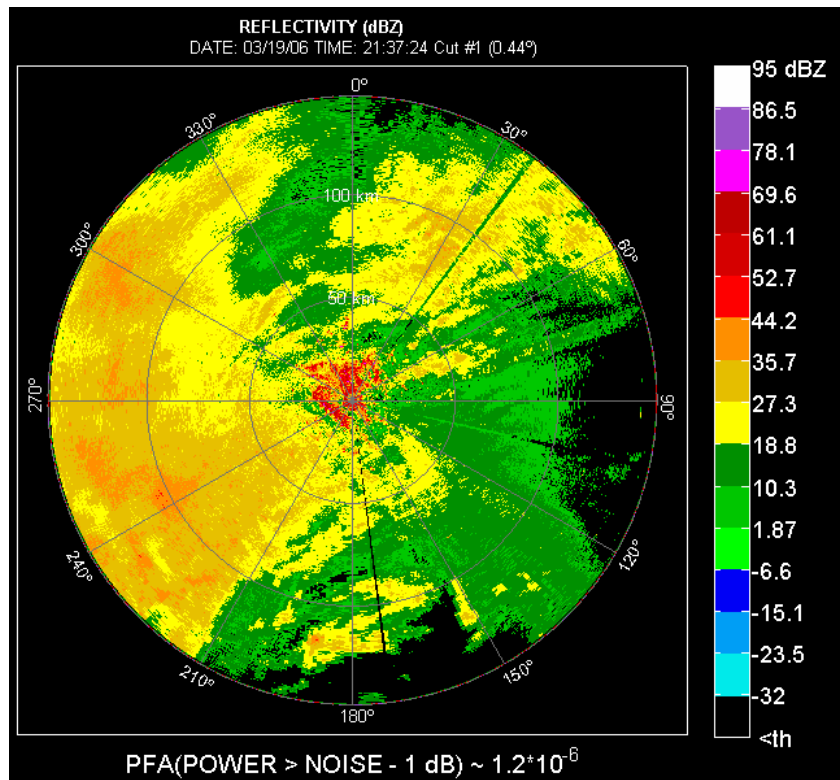
(b)



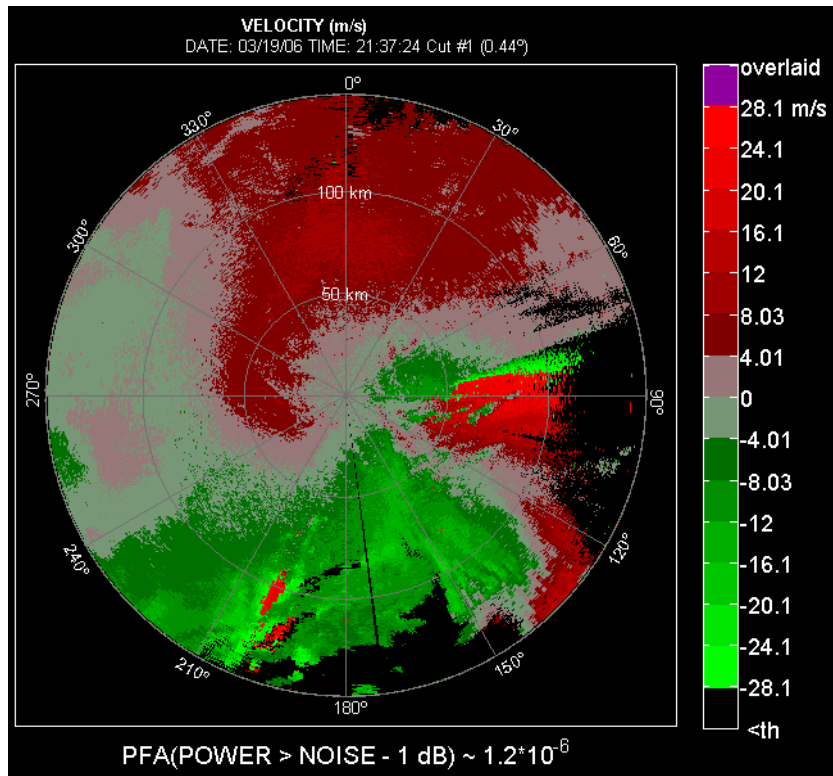
(c)

Figure 6.18 Reflectivity (a) and mean velocity (b) fields with the classification of detections (c) obtained after doubling the noise power, and using the uniform sum for detection.

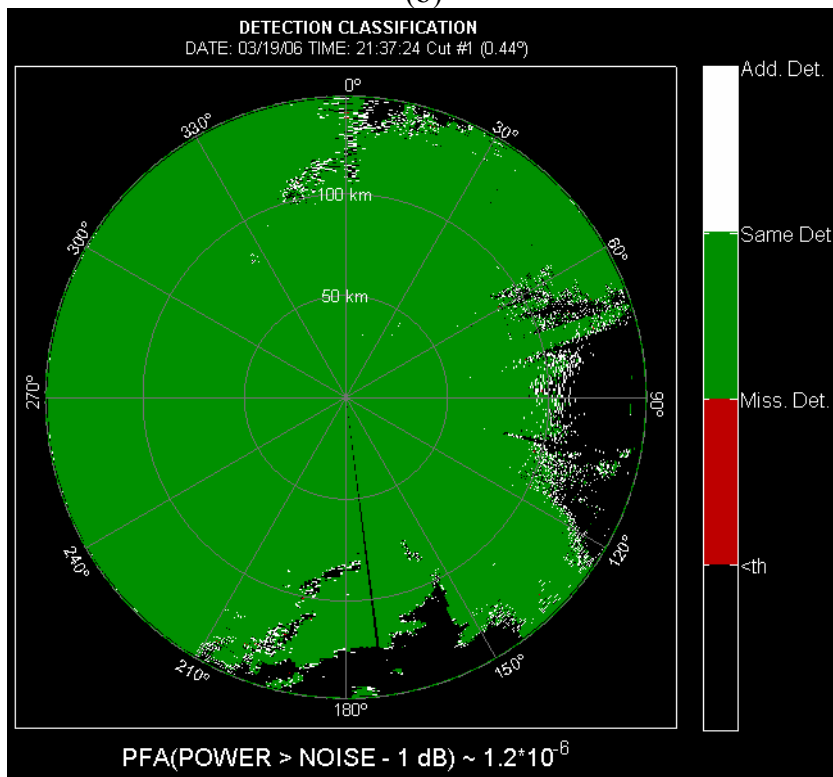
The statistics presented in Table 6.5 indicates that the performance of both weighted sum and uniform sum is extremely similar. The weighted sum produces miniscule improvement of 0.08% in *additional detections* (some improvement is expected as weighted sum is tuned to the actual ratio N_v/N_h). By setting the power threshold to -1 dB above the noise (so the PFA equals that of the weighted/uniform sum), we achieve the performance of a uniform sum when detecting signals that fall below the threshold of 3.5 dB after doubling the noise power (i.e., *bounded detections*). The difference occurs when comparing detections of range bins that fall below the power threshold before doubling noise (i.e., in “single-pol”) but are detected after the noise has been doubled (i.e., in “dual-pol”) using one of the improved detection schemes (i.e., *additional detections*). This comparison shows that the uniform sum detects 3.3% more than the power based thresholding given the same PFA.



(a)



(b)



(c)

Figure 6.19 Reflectivity (a) and mean velocity (b) fields with the classification of detections (c) obtained by lowering the power threshold to -1 dB above the artificially doubled noise.

To better understand to how gains in detections would benefit real operations, and particularly in the case of the Doppler scan, the range unfolded velocities are shown in Figure 6.20 to Figure 6.24. The previous scan with $M = 17$ and a long PRT with unambiguous range of 466 km was used for unfolding. The Figure 6.20 was obtained from the original data using surveillance scan for range unfolding. A range location, that contains several overlaid echoes, is deemed resolved only if a signal exists that is 5 dB larger than the sum of the returns from all other trips.

<i>Decision criteria</i>	$P \geq N_h + 3.5\text{dB}$	$P \geq N_h + 0.5\text{dB}$	$P \geq N_h - 1\text{dB}$	WEIGHTED SUM	UNIFORM SUM
<i>PFA</i>	2.34×10^{-26}	2.14×10^{-10}	1.2×10^{-6}	1.2×10^{-6}	1.2×10^{-6}
<i>Ratio of total detections</i>	0.956255	0.996208	0.999842	1.0	1.0
<i>Ratio of bounded detections</i>	0.055355	0.675441	0.740029	0.741758	0.741758
<i>Ratio of additional detections</i>	0	0.003514	0.016587	0.050202	0.049198

Table 6.5 Real data statistics for Doppler scan with $M = 52$, and weights $\alpha = 1.5$, $\beta = 1.5$, $\gamma = 2$.

Also, if a signal is detected at a range location, but all other range locations, from which potential overlaid echoes can originate in Doppler scan, are classified as noise; such range location is deemed resolved. To simulate the dual-pol situation with the unaltered censoring scheme, Figure 6.21 is obtained using exactly the same processing as for Figure 6.20, except that noise was doubled. By visual comparison, one notices the expected loss of features, especially at ranges beyond 150 km (i.e., unambiguous range of the Doppler scan). Power based thresholds were relaxed to -1 and 0.5 dB for surveillance and Doppler scan, respectively, to obtain Figure 6.22. Visual comparison reveals that lowering power thresholds produces the results similar to the original “single-pol” case.

This conclusion is supported by the statistics in Table 6.6. Namely, if we add the values from the third and the fifth row in column three (i.e., *total* and *additional detections*), we obtain the overall number of detections of approximately 100% of those in the “single-pol”. Note that even though the *ratio of total detections* is ~99%, the overall ~100% is obtained by adding the *additional detections* that amount to ~1%. Small difference in detection distribution can be attributed to statistical uncertainty. The detection threshold for power is even further relaxed to -1 dB in Doppler scan to attain the PFA of 1.2×10^{-6} , which resulted in the velocity field presented in Figure 6.23. Both visual evaluation and the statistics in Table 6.6 suggest a gain of 0.7% with respect to the total body of detections in the “single-pol”. It is interesting to note that in both Figure 6.22, and Figure 6.23 no apparent speckle cluttering is present even though the rate of false detections in surveillance scan is 0.003 (i.e., power threshold is lowered to -1 dB above noise). This is because the PFA in the corresponding Doppler scan remains low. Thus, all of the false detections that occur during the surveillance scan are discarded.

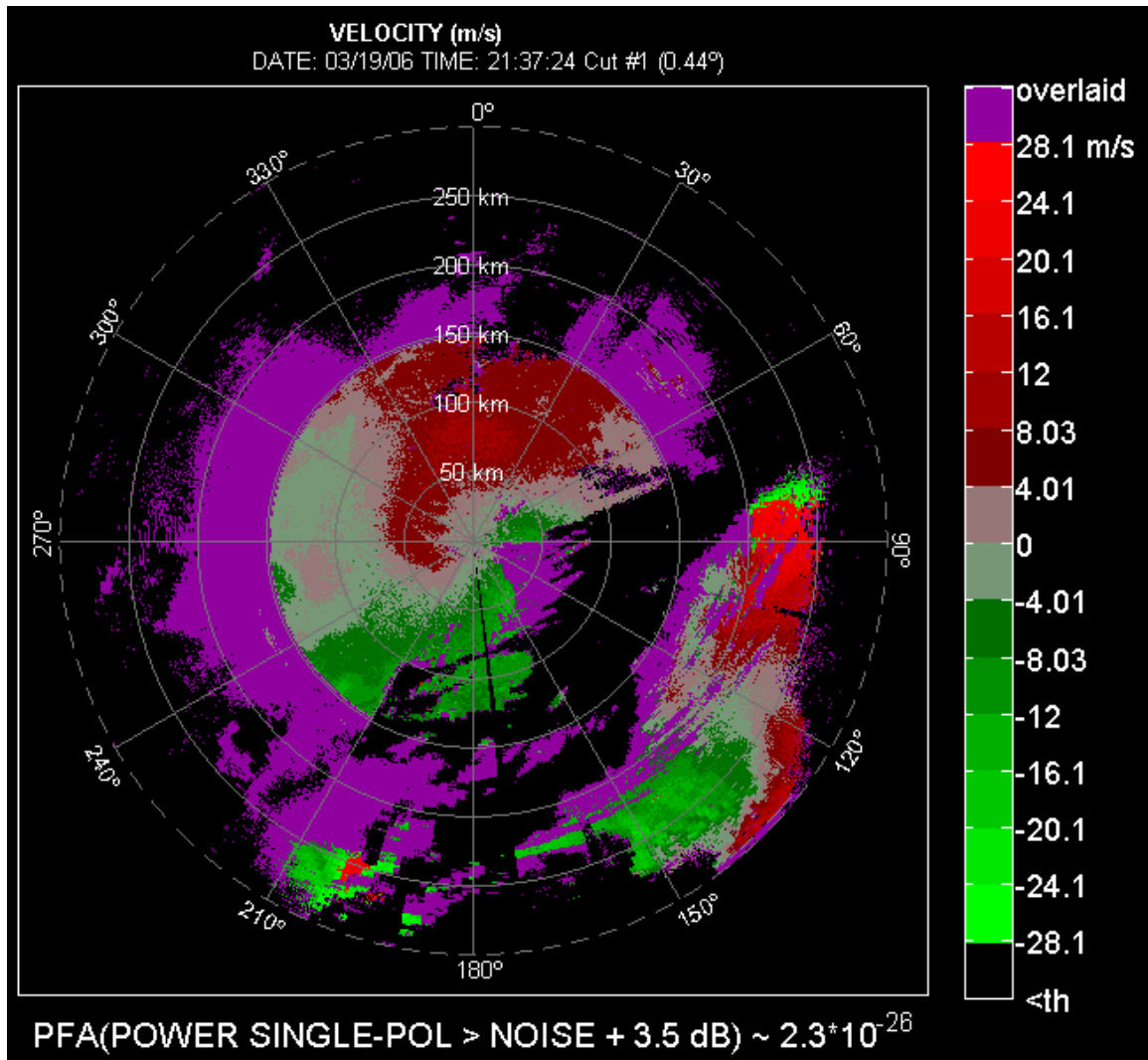


Figure 6.20 Original range unfolded velocity field for *SNR* thresholds of 2 and 3.5 dB in surveillance and Doppler scans, respectively. Sample numbers *M* are 17, and 52 in surveillance and Doppler scans, respectively.

Finally, Figure 6.24 shows the resulting velocity field where the uniform sum was used for detection in both scans. Visual comparison to the “single-pol” image in Figure 6.20 shows noticeable increase in detections. This is further quantitatively verified by statistics in Table 6.6, which shows that the addition of the ratios of *total* and *additional detections* amounts to 2.7% more detections than in “single-pol” case.

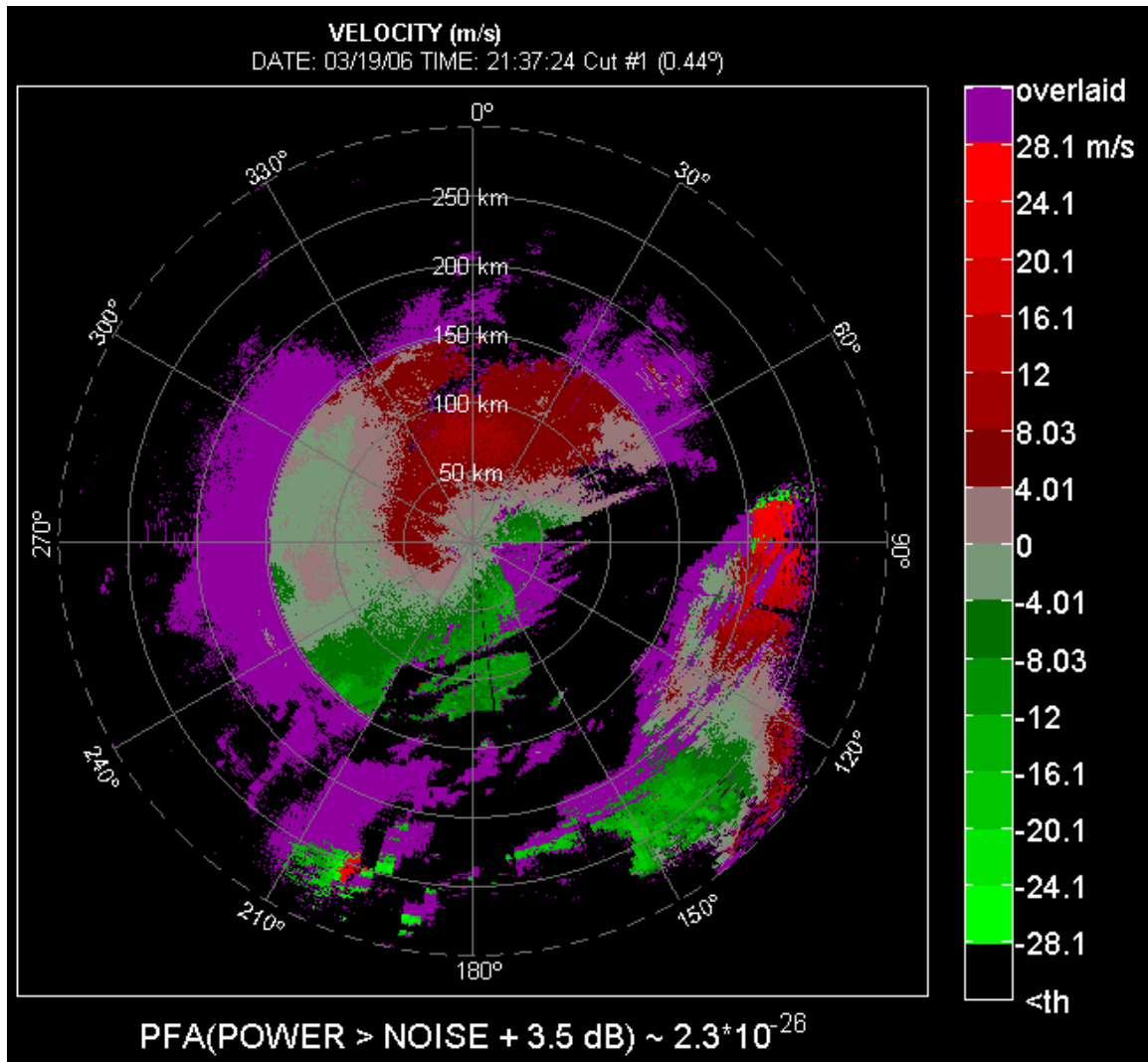


Figure 6.21 Unfolded velocity field obtained after doubling the noise power, but not changing the thresholds.

In Table 6.7 to Table 6.10 real data statistics (for data collected on 03/09/06) dependent on the N_v/N_h ratio for the same weight combinations as in Figure 5.12 and Figure 5.13 is given. The results in Table 6.7 show that the weights $\alpha = 1$, $\beta = 1.5$, and $\gamma = 2$ produce the most detections when compared to the single-pol case, while the uniform sum yields almost the same performance when N_v/N_h equals one and M is 17. When M equals 52 the Table 6.7 shows the performance to be practically the same for all weight combinations. In Table 6.8, Table 6.9, and Table 6.10 the statistics for the *Ratio of*

bounded detections, when M is 17, shows the increase of difference in performance between the best weighted and the uniform sum as the ratio N_v/N_h decreases (i.e., from 0.3% to 2% for N_v/N_h of 0.9 and 0.7). When compared to the curves in Figure 5.12 we notice that the weighted sum producing the best performance in real data statistics is the one yielding the maximum POD at Z_{DR} of 0 dB in Figure 5.12. This can be explained by the fact that, for the fixed horizontal channel SNR, the SNR in the vertical channel is inversely proportional to Z_{DR} resulting in better detections of signals with lower differential reflectivities. Thus, using weights that put more stress on detection of signals with lower Z_{DR} values appear to produce better overall results. Moreover, the curves in Figure 5.12 show the difference between the uniform sum POD and the maximum POD, produced by the weighted sum, at 0 dB to be increasing with the N_v/N_h ratio decrease. This is in agreement with the real data statistics presented in Table 6.7 to Table 6.10. When the number of samples M increases to 52 the real data statistics shows no significant difference in performance among different weighted sums (including the uniform sum). This is in agreement with the simulation results because the curves presented in Figure 5.13 show no significant difference in POD at Z_{DR} values smaller than 3 dB.

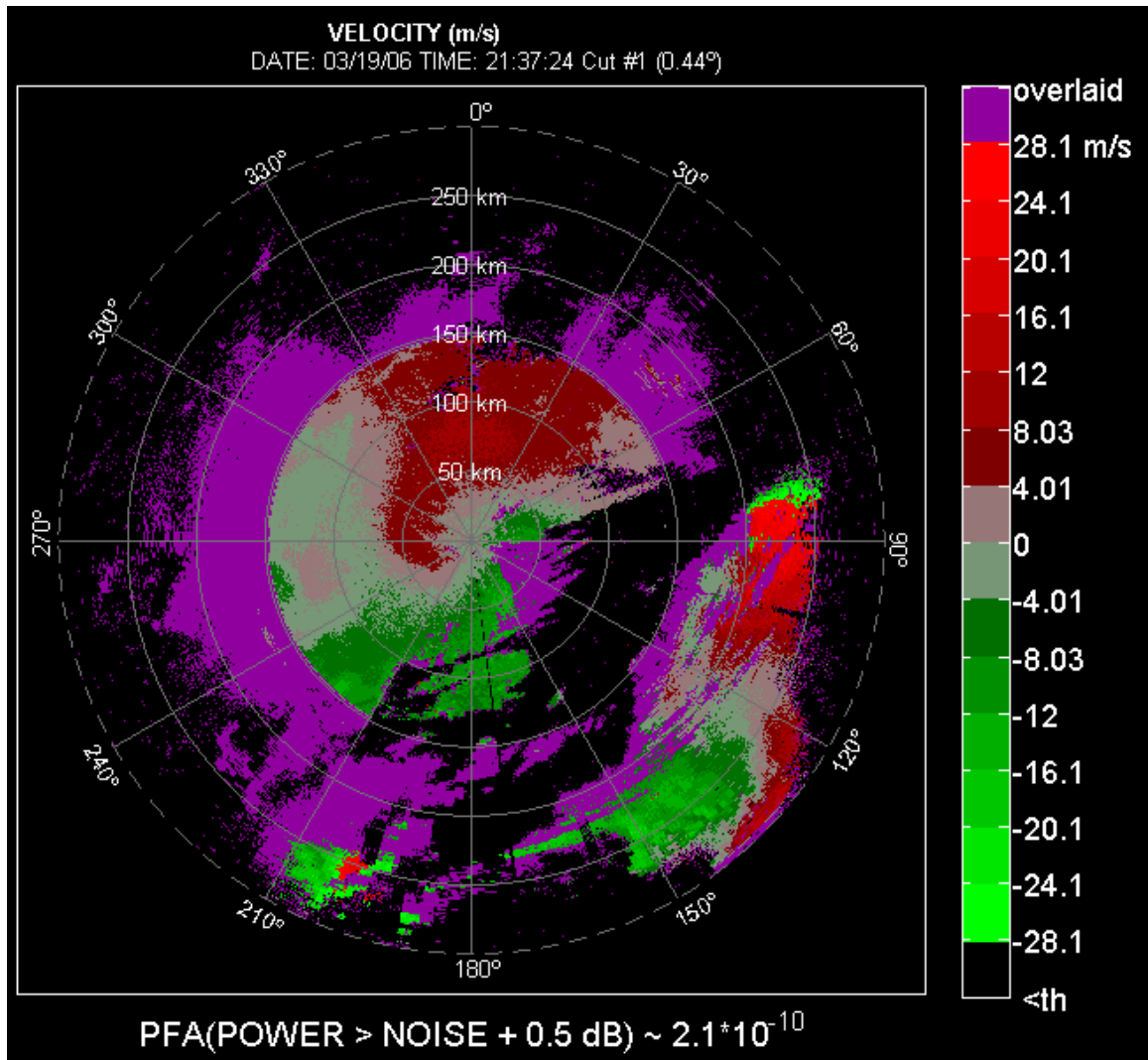


Figure 6.22 Unfolded mean velocity field obtained by lowering the threshold to -1 dB, in surveillance, and to 0.5 dB in Doppler scan, above the artificially doubled noise.

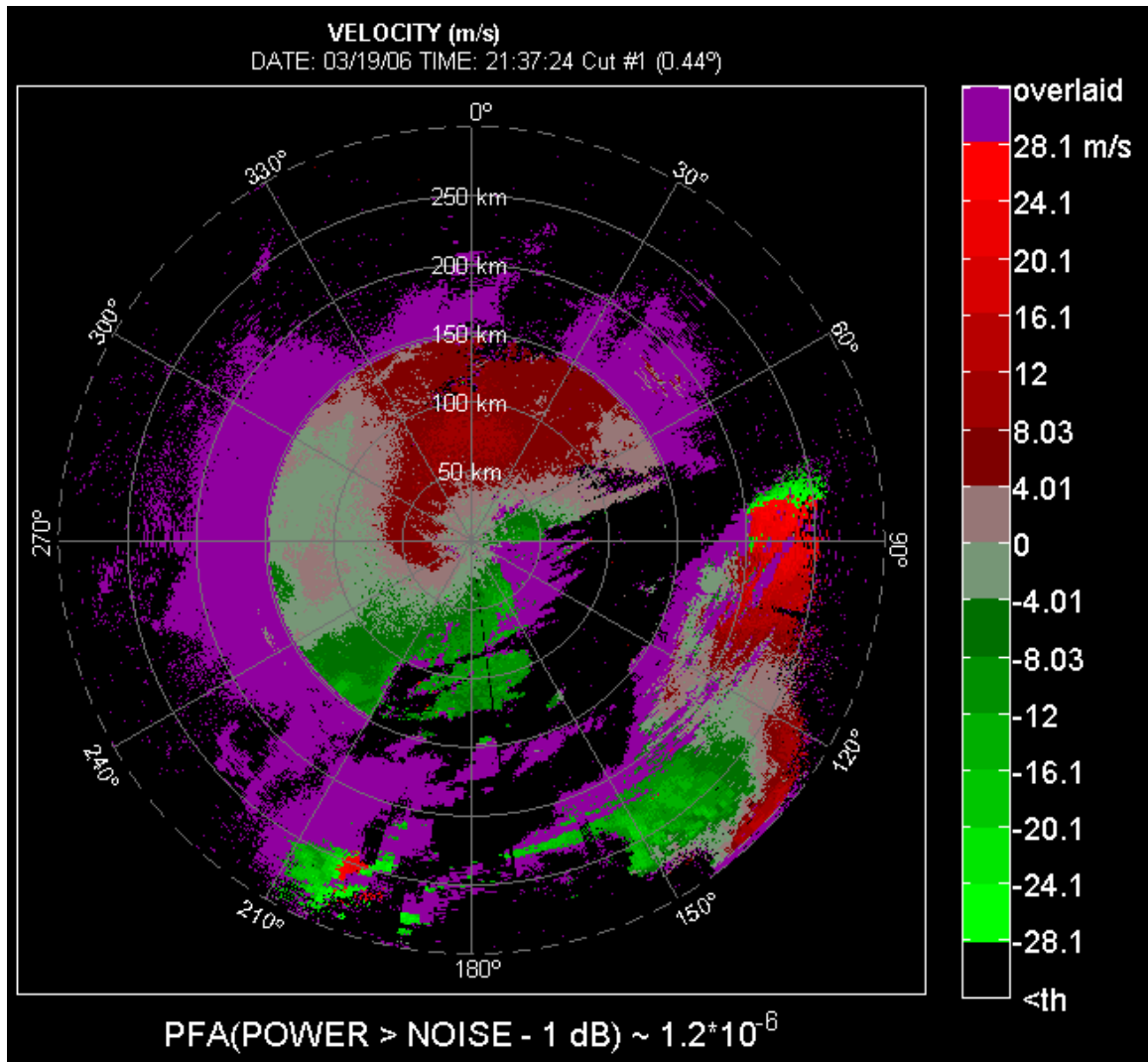


Figure 6.23 Unfolded mean velocity field obtained by lowering the threshold to -1 dB, in both the surveillance and Doppler scan, above the artificially doubled noise.

<i>D</i>	$P \geq N_h + 3.5\text{dB}$	$P \geq N_h + 0.5\text{dB}$	$P \geq N_h - 1\text{dB}$	UNIFORM SUM
<i>PFA</i>	2.34×10^{-26}	2.14×10^{-10}	1.2×10^{-6}	1.2×10^{-6}
<i>Ratio of total detections</i>	0.947989	0.989575	0.991954	0.995178
<i>Ratio of bounded detections</i>	0.044919	0.637883	0.691226	0.724477
<i>Ratio of additional detections</i>	0.003204	0.007643	0.014769	0.033545

Table 6.6 Statistics for range unfolded Doppler scan collected on 03/19/06.

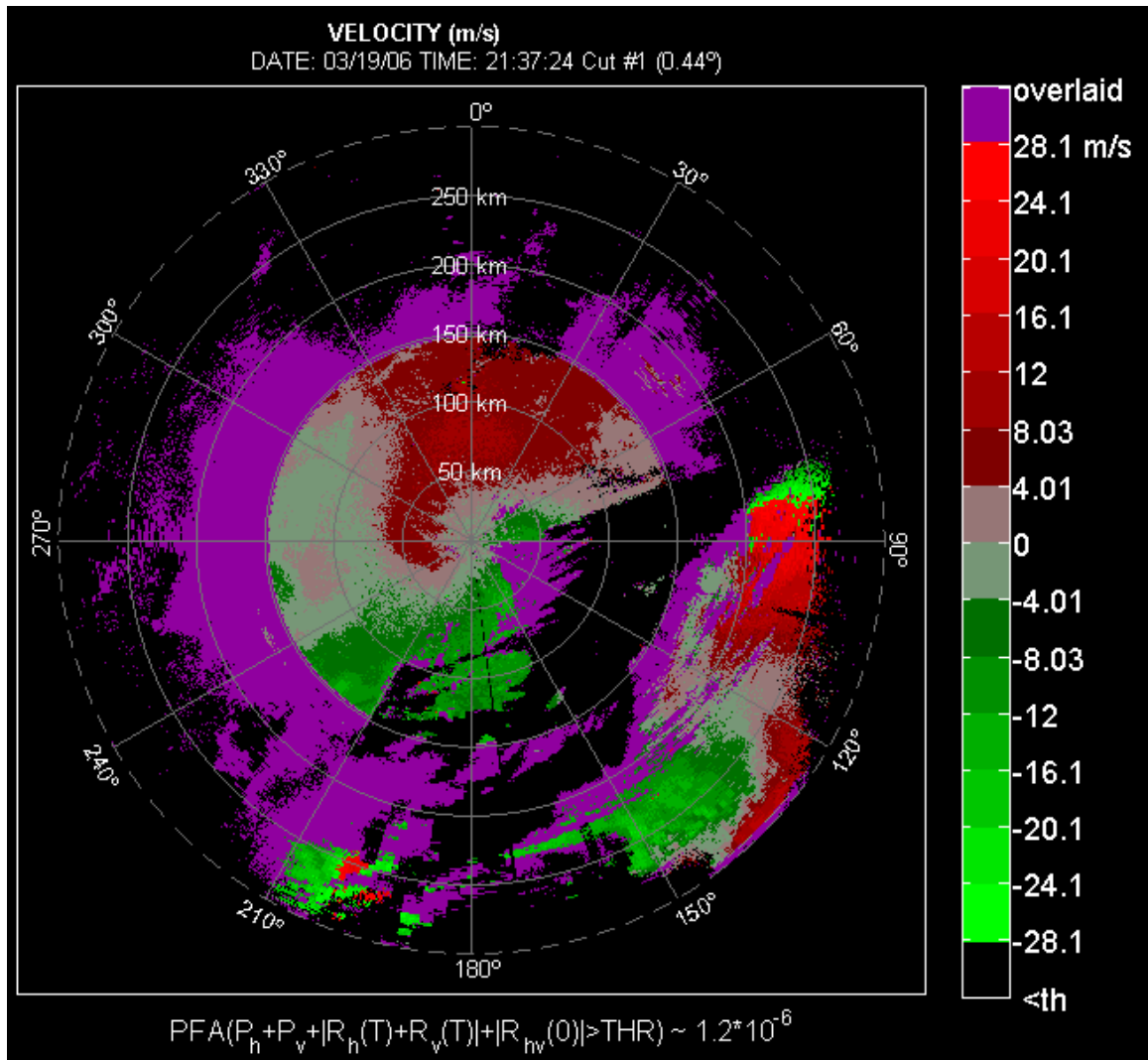


Figure 6.24 Unfolded mean velocity field obtained after doubling the noise power, and using the uniform sum for detection.

α, β, γ	M	1.5, 1.5, 2	1, 1.5, 2	0.5, 1, 1	1, 1, 1
Ratio of total detections	17	0.977888	0.978784	0.977130	0.978486
	52	1	1	1	1
Ratio of bounded detections	17	0.752096	0.759877	0.741156	0.754620
	52	0.741758	0.741758	0.741758	0.741758
Ratio of additional detections	17	0.014702	0.014360	0.011847	0.013726
	52	0.046716	0.047320	0.046451	0.046462

Table 6.7 Real data statistics comparison for various weights in the sum when $M = 17/52$, $N_v/N_h = 1$, and $PFA = 1.2 * 10^{-6}$.

α, β, γ	M	1.5, 1.5, 2	1, 1.5, 2	0.5, 1, 1	1, 1, 1
<i>Ratio of total detections</i>	17	0.982271	0.981958	0.979384	0.981994
	52	1	1	1	1
<i>Ratio of bounded detections</i>	17	0.798968	0.794607	0.765031	0.795916
	52	0.741758	0.741758	0.741758	0.741758
<i>Ratio of additional detections</i>	17	0.017547	0.017293	0.013153	0.016527
	52	0.048520	0.048644	0.047178	0.047896

Table 6.8 Real data statistics comparison for various weights in the sum when $M = 17/52$, $N_v/N_h = 0.9$, and $PFA = 1.2 \cdot 10^{-6}$.

α, β, γ	M	1.5, 1.5, 2	1, 1.5, 2	0.5, 1, 1	1, 1, 1
<i>Ratio of total detections</i>	17	0.985693	0.985348	0.981885	0.984679
	52	1	1	1	1
<i>Ratio of bounded detections</i>	17	0.833819	0.831230	0.795289	0.824392
	52	0.741758	0.741758	0.741758	0.741758
<i>Ratio of additional detections</i>	17	0.021804	0.019748	0.014786	0.018842
	52	0.050867	0.050606	0.048542	0.049746

Table 6.9 Real data statistics comparison for various weights in the sum when $M = 17/52$, $N_v/N_h = 0.8$, and $PFA = 1.2 \cdot 10^{-6}$.

α, β, γ	M	1.5, 1.5, 2	1, 1, 2	3, 2, 3	1, 1, 1
<i>Ratio of total detections</i>	17	0.989157	0.989518	0.989234	0.984679
	52	1	1	1	1
<i>Ratio of bounded detections</i>	17	0.874128	0.877505	0.874646	0.857314
	52	0.741758	0.741758	0.741758	0.741758
<i>Ratio of additional detections</i>	17	0.026079	0.024452	0.028573	0.021606
	52	0.052318	0.051242	0.052369	0.050852

Table 6.10 Real data statistics comparison for various weights in the sum when $M = 17/52$, $N_v/N_h = 0.7$, and $PFA = 1.2 \cdot 10^{-6}$.

Furthermore, another case of weather phenomena is presented. The original reflectivity field of data collected on 04/24/07 is shown in Figure 6.25 and the histogram of the SNR distribution in the horizontal channel is given in Figure 6.26. In this case about 10% of all the detections in the “single-pol” have SNR between 2 and 5 dB. The censored reflectivity field using the same threshold but with additional noise is shown in Figure 6.27. After elevating the threshold to 2 dB above the noise, the field is presented in Figure 6.288. Using the uniform sum yields Figure 6.29. The statistics is given in Table 6.11. We notice that the *Ratio of bounded detections* has decreased for uniform

sum compared to the statistics in Table 6.4. This can be explained by the fact that the ratio N_v/N_h increased from 0.8269 to 0.9378, thus the overall amount of noise in H and V channel is larger.

D	$P \geq N_h - 1 \text{ dB}$	$P \geq N_h + 2 \text{ dB}$	P&UNIFORM SUM	UNIFORM SUM
<i>Ratio of total detections</i>	0.977623	0.893241	0.963456	0.961887
<i>Ratio of bounded detections</i>	0.798316	0.143310	0.687322	0.679773
<i>Ratio of additional detections</i>	0.041272	0.000192	0.024048	0.023965

Table 6.11 Real data statistics for surveillance scan collected on 04/24/07.

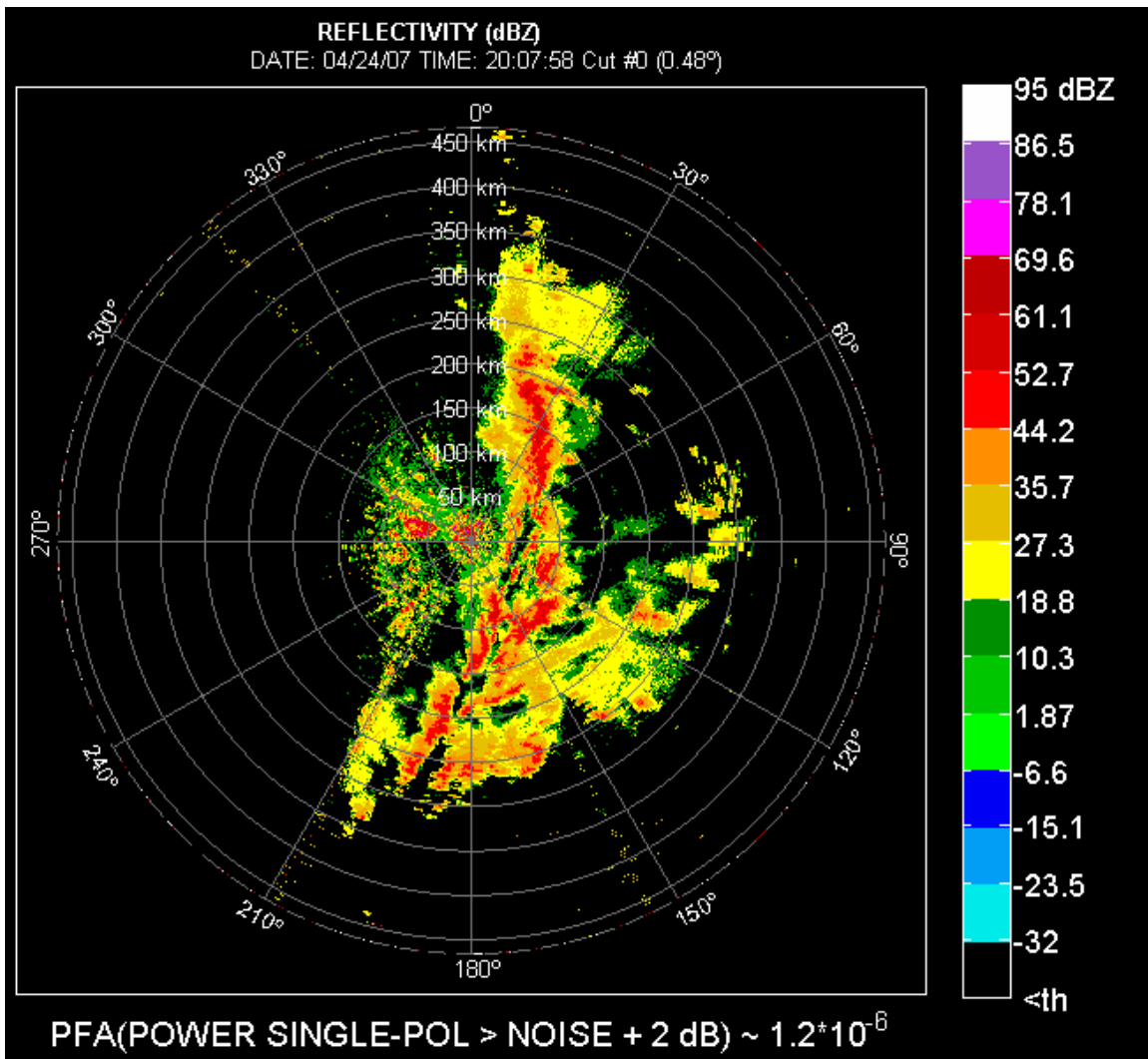


Figure 6.25 The original “single-pol” reflectivity field.

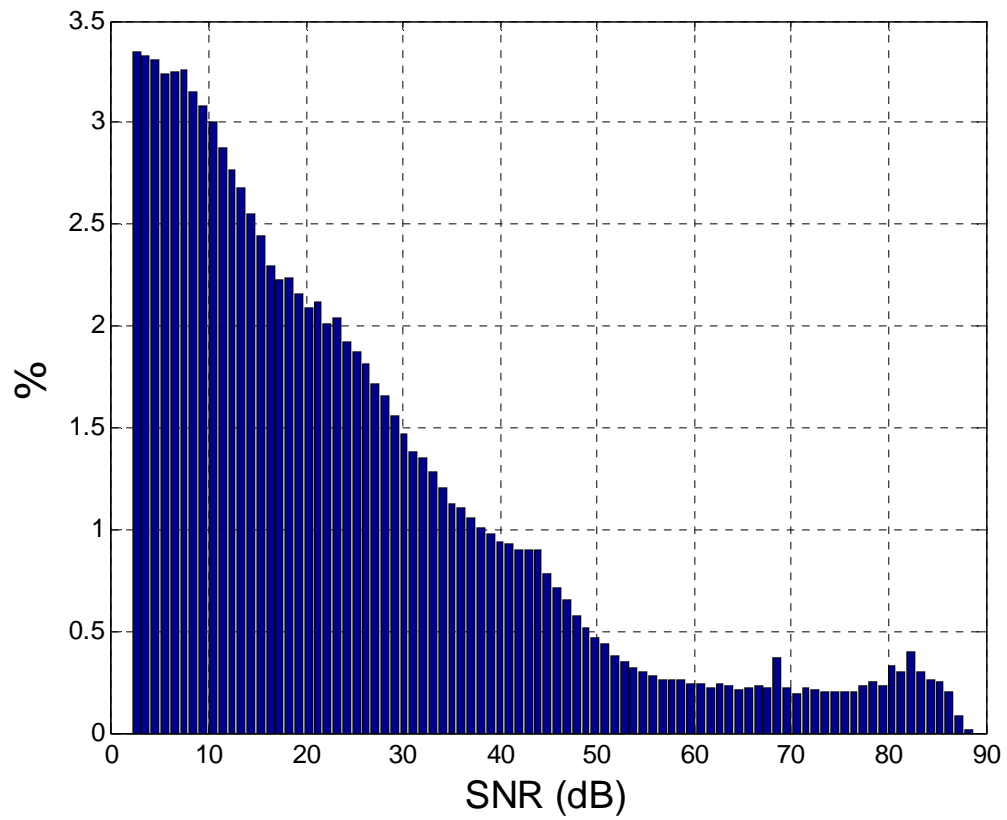
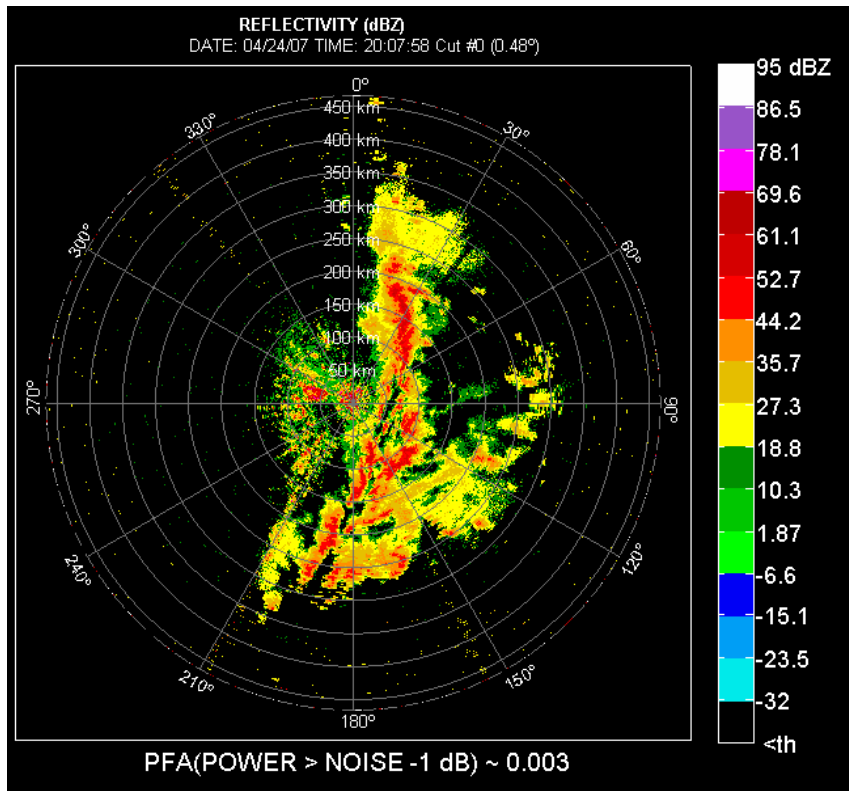
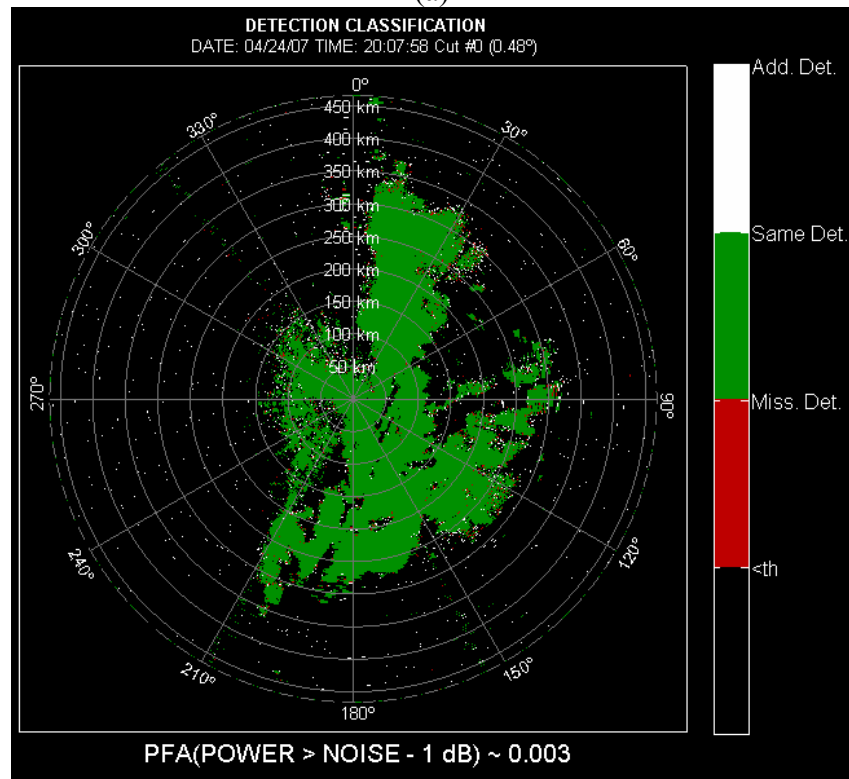


Figure 6.26 The histogram of the SNR distribution in the horizontal channel before the noise power is doubled.

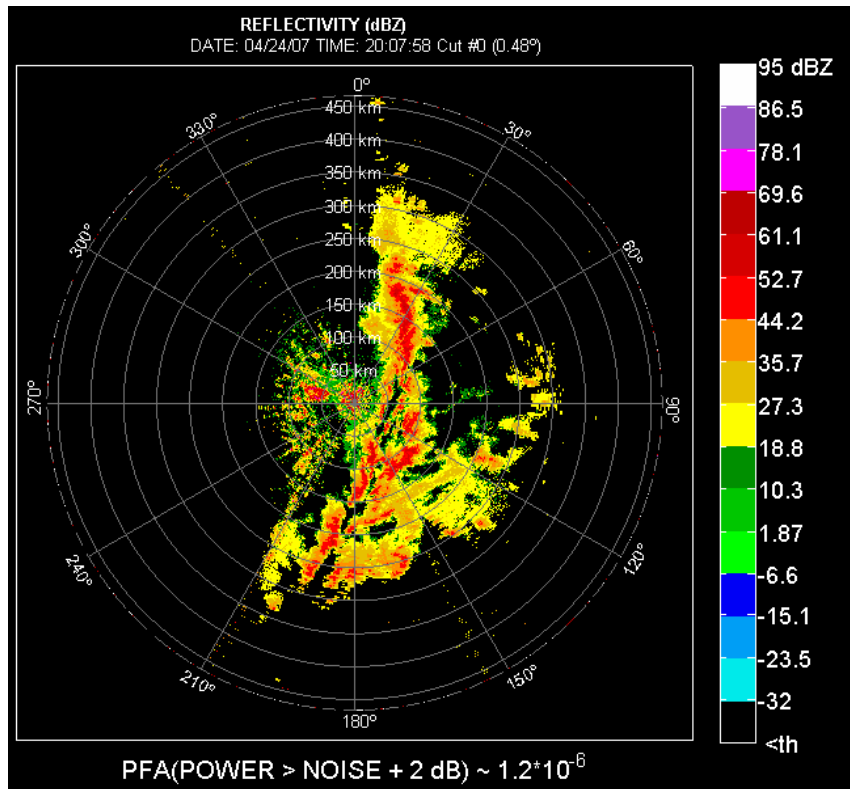


(a)

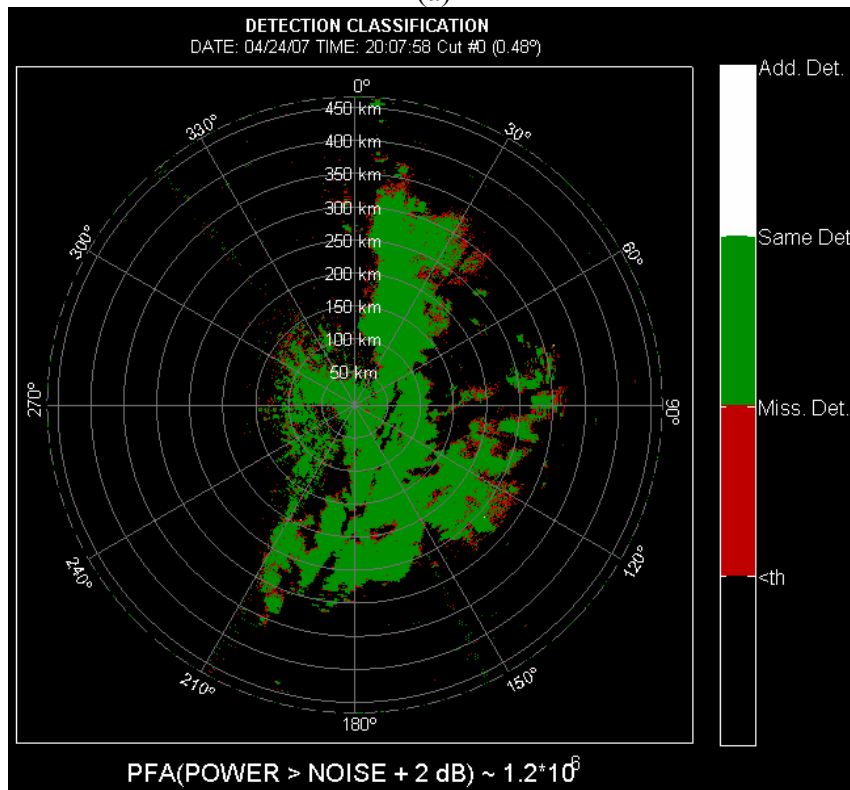


(b)

Figure 6.27 Reflectivity field (a) and the classification of detections (b) obtained after doubling the noise power, but not changing the threshold.

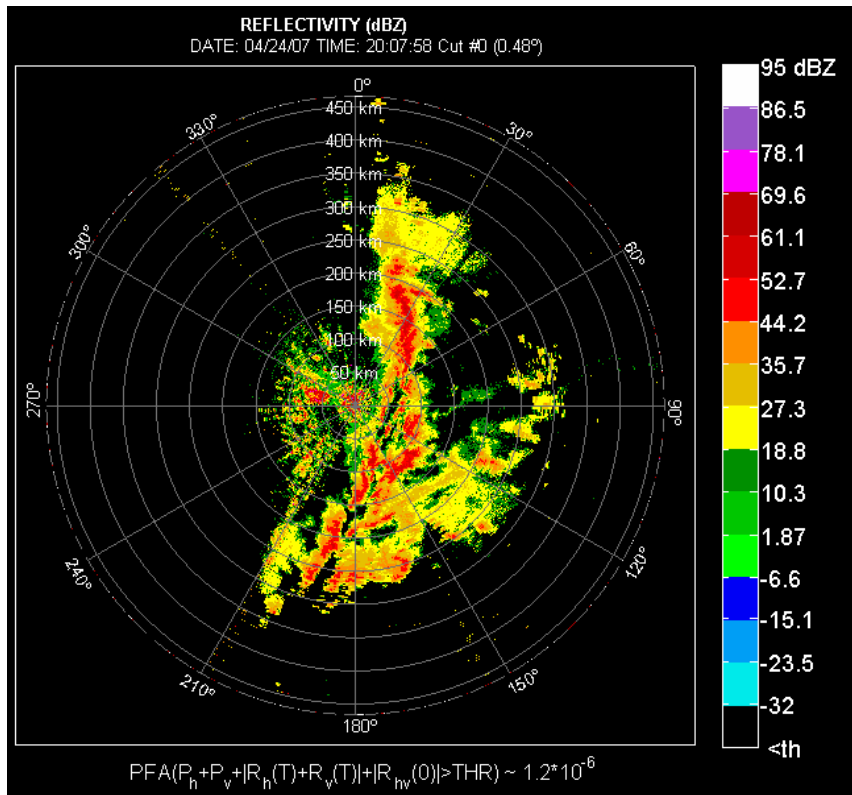


(a)

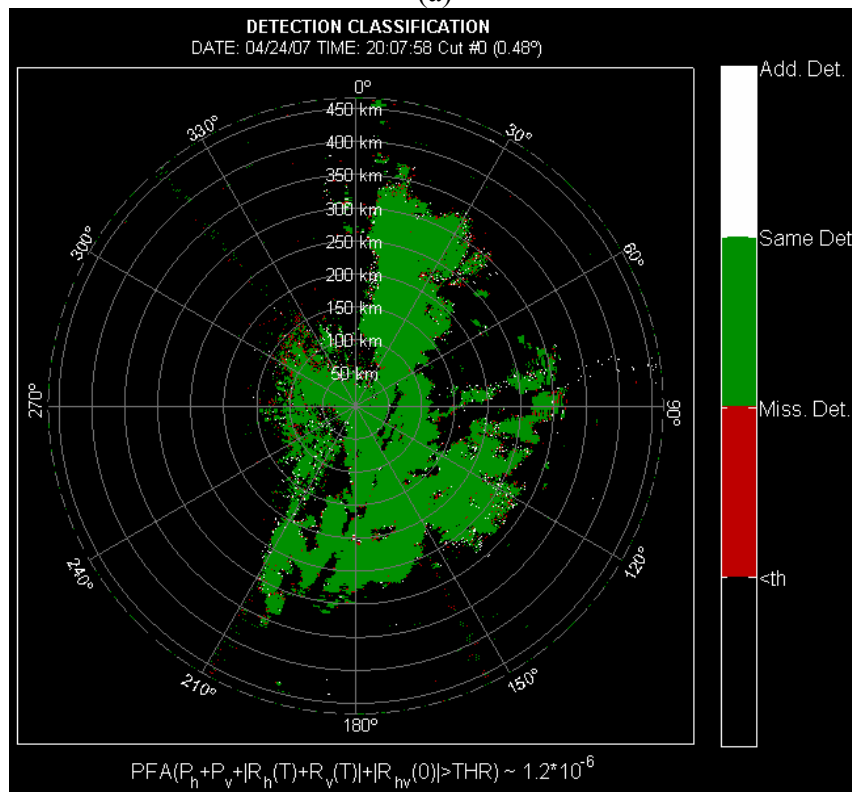


(b)

Figure 6.28 Reflectivity field obtained after doubling the noise power, and increasing the threshold to 2 dB above the doubled noise power.



(a)



(b)

Figure 6.29 Reflectivity field (a) and classification of detections (b) obtained after doubling the noise power, and using the uniform sum for detection.

As in the previous case, a Doppler scan with $M = 52$ and the unambiguous range of 150 km was executed after the surveillance scan. The range unfolded velocities of the original field are presented in Figure 6.30. After the noise is artificially doubled, the field in Figure 6.311 is obtained. Lowering thresholds to -1 dB in surveillance and to 0.5 dB in Doppler scan, above the artificially doubled noise, produces the image in Figure 6.32. Further lowering the threshold in Doppler scan to -1 dB, to obtain the same false alarm rate as used for the uniform sum, produces the image in Figure 6.33. When uniform sum is used for signal detection, one gets velocity field in Figure 6.34. The statistics is given in Table 6.12. Compared to the statistics given in Table 6.6, we notice that the *Ratio of bounded detections* is higher even though the overall amount of noise is larger (i.e., the ratio N_v/N_h is higher). This could be due to the nature of this event where the resolved bounded detections in single-pol are simply more coherent which makes them more susceptible to detection by the uniform sum after increasing the noise power.

D	$P \geq N_h + 3.5\text{dB}$	$P \geq N_h + 0.5\text{dB}$	$P \geq N_h - 1\text{dB}$	UNIFORM SUM
<i>PFA</i>	2.34×10^{-26}	2.14×10^{-10}	$1.2 * 10^{-6}$	$1.2 * 10^{-6}$
<i>Ratio of total detections</i>	0.922536	0.987867	0.988286	0.989894
<i>Ratio of bounded detections</i>	0.053373	0.844268	0.849786	0.866426
<i>Ratio of additional detections</i>	0.003863	0.025328	0.031937	0.072861

Table 6.12 Statistics for range unfolded Doppler scan collected on 04/24/07.

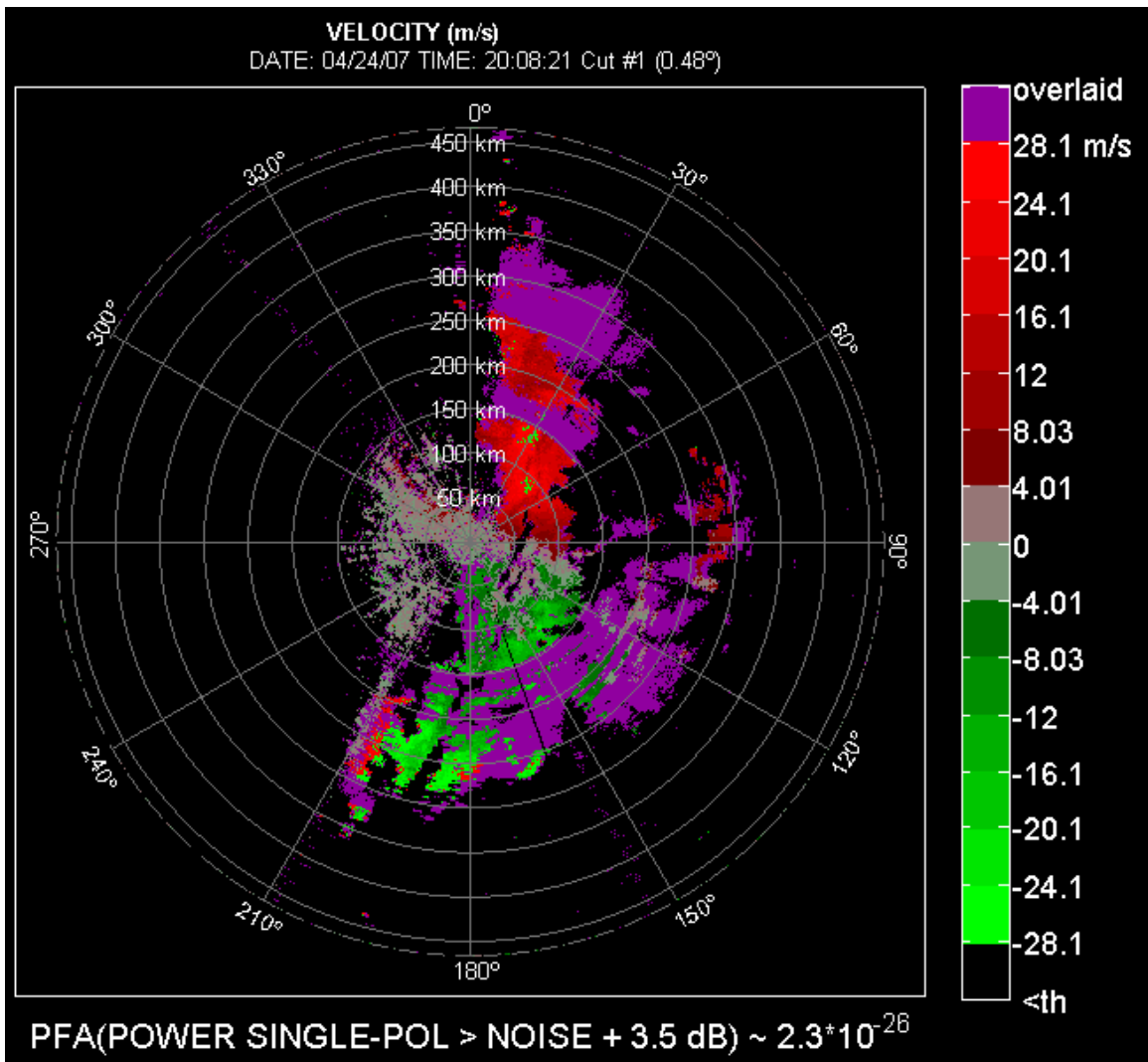


Figure 6.30 Original range unfolded velocity field for *SNR* thresholds of 2 and 3.5 dB in surveillance and Doppler cuts, respectively. Sample numbers *M* are 17, and 52 in surveillance and Doppler scans, respectively.

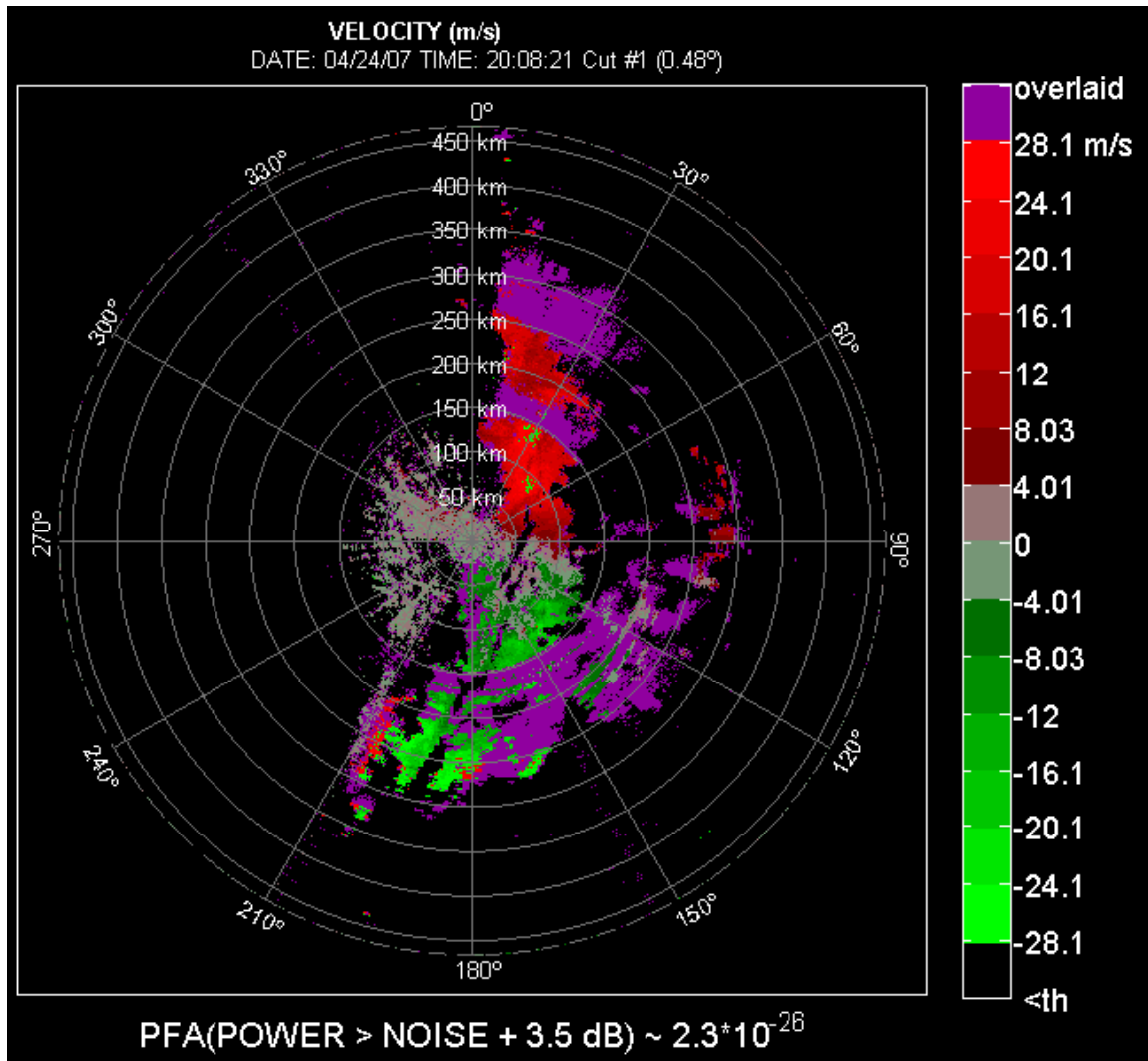


Figure 6.31 Unfolded velocity field obtained after doubling the noise power, but not changing the thresholds.

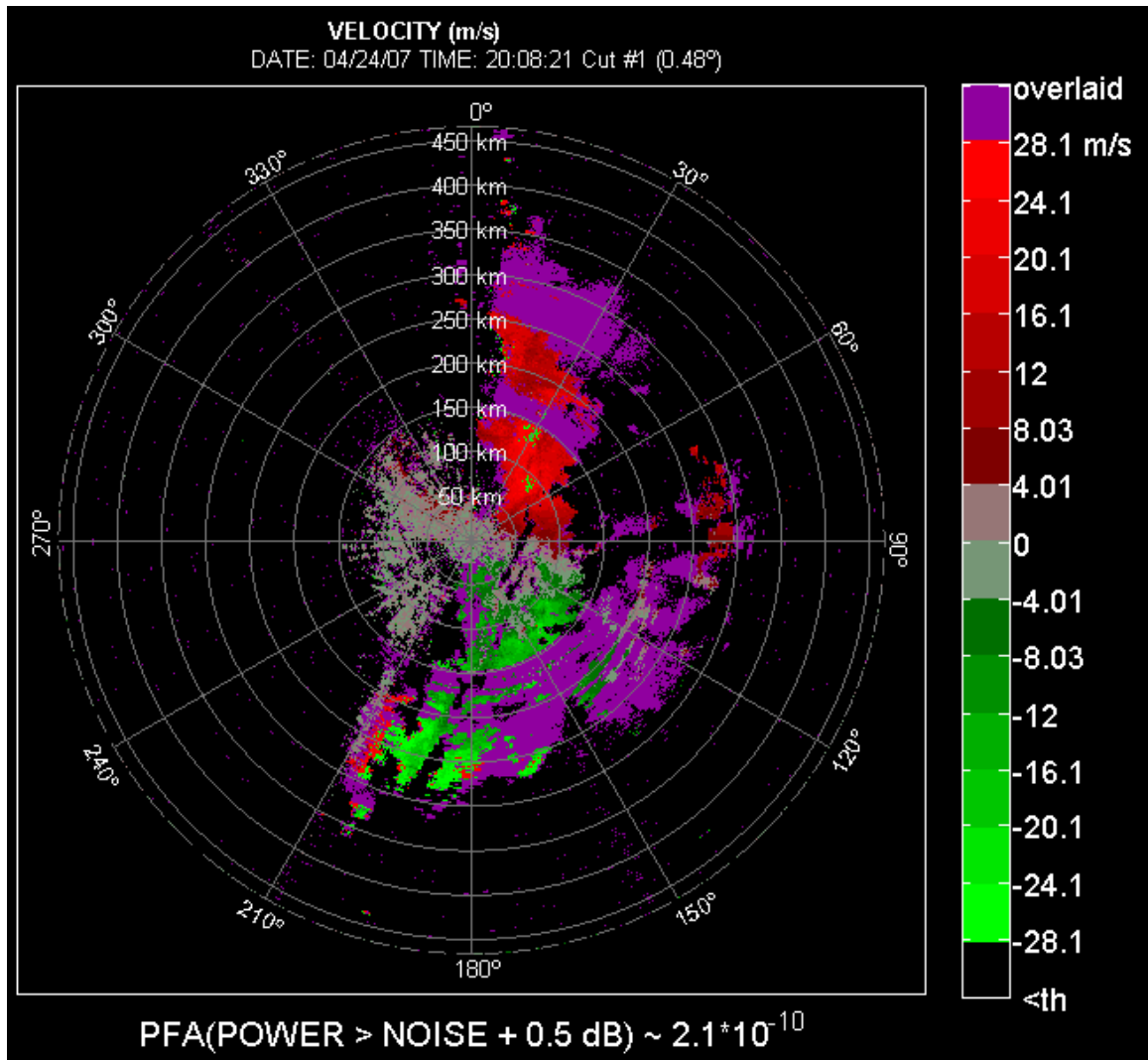


Figure 6.32 Unfolded mean velocity field obtained by lowering the threshold to -1 dB, in surveillance, and to 0.5 dB in Doppler scan, above the artificially doubled noise.

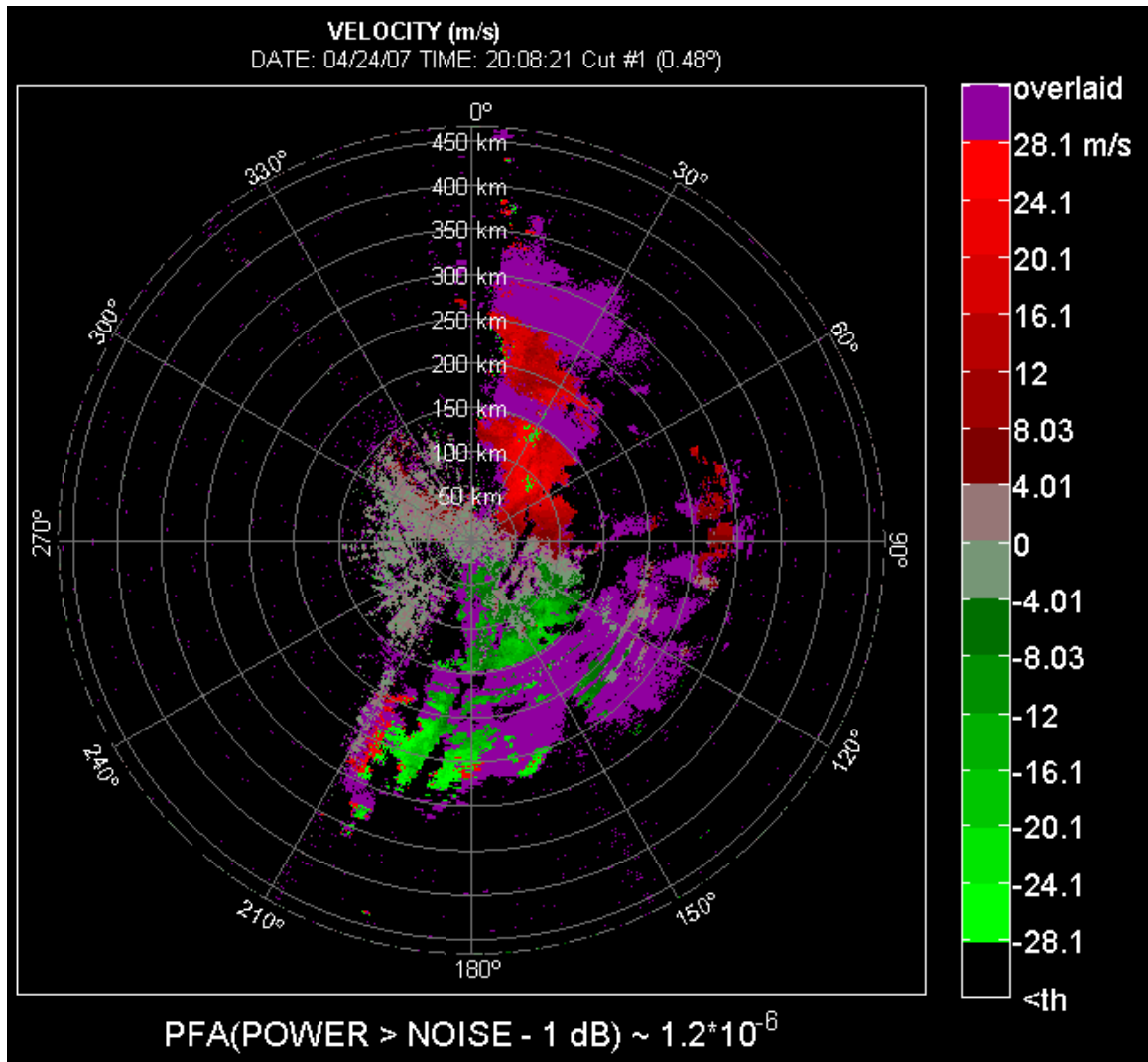


Figure 6.33 Unfolded mean velocity field obtained by lowering the threshold to -1 dB, in both the surveillance and Doppler scan, above the artificially doubled noise.

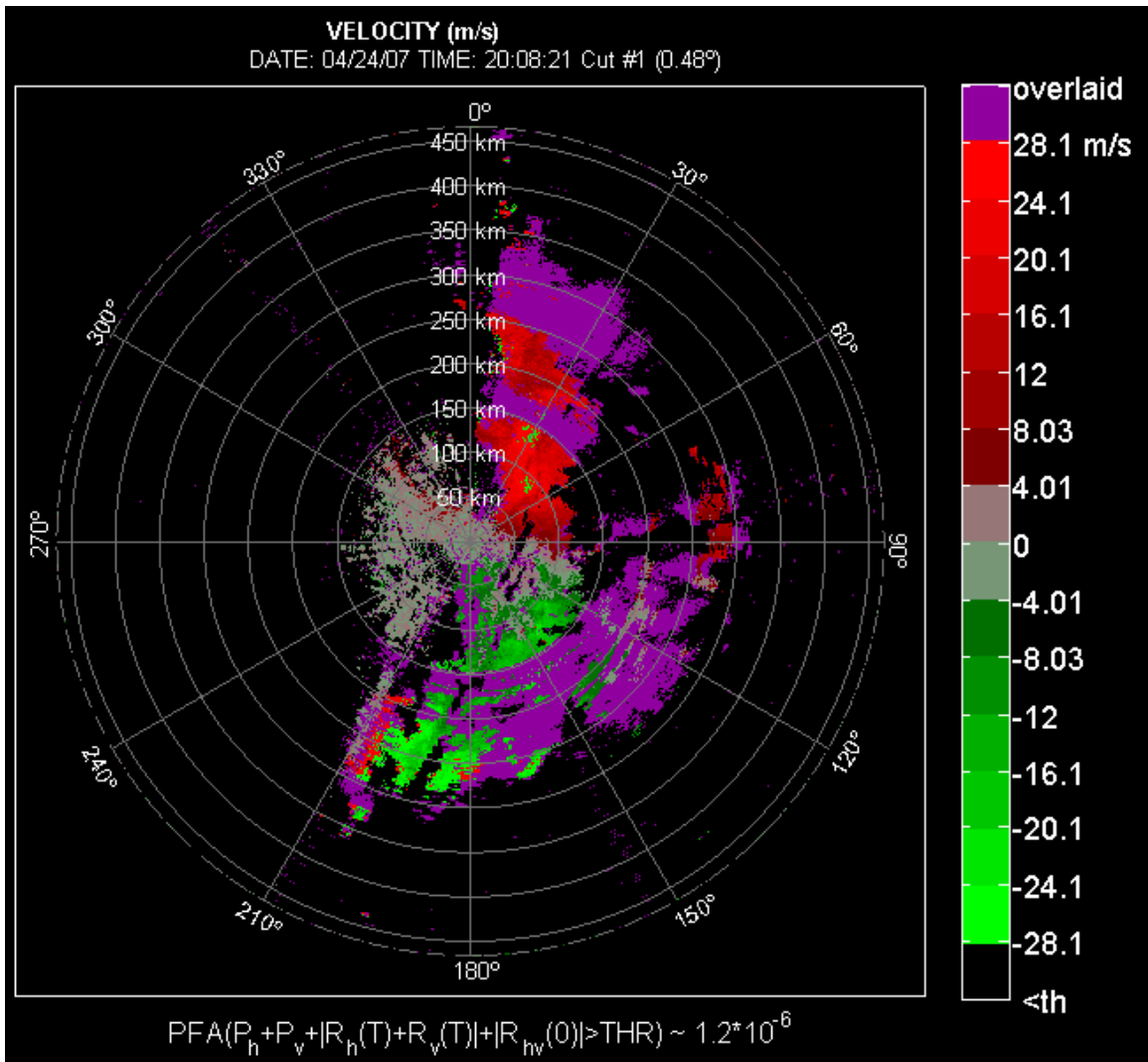


Figure 6.34 Unfolded mean velocity field obtained after doubling the noise power, and using the uniform sum for detection.

7. Real-Time Implementation of the Weighted Sum

Real-time system implementation of the weighted/uniform sum requires a different approach for threshold computation, which needs to be based on the real-time measurement of the ratio N_v/N_h and the number of pulses M in the operational mode. This can be achieved possibly by following the procedure described in section 5.5. Unfortunately, the mathematics behind the implementation of such a procedure is very involved, and the execution times are unacceptable for real-time systems. A viable solution could be look-up tables, where the threshold is pre-computed for each M value available in the operational mode and for a given PFA. Different radar systems, however, have different values of the ratio N_v/N_h , which may vary over time. Let us examine the sensitivity of a PFA to various values of N_v/N_h . The analysis for the uniform sum is shown in Figure 7.1 for several values of M . The curves show that the PFA is extremely sensitive to N_v/N_h . Moreover, the results suggest that if the desired PFA accuracy of $\pm 10\%$ is required, the system ratio N_v/N_h must not differ more than 0.5% from the ratio for which the threshold is calculated. More important, though, is how much the resulting POD varies as the actual ratio N_v/N_h departs from the one for which the threshold is calculated. This is shown in Figure 7.2 and Table 7.1. These show that the POD is moderately sensitive to the variation in N_v/N_h . For instance, for M of 17 a 2% drop of the N_v/N_h produces only 0.5% loss in the detection rate. Moreover, the loss in POD for the same change in noise power ratio decreases as M increases. For $M = 52$ the detection rate is merely 0.05% smaller for the 0.02 drop in the N_v/N_h . To further examine how this reflects on the detection of real signals, the following experiment is performed. The actual measured ratio of N_v/N_h is 0.8269. In order to assess the performance for various

values of N_v/N_h , additional noise power is introduced in the V channel as follows. Let Δ be the amount by which we want the N_v/N_h to be skewed (i.e., the desired difference between the N_v/N_h ratio for which the threshold is given and the true one). Then the additional noise power x , in the V channel, to obtain the desired ratio is

$$\frac{N_v}{N_h} + \Delta = \frac{N_v + x}{2N_h} \Rightarrow x = N_v + 2\Delta N_h. \quad (7.1)$$

The results of various Δ are given in Table 7.2 and Table 7.3, for $M = 17$, and $M = 52$, respectively. These results agree with the simulation results in Table 7.1.

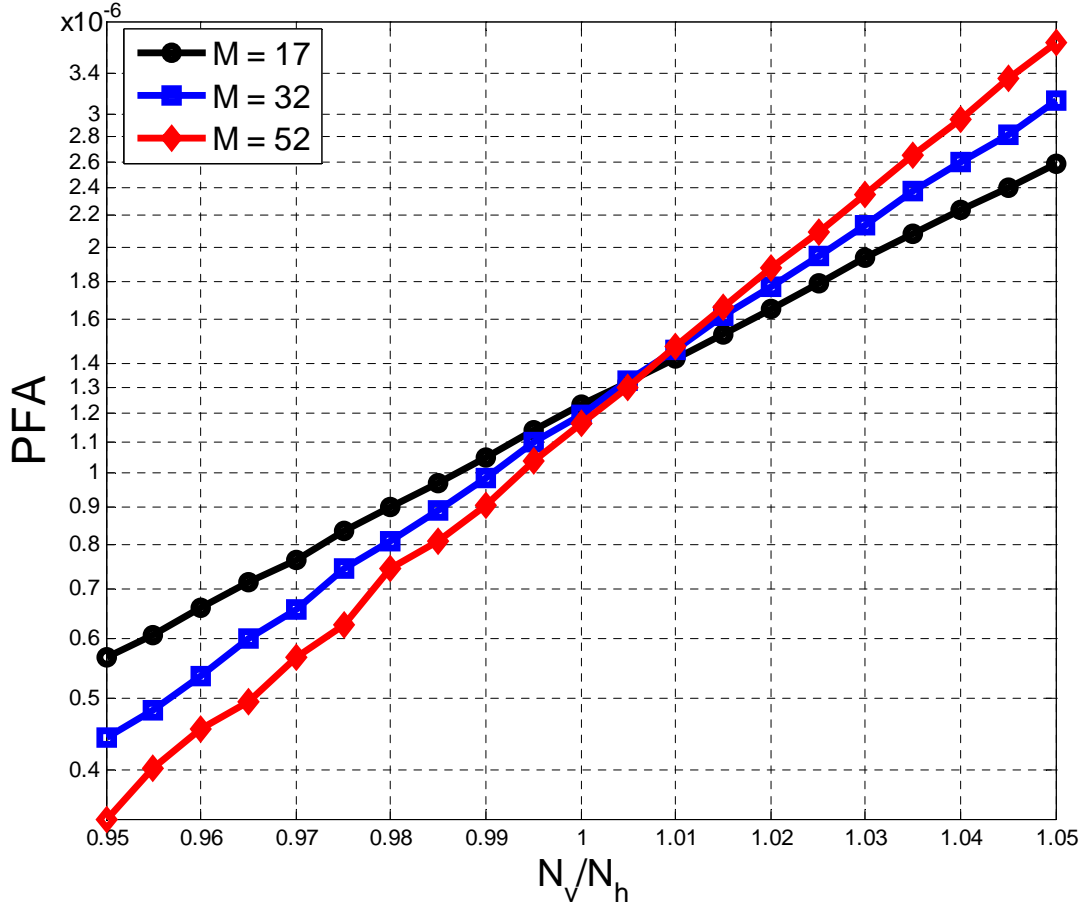


Figure 7.1 Uniform sum PFA sensitivity to change in the ratio N_v/N_h for threshold adjusted for PFA of 1.2×10^{-6} , and the unity ratio N_v/N_h .

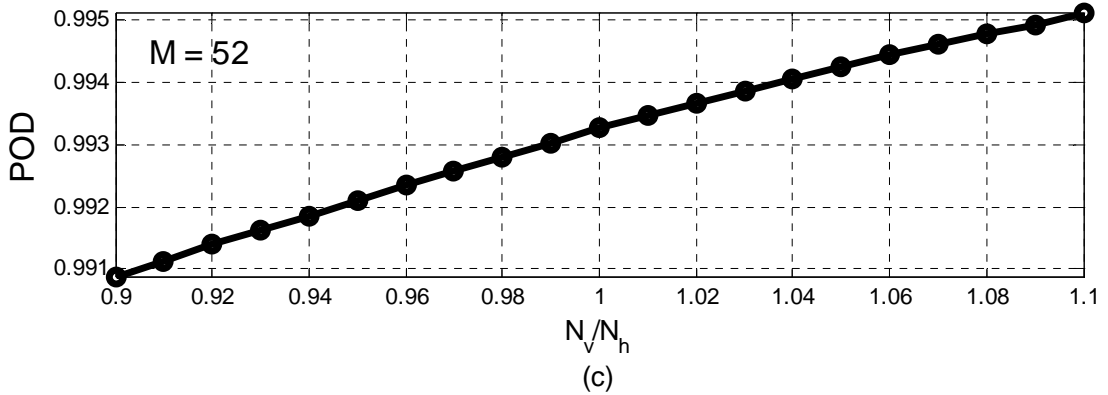
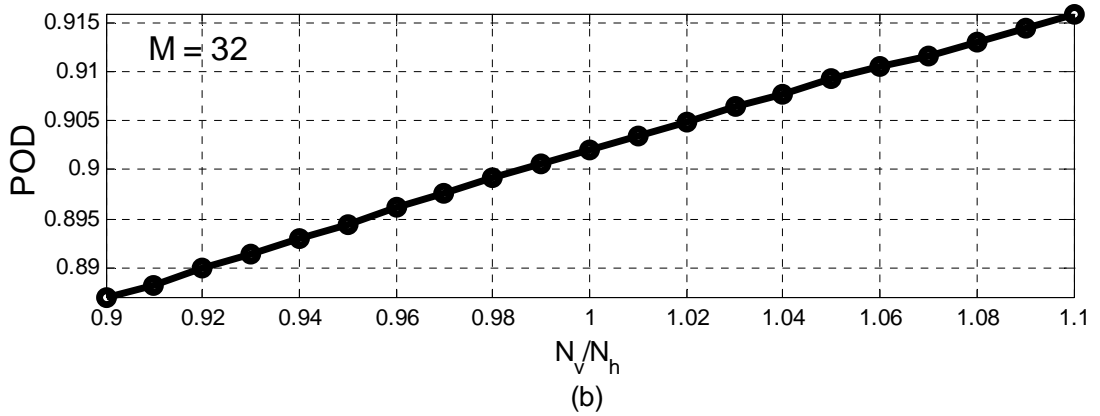
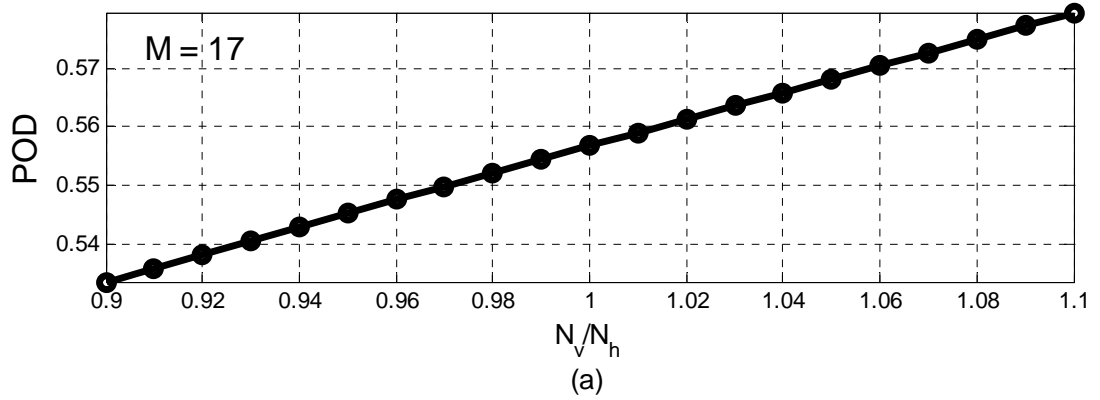


Figure 7.2 Uniform sum POD sensitivity to change in the ratio N_v/N_h for threshold set to PFA of 1.2×10^{-6} , for the unity ratio N_v/N_h , and signal parameters $SNR = 0$ dB, $\sigma_v = 2 \text{ m s}^{-1}$, $Z_{DR} = 1 \text{ dB}$, $\rho_{hv} = 0.96$.

The previous analysis implies that for each M , an efficient method for threshold computation based on the measured N_v/N_h ratio, should be devised. The results in Figure 7.3 exhibit the threshold as function of the N_v/N_h ratio for $M = 17$ and $PFA = 1.2 \times 10^{-6}$. The circles denote the thresholds for N_v/N_h ranging from 0.5 to 1 with the step of 0.05.

The dashed line is the least squares fit, to the data (denoted by circles), using function $x^B e^{A+Cx}$, where $x = N_v/N_h$, and the coefficients A , B , and C are obtained as described in Appendix L. As an assessment of the interpolation quality, red square markers are placed on top of the interpolation curve. These represent the estimated thresholds for N_v/N_h ratio ranging from 0.6 to 0.98 with the step of 0.02. This shows that the least square fitted curve is an excellent approximation and can be used to efficiently calculate the threshold for any ratio of noise powers in H and V channels. Moreover, when the fitting function coefficients are found for the unity noise power in H channel and the desired PFA, the threshold for any system can be obtained by plugging the measured N_v/N_h ratio into the function and multiplying the output with the measured N_h . Notice that the fitting function found for the unit N_h and the N_v/N_h ratio range of $[1-\varepsilon, 1]$, where $\varepsilon \in [0, 1]$ (i.e., when $N_v < N_h$), can be reused for the case when $N_h/N_v \in [1-\varepsilon, 1]$ (i.e., when $N_v > N_h$) by simply swapping the places of N_h and N_v . The threshold is then found as

$$THR = \max(N_h, N_v) \cdot \left(\frac{\min(N_h, N_v)}{\max(N_h, N_v)} \right)^B \cdot \exp \left(A + C \cdot \frac{\min(N_h, N_v)}{\max(N_h, N_v)} \right). \quad (7.2)$$

Coefficients for some M values used in operation are given in Table 7.4.

$\Delta N_v/N_h$	-0.01	-0.02	-0.03	-0.04	-0.05	-0.06
Δ POD (M=17)	-2.28×10^{-3}	-4.57×10^{-3}	-6.91×10^{-3}	-9.19×10^{-3}	-1.15×10^{-2}	-1.39×10^{-2}
Δ POD (M=32)	-1.44×10^{-3}	-2.86×10^{-3}	-4.5×10^{-3}	-5.84×10^{-3}	-7.65×10^{-3}	-9.11×10^{-3}
Δ POD (M=52)	-2.45×10^{-4}	-4.71×10^{-4}	-6.9×10^{-4}	-9.28×10^{-4}	-1.16×10^{-3}	-1.41×10^{-3}

Table 7.1 The estimated drop in uniform sum POD vs. the drop in the ratio of N_v/N_h for threshold set to PFA of 1.2×10^{-6} , for the unity ratio N_v/N_h , and signal parameters $SNR = 0$ dB, $\sigma_v = 2$ m s⁻¹, $Z_{DR} = 1$ dB, $\rho_{hv} = 0.96$.

Δ	0	-0.01	-0.02	-0.05	-0.1	-0.2
Ratio of total detections	0.984366	0.983747	0.983924	0.983573	0.982610	0.980850
Ratio of bounded detections	0.822027	0.814692	0.814696	0.812835	0.800011	0.782148
Ratio of additional detections	0.021714	0.021760	0.021615	0.020041	0.018912	0.015892

Table 7.2 The uniform sum detections vs. the difference between the actual ratio of N_v/N_h and the one the threshold was adjusted for, in case of $M = 17$, and PFA of 1.2×10^{-6} .

Δ	0	-0.02	-0.05	-0.1	-0.2	-0.4
Ratio of total detections	1	1	1	1	1	1
Ratio of bounded detections	0.741758	0.741758	0.741758	0.741758	0.741758	0.741758
Ratio of additional detections	0.471704	0.466731	0.457801	0.451406	0.437871	0.404143

Table 7.3 The uniform sum detections vs. the difference between the actual ratio of N_v/N_h and the one the threshold was adjusted for, in case of $M = 52$, and PFA of 1.2×10^{-6} .

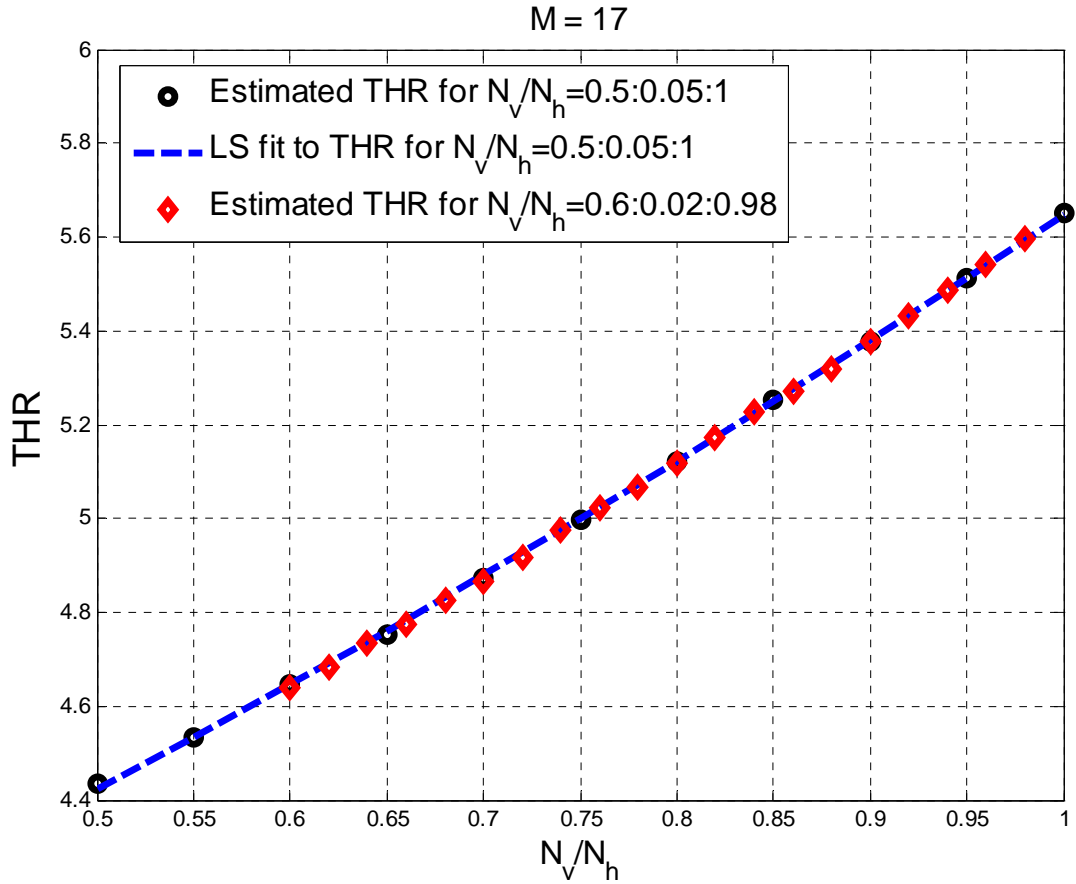


Figure 7.3 Least squares approximation using $x^B e^{A+Cx}$ yielding function that takes the N_v/N_h ratio as an input and outputs threshold for PFA = 1.2×10^{-6} .

M/PFA		5×10^{-7}	6×10^{-7}	7×10^{-7}	8×10^{-7}	9×10^{-7}	1×10^{-6}	1.1×10^{-6}	1.2×10^{-6}
10	A	1.4207	1.4156	1.4127	1.4137	1.4071	1.4020	1.3988	1.3975
	B	-0.1047	-0.1027	-0.1001	-0.0947	-0.0961	-0.0965	-0.0957	-0.0939
	C	0.6079	0.6062	0.6030	0.5968	0.5990	0.5999	0.5994	0.5973
11	A	1.3904	1.3873	1.3762	1.3697	1.3709	1.3668	1.3653	1.3615
	B	-0.0859	-0.0825	-0.0863	-0.0873	-0.0823	-0.0821	-0.0802	-0.0803
	C	0.5857	0.5821	0.5872	0.5888	0.5832	0.5833	0.5811	0.5816
12	A	1.3534	1.3473	1.3443	1.3395	1.3410	1.3349	1.3338	1.3298
	B	-0.0767	-0.0758	-0.0736	-0.0731	-0.0681	-0.0697	-0.0676	-0.0679
	C	0.5774	0.5771	0.5745	0.5745	0.5687	0.5710	0.5684	0.5693
16	A	1.2242	1.2281	1.2252	1.2134	1.2204	1.2084	1.2048	1.2036
	B	-0.0595	-0.0517	-0.0494	-0.0549	-0.0459	-0.0525	-0.0526	-0.0511
	C	0.5650	0.5551	0.5530	0.5606	0.5496	0.5583	0.5587	0.5570
17	A	1.2201	1.2175	1.2099	1.1990	1.1965	1.1936	1.2064	1.2039
	B	-0.0402	-0.0381	-0.0395	-0.0439	-0.0425	-0.0419	-0.0300	-0.0293
	C	0.5404	0.5369	0.5399	0.5468	0.5456	0.5450	0.5285	0.5285
21	A	1.1271	1.1217	1.1149	1.1103	1.1056	1.1040	1.1087	1.1026
	B	-0.0351	-0.0353	-0.0359	-0.0364	-0.0369	-0.0356	-0.0292	-0.0319
	C	0.5405	0.5406	0.5433	0.5439	0.5453	0.5437	0.5356	0.5396
25	A	1.0785	1.0733	1.0728	1.0703	1.0678	1.0644	1.0648	1.0622
	B	-0.0141	-0.0142	-0.0109	-0.0097	-0.0088	-0.0089	-0.0064	-0.0062
	C	0.5180	0.5181	0.5145	0.5133	0.5125	0.5129	0.5098	0.5100
28	A	1.0457	1.0408	1.0378	1.0352	1.0326	1.0313	1.0282	1.0280
	B	-3.77e-3	-3.42e-3	-2.56e-3	-1.53e-3	-9.05e-4	5.05e-4	3.24e-4	2.19e-3
	C	0.5064	0.5067	0.5055	0.5046	0.5041	0.5025	0.5031	0.5009
29	A	1.0227	1.0232	1.0189	1.0148	1.0099	1.0090	1.0068	1.0098
	B	-9.29e-3	-5.25e-3	-5.11e-3	-5.29e-3	-6.4e-3	-4.8e-3	-4.32e-3	-2.64e-4
	C	0.5171	0.5118	0.5122	0.5129	0.5147	0.5127	0.5125	0.5072
32	A	0.9939	0.9966	0.9869	0.9916	0.9907	0.9872	0.9847	0.9848
	B	-1.21e-3	4.3e-3	4.25e-4	5.99e-3	8.1e-3	7.71e-3	7.02e-3	9.02e-3
	C	0.5103	0.5028	0.5089	0.5005	0.4986	0.4994	0.4994	0.4970
37	A	0.9472	0.9462	0.9430	0.9422	0.9409	0.9374	0.9354	0.9350
	B	4.74e-3	7.63e-3	8.14e-3	1.01e-2	1.14e-2	1.09e-2	1.14e-2	1.27e-2
	C	0.5062	0.5030	0.5026	0.5001	0.4986	0.4996	0.4993	0.4976
41	A	0.9312	0.9431	0.9516	0.9339	0.9391	0.9365	0.9361	0.9352
	B	0.0197	0.0317	0.0414	0.0297	0.0373	0.0371	0.0388	0.0398
	C	0.4873	0.4710	0.4588	0.4737	0.4661	0.4662	0.4646	0.4634
43	A	0.9271	0.9382	0.9343	0.9375	0.9125	0.9247	0.9221	0.9155
	B	0.0288	0.0399	0.0393	0.0441	0.0277	0.0395	0.0393	0.0359
	C	0.4754	0.4604	0.4609	0.4542	0.4773	0.4625	0.4630	0.4677
46	A	0.9022	0.9014	0.8983	0.9041	0.9064	0.8942	0.8955	0.8969
	B	0.0275	0.0301	0.0304	0.0372	0.0416	0.0340	0.0372	0.0394
	C	0.4801	0.4768	0.4765	0.4679	0.4633	0.4734	0.4700	0.4665

52	A	0.8782	0.8715	0.8579	0.8564	0.8729	0.8735	0.8745	0.8572
	B	0.0404	0.0377	0.0299	0.0310	0.0464	0.0480	0.0508	0.0394
	C	0.4673	0.4699	0.4806	0.4793	0.4602	0.4573	0.4543	0.4704
56	A	0.8368	0.8422	0.8406	0.8431	0.8411	0.8359	0.8368	0.8342
	B	0.0265	0.0330	0.0347	0.0385	0.0389	0.0369	0.0396	0.0388
	C	0.4871	0.4778	0.4766	0.4713	0.4709	0.4741	0.4716	0.4722
60	A	0.8352	0.8348	0.8319	0.8338	0.8319	0.8207	0.8252	0.8252
	B	0.0405	0.0430	0.0429	0.0469	0.0467	0.0405	0.0451	0.0467
	C	0.4686	0.4659	0.4656	0.4610	0.4606	0.4700	0.4636	0.4618
63	A	0.8377	0.8412	0.8236	0.8336	0.8210	0.8276	0.8238	0.8246
	B	0.0538	0.0588	0.0485	0.0576	0.0505	0.0567	0.0552	0.0576
	C	0.4528	0.4457	0.4607	0.4476	0.4588	0.4497	0.4515	0.4492
64	A	0.8202	0.8211	0.8107	0.8160	0.8100	0.8085	0.8121	0.8052
	B	0.0441	0.0474	0.0422	0.0478	0.0448	0.0456	0.0498	0.0461
	C	0.4663	0.4619	0.4696	0.4616	0.4652	0.4648	0.4593	0.4646
70	A	0.8056	0.8211	0.7950	0.7969	0.8031	0.8024	0.7897	0.7985
	B	0.0525	0.0673	0.0492	0.0532	0.0594	0.0602	0.0521	0.0606
	C	0.4568	0.4381	0.4615	0.4575	0.4489	0.4475	0.4588	0.4487
87	A	0.7601	0.7510	0.7447	0.7379	0.7324	0.7542	0.7433	0.7718
	B	0.0615	0.0586	0.0530	0.0519	0.0488	0.0668	0.0599	0.0827
	C	0.4477	0.4544	0.4577	0.4630	0.4667	0.4423	0.4524	0.4216
88	A	0.7150	0.7596	0.7450	0.7438	0.7495	0.7417	0.7495	0.7407
	B	0.0285	0.0663	0.0573	0.0592	0.0634	0.0593	0.0662	0.0610
	C	0.4912	0.4429	0.4554	0.4551	0.4462	0.4525	0.4427	0.4505

Table 7.4 Parameters for the uniform sum threshold calculation as $THR = \max(N_h, N_v) \cdot (\min(N_h, N_v) / \max(N_h, N_v))^B \cdot \exp(A + C \cdot \min(N_h, N_v) / \max(N_h, N_v))$.

When the batch mode⁽⁵⁾ is used, there are cases in which only several pulses with long PRT are transmitted (i.e., surveillance). For example, only 6 pulses are used for surveillance in the batch mode of VCP 11. If power based censoring is used with the threshold of 3.5 dB above the noise power, the rate of false detections can be obtained using eq. (A.11) in Appendix A, which gives the PFA of 1.1078×10^{-4} . The coefficients for least squares fit, for such case, are given in Table 7.5.

⁵ This is mode where several long PRT pulses are followed by a large number of short PRT ones

M/PFA	5×10^{-5}	6×10^{-5}	7×10^{-5}	8×10^{-5}	9×10^{-5}	1×10^{-4}	1.1×10^{-4}	1.2×10^{-4}	
6	A	1.4783	1.4664	1.4758	1.4558	1.4507	1.4463	1.4424	1.4425
	B	-0.1114	-0.1114	-0.0975	-0.1054	-0.1027	-0.1011	-0.0991	-0.0956
	C	0.6228	0.6240	0.6050	0.6168	0.6151	0.6126	0.6105	0.6047

Table 7.5 Parameters for threshold calculation as $THR = \max(N_h, N_v) \cdot (\min(N_h, N_v) / \max(N_h, N_v))^B \cdot \exp(A + C \cdot \min(N_h, N_v) / \max(N_h, N_v))$.

Similarly, when 8 pulses are used, the resulting false alarm rate is 1.1713×10^{-5} . The coefficients for the fit are given in Table 7.6.

M/PFA	7×10^{-6}	8×10^{-6}	9×10^{-6}	1×10^{-5}	1.1×10^{-5}	1.2×10^{-4}	1.3×10^{-4}	1.4×10^{-4}	
8	A	1.4396	1.4429	1.4383	1.4358	1.4296	1.4170	1.4263	1.4067
	B	-0.0965	-0.0890	-0.0878	-0.0857	-0.0863	-0.0931	-0.0822	-0.0947
	C	0.6016	0.5918	0.5908	0.5881	0.5898	0.5983	0.5850	0.6012

Table 7.6 Parameters for threshold calculation as $THR = \max(N_h, N_v) \cdot (\min(N_h, N_v) / \max(N_h, N_v))^B \cdot \exp(A + C \cdot \min(N_h, N_v) / \max(N_h, N_v))$.

8. Summary and Conclusions

A number of different approaches for thresholding spectral moment and polarimetric data aiming at optimal detection were developed and assessed using both simulations and real data. Initially, a detection scheme within the framework of the classical probability theory was developed. It was concluded that the classical likelihood-ratio test (which yields the best possible detection rate) is not practical for implementation, in real-time, on current systems due to excessive computational requirements. Therefore, alternative approaches tailored for real-time implementation, based on intermediate computations used for computing Doppler spectral moments and polarimetric variables, were investigated. A promising scheme that directly sums the powers as well as auto- and cross-correlations produces the high rate of detection. It is termed the “uniform sum” and its performance was compared to the likelihood-ratio. The analysis indicates that the uniform sum has satisfactory performance but it still falls somewhat short of the best possible detection rate produced by the maximum likelihood approach. One of the possible reasons is that the maximum likelihood approach utilizes the information about the signal velocity and the cross-correlation phase for detection, in addition to powers, absolute values of autocorrelations and the cross-correlation used in the uniform sum. Thus, more information about the signal is used for detection in case of the maximum likelihood method than in the uniform sum approach. In reality, though, we have no prior knowledge about the signal velocity and the cross-correlation phase (as these are the parameters we need to measure). Additionally, detection using the signal velocity and cross correlation phase has detrimental effect as the detection rate produced by the maximum likelihood method rapidly declines if the actual signal velocity and the cross-

correlation phase deviate from the values that the likelihood-ratio detector is tuned to. The uniform sum, on the other hand, is not limited by this issue. It is ascertained that the performance of the uniform sum, when detecting weather signals with high correlation between H and V components, depends mostly on the SNR in the horizontal and the vertical channel and to a lesser extent on the spectrum width. Moreover, compared to the power thresholds, the uniform sum exhibits more stable detection rates with varying σ_v . This is because the variance of the power estimates declines with increasing σ_v , producing better detection rates for signals that are less coherent, and vice versa. The uniform sum estimates, however, balance out this phenomenon by using the autocorrelation measurements that have higher values for strongly coherent signals, thus offsetting the mean of uniform sum away from the threshold, effectively producing less variation in detection for various spectrum widths. Secondly, comparison to maximum likelihood method may imply that the uniform sum does not achieve the best possible detection rate given the signal information embedded in it. Consequently, it is speculated that the detection can be improved by appropriately weighting the terms in the uniform sum. This approach was investigated and it was shown that the weighting produces marginal improvements compared to the uniform sum.

Further, the guidelines for operational implementation of the uniform sum for detection were developed. Given the desired rate of false detections, the threshold value is dependent on the number of samples M and the ratio of noise powers in the horizontal and the vertical channel. The procedure for calculating the thresholds based on these parameters is devised and described. It involves assessing the probability rates of rare events for which no analytical probability distribution function can be obtained. Due to

this, Monte Carlo simulations with variance reduction techniques are used for threshold calculation yielding the procedure that is mathematically and computationally extremely intensive. Thus, it is recommended that the results be presented in a form of a look-up table with entries for each number of samples and the desired false alarm rate. The table contains coefficients which, when plugged in the appropriate formula along with the measured noise powers in horizontal and vertical channel, produce the threshold for the desired false detection rate.

This research is motivated by the desire to improve detection on dual-polarized weather radars. It was prompted by the 3 dB SNR loss in radars that transmit (and receive) simultaneously electromagnetic waves at horizontal and vertical polarizations. The forthcoming dual polarization upgrade of the WSR-88D network will employ this technique. Thus the goal is to mitigate the effects of this loss in sensitivity. The uniform sum exhibited significant improvement in signal detection rate compared to the legacy power-based censoring, hence it presents a viable solution for enhancing the signal detection capabilities in dual-polarization weather radars.

From the research work presented in this dissertation, the following topics are suggested for future study:

1. Similar approach utilizing the signal coherency along-sample time (i.e., autocorrelation) can be derived for single-polarization weather radars. The sum, in this case, would consist of the power and the autocorrelation absolute value estimates. These may be weighted for improved performance. Similar analysis ought to be performed to produce the threshold values.

2. Analysis of signal detection for oversampled signals where additional coherency in range can be used to enhance the detection. The absolute value of the lag 1 correlation in range can be added as the additional term in the sum. This may have the potential to enhance the detection because the coherency in range for oversampled signals is very stable. In case of oversampled signals, though, the SNR is decreased as opposed to non-oversampled case because of the increased receiver bandwidth. Thus, care should be taken when devising the detection scheme so that the maximum possible improvement can be achieved by using the correlation in range.

3. Investigate the possibility of signal detection in the spectral domain. The natural approach to detection in the spectral domain would be to utilize the periodogram. The signal power is concentrated in a few coefficients as opposed to the noise that is evenly spread across the entire spectrum; thus, the largest power spectrum coefficient can be used for comparison to some threshold. When working with signals from dual-polarized radar it makes sense to work with the cross-spectrum in order to utilize the cross-correlation among H and V samples. The cross-spectrum is found as $\hat{A}_{hv}(k) = \hat{A}_h^*(k) \hat{A}_v(k)$, where $\hat{A}_h(k)$ and $\hat{A}_v(k)$ are the Fourier coefficients obtained from samples in horizontal and vertical channels, respectively.

In general, this work explored the use of partial coherency in signals to enhance detection in presence of noise. Principles and approaches developed during the course of the research are not limited to dual-polarized weather radars and can be applied (with

some modification) to any case where sensing of partially coherent signals is of interest (e.g., single-polarized radars, sodars, lidars, etc.).

References

1. Crum, T.D., and R.L. Alberty, 1993: The WSR-88D and the WSR-88D Operational Support Facility. *Bull. Amer. Meteor. Soc.*, **74**, 1669–1687.
2. De Boer P-T., D.P Kroese, S. Mannor and R.Y. Rubinstein, 2005: A Tutorial on the Cross-Entropy Method. *Annals of Operations Research*, **134** (1), 19--67.
3. Denny M., 2001: Introduction to importance sampling in rare-event simulations, *European Journal of Physics*, **22**, 403-411.
4. Doviak, R.J. and D.S. Zrnić, 1993: *Doppler radar and weather observations*, Academic Press, Orlando.
5. Doviak, R. J., V. Bringi, A. Ryzhkov, A. Zahrai and D. Zrnić, 2000: Considerations for Polarimetric Upgrades to Operational WSR-88D Radars. *J. Atmos. Oceanic Technol.*, **17**, 257–278.
6. Erchard, J.D., 1991: Estimation of Radar Detection and False Alarm Probabilities, *IEEE Transactions on Aerospace and Electronic Systems*, **27**, 255-260.
7. Fang M., R. J. Doviak, and V. Melnikov, 2003: Spectrum Width Measured by WSR-88D: Error Sources and Statistics of Various Weather Phenomena, *JTECH*, **21**, 888-904
8. Keeler, R.J., and R.E. Passarelli, 1990: Signal Processing for Atmospheric Radars, *Radar in Meteorology*, D. Atlas, Ed., Amer. Meteor. Soc., 287-315.
9. Melnikov, V.M., 2004: Simultaneous Transmission Mode for the Polarimetric WSR-88D, NOAA/NSSL Report, 84 pp.
10. Miller, K.S., 1969: Complex Gaussian Processes, *SIAM Review*, **11**, 544-567.
11. Milton Abramowitz and Irene A. Stegun, 1964: *Handbook of Mathematical Functions*, Dover Publications, New York.
12. Mitchell R.L., 1981: Importance Sampling Applied to Simulations of False Alarm Statistics, *IEEE Transactions on Aerospace and Electronic Systems*, AES-17, No. 1, pp 15-24.
13. Raff M. S., 1970: On Calculating the Gamma Function on Non-Integral Arguments, *The American Statistician*, 22-24
14. Rubinstein R. Y., 1981: *Simulation and the Monte Carlo Method*, John Wiley & Sons, New York.

15. Neyman J. and E.S. Pearson, 1933: On the Problem of the Most Efficient Tests of Statistical Hypotheses, *Philosophical Transactions of the Royal Society of London. Series A, Containing Papers of a Mathematical or Physical Character*, Vol. 231. (1933), pp. 289-337.
16. Papoulis A., and S.U. Pillai, 2002: *Probability, Random Variables and Stochastic Processes*, Tata McGraw-Hill Edition.
17. Sachidananda, M., and D.S. Zrnić, 1985: Z_{DR} Measurement Consideration for a Fast Scan Capability Radar, *Radio Sci.*, **20**, 907-922.
18. Sachidananda, M., and D.S. Zrnić, 1986: Differential Propagation Phase Shift and Rainfall Rate Estimation. *Radio Sci.*, **21**, 235-247.
19. Scharfenberg K. A., K. L. Elmore, E. Forren, V. Melnikov, and D. S. Zrnić, 2005: Estimating the impact of a 3-dB sensitivity loss on WSR-88D data , *32nd Conference on Radar Meteorology*.
20. Schuur T. J., D.W. Burgess, A. V. Ryzhkov, 2003: The Joint Polarization Experiment - An Operational Demonstration of the Polarimetric WSR-88D Radar, *31st Conference on Radar Meteorology*.
21. Seliga, T.A., and V.N. Bringi, 1976: Potential use of radar differential reflectivity measurements at orthogonal polarizations for measuring precipitation. *J. Appl. Meteor.*, **15**, 69-76.
22. SIGMET, 2006: Chapter 5, *RVP8 User's Manual*, p. 36.
23. Srinivasan R., 2002: *Importance Sampling: Applications in Communications and Detection*, Springer.
24. Stacy, E. W., 1962: A Generalization of the Gamma Distribution, *Annals of Mathematical Statistics*, XXXIII (September 1962), 1187-1192.
25. Stumpf G. J., A. Witt, E. D.W. Mitchell, P. L. Spencer, J. T. Johnson, M. D. Eilts, K. W. Thomas, and D. W. Burgess, 1998: The National Severe Storms Laboratory Mesocyclone Detection Algorithm for the WSR-88D, *Weather and Forecasting*, **13**, 2, 304–326.
26. Swerling P., 1954: Probability of Detection for Fluctuating Targets, *Research Memorandum*, p. 37.
27. Tjalling J. Ypma, 1995: Historical development of the Newton-Raphson method, *SIAM Review* **37** (4), 531–551.
28. Torres, S.M., 2001: Estimation of Doppler and polarimetric variables for weather radar. Ph.D. dissertation. The University of Oklahoma, 158 pp.

29. Zrnić D.S., 1975: Simulation of weather like Doppler spectra and signals, *J. Appl. Meteorol.*, 619-620.

Appendix A

PFA Calculation for Power Based Signal Detection

The requirement of signal censoring for weather surveillance radars is that PFA is sufficiently small so that false detections do not clutter the PPI images. Moreover, because meteorological radars deal with distributed targets, missing 5 to 10 out of 100 is an acceptable trade-off for achieving low PFA. Consequently, calculation of PFA for a given threshold requires integral evaluation at the tail of *pdf*. This makes Monte Carlo methods extremely time consuming and makes it imperative to know the *pdf* in a functional form.

It is a well known fact that the sum

$$X = \sum_{m=0}^{M-1} X_m, \quad (\text{A.1})$$

of M independent exponentially distributed random variables X_m with:

$$f(y; \theta^{-1}) = \begin{cases} \frac{1}{\theta} e^{-y/\theta} & , y \geq 0 \\ 0 & , y < 0 \end{cases}, \quad (\text{A.2})$$

has gamma distribution. For completeness the proof is given as follows.

Proof: The moment generating function for each X_m is:

$$M_{X_m}(t) = (1 - \theta t)^{-1}. \quad (\text{A.3})$$

Hence,

$$M_X(t) = \sum_{m=0}^{M-1} M_{X_m}(t) = (1 - \theta t)^{-M}. \quad (\text{A.4})$$

This is the same as the moment generating function for gamma distribution with parameters:

$$f(x; M; \theta) = x^{M-1} \frac{e^{-x/\theta}}{\theta^M (M-1)!} \text{ for } x > 0. \quad (\text{A.5})$$

The formula used for power estimate is:

$$\hat{P} = \frac{1}{M} \sum_{k=0}^{M-1} P_k, \quad (\text{A.6})$$

with the mean and variance P and P^2/M , respectively. Equating these values with the mean and the variance for (A.5) (i.e., $M\theta$ and $M\theta^2$) gives $\theta = P/M$ from which we get:

$$f_N(p; M; P) = M^M p^{M-1} \frac{e^{-p \frac{M}{P}}}{P^M (M-1)!} \text{ for } p > 0, \quad (\text{A.7})$$

which after replacing P with the noise power N gives us the following PFA for a certain threshold as a function of THR :

$$PFA(M; THR) = \frac{M}{N \cdot (M-1)!} \int_{THR}^{\infty} \left(\frac{M}{N} p \right)^{M-1} e^{-p \frac{M}{N}} dp = \Gamma_{inc} \left(THR \frac{M}{N}, M \right), \quad (\text{A.8})$$

where $\Gamma_{inc}(x, \alpha)$ is the incomplete gamma function defined as:

$$\Gamma_{inc}(x, \alpha) = \frac{1}{\Gamma(\alpha)} \int_x^{\infty} e^{-t} t^{\alpha-1} dt. \quad (\text{A.9})$$

We can express THR as a function of N as:

$$THR = N \left(1 + 10^{THR_{dB}/10} \right), \quad (\text{A.10})$$

where THR_{dB} is the threshold expressed in dB relative to the noise power N (i.e., $THR_{dB} = 10 \log_{10}(THR/N)$). Note that in operation, the known (measured) noise power is always subtracted from the estimate. Hence, the effective threshold for (A.6) is as above. Now we can calculate the PFA for power threshold as:

$$PFA \left[M; N \cdot \left(1 + 10^{THR_{dB}/10} \right) \right] = \Gamma_{inc} \left[M \cdot \left(1 + 10^{THR_{dB}/10} \right), M \right]. \quad (\text{A.11})$$

If we put the power threshold to be 2 dB above the noise level this gives us low PFA of only 1.1749×10^{-6} . If the threshold is lowered to -1 dB above noise the PFA increases to 0.003. If we desire to have PFA to be 10^{-5} , then the threshold needs to be set to 1.4183 dB above noise.

In the remainder of this appendix we also find the general moment expression for noise power estimates. We have:

$$M_{\hat{p}}(t) = \left(1 - \frac{P}{M}t\right)^{-M} \quad \text{and} \quad E\{\hat{P}^n\} = \left. \frac{d^n}{dt^n} \right|_{t=0} M_{\hat{p}}(t), \quad (\text{A.12})$$

which gives

$$\begin{aligned} E\{\hat{P}\} &= \left. \left(1 - \frac{P}{M}t\right)^{-M-1} (-M) \left(-\frac{P}{M}\right) \right|_{t=0} = P, \\ E\{\hat{P}^2\} &= P \left. \left(1 - \frac{P}{M}t\right)^{-M-2} (-M-1) \left(-\frac{P}{M}\right) \right|_{t=0} = \frac{M+1}{M} P^2, \\ E\{\hat{P}^3\} &= \frac{M+1}{M} P^2 \left. \left(1 - \frac{P}{M}t\right)^{-M-3} (-M-2) \left(-\frac{P}{M}\right) \right|_{t=0} = \frac{(M+1)(M+2)}{M^2} P^3. \end{aligned} \quad (\text{A.13})$$

In general:

$$\begin{aligned} E\{\hat{P}^n\} &= \frac{M^M}{P^M (M-1)!} \int_0^\infty p^{M-1+n} e^{-p \frac{M}{P}} dp = \frac{P^n \Gamma(M+n)}{M^n (M-1)!} = \frac{(M+n-1)!}{M!} \frac{P^n}{M^{n-1}} \\ &= \frac{\prod_{i=1}^{n-1} (M+i)}{M^{n-1}} P^n. \end{aligned} \quad (\text{A.14})$$

Appendix B

Use of Gamma Distribution and Generalized Laguerre Polynomials for *pdf* Approximation and Moment Interpolation

Gamma distribution is defined as:

$$f(x) = \begin{cases} \frac{x^\alpha e^{-x/\theta}}{\theta^{\alpha+1} \Gamma(\alpha+1)} & \text{if } x > 0, \\ 0 & \text{if } x < 0. \end{cases} \quad (\text{B.1})$$

It is known fact that the mean and the variance of this distribution are:

$$\begin{aligned} m &= (\alpha+1)\theta \\ \sigma^2 &= (\alpha+1)\theta^2. \end{aligned} \quad (\text{B.2})$$

Knowing this we can express the parameters α and θ in terms of m and σ^2 as:

$$\begin{aligned} \alpha+1 &= m^2/\sigma^2 \\ \theta &= \sigma^2/m. \end{aligned} \quad (\text{B.3})$$

Thus, if the mean and the variance of a *pdf* are known we can approximate it with the gamma distribution. If matching to more than just the first two moments is desired, an error correction must be applied as described in Chapter 10. When the weighting function is gamma distribution, to achieve error correction we turn to **generalized Laguerre polynomials** which are defined as:

$$L_n^{(\alpha)}(x) = \frac{x^{-\alpha} e^x}{n!} \frac{d^n}{dx^n} (e^{-x} x^{n+\alpha}). \quad (\text{B.4})$$

The associated Laguerre polynomials are orthogonal over $[0, \infty)$ with respect to the weighting function $x^\alpha e^{-x}$:

$$\int_0^\infty e^{-x} x^\alpha L_n^{(\alpha)}(x) L_m^{(\alpha)}(x) dx = \frac{\Gamma(n+\alpha+1)}{n!} \delta_{nm}. \quad (\text{B.5})$$

The generalized Laguerre polynomial of degree n is:

$$L_n^{(\alpha)}(x) = \sum_{m=0}^n \binom{n+\alpha}{n-m} \frac{(-x)^m}{m!} = \sum_{m=0}^n \frac{\Gamma(n+\alpha+1)}{(n-m)!\Gamma(\alpha+m+1)} \frac{(-x)^m}{m!}. \quad (\text{B.6})$$

The first five generalized Laguerre polynomials are:

$$\begin{aligned} L_0^{(\alpha)}(x) &= 1 \\ L_1^{(\alpha)}(x) &= -x + \alpha + 1 \\ L_2^{(\alpha)}(x) &= \frac{1}{2} \left(x^2 - 2x(\alpha + 2) + (\alpha + 2)(\alpha + 1) \right) \\ L_3^{(\alpha)}(x) &= \frac{1}{6} \left(-x^3 + 3x^2(\alpha + 3) - 3x \prod_{i=2}^3 (\alpha + i) + \prod_{i=1}^3 (\alpha + i) \right) \\ L_4^{(\alpha)}(x) &= \frac{1}{24} \left(x^4 - 4x^3(\alpha + 4) + 6x^2 \prod_{i=3}^4 (\alpha + i) - 4x \prod_{i=2}^4 (\alpha + i) + \prod_{i=1}^4 (\alpha + i) \right) \\ L_5^{(\alpha)}(x) &= \frac{1}{120} \left(-x^5 + 5x^4(\alpha + 5) - 10x^3 \prod_{i=4}^5 (\alpha + i) + 10x^2 \prod_{i=3}^5 (\alpha + i) - \right. \\ &\quad \left. 5x \prod_{i=2}^5 (\alpha + i) + \prod_{i=1}^5 (\alpha + i) \right). \end{aligned} \quad (\text{B.7})$$

Apparently, if we use gamma approximation as previously shown the first two moments of the approximation will be the same as those of the true *pdf*. Unfortunately, this is not valid for higher moments. Let's say we want to perform error correction up to the n -th moment. Let our approximation function be:

$$pdf \approx f(x) = \frac{x^\alpha e^{-x/\theta}}{\theta^{\alpha+1} \Gamma(\alpha+1)} \sum_{k=0}^n C_k L_k^{(\alpha)} \left(\frac{x}{\theta} \right), \quad (\text{B.8})$$

where C_k are coefficients which need to be determined so that $m_k = m'_k$ (where m_k is true *pdf* k -th moment, and m'_k is the approximation k -th moment) for $k = 0, \dots, n$.

For $f(x)$ to be *pdf* it must satisfy:

$$\int_0^{\infty} 1 \cdot f(x) dx = 1. \quad (\text{B.9})$$

Apparently, $1 = L_0^{(\alpha)}(x/\theta)$ so we write:

$$\int_0^{\infty} 1 \cdot f(x) dx = \frac{1}{\theta \Gamma(\alpha + 1)} \sum_{k=0}^n C_k \int_0^{\infty} \frac{x^\alpha}{\theta^\alpha} e^{-x/\theta} L_0^{(\alpha)}\left(\frac{x}{\theta}\right) L_k^{(\alpha)}\left(\frac{x}{\theta}\right) dx, \quad (\text{B.10})$$

which after taking $x/\theta = t$ becomes

$$\int_0^{\infty} 1 \cdot f(x) dx = \frac{1}{\Gamma(\alpha + 1)} \sum_{k=0}^n C_k \int_0^{\infty} t^\alpha e^{-t} L_0^{(\alpha)}(t) L_k^{(\alpha)}(t) dt. \quad (\text{B.11})$$

Using (B.5) we get:

$$\int_0^{\infty} 1 \cdot f(x) dx = \frac{1}{\Gamma(\alpha + 1)} \cdot C_0 \frac{\Gamma(\alpha + 1)}{0!} = C_0 = 1. \quad (\text{B.12})$$

To find C_1 :

$$\begin{aligned} \int_0^{\infty} x \cdot f(x) dx &= \frac{1}{\theta \Gamma(\alpha + 1)} \sum_{k=0}^n C_k \int_0^{\infty} \frac{x^\alpha}{\theta^\alpha} e^{-x/\theta} \theta \left(-L_1^{(\alpha)}\left(\frac{x}{\theta}\right) + (\alpha + 1)L_0^{(\alpha)}\left(\frac{x}{\theta}\right) \right) L_k^{(\alpha)}\left(\frac{x}{\theta}\right) dx \\ &= \frac{\theta}{\Gamma(\alpha + 1)} \sum_{k=0}^n C_k \int_0^{\infty} t^\alpha e^{-t} \left(-L_1^{(\alpha)}(t) + (\alpha + 1)L_0^{(\alpha)}(t) \right) L_k^{(\alpha)}(t) dt \\ &= \frac{\theta}{\Gamma(\alpha + 1)} \left(-C_1 \frac{\Gamma(\alpha + 2)}{2!} + (\alpha + 1)C_0 \Gamma(\alpha + 1) \right) \\ &= -\frac{\theta}{\Gamma(\alpha + 1)} C_1 \frac{\Gamma(\alpha + 2)}{2!} + (\alpha + 1)\theta. \end{aligned} \quad (\text{B.13})$$

Apparently, from (B.2) we have $C_1 = 0$. Following the same approach we also get $C_2 = 0$.

This is expected as gamma distribution parameters are set so that the first two moments are the same as those of true *pdf*, hence do not need correction. Notice that because Laguerre polynomials are orthogonal to each other and each x^k is represented uniquely as a linear combination of $L_n^{(\alpha)}$'s where $n \leq k$, the value of each C_k influences only the moments of order greater than or equal to k . This enables for the moment correction in a step-wise manner, where the values obtained in each stage have no bearing on the values yielded by previous steps. To demonstrate this let us find the value of C_3 .

$$\int_0^{\infty} x^3 f(x) dx = \frac{\theta^2}{\Gamma(\alpha+1)} \sum_{k=0}^3 C_k \int_0^{\infty} \frac{x^\alpha}{\theta^\alpha} e^{-x/\theta} \left(-6L_3^{(\alpha)}\left(\frac{x}{\theta}\right) + \sum_{j=0}^2 A_j L_j^{(\alpha)}\left(\frac{x}{\theta}\right) \prod_{i=j+1}^3 (\alpha+i) \right) \times L_k^{(\alpha)}\left(\frac{x}{\theta}\right) dx, \quad (\text{B.14})$$

where $A_0 = 1$, $A_1 = -3$, and $A_2 = 6$. Then:

$$m_3 = \frac{\theta^3}{\Gamma(\alpha+1)} \left(-C_3 6 \frac{\Gamma(\alpha+4)}{6} + \Gamma(\alpha+1)(\alpha+1)(\alpha+2)(\alpha+3) \right). \quad (\text{B.15})$$

Finally we have:

$$C_3 = 1 - \frac{\Gamma(\alpha+1)}{\Gamma(\alpha+4)} \frac{m_3}{\theta^3} = 1 - \frac{1}{(\alpha+2)(\alpha+3)} \frac{m}{(\sigma^2)^2} m_3. \quad (\text{B.16})$$

Following this procedure we can perform error correction up to the n -th moment. Listed below are coefficient values for error correction up to the 5-th moment:

$$\begin{aligned} C_4 &= -1 + 4C_3 + \frac{\Gamma(\alpha+1)}{\Gamma(\alpha+5)} \frac{m_4}{\theta^4} = 3 - \frac{4}{\prod_{i=2}^3 (\alpha+i)} \frac{m}{(\sigma^2)^2} m_3 + \frac{1}{\prod_{i=2}^4 (\alpha+i)} \frac{m^2}{(\sigma^2)^3} m_4 \\ C_5 &= 1 - 10C_3 + 5C_4 - \frac{\Gamma(\alpha+1)}{\Gamma(\alpha+6)} \frac{m_5}{\theta^5} \\ &= 6 - \frac{10}{\prod_{i=2}^3 (\alpha+i)} \frac{m}{(\sigma^2)^2} m_3 + \frac{5}{\prod_{i=2}^4 (\alpha+i)} \frac{m^2}{(\sigma^2)^3} m_4 - \frac{1}{\prod_{i=2}^5 (\alpha+i)} \frac{m^3}{(\sigma^2)^4} m_5. \end{aligned} \quad (\text{B.17})$$

General coefficient is:

$$C_n = (-1)^{n+1} \left(1 + \sum_{k=3}^{n-1} \frac{n!}{(n-k)!k!} (-1)^k C_k - \frac{\Gamma(\alpha+1)}{\Gamma(\alpha+n+1)} \frac{m_n}{\theta^n} \right). \quad (\text{B.18})$$

Taking into account that $C_0 = 1$, and $C_1, C_2 = 0$ the approximation expression with error corrected up to the n -th moment is:

$$pdf \approx \frac{x^\alpha e^{-x/\theta}}{\theta^{\alpha+1} \Gamma(\alpha+1)} \left(1 + \sum_{k=3}^n C_k L_k^{(\alpha)}\left(\frac{x}{\theta}\right) \right). \quad (\text{B.19})$$

Given the approximation (B.19) we can now interpolate the moments as described in section 5.4. Substituting $y = x^{1/2}$ and using formula we get:

$$\begin{aligned} f_Y(y) &\approx \frac{2y^{2\alpha+1}e^{-y^2/\theta}}{\theta^{\alpha+1}\Gamma(\alpha+1)} \left(1 + \sum_{k=3}^n C_k L_k^{(\alpha)} \left(\frac{y^2}{\theta} \right) \right) \\ &\approx \frac{2y^{2\alpha+1}e^{-y^2/\theta}}{\theta^{\alpha+1}\Gamma(\alpha+1)} \left(1 + \sum_{k=3}^n C_k \sum_{m=0}^k \frac{\Gamma(n+\alpha+1)}{m!(n-m)!\Gamma(\alpha+m+1)} \frac{(-y^2)^m}{\theta^m} \right). \end{aligned} \quad (\text{B.20})$$

Thus the moment approximation formula is:

$$\begin{aligned} E\{Y^n\} &\approx \frac{2}{\theta^{\alpha+1}\Gamma(\alpha+1)} \left(\int_0^\infty y^{2\alpha+n+1} e^{-\frac{y^2}{\theta}} dy + \right. \\ &\quad \left. \sum_{k=3}^n C_k \sum_{m=0}^k \frac{\Gamma(n+\alpha+1)(-1)^m}{m!(n-m)!\Gamma(\alpha+m+1)} \int_0^\infty y^{2\alpha+n+1} e^{-\frac{y^2}{\theta}} \left(\frac{y^2}{\theta} \right)^m dy \right). \end{aligned} \quad (\text{B.21})$$

General expression that we need to solve is:

$$\int_0^\infty y^{2\alpha+n+1} e^{-\frac{y^2}{\theta}} \frac{y^{2k}}{\theta^k} dy = \theta^{\alpha+\frac{n+1}{2}} \int_0^\infty \left(\frac{y^2}{\theta} \right)^{\alpha+\frac{n+1}{2}} e^{-\frac{y^2}{\theta}} \left(\frac{y^2}{\theta} \right)^k dy. \quad (\text{B.22})$$

Let us do the following substitution:

$$\frac{y^2}{\theta} = t \Rightarrow \frac{2y}{\theta} dy = dt \Rightarrow dy = \frac{\theta}{2y} dt = \frac{\sqrt{\theta}}{2\sqrt{t}} dt. \quad (\text{B.23})$$

Thus we get:

$$\begin{aligned} \int_0^\infty y^{2\alpha+n+1} e^{-\frac{y^2}{\theta}} \frac{y^{2k}}{\theta^k} dy &= \theta^{\alpha+\frac{n+1}{2}} \int_0^\infty t^{\alpha+\frac{n+1}{2}} e^{-t} t^k \frac{\sqrt{\theta}}{2\sqrt{t}} dt \\ &= \frac{\theta^{\alpha+\frac{n+1}{2}}}{2} \int_0^\infty t^{\alpha+\frac{n}{2}+k+1-1} e^{-t} dt \\ &= \frac{\theta^{\alpha+\frac{n+1}{2}}}{2} \Gamma\left(\alpha + \frac{n}{2} + k + 1\right). \end{aligned} \quad (\text{B.24})$$

Finally:

$$E\{Y^n\} \approx \frac{\theta^{\frac{n}{2}}}{\Gamma(\alpha+1)} \left(\Gamma\left(\alpha + \frac{n}{2} + 1\right) + \sum_{k=3}^n C_k \sum_{m=0}^k \frac{(-1)^m \Gamma(n+\alpha+1)}{m!(n-m)! \Gamma(\alpha+m+1)} \Gamma\left(\alpha + \frac{n}{2} + m + 1\right) \right). \quad (\text{B.25})$$

In order to approximate using an exponential distribution, we use the previous derivation by noting that if we set $\alpha = 0$ and $\theta = m$, gamma distribution becomes exponential with the mean m . Because exponential distribution has only one degree of freedom the correction starts from the second moment. Then we have:

$$E\{Y^n\} \approx m^{\frac{n}{2}} \left[\Gamma\left(\frac{n}{2} + 1\right) + \sum_{k=2}^n C_k \sum_{l=0}^k \frac{(-1)^l n!}{(l!)^2 (n-l)!} \Gamma\left(\frac{n}{2} + l + 1\right) \right] \approx m^{\frac{n}{2}} \Gamma\left(\frac{n}{2} + 1\right) \left[1 + \sum_{k=2}^n C_k \left(1 + \sum_{l=1}^k \frac{(-1)^l n!}{(l!)^2 (n-l)!} \left(\frac{n}{2} + 1\right) \cdots \left(\frac{n}{2} + l\right) \right) \right], \quad (\text{B.26})$$

where each coefficient is found as:

$$C_n = (-1)^{n+1} \left(1 + \sum_{k=2}^{n-1} \frac{n!}{(n-k)! k!} (-1)^k C_k - \frac{1}{n!} \frac{m_n}{m^n} \right). \quad (\text{B.27})$$

Appendix C

Use of Generalized Gamma Distribution for *pdf* Approximation and Moment Interpolation

The generalized gamma distribution is given as (Stacy 1962):

$$f(x) = \begin{cases} \frac{x^{p-1} e^{-\left(\frac{x}{a}\right)^{\frac{1}{q}}}}{qa^p \Gamma(qp)} & \text{if } x \geq 0 \\ 0 & \text{if } x < 0 \end{cases} \quad (\text{C.1})$$

This distribution has three degrees of freedom hence if matching to more than the first three moments is required the correction needs to be performed. Unfortunately, this distribution does not have the family of polynomials that are orthogonal with respect to it. Consequently, orthogonal polynomials must be derived following the procedure given in section 5.2. To do this, we need to define the inner product as:

$$\langle f(x), g(x) \rangle = \int_0^{\infty} f(x) g(x) \frac{x^{p-1} e^{-\left(\frac{x}{a}\right)^{\frac{1}{q}}}}{qa^p \Gamma(qp)} dx \quad (\text{C.2})$$

Because in our case $f(x)$ and $g(x)$ are polynomials it is convenient to note that:

$$\langle x^n, 1 \rangle = \int_0^{\infty} x^n \frac{x^{p-1} e^{-\left(\frac{x}{a}\right)^{\frac{1}{q}}}}{qa^p \Gamma(qp)} dx = a^n \frac{\Gamma(qp + qn)}{\Gamma(qp)} \quad (\text{C.3})$$

Then, the inner product of two polynomials is carried by multiplying them to obtain new polynomial in which each variable power of n is replaced by (C.3). This provides an avenue for efficiently evaluating inner products. Despite of this, the derivation of higher order polynomials and the correction coefficients proves extremely involved. Because of that, it is done with the aid of the MATLAB symbolic toolbox. In that regard, all further

formulas in this chapter will be given in MATLAB format. The procedure is described next.

Let us introduce the following notation:

$$\begin{aligned}
 G &= \text{gamma}(q*p); \\
 G1 &= \text{gamma}(q*p+q); \\
 G2 &= \text{gamma}(q*p+2*q); \\
 G3 &= \text{gamma}(q*p+3*q); \\
 G4 &= \text{gamma}(q*p+4*q); \\
 G5 &= \text{gamma}(q*p+5*q); \\
 G6 &= \text{gamma}(q*p+6*q); \\
 G7 &= \text{gamma}(q*p+7*q); \\
 G8 &= \text{gamma}(q*p+8*q); \\
 G9 &= \text{gamma}(q*p+9*q); \\
 G10 &= \text{gamma}(q*p+10*q);
 \end{aligned}
 \tag{C.4}$$

First we set symbolic variables as:

```
>> syms x a G G1 G2 G3 G4 G5 G6 G7 G8
```

Then we choose the zeroth and the first polynomials as:

```
>> p0 = 1
```

```
>> p1 = x - a*G1/G
```

Then we need to find the coefficient b_2 as:

```
>> collect(x*p1*p1)
```

Replace the powers of x as in the Table C.1.

x^6	a^6*G6/G
x^5	a^5*G5/G
x^4	a^4*G4/G
x^3	a^3*G3/G
x^2	a^2*G2/G
x	$a*G1/G$

Table C.1 Variable replacement.

We get:

```
>> t0 = a^3*G3/G-2*a^2*G2/G+a*G1/G+a*G1/G*a^2*G1^2/G^2
```

Then:

```
>> collect(p1*p1)
```

Again replace the powers of x to get:

```
>> t1 = a^2*G2/G-2*a*G1/G*a*G1/G+a^2*G1^2/G^2
```

The b_2 coefficient is then found as:

```
>> b2 = simplify(t0/t1)
```

The similar procedure is then followed to obtain c_2 . It goes as:

```
>> collect(x*p1*p0)
```

Because p_0 equals one:

```
>> c2 = a^2*G2/G-a*G1/G*a*G1/G
```

Get the p_2 polynomial as:

```
>> p2=collect(simplify((x-b2)*p1-c2*p0))
```

```
>> p2 = x^2+(-a*G3*G+G2*a*G1)/(G2*G-G1^2)*x+(a^2*G3*G1-a^2*G2^2)/(G2*G-G1^2);
```

The polynomial p_3 is obtained in a similar manner as:

```
>> collect(x*p2*p2)
```

Replace powers of x to obtain t_0 .

```
>> collect(p2*p2)
```

Replace powers of x to obtain t_1 .

Get b_3 as:

```
>> b3 = simplify(t0/t1)
```

Then,

```
>> collect(x*p2*p1)
```

Replace powers of x to obtain t_0 .

```
>> collect(p1*p1)
```

Replace powers of x to obtain $t1$.

Get $c3$ as:

```
>> c3 = simplify(t0/t1)
```

Get $p3$ as:

```
>> p3=collect(simplify((x-b3)*g2-c3*g1))
```

By now the expression for the third polynomial has grown so large and we shall omit the expression itself because it does not contribute to the clarity of the procedure description.

We calculate the fourth polynomial next (using the same procedure already described for the first three polynomials). The C_4 correction coefficient is now:

$$C_4 = \frac{m_4 - a^4 \frac{\Gamma(qp + 4q)}{\Gamma(qp)}}{\langle x^4, p_4 \rangle} . \quad (C.5)$$

Thus, we need to calculate the inner product in the denominator. This is done as:

```
>> collect(x^4*p4)
```

Replace powers of x to obtain $t0$. Then,

```
>> C4 = (m4 - a^4*G4/G)/simplify(t0)
```

We could continue by finding the $p5$ and $C5$, but it is the experience of the author that the correction, in MATLAB, for moments beyond the 4-th fails due to the rounding errors.

Hence, when the general gamma distribution is used for approximation of the correction only up to the 4-th moment is numerically possible.

The approximation function is now:

$$f(x) \approx \frac{x^{p-1} e^{-\left(\frac{x}{a}\right)^{1/q}}}{qa^p \Gamma(qp)} (1 + C_4 p_4(x)) . \quad (C.6)$$

Let us now analyze how to achieve the interpolation of odd moments. Substituting $y = x^{1/2}$ we get:

$$f(y) \approx 2 \frac{y^{2p-1} e^{-\left(\frac{y^2}{a}\right)^{1/q}}}{qa^p \Gamma(qp)} \left(1 + C_4 p_4(y^2)\right) = 2 \frac{y^{2p-1} e^{-\left(\frac{y^2}{a}\right)^{1/q}}}{qa^p \Gamma(qp)} \left(1 + C_4 \sum_{k=0}^4 c_{p4}(k) y^{2k}\right), \quad (\text{C.7})$$

where $c_{p4}(k)$ are the coefficients of the polynomial. Then the n -th moment is:

$$\begin{aligned} m_n &\approx \int_0^\infty 2 \frac{y^{2p-1} e^{-\left(\frac{y^2}{a}\right)^{1/q}}}{qa^p \Gamma(qp)} \left(1 + C_4 \sum_{k=0}^4 c_{p4}(k) y^{2k}\right) dy \\ &\approx a^{\frac{n}{2}} \frac{\Gamma\left(q\left(p + \frac{n}{2}\right)\right)}{\Gamma(qp)} + C_4 \sum_{k=0}^4 c_{p4}(k) a^{\frac{n}{2}+k} \frac{\Gamma\left(q\left(p+k + \frac{n}{2}\right)\right)}{\Gamma(qp)} y^{2k}. \end{aligned} \quad (\text{C.8})$$

Appendix D

Gaussian Random Variable Product Mathematical Expectation

In Papoulis (2002) (pg. 258) it is shown that the product of four jointly normal random variables with zero mean is:

$$E\{V_1V_2V_3V_4\} = C_{12}C_{34} + C_{13}C_{24} + C_{14}C_{23} \quad (\text{D.1})$$

where $C_{ij} = E\{V_iV_j\}$. In our applications, however, we encounter cases where we desire to evaluate the mathematical expectation of the product of six or more jointly normal random variables. Following the same procedure as in Papoulis (2002), it can be proved that in general:

$$E\{V_1 \dots V_n\} = \sum C_{m_1m_2} \dots C_{m_{n-1}m_n}, \quad (\text{D.2})$$

where the sum in this particular case denotes the sum of all products $C_{m_1m_2} \dots C_{m_{n-1}m_n}$ obtained by taking all possible $n/2$ -combinations of the elements of the set $A = \{(m_1, m_2), \dots, (m_{n-1}, m_n)\}$ such that $m_1 \neq m_2 \neq \dots \neq m_n$. The set A is obtained by taking all possible 2-combinations from the set $\{1, \dots, n\}$.

Proof: From Papoulis (2002) we have (pg. 257, eq. 7-60):

$$E\left\{e^{j(\omega_1V_1 + \dots + \omega_nV_n)}\right\} = \exp\left\{-\frac{1}{2} \sum_{m=1}^n \sum_{k=1}^n \omega_m \omega_k C_{mk}\right\}. \quad (\text{D.3})$$

We expand exponentials on both sides of (D.3) and show explicitly only the terms containing the product $\omega_1 \dots \omega_n$:

$$\begin{aligned}
E\left\{e^{j(\omega_1 V_1 + \dots + \omega_n V_n)}\right\} &= \dots + \frac{j^n}{n!} E\left\{(\omega_1 V_1 + \dots + \omega_n V_n)^n\right\} + \dots \\
&= \dots + \frac{j^n}{n!} E\left\{\sum_{k_1 + \dots + k_n = n} \frac{n!}{k_1! \dots k_n!} (\omega_1 V_1)^{k_1} \dots (\omega_n V_n)^{k_n}\right\} + \dots \\
&= \dots + (-1)^{\frac{n}{2}} \frac{n!}{n!} E\{V_1 \dots V_n\} \omega_1 \dots \omega_n + \dots
\end{aligned} \tag{D.4}$$

$$\exp\left\{-\frac{1}{2} \sum_{m=1}^n \sum_{k=1}^n \omega_m \omega_k C_{mk}\right\} = \dots + \frac{1}{(n/2)!} \left(-\frac{1}{2} \sum_{m=1}^n \sum_{k=1}^n \omega_m \omega_k C_{mk}\right)^{\frac{n}{2}} + \dots$$

Because $\omega_m \omega_k C_{mk} = \omega_k \omega_m C_{km}$, we can write the double summation term as:

$$\sum_{m=1}^n \sum_{k=1}^n \omega_m \omega_k C_{mk} = \sum_{k=1}^n (\omega_k)^2 C_{kk} + 2 \sum_{m,k,m \neq k} \omega_m \omega_k C_{mk}. \tag{D.5}$$

The second term denotes the sum of all elements $\omega_m \omega_k C_{mk}$, where each (m,k) is a two element combination (i.e., 2-combination) from the set $\{1, \dots, n\}$. Because we are interested only in terms containing the product $\omega_1 \dots \omega_n$ we can write:

$$\begin{aligned}
\exp\left\{-\frac{1}{2} \sum_{m=1}^n \sum_{k=1}^n \omega_m \omega_k C_{mk}\right\} &= \dots + \frac{(-1)^{\frac{n}{2}}}{2^{n/2} (n/2)!} \left(\sum_{k=1}^n (\omega_k)^2 C_{kk} + 2 \sum_{m,k,m \neq k} \omega_m \omega_k C_{mk}\right)^{\frac{n}{2}} + \dots \\
&= \dots + \frac{(-1)^{\frac{n}{2}}}{(n/2)!} \left(\sum_{m,k,m \neq k} \omega_m \omega_k C_{mk}\right)^{\frac{n}{2}} + \dots \\
&= \dots + \frac{(-1)^{\frac{n}{2}}}{(n/2)!} \sum_{l_1 + \dots + l_{n/2} = n/2} \frac{(n/2)!}{l_1! \dots l_{n/2}!} (\omega_{m_1} \omega_{k_1} C_{m_1 k_1})^{l_1} \dots \\
&\quad (\omega_{m_{n/2}} \omega_{k_{n/2}} C_{m_{n/2} k_{n/2}})^{l_{n/2}} + \dots
\end{aligned} \tag{D.6}$$

Again, we are interested only in terms containing the product $\omega_1 \dots \omega_n$, hence we have $l_i = 1$ ($i=1, \dots, n/2$). Note also that in the above formula not all cases when $l_i = 1$ will have the product $\omega_1 \dots \omega_n$ as some of the subscripts values in ω will repeat. Thus, we choose only the terms where all ω subscripts are different. Finally, to single out the terms with the product $\omega_1 \dots \omega_n$ we write those as:

$$\exp\left\{-\frac{1}{2}\sum_{m=1}^n\sum_{k=1}^n\omega_m\omega_k C_{mk}\right\}=\dots+(-1)^{\frac{n}{2}}\sum\omega_1\dots\omega_n C_{m_1m_2}\dots C_{m_{n-1}m_n}+\dots, \quad (\text{D.7})$$

where each $\{(m_1, m_2)\dots(m_{n-1}, m_n)\}$ is a $n/2$ -combination of the elements taken from the set of all possible 2-combinations of the set $\{1, \dots, n\}$ such that $m_1 \neq m_2 \neq \dots \neq m_n$. This proves (D.2).

In particular, for $n = 6$ we have:

$$\begin{aligned} E\{V_1V_2V_3V_4V_5V_6\} &= C_{12}C_{34}C_{56} + C_{12}C_{35}C_{46} + C_{12}C_{36}C_{45} + \\ &C_{13}C_{24}C_{56} + C_{13}C_{25}C_{46} + C_{13}C_{26}C_{45} + \\ &C_{14}C_{23}C_{56} + C_{14}C_{25}C_{36} + C_{14}C_{26}C_{35} + \\ &C_{15}C_{23}C_{46} + C_{15}C_{34}C_{26} + C_{15}C_{36}C_{45} + \\ &C_{16}C_{34}C_{25} + C_{16}C_{23}C_{45} + C_{16}C_{24}C_{35}. \end{aligned} \quad (\text{D.8})$$

We deal with complex random variables and the form we encounter is $E\{V_1V_2^*V_3V_4^*V_5V_6^*\}$.

The weather radar voltage sample is of the form (Doviak and Zrnić 1993):

$$V_k = s_k e^{j\theta_k} + n_k e^{j\alpha_k}, \quad (\text{D.9})$$

where s_k and n_k are the signal and the noise amplitudes, respectively. Both are independent Rayleigh distributed random variables. Uniformly distributed random variables α_k and θ_k represent signal and noise phases, respectively. Let us now consider:

$$E\{V_k V_l\} = E\{s_k s_l\} E\{e^{j(\theta_k + \theta_l)}\} + E\{n_k n_l\} E\{e^{j(\alpha_k + \alpha_l)}\}. \quad (\text{D.10})$$

We claim that:

$$E\{V_k V_l\} = 0, \text{ because } E\{e^{j(\beta_k + \beta_l)}\} = 0. \quad (\text{D.11})$$

for every two uniformly distributed random variables β_k and β_l between $[-\pi, \pi]$.

Proof: The resultant pdf of the sum $\gamma = \beta_k + \beta_l$ is:

Case 1: If $k = l$

$$P(a < 2\beta_k < b) = P\left(\frac{a}{2} < \beta_k < \frac{b}{2}\right) = \frac{1}{2\pi} \int_{a/2}^{b/2} d\beta_k = \frac{1}{4\pi} \int_a^b d\gamma. \quad (\text{D.12})$$

Hence, the sum is uniformly distributed between $[-2\pi, 2\pi]$. Then we have:

$$E\left\{e^{j(\beta_k + \beta_l)}\right\} = E\left\{e^{j\gamma}\right\} = \frac{1}{4\pi} \int_{-2\pi}^{2\pi} e^{j\gamma} d\gamma = \frac{e^{j2\pi} - e^{-j2\pi}}{j4\pi} = 0. \quad (\text{D.13})$$

Case 2: If $k \neq l$

$$P(a < \beta_k + \beta_l < b) = \frac{1}{(2\pi)^2} \int_a^{b-\pi} \int_{\gamma-\pi}^{\gamma+\pi} d\beta_k d\gamma = \frac{1}{2\pi} \int_a^b d\gamma. \quad (\text{D.14})$$

Hence, the sum is uniformly distributed between $[-\pi, \pi]$. Then we have:

$$E\left\{e^{j(\beta_k + \beta_l)}\right\} = E\left\{e^{j\gamma}\right\} = \frac{1}{2\pi} \int_{-\pi}^{\pi} e^{j\gamma} d\gamma = \frac{e^{j\pi} - e^{-j\pi}}{j2\pi} = 0. \quad (\text{D.15})$$

Using (D.8) we write:

$$E\left\{V_1 V_2^* V_3 V_4^* V_5 V_6^*\right\} = C_{12} C_{34} C_{56} + C_{12} C_{36} C_{45} + C_{14} C_{23} C_{56} + C_{14} C_{25} C_{36} + C_{16} C_{34} C_{25} + C_{16} C_{23} C_{45}. \quad (\text{D.16})$$

Similarly,

$$\begin{aligned} E\left\{V_1 V_2^* V_3 V_4^* V_5 V_6^* V_7 V_8^*\right\} = & \\ & C_{12} (C_{34} C_{56} C_{78} + C_{34} C_{58} C_{67} + C_{36} C_{45} C_{78} + C_{36} C_{47} C_{58} + C_{38} C_{56} C_{47} + C_{38} C_{45} C_{67}) + \\ & C_{14} (C_{32} C_{56} C_{78} + C_{32} C_{58} C_{67} + C_{36} C_{25} C_{78} + C_{36} C_{27} C_{58} + C_{38} C_{56} C_{27} + C_{38} C_{25} C_{67}) + \\ & C_{16} (C_{32} C_{54} C_{78} + C_{32} C_{58} C_{47} + C_{34} C_{25} C_{78} + C_{34} C_{27} C_{58} + C_{38} C_{54} C_{27} + C_{38} C_{25} C_{47}) + \\ & C_{18} (C_{32} C_{54} C_{76} + C_{32} C_{56} C_{47} + C_{34} C_{25} C_{76} + C_{34} C_{27} C_{56} + C_{36} C_{54} C_{27} + C_{36} C_{25} C_{47}). \end{aligned} \quad (\text{D.17})$$

and,

$$\begin{aligned}
& E\{V_1V_2^*V_3V_4^*V_5V_6^*V_7V_8^*V_9V_{10}^*\} = \\
& C_{12} \left[C_{34} (C_{56}C_{78}C_{9,10} + C_{56}C_{7,10}C_{89} + C_{58}C_{67}C_{9,10} + C_{58}C_{69}C_{7,10} + C_{510}C_{78}C_{69} + C_{5,10}C_{67}C_{89}) + \right. \\
& \quad C_{36} (C_{54}C_{78}C_{9,10} + C_{54}C_{7,10}C_{89} + C_{58}C_{47}C_{9,10} + C_{58}C_{49}C_{7,10} + C_{5,10}C_{78}C_{49} + C_{5,10}C_{47}C_{89}) + \\
& \quad \left. C_{38} (C_{56}C_{74}C_{9,10} + C_{56}C_{7,10}C_{49} + C_{54}C_{67}C_{9,10} + C_{54}C_{69}C_{7,10} + C_{5,10}C_{74}C_{69} + C_{5,10}C_{67}C_{49}) \right] + \\
& C_{14} \left[C_{32} (C_{56}C_{78}C_{9,10} + C_{56}C_{7,10}C_{89} + C_{58}C_{67}C_{9,10} + C_{58}C_{69}C_{7,10} + C_{5,10}C_{78}C_{69} + C_{5,10}C_{67}C_{89}) + \right. \\
& \quad C_{36} (C_{52}C_{78}C_{9,10} + C_{52}C_{7,10}C_{89} + C_{58}C_{27}C_{9,10} + C_{58}C_{29}C_{7,10} + C_{5,10}C_{78}C_{29} + C_{5,10}C_{27}C_{89}) + \\
& \quad \left. C_{38} (C_{56}C_{72}C_{9,10} + C_{56}C_{7,10}C_{29} + C_{52}C_{67}C_{9,10} + C_{52}C_{69}C_{7,10} + C_{5,10}C_{72}C_{69} + C_{5,10}C_{67}C_{29}) \right] + \\
& C_{16} \left[C_{34} (C_{52}C_{78}C_{9,10} + C_{52}C_{7,10}C_{89} + C_{58}C_{27}C_{9,10} + C_{58}C_{29}C_{7,10} + C_{5,10}C_{78}C_{29} + C_{5,10}C_{27}C_{89}) + \right. \\
& \quad C_{32} (C_{54}C_{78}C_{9,10} + C_{54}C_{7,10}C_{89} + C_{58}C_{47}C_{9,10} + C_{58}C_{49}C_{7,10} + C_{5,10}C_{78}C_{49} + C_{5,10}C_{47}C_{89}) + \\
& \quad \left. C_{38} (C_{52}C_{74}C_{9,10} + C_{52}C_{7,10}C_{49} + C_{54}C_{27}C_{9,10} + C_{54}C_{29}C_{7,10} + C_{5,10}C_{74}C_{29} + C_{5,10}C_{27}C_{49}) \right] \\
& C_{18} \left[C_{34} (C_{56}C_{72}C_{9,10} + C_{56}C_{7,10}C_{29} + C_{52}C_{67}C_{9,10} + C_{52}C_{69}C_{7,10} + C_{5,10}C_{72}C_{69} + C_{5,10}C_{67}C_{29}) + \right. \\
& \quad C_{36} (C_{54}C_{72}C_{9,10} + C_{54}C_{7,10}C_{29} + C_{52}C_{47}C_{9,10} + C_{52}C_{49}C_{7,10} + C_{5,10}C_{72}C_{49} + C_{5,10}C_{47}C_{29}) + \\
& \quad \left. C_{32} (C_{56}C_{74}C_{9,10} + C_{56}C_{7,10}C_{49} + C_{54}C_{67}C_{9,10} + C_{54}C_{69}C_{7,10} + C_{5,10}C_{74}C_{69} + C_{5,10}C_{67}C_{49}) \right] \\
& C_{1,10} \left[C_{34} (C_{56}C_{78}C_{92} + C_{56}C_{72}C_{89} + C_{58}C_{67}C_{92} + C_{58}C_{69}C_{72} + C_{52}C_{78}C_{69} + C_{52}C_{67}C_{89}) + \right. \\
& \quad C_{36} (C_{54}C_{78}C_{92} + C_{54}C_{72}C_{89} + C_{58}C_{47}C_{92} + C_{58}C_{49}C_{72} + C_{52}C_{78}C_{49} + C_{52}C_{47}C_{89}) + \\
& \quad \left. C_{38} (C_{56}C_{74}C_{92} + C_{56}C_{72}C_{49} + C_{54}C_{67}C_{92} + C_{54}C_{69}C_{72} + C_{52}C_{74}C_{69} + C_{52}C_{67}C_{49}) \right]. \tag{D.18}
\end{aligned}$$

Apparently, it does not appear profitable to proceed any further. As previously shown, in case of complex samples we combine only complex conjugates with the ones that are not.

Thus we can modify (D.2) as:

$$E\{V_1V_2^* \dots V_{n-1}V_n^*\} = \sum_{Perm(m_1, \dots, m_{n/2})}^{\{2, 4, \dots, n\}} C_{1m_1} C_{3m_2} \dots C_{(n-3)m_{n/2-1}} C_{(n-1)m_{n/2}} \tag{D.19}$$

where the sum in this particular case denotes the sum of all possible products

$C_{1m_1} C_{3m_2} \dots C_{(n-3)m_{n/2-1}} C_{(n-1)m_{n/2}}$ where each $m_1, m_2, \dots, m_{n/2-1}, m_{n/2}$ is a $n/2$ -permutation of the elements of the set $\{2, 4, 6, \dots, n\}$.

Appendix E

Noise Moment Computation for $|\hat{R}_{hv}(0)|^n$

The *pdf* for $|\hat{R}_{hv}(0)|$ is given by (Jong-Sen Lee et al. 1994, eq. 32):

$$f(x) = \frac{4M^{M+1}x^M}{\Gamma(M)(\sqrt{N_h N_v})^{M+1}} K_{M-1} \left(\frac{2Mx}{\sqrt{N_h N_v}} \right), \quad (\text{E.1})$$

where K_{M-1} is the modified Bessel function of the second kind. Using the infinite sum identity for K_{M-1} we can express $f(x)$ as:

$$f(x) = \frac{4M^{M+1}x^M}{\Gamma(M)(\sqrt{N_h N_v})^{M+1}} \sqrt{\frac{\pi}{2}} e^{-\frac{2Mx}{\sqrt{N_h N_v}}} \times \sum_{m=0}^{\infty} \frac{\Gamma(M+m-1/2)}{\Gamma(m+1)\Gamma(M-m-1/2)} 2^{-m} \left(\frac{2Mx}{\sqrt{N_h N_v}} \right)^{-m-\frac{1}{2}} \quad (\text{E.2})$$

Consequently, the general moment expression is:

$$\begin{aligned} m_k &= \int_{-\infty}^{\infty} x^k f(x) dx \\ &= \frac{4M^{M+1} \sqrt{\frac{\pi}{2}}}{\Gamma(M)(\sqrt{N_h N_v})^{M+1}} \sum_{m=0}^{\infty} \frac{2^{-m} \Gamma(M+m-1/2)}{\Gamma(m+1)\Gamma(M-m-1/2)} \times \\ &\quad \int_0^{\infty} x^{M+k} \left(\frac{2Mx}{\sqrt{N_h N_v}} \right)^{-m-\frac{1}{2}} e^{-\frac{2Mx}{\sqrt{N_h N_v}}} dx. \end{aligned} \quad (\text{E.3})$$

After taking the variable substitution $t = 2Mx/\sqrt{N_h N_v}$ and solving the integral, the general moment expression becomes:

$$\begin{aligned}
m_k &= \frac{4M^{M+1} \left(\frac{\sqrt{N_h N_v}}{2M} \right)^{M+k+1}}{\Gamma(M) (\sqrt{N_h N_v})^{M+1}} \sqrt{\frac{\pi}{2}} \sum_{m=0}^{\infty} \frac{2^{-m} \Gamma(M+m-1/2)}{\Gamma(m+1) \Gamma(M-m-1/2)} \int_0^{\infty} e^{-t} t^{M+k-m+\frac{1}{2}-1} dt \\
&= \frac{4 \left(\sqrt{N_h N_v} \right)^k}{\Gamma(M) M^k 2^{M+k+1}} \sqrt{\frac{\pi}{2}} \sum_{m=0}^{\infty} \frac{\Gamma(M+m-1/2) \Gamma(M+k-m+1/2)}{\Gamma(m+1) \Gamma(M-m-1/2)} 2^{-m}.
\end{aligned} \tag{E.4}$$

The above formula was programmed in MATLAB as:

```

k = 1:mn;
m_R0Nhv = zeros(1, mn);
for m=0:17
    m_R0Nhv = m_R0Nhv+...
        4*sqrt(Nh*Nv).^k./(gamma(M)*2.^(M+k+1).*M.^k).*sqrt(pi/2).*...
        2^(-m).*exp(gammaln(M+k-m+1/2)-gammaln(m+1)).*exp(gammaln(M-
        1+m+1/2)-...
        gammaln(M-1-m+1/2));
end

```

where mn is the number of desired moments to be calculated, and m stands for the term number in the (E.4) sum. It was established that if $m > 18$ MATLAB gives NaN as a result. This is most likely due to the overflows/underflows in the computation. Nevertheless, it appeared that taking the first 17 terms in the sum yields outputs that do not change even when the number of terms in the sum is increased. There is no certain way to verify the accuracy of all the results yielded by the (E.4) formula. We know for certain, though, that for the noise case the exact formula for the second moment is:

$$m_2 = E \left\{ \left| \hat{R}_{hv}(0) \right|^2 \right\} = \frac{N_h N_v}{M}. \tag{E.5}$$

For the values $N_h = 3.4174e-006$, $N_v = 2.8259e-006$, $M = 17$, the above formula yields $m_2 = 5.680724e-013$, while (E.4) gives $m_2 = 5.681313e-013$. These two results are in good agreement which gives us confidence in other values obtained using (E.4).

In case really high accuracy is needed we shall derive the exact formula for $E \left\{ \left| \hat{R}_{hv}(0) \right|^{2k} \right\}$.

We have:

$$\begin{aligned}
M^{2k} E \left\{ \left| \hat{R}_{hv}(0) \right|^{2k} \right\} &= \sum_{m_1=0}^{M-1} \cdots \sum_{m_{2k}=0}^{M-1} E \left\{ \prod_{n0=1}^k V_h(m_{n0}) V_v^*(m_{n0}) \prod_{n1=k+1}^{2k} V_v(m_{n1}) V_h^*(m_{n1}) \right\} \\
&= \sum_{m_1=0}^{M-1} \cdots \sum_{m_{2k}=0}^{M-1} E \left\{ \prod_{n0=1}^k V_h(m_{n0}) V_h^*(m_{n0+k}) \right\} E \left\{ \prod_{n1=1}^k V_v(m_{n1+k}) V_v^*(m_{n1}) \right\} \\
&= \sum_{m_1=0}^{M-1} \cdots \sum_{m_{2k}=0}^{M-1} \sum_{Perm\{l_1, \dots, l_k\}}^{\{m_{k+1}, \dots, m_{2k}\}} \prod_{n0=1}^k C_{m_{n0}l_{n0}}^h \sum_{Perm\{q_1, \dots, q_k\}}^{\{m_1, \dots, m_k\}} \prod_{n1=1}^k C_{(m_{n1+k})q_k}^v.
\end{aligned} \tag{E.6}$$

We now proceed by attempting to derive the recursion formula by examining how pairing of $V_h(m_0)$ sample with each other sample in horizontal channel affects the samples in vertical channel.

$$\begin{aligned}
M^{2k} E \left\{ \left| \hat{R}_{hv}(0) \right|^{2k} \right\} &= \sum_{m_1=0}^{M-1} \cdots \sum_{m_{2k}=0}^{M-1} \sum_{Perm\{l_2, \dots, l_k\}}^{\{m_{k+2}, \dots, m_{2k}\}} C_{m_1 m_{k+1}}^h \prod_{n0=2}^k C_{m_{n0}l_{n0}}^h \sum_{Perm\{q_1, \dots, q_k\}}^{\{m_1, \dots, m_k\}} \prod_{n1=1}^k C_{m_{n1+k}q_k}^v + \\
&\cdots \sum_{m_1=0}^{M-1} \cdots \sum_{m_{2k}=0}^{M-1} \sum_{Perm\{l_1, \dots, l_{i-1}, l_{i+1}, \dots, l_k\}}^{\{m_{k+2}, \dots, m_{2k}\}} \prod_{n0=1}^{i-1} C_{m_{n0}l_{n0}}^h C_{m_i m_{k+1}}^h \prod_{n0=i+1}^k C_{m_{n0}l_{n0}}^h \sum_{Perm\{q_1, \dots, q_k\}}^{\{m_1, \dots, m_k\}} \prod_{n1=1}^k C_{m_{n1+k}q_k}^v + \cdots \\
&\sum_{m_1=0}^{M-1} \cdots \sum_{m_{2k}=0}^{M-1} \sum_{Perm\{l_2, \dots, l_k\}}^{\{m_{k+2}, \dots, m_{2k}\}} \prod_{n0=1}^{k-1} C_{m_{n0}l_{n0}}^h C_{m_k m_{k+1}}^h \sum_{Perm\{q_1, \dots, q_k\}}^{\{m_1, \dots, m_k\}} \prod_{n1=1}^k C_{m_{n1+k}q_k}^v
\end{aligned} \tag{E.7}$$

Notice that all terms on the right side of (E.7) have the same expected values. Let us now calculate the general term:

$$\begin{aligned}
\frac{M^{2k}}{k} E \left\{ \left| \hat{R}_{hv}(0) \right|^{2k} \right\} &= \sum_{m_1=0}^{M-1} \cdots \sum_{m_{2k}=0}^{M-1} \sum_{\text{Perm}\{l_1, \dots, l_{i-1}, l_{i+1}, \dots, l_k\}}^{\{m_{k+2}, \dots, m_{2k}\}} \prod_{n=0}^{i-1} C_{m_n 0 l_{n0}}^h C_{m_i m_{k+1}}^h \prod_{n=0}^k C_{m_n 0 l_{n0}}^h \\
&\quad \sum_{\text{Perm}\{q_1, \dots, q_k\}}^{\{m_1, \dots, m_k\}} \prod_{n=1}^k C_{m_{n1+k} q_{n1}}^v \\
&= N_h \sum_{m_1=0}^{M-1} \cdots \sum_{m_{i-1}=0}^{M-1} \sum_{m_{i+1}=0}^{M-1} \cdots \sum_{m_{2k}=0}^{M-1} \sum_{\text{Perm}\{l_1, \dots, l_{i-1}, l_{i+1}, \dots, l_k\}}^{\{m_{k+2}, \dots, m_{2k}\}} \prod_{n=0}^{i-1} C_{m_n 0 l_{n0}}^h \prod_{n=0}^k C_{m_n 0 l_{n0}}^h \\
&\quad \sum_{\text{Perm}\{q_1, \dots, q_k\}}^{\{m_1, \dots, m_{i-1}, m_{k+1}, m_{i+1}, \dots, m_k\}} \prod_{n=1}^k C_{m_{n1+k} q_{n1}}^v \\
&= N_h M^{2k-1} E \left\{ \left| \hat{R}_{hv}(0) \right|^{2k-2} \hat{P}_v \right\}.
\end{aligned} \tag{E.8}$$

Thus,

$$E \left\{ \left| \hat{R}_{hv}(0) \right|^{2k} \right\} = \frac{k}{M} N_h E \left\{ \left| \hat{R}_{hv}(0) \right|^{2k-2} \hat{P}_v \right\}. \tag{E.9}$$

After applying this formula recursively we get:

$$E \left\{ \left| \hat{R}_{hv}(0) \right|^{2k} \right\} = \frac{k!}{M^k} N_h^k E \left\{ \hat{P}_v^k \right\} = \frac{k!}{M^{2k-1}} \frac{(M+k-1)!}{M!} N_h^k N_v^k. \tag{E.10}$$

Knowing even moments one can, due to the numerical stability, choose to use the polynomial approximation to obtain odd moments. Further, these can be used for enhanced estimation using control variates (as described in section 5.4). It is the experience of the author that the polynomial approximation using gamma distribution with error correction up to the 5-th moment yields satisfactory results.

Appendix F

Evaluation of Noise Moments for $\left|\hat{R}_h(T) + \hat{R}_v(T)\right|^n$

The evaluation when n is even can be performed analytically. To evaluate odd moments we can apply the approach given in section 5.4. Hence, we shall calculate the even powers and use those to find an approximation to the $pdf\left(\left|\hat{R}_h(T) + \hat{R}_v(T)\right|^2\right)$, which can be used to approximate $pdf\left(\left|\hat{R}_h(T) + \hat{R}_v(T)\right|\right)$, and hence all other odd moments. These approximations can be used for enhanced odd moment estimation using control variates. To make it consistent with the notation in section 5.4 we have:

$$P = \left|\hat{R}_h(T) + \hat{R}_v(T)\right|^2 \quad \text{and} \quad Y = P^{1/2} = \left|\hat{R}_h(T) + \hat{R}_v(T)\right|. \quad (\text{F.1})$$

We now proceed by finding the moments:

$$\begin{aligned} E\left\{\left|\hat{R}_h(T) + \hat{R}_v(T)\right|^2\right\} &= \frac{1}{(M-1)^2} E\left\{\sum_{m=0}^{M-2} \left[V_h^*(m)V_h(m+1) + V_v^*(m)V_v(m+1)\right] \times \right. \\ &\quad \left. \sum_{n=0}^{M-2} \left[V_h(n)V_h^*(n+1) + V_v(n)V_v^*(n+1)\right]\right\} \\ &= E\left\{\left(\hat{R}_h(T) + \hat{R}_v(T)\right)\left(\hat{R}_h^*(T) + \hat{R}_v^*(T)\right)\right\} \\ &= E\left\{\left|\hat{R}_h(T)\right|^2\right\} + E\left\{\hat{R}_h(T)\hat{R}_v^*(T)\right\} + E\left\{\hat{R}_v(T)\hat{R}_h^*(T)\right\} + \\ &\quad E\left\{\left|\hat{R}_v^*(T)\right|^2\right\} \\ &= \frac{N_h^2 + N_v^2}{M-1}, \end{aligned} \quad (\text{F.2})$$

because

$$\begin{aligned}
E \left\{ \left| \hat{R}(T) \right|^2 \right\} &= \frac{1}{(M-1)^2} E \left\{ \sum_{m=0}^{M-2} V^*(m) V(m+1) \sum_{n=0}^{M-2} V(n) V^*(n+1) \right\} \\
&= \frac{1}{(M-1)^2} \sum_{m=0}^{M-2} \sum_{n=0}^{M-2} \left[E \{ V^*(m) V(m+1) \} E \{ V(n) V^*(n+1) \} + \right. \\
&\quad \left. E \{ V^*(m) V(n) \} E \{ V(m+1) V^*(n+1) \} \right] \\
&= \frac{N^2}{M-1},
\end{aligned} \tag{F.3}$$

and

$$E \{ \hat{R}_h(T) \hat{R}_v^*(T) \} = E \{ \hat{R}_h(T) \} E \{ \hat{R}_v^*(T) \} = 0. \tag{F.4}$$

For $n = 4$:

$$\begin{aligned}
E \left\{ \left| \hat{R}_h(T) + \hat{R}_v(T) \right|^4 \right\} &= E \left\{ \left(\hat{R}_h(T) + \hat{R}_v(T) \right)^2 \left(\hat{R}_h^*(T) + \hat{R}_v^*(T) \right)^2 \right\} \\
&= E \left\{ \left| \hat{R}_h(T) \right|^4 + 2 \hat{R}_h(T)^2 \hat{R}_h^*(T) \hat{R}_v^*(T) + \hat{R}_h(T)^2 \hat{R}_v^*(T)^2 + \right. \\
&\quad \left. 2 \hat{R}_h^*(T)^2 \hat{R}_h(T) \hat{R}_v(T) + 4 \left| \hat{R}_h(T) \right|^2 \left| \hat{R}_v(T) \right|^2 + 2 \hat{R}_v^*(T)^2 \hat{R}_h(T) \hat{R}_v(T) + \right. \\
&\quad \left. \hat{R}_h^*(T)^2 \hat{R}_v(T)^2 + 2 \hat{R}_v(T)^2 \hat{R}_h^*(T) \hat{R}_v^*(T) + \left| \hat{R}_v(T) \right|^4 \right\}.
\end{aligned} \tag{F.5}$$

We can readily see that the mathematical expectation of all terms except the first, the middle, and the last is zero. Consequently:

$$E \left\{ \left| \hat{R}_h(T) + \hat{R}_v(T) \right|^4 \right\} = E \left\{ \left| \hat{R}_h(T) \right|^4 \right\} + 4 E \left\{ \left| \hat{R}_h(T) \right|^2 \right\} E \left\{ \left| \hat{R}_v(T) \right|^2 \right\} + E \left\{ \left| \hat{R}_v(T) \right|^4 \right\}. \tag{F.6}$$

We already know:

$$E \left\{ \left| \hat{R}_h(T) \right|^2 \right\} E \left\{ \left| \hat{R}_v(T) \right|^2 \right\} = \frac{N_h^2 N_v^2}{(M-1)^2}. \tag{F.7}$$

To find $E \left\{ \left| \hat{R}(T) \right|^4 \right\}$ we first write it as:

$$\begin{aligned}
E \left\{ \left| \hat{R}(T) \right|^4 \right\} &= \frac{1}{(M-1)^4} E \left\{ \sum_{m_1=0}^{M-2} V^*(m_1) V(m_1+1) \sum_{m_2=0}^{M-2} V(m_2) V^*(m_2+1) \times \right. \\
&\quad \left. \sum_{m_3=0}^{M-2} V^*(m_3) V(m_3+1) \sum_{m_4=0}^{M-2} V(m_4) V^*(m_4+1) \right\} \\
&= \frac{1}{(M-1)^4} \sum_{m_1=0}^{M-2} \sum_{m_2=0}^{M-2} \sum_{m_3=0}^{M-2} \sum_{m_4=0}^{M-2} E \left\{ V(m_1+1) V^*(m_1) V(m_2) V^*(m_2+1) \right. \\
&\quad \left. V(m_3+1) V^*(m_3) V(m_4) V^*(m_4+1) \right\}.
\end{aligned} \tag{F.8}$$

Apparently, we can utilize formula (D.19) to evaluate the mathematical expectation as:

$$\begin{aligned}
E \left\{ \left| \hat{R}(T) \right|^4 \right\} &= \frac{1}{(M-1)^4} \sum_{m_1=0}^{M-2} \sum_{m_2=0}^{M-2} \sum_{m_3=0}^{M-2} \sum_{m_4=0}^{M-2} \sum_{\text{Perm}(n_1, n_2, n_3, n_4)}^{\{m_1, m_2+1, m_3, m_4+1\}} E \left\{ V(m_1+1) V^*(n_1) \right\} \times \\
&\quad E \left\{ V(m_2) V^*(n_2) \right\} E \left\{ V(m_3+1) V^*(n_3) \right\} E \left\{ V(m_4) V^*(n_4) \right\}.
\end{aligned} \tag{F.9}$$

We approach this in a somewhat unconventional manner. First, we notice that in the case of noise samples

$$E \left\{ V(m) V^*(n) \right\} = \begin{cases} N & m = n \\ 0 & m \neq n \end{cases} = N \delta(m, n). \tag{F.10}$$

Hence, evaluating (F.8) reduces to counting the sum of products $\delta(m_1+1, n_1) \delta(m_2, n_2) \delta(m_3+1, n_3) \delta(m_4, n_4) N^4$ as m_1, m_2, m_3, m_4 are ranged through values 0 to $M-2$, for each 4-permutation (n_1, n_2, n_3, n_4) of the set $\{m_1, m_2+1, m_3, m_4+1\}$. Consequently, we rewrite (F.9) as:

$$\begin{aligned}
E \left\{ \left| \hat{R}(T) \right|^4 \right\} &= \frac{N^4}{(M-1)^4} \sum_{m_1=0}^{M-2} \sum_{m_2=0}^{M-2} \sum_{m_3=0}^{M-2} \sum_{m_4=0}^{M-2} \sum_{\text{Perm}(n_1, \dots, n_4)}^{\{m_1, m_2+1, m_3, m_4+1\}} \delta(m_1+1, n_1) \delta(m_2, n_2) \\
&\quad \delta(m_3+1, n_3) \delta(m_4, n_4).
\end{aligned} \tag{F.11}$$

By looking at (F.11) we notice that the quadruple sum has the most products $\delta(m_1+1, n_1) \delta(m_2, n_2) \delta(m_3+1, n_3) \delta(m_4, n_4)$ equal to one when $n_1=m_2+1, n_2 = m_1, n_3 = m_4+1,$

and $n_4 = m_3$. This gives $m_1=m_2$ and $m_3 = m_4$, for which case the quadruple sum is $(M-1)^2$.

This tells us that $E \left\{ \left| \hat{R}(T) \right|^4 \right\}$ is of the form:

$$E \left\{ \left| \hat{R}(T) \right|^4 \right\} = \frac{N^4}{(M-1)^4} (AM^2 + BM + C), \quad (\text{F.12})$$

where A , B , and C are some unknown integer constants. Given the conclusions so far, one can easily see that the quadruple sum computation can be easily programmed using *for* loops in any programming language, thus allowing us to compute the expression AM^2+BM+C for arbitrary M . To determine the constants A , B , and C all we need to do is to compute AM^2+BM+C for three arbitrary values of M thus setting the system of three linear equations with three unknowns. Moreover, we can generalize this approach for any arbitrary even integer k as:

$$\begin{aligned} E \left\{ \left| \hat{R}(T) \right|^k \right\} &= \frac{N^k}{(M-1)^k} \sum_{m_1=0}^{M-2} \cdots \sum_{m_k=0}^{M-2} \sum_{\text{Perm}(n_1, \dots, n_k)}^{\{m_1, m_2+1, \dots, m_{k-1}, m_k+1\}} \delta(m_1+1, n_1) \delta(m_2, n_2) \\ &\quad \delta(m_3+1, n_3) \delta(m_4, n_4) \cdots \delta(m_{k-1}+1, n_{k-1}) \delta(m_k, n_k) \quad (\text{F.13}) \\ &= \frac{N^k}{(M-1)^k} \left(C_{k/2} M^{\frac{k}{2}} + C_{k/2-1} M^{\frac{k}{2}-1} + \dots + C_0 \right). \end{aligned}$$

We also notice that we can deduce the value of the first coefficient (i.e., $C_{k/2}$) by the following rationale. To get the maximum sum (i.e., $(M-1)^{k/2}$), we fix the permutation in positions n_1, n_3, \dots, n_{k-1} where given permutation is chosen from the set $\{m_2+1, m_4+1, \dots, m_k+1\}$. The choice in these positions determines the values of n_2, n_4, \dots, n_k . For instance, if n_1 is chosen to be m_2+1 then n_2 must equal m_1 , in order for the first and second sum combined to yield $(M-1)$, and so forth. This tells us that the coefficient $C_{k/2} = (k/2)!$.

In particular:

$$E \left\{ \left| \hat{R}(T) \right|^4 \right\} = \frac{2M^2 + 2M - 8}{(M-1)^4} N^4, \quad (\text{F.14})$$

$$E \left\{ \left| \hat{R}(T) \right|^6 \right\} = \frac{6M^3 + 36M^2 - 6M - 180}{(M-1)^6} N^6, \quad (\text{F.15})$$

$$E \left\{ \left| \hat{R}(T) \right|^8 \right\} = \frac{24M^4 + 336M^3 + 1128M^2 - 1488M - 8064}{(M-1)^8} N^8, \quad (\text{F.16})$$

$$E \left\{ \left| \hat{R}(T) \right|^{10} \right\} = \frac{120M^5 + 3000M^4 + 24600M^3 + 54600M^2 - 168720M - 604800}{(M-1)^{10}} N^{10}. \quad (\text{F.17})$$

We can now calculate:

$$E \left\{ \left| \hat{R}_h(T) + \hat{R}_v(T) \right|^4 \right\} = \frac{2M^2 + 2M - 8}{(M-1)^4} (N_h^4 + N_v^4) + 4 \frac{N_h^2 N_v^2}{(M-1)^2}, \quad (\text{F.18})$$

$$\begin{aligned} E \left\{ \left| \hat{R}_h(T) + \hat{R}_v(T) \right|^6 \right\} &= E \left\{ \left(\hat{R}_h(T) + \hat{R}_v(T) \right)^3 \left(\hat{R}_h^*(T) + \hat{R}_v^*(T) \right)^3 \right\} \\ &= E \left\{ \left(\hat{R}_h(T)^3 + 3\hat{R}_h(T)^2 \hat{R}_v(T) + 3\hat{R}_h(T) \hat{R}_v(T)^2 + \hat{R}_v(T)^3 \right) \times \right. \\ &\quad \left. \left(\hat{R}_h^*(T)^3 + 3\hat{R}_h^*(T)^2 \hat{R}_v^*(T) + 3\hat{R}_h^*(T) \hat{R}_v^*(T)^2 + \hat{R}_v^*(T)^3 \right) \right\} \\ &= E \left\{ \left| \hat{R}_h(T) \right|^6 \right\} + 9E \left\{ \left| \hat{R}_h(T) \right|^4 \left| \hat{R}_v(T) \right|^2 \right\} + \\ &\quad 9E \left\{ \left| \hat{R}_h(T) \right|^2 \left| \hat{R}_v(T) \right|^4 \right\} + E \left\{ \left| \hat{R}_v(T) \right|^6 \right\} \\ &= \frac{6M^3 + 36M^2 - 6M - 180}{(M-1)^6} (N_h^6 + N_v^6) + \\ &\quad 9 \frac{2M^2 + 2M - 8}{(M-1)^5} (N_h^4 N_v^2 + N_h^2 N_v^4), \end{aligned} \quad (\text{F.19})$$

$$\begin{aligned}
E \left\{ \left| \hat{R}_h(T) + \hat{R}_v(T) \right|^8 \right\} &= E \left\{ \left(\hat{R}_h(T) + \hat{R}_v(T) \right)^4 \left(\hat{R}_h^*(T) + \hat{R}_v^*(T) \right)^4 \right\} \\
&= E \left\{ \left(\hat{R}_h(T)^4 + 4\hat{R}_h(T)^3 \hat{R}_v(T) + 6\hat{R}_h(T)^2 \hat{R}_v(T)^2 + 4\hat{R}_h(T) \hat{R}_v(T)^3 + \hat{R}_v(T)^4 \right) \times \right. \\
&\quad \left. \left(\hat{R}_h^*(T)^4 + 4\hat{R}_h^*(T)^3 \hat{R}_v^*(T) + 6\hat{R}_h^*(T)^2 \hat{R}_v^*(T)^2 + 4\hat{R}_h^*(T) \hat{R}_v^*(T)^3 + \hat{R}_v^*(T)^4 \right) \right\} \\
&= E \left\{ \left| \hat{R}_h(T) \right|^8 \right\} + 16E \left\{ \left| \hat{R}_h(T) \right|^6 \left| \hat{R}_v(T) \right|^2 \right\} + 36E \left\{ \left| \hat{R}_h(T) \right|^4 \left| \hat{R}_v(T) \right|^4 \right\} + \\
&\quad 16E \left\{ \left| \hat{R}_h(T) \right|^2 \left| \hat{R}_v(T) \right|^6 \right\} + E \left\{ \left| \hat{R}_v(T) \right|^8 \right\} \\
&= \frac{24M^4 + 336M^3 + 1128M^2 - 1488M - 8064}{(M-1)^8} (N_h^8 + N_v^8) + \\
&\quad 16 \frac{6M^3 + 36M^2 - 6M - 180}{(M-1)^7} (N_h^6 N_v^2 + N_h^2 N_v^6) + \\
&\quad 36 \frac{(2M^2 + 2M - 8)^2}{(M-1)^8} N_h^4 N_v^4, \tag{F.20}
\end{aligned}$$

$$\begin{aligned}
E \left\{ \left| \hat{R}_h(T) + \hat{R}_v(T) \right|^{10} \right\} &= E \left\{ \left(\hat{R}_h(T) + \hat{R}_v(T) \right)^5 \left(\hat{R}_h^*(T) + \hat{R}_v^*(T) \right)^5 \right\} \\
&= E \left\{ \left| \hat{R}_h(T) \right|^{10} + 25 \left| \hat{R}_h(T) \right|^8 \left| \hat{R}_v(T) \right|^2 + 100 \left| \hat{R}_h(T) \right|^6 \left| \hat{R}_v(T) \right|^4 + \right. \\
&\quad \left. 100 \left| \hat{R}_h(T) \right|^4 \left| \hat{R}_v(T) \right|^6 + 25 \left| \hat{R}_h(T) \right|^2 \left| \hat{R}_v(T) \right|^8 + \left| \hat{R}_v(T) \right|^{10} \right\} \\
&= E \left\{ \left| \hat{R}_h(T) \right|^{10} \right\} + 25E \left\{ \left| \hat{R}_h(T) \right|^8 \right\} E \left\{ \left| \hat{R}_v(T) \right|^2 \right\} + 100E \left\{ \left| \hat{R}_h(T) \right|^6 \right\} E \left\{ \left| \hat{R}_v(T) \right|^4 \right\} + \\
&\quad 100E \left\{ \left| \hat{R}_h(T) \right|^4 \right\} E \left\{ \left| \hat{R}_v(T) \right|^6 \right\} + 25E \left\{ \left| \hat{R}_h(T) \right|^2 \right\} E \left\{ \left| \hat{R}_v(T) \right|^8 \right\} + E \left\{ \left| \hat{R}_v(T) \right|^{10} \right\} \\
&= \frac{120M^5 + 3000M^4 + 24600M^3 + 54600M^2 - 168720M - 604800}{(M-1)^{10}} (N_h^{10} + N_v^{10}) + \\
&\quad 25 \frac{24M^4 + 336M^3 + 1128M^2 - 1488M - 8064}{(M-1)^9} (N_h^8 N_v^2 + N_h^2 N_v^8) + \\
&\quad 100 \frac{6M^3 + 36M^2 - 6M - 180}{(M-1)^6} \times \frac{2M^2 + 2M - 8}{(M-1)^4} (N_h^6 N_v^4 + N_h^4 N_v^6). \tag{F.21}
\end{aligned}$$

To validate the above formulae, the first 20 moments of $\left| \hat{R}_h(T) + \hat{R}_v(T) \right|$ were found through simulation and using the approximation, for odd moments, with the exponential

function and correction up to the 5-th moment of $|\hat{R}_h(T) + \hat{R}_v(T)|^2$. Four simulation runs were executed and the results are shown in Figure F.1. The approximation and the simulation appear to be in a very good agreement up to the 15th moment when the simulation variance becomes more apparent.

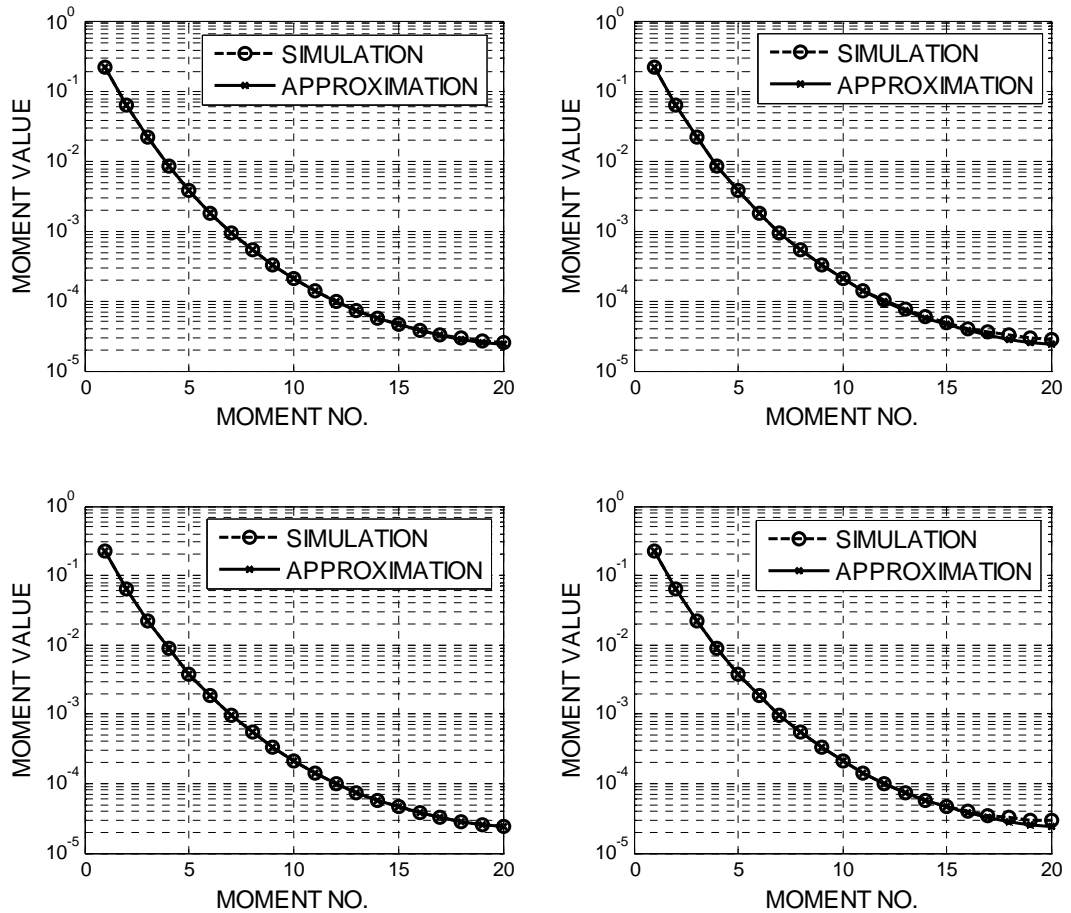


Figure F.1 Comparison between moments obtained through simulation and approximation.

Appendix G

Evaluation of Noise Moments for $\hat{P}_h^{kh} \left| \hat{R}_{hv}(0) \right|^n$ and $\hat{P}_h^{kh} \hat{P}_v^{kv} \left| \hat{R}_{hv}(0) \right|^n$

We start by evaluating $E \left\{ \hat{P}_h^2 \left| \hat{R}_{hv}(0) \right|^2 \right\}$ as

$$E \left\{ \hat{P}_h^2 \left| \hat{R}_{hv}(0) \right|^2 \right\} = \frac{1}{M^4} \sum_{m_1=0}^{M-1} \sum_{m_2=0}^{M-1} \sum_{m_3=0}^{M-1} \sum_{m_4=0}^{M-1} E \left\{ V_h(m_1) V_h^*(m_1) V_h(m_2) V_h^*(m_2) \right. \\ \left. V_v(m_3) V_h^*(m_3) V_h(m_4) V_v^*(m_4) \right\}. \quad (\text{G.1})$$

Note that because noise samples in H and V channel are independent we can discard all permutations where $V_v(m_3)$ and $V_v^*(m_4)$ are not paired together. Thus we rewrite (G.1) as:

$$E \left\{ \hat{P}_h^2 \left| \hat{R}_{hv}(0) \right|^2 \right\} = \frac{1}{M^4} \sum_{m_1=0}^{M-1} \sum_{m_2=0}^{M-1} \sum_{m_3=0}^{M-1} \sum_{m_4=0}^{M-1} E \left\{ V_h(m_1) V_h^*(m_1) V_h(m_2) V_h^*(m_2) \right. \\ \left. V_h^*(m_3) V_h(m_4) \right\} E \left\{ V_v(m_3) V_v^*(m_4) \right\}. \quad (\text{G.2})$$

Further, because noise samples are uncorrelated $m_3 = m_4$, so we have:

$$E \left\{ \hat{P}_h^2 \left| \hat{R}_{hv}(0) \right|^2 \right\} = \frac{1}{M^4} \sum_{m_1=0}^{M-1} \sum_{m_2=0}^{M-1} \sum_{m_3=0}^{M-1} E \left\{ V_h(m_1) V_h^*(m_1) V_h(m_2) V_h^*(m_2) V_h(m_3) V_h^*(m_3) \right\} \\ E \left\{ V_v(m_3) V_v^*(m_3) \right\} \\ = \frac{N_v}{M} E \left\{ \hat{P}_h^3 \right\}. \quad (\text{G.3})$$

Finally, using the result (A.14) we get:

$$E \left\{ \hat{P}_h^2 \left| \hat{R}_{hv}(0) \right|^2 \right\} = \frac{(M+1)(M+2)}{M^3} N_h^3 N_v = \frac{M^2 + 3M + 2}{M^3} N_h^3 N_v. \quad (\text{G.4})$$

We proceed in a similar fashion for higher moments:

$$\begin{aligned}
E \left\{ \hat{P}_h^4 \left| \hat{R}_{hv}(0) \right|^4 \right\} &= \frac{1}{M^8} \sum_{m_1=0}^{M-1} \cdots \sum_{m_8=0}^{M-1} E \left\{ V_h(m_1) V_h^*(m_1) \cdots V_h(m_4) V_h^*(m_4) \right. \\
&\quad \left. V_h(m_5) V_h^*(m_5) V_h(m_6) V_h^*(m_6) V_h(m_7) V_h^*(m_7) V_h(m_8) V_h^*(m_8) \right\} \\
&= \frac{1}{M^8} \sum_{m_1=0}^{M-1} \cdots \sum_{m_8=0}^{M-1} E \left\{ V_h(m_1) V_h^*(m_1) \cdots V_h(m_4) V_h^*(m_4) V_h(m_5) V_h^*(m_7) \right. \\
&\quad \left. V_h(m_6) V_h^*(m_8) \right\} E \left\{ V_v(m_7) V_v^*(m_5) V_v(m_8) V_v^*(m_6) \right\} \quad (G.5) \\
&= \frac{1}{M^8} \sum_{m_1=0}^{M-1} \cdots \sum_{m_8=0}^{M-1} E \left\{ V_h(m_1) V_h^*(m_1) \cdots V_h(m_4) V_h^*(m_4) V_h(m_5) V_h^*(m_7) \right. \\
&\quad \left. V_h(m_6) V_h^*(m_8) \right\} \left(E \left\{ V_v(m_7) V_v^*(m_5) \right\} E \left\{ V_v(m_8) V_v^*(m_6) \right\} + \right. \\
&\quad \left. E \left\{ V_v(m_7) V_v^*(m_6) \right\} E \left\{ V_v(m_8) V_v^*(m_5) \right\} \right).
\end{aligned}$$

The first product term in the brackets imposes $m_5=m_7$ and $m_6=m_8$, whereas the second one $m_6=m_7$ and $m_5=m_8$. Hence:

$$\begin{aligned}
E \left\{ \hat{P}_h^4 \left| \hat{R}_{hv}(0) \right|^4 \right\} &= \frac{1}{M^8} \sum_{m_1=0}^{M-1} \cdots \sum_{m_6=0}^{M-1} E \left\{ V_h(m_1) V_h^*(m_1) \cdots V_h(m_4) V_h^*(m_4) V_h(m_5) V_h^*(m_5) \right. \\
&\quad \left. V_h(m_6) V_h^*(m_6) \right\} E \left\{ V_v(m_5) V_v^*(m_5) \right\} E \left\{ V_v(m_6) V_v^*(m_6) \right\} + \quad (G.6) \\
&\quad \frac{1}{M^8} \sum_{m_1=0}^{M-1} \cdots \sum_{m_6=0}^{M-1} E \left\{ V_h(m_1) V_h^*(m_1) \cdots V_h(m_4) V_h^*(m_4) V_h(m_5) V_h^*(m_6) \right. \\
&\quad \left. V_h(m_6) V_h^*(m_5) \right\} E \left\{ V_v(m_6) V_v^*(m_6) \right\} E \left\{ V_v(m_5) V_v^*(m_5) \right\}.
\end{aligned}$$

Apparently, two terms in the sum are the same so we can readily write:

$$\begin{aligned}
E \left\{ \hat{P}_h^4 \left| \hat{R}_{hv}(0) \right|^4 \right\} &= 2 \frac{(M+1) \cdots (M+5)}{M^7} N_h^6 N_v^2 \\
&= \frac{2M^6 + 30M^5 + 170M^4 + 450M^3 + 548M^2 + 240M}{M^8} N_h^6 N_v^2. \quad (G.7)
\end{aligned}$$

To find $E \left\{ \hat{P}_h^6 \left| \hat{R}_{hv}(0) \right|^6 \right\}$ we write:

$$\begin{aligned}
E \left\{ \hat{P}_h^6 \left| \hat{R}_{hv}(0) \right|^6 \right\} &= \frac{1}{M^{12}} \sum_{m_1=0}^{M-1} \cdots \sum_{m_{12}=0}^{M-1} E \left\{ V_h(m_1) V_h^*(m_1) \cdots V_h(m_6) V_h^*(m_6) \right. \\
&\quad \left. V_h(m_7) V_v^*(m_7) \cdots V_h(m_9) V_v^*(m_9) V_v(m_{10}) V_h^*(m_{10}) \cdots V_v(m_{12}) V_h^*(m_{12}) \right\} \\
&= \frac{1}{M^{12}} \sum_{m_1=0}^{M-1} \cdots \sum_{m_{12}=0}^{M-1} E \left\{ V_v(m_{10}) V_v^*(m_7) V_v(m_{11}) V_v^*(m_8) V_v(m_{12}) V_v^*(m_9) \right\} \\
&\quad E \left\{ V_h(m_1) V_h^*(m_1) \cdots V_h(m_6) V_h^*(m_6) V_h(m_7) \cdots V_h(m_9) V_h^*(m_{10}) \cdots V_h^*(m_{12}) \right\}.
\end{aligned} \tag{G.8}$$

Given that there are 3! permutations in the expected value for V samples, and for each case the expectation for H samples is the same we can calculate the sum for just one and multiply it by 6 to obtain the total sum as

$$\begin{aligned}
E \left\{ \hat{P}_h^6 \left| \hat{R}_{hv}(0) \right|^6 \right\} &= \frac{6}{M^{12}} \sum_{m_1=0}^{M-1} \cdots \sum_{m_9=0}^{M-1} E \left\{ V_v(m_7) V_v^*(m_7) \right\} E \left\{ V_v(m_8) V_v^*(m_8) \right\} \times \\
&\quad E \left\{ V_v(m_9) V_v^*(m_9) \right\} \times \\
&\quad E \left\{ V_h(m_1) V_h^*(m_1) \cdots V_h(m_6) V_h^*(m_6) V_h(m_7) V_h^*(m_7) \cdots V_h(m_9) V_h^*(m_9) \right\} \\
&= \frac{6N_v^3}{M^3} \left(\frac{1}{M} \sum_{m=0}^{M-1} \hat{P}_h(m) \right)^9 = 6 \frac{(M+1) \cdots (M+8)}{M^{11}} N_v^3 N_h^9.
\end{aligned} \tag{G.9}$$

Based on the previous derivations we can write the general formula for $E \left\{ \hat{P}_h^k \left| \hat{R}_{hv}(0) \right|^{2n} \right\}$ as

$$\begin{aligned}
E \left\{ \hat{P}_h^k \left| \hat{R}_{hv}(0) \right|^{2n} \right\} &= \\
&\quad \frac{1}{M^{2n+k}} \sum_{m_1=0}^{M-1} \cdots \sum_{m_{2n+k}=0}^{M-1} E \left\{ V_v(m_{k+n+1}) V_v^*(m_{k+1}) \cdots V_v(m_{k+2n}) V_v^*(m_{k+n}) \right\} \\
&\quad E \left\{ V_h(m_1) V_h^*(m_1) \cdots V_h(m_k) V_h^*(m_k) V_h(m_{k+1}) \cdots V_h(m_{k+n}) V_h^*(m_{k+n+1}) \cdots V_h^*(m_{k+n+1}) \right\} \\
&= \frac{n!}{M^{2n+k}} \sum_{m_1=0}^{M-1} \cdots \sum_{m_{k+n}=0}^{M-1} E \left\{ V_v(m_{k+1}) V_v^*(m_{k+1}) \right\} \cdots E \left\{ V_v(m_{k+n}) V_v^*(m_{k+n}) \right\} \\
&\quad E \left\{ V_h(m_1) V_h^*(m_1) \cdots V_h(m_{k+n}) V_h^*(m_{k+n}) \right\} \\
&= n! \frac{N_v^n}{M^n} \left(\frac{1}{M} \sum_{m=0}^{M-1} \hat{P}_h(m) \right)^{k+n} = n! \frac{(M+1) \cdots (M+k+n-1)}{M^{k+2n-1}} N_v^n N_h^{k+n},
\end{aligned} \tag{G.10}$$

from which we get:

$$E \left\{ \hat{P}_h^8 \left| \hat{R}_{hv}(0) \right|^8 \right\} = 24 \frac{(M+1) \cdots (M+11)}{M^{15}} N_v^4 N_h^{12}. \quad (\text{G.11})$$

Using previous derivations we find

$$\begin{aligned} E \left\{ \hat{P}_v^{kv} \hat{P}_h^{kh} \left| \hat{R}_{hv}(0) \right|^{2n} \right\} &= \frac{1}{M^{kv+kh+2n}} \sum_{m_1=0}^{M-1} \cdots \sum_{m_{kv+kh+2n}=0}^{M-1} E \left\{ \prod_{n_0=kv+1}^{kv+kh} V_h(m_{n_0}) V_h^*(m_{n_0}) \right. \\ &\quad \left. \prod_{n_1=kh+kv+1}^{kh+kv+n} V_h(m_{n_1}) V_h^*(m_{n_1+n}) \right\} E \left\{ \prod_{n_2=1}^{kv} V_v(m_{n_2}) V_v^*(m_{n_2}) \prod_{n_3=kh+kv+1}^{kh+kv+n} V_v(m_{n_3+n}) V_v^*(m_{n_3}) \right\} \\ &= A + B + C, \end{aligned} \quad (\text{G.12})$$

where:

$$\begin{aligned} A &= \frac{1}{M^{kv+kh+2n}} \sum_{m_1=0}^{M-1} \cdots \sum_{m_{2n+kh+kv}=0}^{M-1} E \left\{ \prod_{n_0=kv+1}^{kv+kh} V_h(m_{n_0}) V_h^*(m_{n_0}) \prod_{n_1=kh+kv+1}^{kh+kv+n} V_h(m_{n_1}) V_h^*(m_{n_1+n}) \right\} \\ &\quad E \left\{ V_v(m_1) V_v^*(m_1) \right\} E \left\{ \prod_{n_2=2}^{kv} V_v(m_{n_2}) V_v^*(m_{n_2}) \prod_{n_3=kh+kv+1}^{kh+kv+n} V_v(m_{n_3+n}) V_v^*(m_{n_3}) \right\} \\ &= N_v E \left\{ \hat{P}_v^{kv-1} \hat{P}_h^{kh} \left| \hat{R}_{hv}(0) \right|^{2n} \right\}, \end{aligned} \quad (\text{G.13})$$

$$\begin{aligned} B &= \frac{(kv-1)}{M^{kv+kh+2n}} \sum_{m_1=0}^{M-1} \cdots \sum_{m_{kv+kh+2n}=0}^{M-1} E \left\{ \prod_{n_0=kv+1}^{kv+kh} V_h(m_{n_0}) V_h^*(m_{n_0}) \prod_{n_1=kh+kv+1}^{kh+kv+n} V_h(m_{n_1}) V_h^*(m_{n_1+n}) \right\} \\ &\quad E \left\{ V_v(m_1) V_v^*(m_2) \right\} \\ &\quad E \left\{ V_v(m_2) V_v^*(m_1) \prod_{n_2=3}^{kv} V_v(m_{n_2}) V_v^*(m_{n_2}) \prod_{n_3=kh+kv+1}^{kh+kv+n} V_v(m_{n_3+n}) V_v^*(m_{n_3}) \right\} \\ &= \frac{(kv-1)}{M^{kv+kh+2n}} \sum_{m_2=0}^{M-1} \cdots \sum_{m_{kv+kh+2n}=0}^{M-1} E \left\{ \prod_{n_0=kv+1}^{kv+kh} V_h(m_{n_0}) V_h^*(m_{n_0}) \prod_{n_1=kh+kv+1}^{kh+kv+n} V_h(m_{n_1}) V_h^*(m_{n_1+n}) \right\} \\ &\quad N_v E \left\{ \prod_{n_2=2}^{kv} V_v(m_{n_2}) V_v^*(m_{n_2}) \prod_{n_3=kh+kv+1}^{kh+kv+n} V_v(m_{n_3+n}) V_v^*(m_{n_3}) \right\} \\ &= (kv-1) \frac{N_v}{M} E \left\{ \hat{P}_v^{kv-1} \hat{P}_h^{kh} \left| \hat{R}_{hv}(0) \right|^{2n} \right\}, \end{aligned} \quad (\text{G.14})$$

$$\begin{aligned}
C &= \frac{n}{M^{kv+kh+2n}} \sum_{m_1=0}^{M-1} \cdots \sum_{m_{kv+kh+2n}=0}^{M-1} E \left\{ \prod_{n0=kv+1}^{kv+kh} V_h(m_{n0}) V_h^*(m_{n0}) \prod_{n1=kh+kv+1}^{kh+kv+n} V_h(m_{n1}) V_h^*(m_{n1+n}) \right\} \\
&\quad E \left\{ V_v(m_1) V_v^*(m_{kv+kh+1}) \right\} \\
&\quad E \left\{ V_v(m_{kv+kv+1+n}) V_v^*(m_1) \prod_{n2=3}^{kv} V_v(m_{n2}) V_v^*(m_{n2}) \prod_{n3=kh+kv+2}^{kh+kv+n} V_v(m_{n3+n}) V_v^*(m_{n3}) \right\} \\
&= \frac{n}{M^{kv+kh+2n}} \sum_{m_2=0}^{M-1} \cdots \sum_{m_{kv+kh+2n}=0}^{M-1} E \left\{ \prod_{n0=kv+1}^{kv+kh} V_h(m_{n0}) V_h^*(m_{n0}) \prod_{n1=kh+kv+1}^{kh+kv+n} V_h(m_{n1}) V_h^*(m_{n1+n}) \right\} \\
&\quad N_v E \left\{ \prod_{n2=2}^{kv} V_v(m_{n2}) V_v^*(m_{n2}) \prod_{n3=kh+kv+1}^{kh+kv+n} V_v(m_{n3+n}) V_v^*(m_{n3}) \right\} \\
&= n \frac{N_v}{M} E \left\{ \hat{P}_v^{kv-1} \hat{P}_h^{kh} \left| \hat{R}_{hv}(0) \right|^{2n} \right\}.
\end{aligned} \tag{G.15}$$

Finally:

$$\begin{aligned}
E \left\{ \hat{P}_v^{kv} \hat{P}_h^{kh} \left| \hat{R}_{hv}(0) \right|^{2n} \right\} &= \frac{M+kv-1+n}{M} N_v E \left\{ \hat{P}_v^{kv-1} \hat{P}_h^{kh} \left| \hat{R}_{hv}(0) \right|^{2n} \right\} \\
&= \frac{(M+n) \cdots (M+kv-1+n)}{M^{kv}} N_v^{kv} E \left\{ \hat{P}_h^{kh} \left| \hat{R}_{hv}(0) \right|^{2n} \right\} \\
&= \frac{(M+n) \cdots (M+kv-1+n)}{M^{kv}} N_v^{kv} \frac{n! N_v^n}{M^n} \left(\frac{1}{M^{kh+n}} \sum_{m=0}^{M-1} \hat{P}_h(m) \right)^{kh+n} \\
&= n! \frac{\prod_{i=n}^{M+kv+n-1} (M+i) \prod_{j=1}^{M+kh+n-1} (M+j)}{M^{kv+kh+2n-1}} N_v^{kv+n} N_h^{kh+n}.
\end{aligned} \tag{G.16}$$

Appendix H

Evaluation of Noise Moments for $\hat{P}_v^{vk} \hat{P}_h^{hk} \left| \hat{R}_h(T) + \hat{R}_v(T) \right|^{2n}$

To find these moments we shall first derive result which will be of general importance for further derivations. Namely, we shall show that in the case of noise samples:

$$E \left\{ \hat{P}^k \left| \hat{R}(T) \right|^{2n} \right\} = \frac{(M+2n) \cdots (M+k-1+2n)}{M^k} E \left\{ \left| \hat{R}(T) \right|^{2n} \right\} N^k \quad \text{where } k, n \in N. \quad (\text{H.1})$$

First we represent the expression as:

$$E \left\{ \hat{P}^k \left| \hat{R}(T) \right|^{2n} \right\} = \frac{1}{M^k (M-1)^{2n}} \sum_{m_1=0}^{M-1} \cdots \sum_{m_k=0}^{M-1} \sum_{m_{k+1}=0}^{M-2} \cdots \sum_{m_{2n}=0}^{M-2} E \left\{ V(m_1) V^*(m_1) \cdots \right. \\ \left. V(m_k) V^*(m_k) V(m_{k+1}) V^*(m_{k+1}+1) \cdots V(m_{k+n}) V^*(m_{k+n}+1) \right. \\ \left. V(m_{k+n+1}+1) V^*(m_{k+n+1}) \cdots V(m_{k+2n}+1) V^*(m_{k+2n}) \right\}. \quad (\text{H.2})$$

Using formula (D.19) we can write (notice that for notational simplicity both sides are multiplied by $M^k (M-1)^{2n}$):

$$\begin{aligned}
& M^k (M-1)^{2n} E \left\{ \hat{P}^k \left| \hat{R}(T) \right|^{2n} \right\} = \\
& \sum_{m_1=0}^{M-1} \cdots \sum_{m_k=0}^{M-1} \sum_{m_{k+1}=0}^{M-2} \cdots \sum_{m_{k+2n}=0}^{M-2} \sum_{\text{Perm}(n_1, \dots, n_{k+2n})}^{\{m_1, \dots, m_{k+n}, m_{k+n+1}+1, \dots, m_{k+2n}+1\}} C_{m_1 n_1} \cdots C_{m_k n_k} C_{(m_{k+1}+1)n_{k+1}} \cdots C_{(m_{k+n}+1)n_{k+n}} \\
& \quad C_{m_{k+n+1}n_{k+n+1}} \cdots C_{m_{k+2n}n_{k+2n}} \\
& = \sum_{m_1=0}^{M-1} \cdots \sum_{m_k=0}^{M-1} \sum_{m_{k+1}=0}^{M-2} \cdots \sum_{m_{k+2n}=0}^{M-2} \sum_{\text{Perm}(n_2, \dots, n_{k+2n})}^{\{m_2, \dots, m_{k+n}, m_{k+n+1}+1, \dots, m_{k+2n}+1\}} C_{m_1 m_1} C_{m_2 n_2} \cdots C_{m_k n_k} C_{(m_{k+1}+1)n_{k+1}} \cdots \\
& \quad C_{(m_{k+n}+1)n_{k+n}} C_{m_{k+n+1}n_{k+n+1}} \cdots C_{m_{k+2n}n_{k+2n}} + \\
& \sum_{m_1=0}^{M-1} \cdots \sum_{m_k=0}^{M-1} \sum_{m_{k+1}=0}^{M-2} \cdots \sum_{m_{k+2n}=0}^{M-2} \sum_{\text{Perm}(n_1, \dots, n_{k+2n}) \wedge n_1 \neq m_1}^{\{m_1, \dots, m_{k+n}, m_{k+n+1}+1, \dots, m_{k+2n}+1\}} C_{m_1 n_1} \cdots C_{m_k n_k} C_{(m_{k+1}+1)n_{k+1}} \cdots \\
& \quad C_{(m_{k+n}+1)n_{k+n}} C_{m_{k+n+1}n_{k+n+1}} \cdots C_{m_{k+2n}n_{k+2n}} \\
& = M^k (M-1)^{2n} NE \left\{ \hat{P}^{k-1} \left| \hat{R}(T) \right|^{2n} \right\} + \\
& \sum_{m_1=0}^{M-1} \cdots \sum_{m_k=0}^{M-1} \sum_{m_{k+1}=0}^{M-2} \cdots \sum_{m_{k+2n}=0}^{M-2} \sum_{\text{Perm}(n_1, \dots, n_{k+2n}) \wedge n_1 \neq m_1}^{\{m_1, \dots, m_{k+n}, m_{k+n+1}+1, \dots, m_{k+2n}+1\}} C_{m_1 n_1} \cdots C_{m_k n_k} C_{(m_{k+1}+1)n_{k+1}} \cdots \\
& \quad C_{(m_{k+n}+1)n_{k+n}} C_{m_{k+n+1}n_{k+n+1}} \cdots C_{m_{k+2n}n_{k+2n}}. \tag{H.3}
\end{aligned}$$

We now proceed further by calculating the second term which we will designate as A:

$$\begin{aligned}
A & = \sum_{m_1=0}^{M-1} \cdots \sum_{m_k=0}^{M-1} \sum_{m_{k+1}=0}^{M-2} \cdots \sum_{m_{k+2n}=0}^{M-2} \sum_{\text{Perm}(n_1, \dots, n_{k+2n}) \wedge n_1 \neq m_1}^{\{m_1, \dots, m_{k+n}, m_{k+n+1}+1, \dots, m_{k+2n}+1\}} C_{m_1 n_1} \cdots C_{m_k n_k} \\
& \quad C_{(m_{k+1}+1)n_{k+1}} \cdots C_{(m_{k+n}+1)n_{k+n}} C_{m_{k+n+1}n_{k+n+1}} \cdots C_{m_{k+2n}n_{k+2n}} \\
& = \sum_{m_1=0}^{M-1} \cdots \sum_{m_k=0}^{M-1} \sum_{m_{k+1}=0}^{M-2} \cdots \sum_{m_{k+2n}=0}^{M-2} \sum_{\text{Perm}(n_1, n_3, \dots, n_{k+2n})}^{\{m_2, \dots, m_{k+n}, m_{k+n+1}+1, \dots, m_{k+2n}+1\}} C_{m_1 n_1} C_{m_2 m_1} C_{m_3 n_3} \cdots C_{m_k n_k} \\
& \quad C_{(m_{k+1}+1)n_{k+1}} \cdots C_{(m_{k+n}+1)n_{k+n}} C_{m_{k+n+1}n_{k+n+1}} \cdots C_{m_{k+2n}n_{k+2n}} + \\
& \sum_{m_1=0}^{M-1} \cdots \sum_{m_k=0}^{M-1} \sum_{m_{k+1}=0}^{M-2} \cdots \sum_{m_{k+2n}=0}^{M-2} \sum_{\text{Perm}(n_1, n_2, n_4, \dots, n_{k+2n})}^{\{m_2, \dots, m_{k+n}, m_{k+n+1}+1, \dots, m_{k+2n}+1\}} C_{m_1 n_1} C_{m_2 n_2} C_{m_3 m_1} \cdots C_{m_k n_k} \\
& \quad C_{(m_{k+1}+1)n_{k+1}} \cdots C_{(m_{k+n}+1)n_{k+n}} C_{m_{k+n+1}n_{k+n+1}} \cdots C_{m_{k+2n}n_{k+2n}} + \cdots \\
& \sum_{m_1=0}^{M-1} \cdots \sum_{m_k=0}^{M-1} \sum_{m_{k+1}=0}^{M-2} \cdots \sum_{m_{k+2n}=0}^{M-2} \sum_{\text{Perm}(n_1, \dots, n_{k-1}, n_{k+1}, \dots, n_{k+2n})}^{\{m_2, \dots, m_{k+n}, m_{k+n+1}+1, \dots, m_{k+2n}+1\}} C_{m_1 n_1} \cdots C_{m_3 n_{k-1}} C_{m_k m_1} \\
& \quad C_{(m_{k+1}+1)n_{k+1}} \cdots C_{(m_{k+n}+1)n_{k+n}} C_{m_{k+n+1}n_{k+n+1}} \cdots C_{m_{k+2n}n_{k+2n}} + \\
& \sum_{m_1=0}^{M-1} \cdots \sum_{m_k=0}^{M-1} \sum_{m_{k+1}=0}^{M-2} \cdots \sum_{m_{k+2n}=0}^{M-2} \sum_{\text{Perm}(n_1, \dots, n_{k+2n}) \wedge n_i \neq m_1, i=1, \dots, k}^{\{m_1, \dots, m_{k+n}, m_{k+n+1}+1, \dots, m_{k+2n}+1\}} C_{m_1 n_1} \cdots C_{m_k n_k} C_{(m_{k+1}+1)n_{k+1}} \cdots C_{(m_{k+n}+1)n_{k+n}} \\
& \quad C_{m_{k+n+1}n_{k+n+1}} \cdots C_{m_{k+2n}n_{k+2n}}. \tag{H.4}
\end{aligned}$$

By examining the first two terms in the sum we notice that if we replace $m_2 = m_3$ and $m_3 = m_2$ the second term becomes the same as the first one, and so forth. Consequently, we can write:

$$\begin{aligned}
A = & (k-1) \sum_{m_1=0}^{M-1} \cdots \sum_{m_k=0}^{M-1} \sum_{m_{k+1}=0}^{M-2} \cdots \sum_{m_{k+2n}=0}^{M-2} \sum_{\substack{\{m_2, \dots, m_{k+n}, m_{k+n+1}+1, \dots, m_{k+2n}+1\} \\ \text{Perm}(n_1, n_3, \dots, n_{k+2n})}} C_{m_1 n_1} C_{m_2 m_1} C_{m_3 n_3} \cdots C_{m_k n_k} \\
& C_{(m_{k+1}+1)n_{k+1}} \cdots C_{(m_{k+n}+1)n_{k+n}} C_{m_{k+n+1} n_{k+n+1}} \cdots C_{m_{k+2n} n_{k+2n}} + \\
& \sum_{m_1=0}^{M-1} \cdots \sum_{m_k=0}^{M-1} \sum_{m_{k+1}=0}^{M-2} \cdots \sum_{m_{k+2n}=0}^{M-2} \sum_{\substack{\{m_1, \dots, m_{k+n}, m_{k+n+1}+1, \dots, m_{k+2n}+1\} \\ \text{Perm}(n_1, \dots, n_{k+2n}) \wedge n_i \neq m_1, i=1, \dots, k}} C_{m_1 n_1} \cdots C_{m_k n_k} C_{(m_{k+1}+1)n_{k+1}} \cdots C_{(m_{k+n}+1)n_{k+n}} \\
& C_{m_{k+n+1} n_{k+n+1}} \cdots C_{m_{k+2n} n_{k+2n}}
\end{aligned} \tag{H.5}$$

Because in the case of noise samples:

$$C_{m_2 m_1} = \begin{cases} N & m_1 = m_2 \\ 0 & m_1 \neq m_2 \end{cases}. \tag{H.6}$$

The first term in A which we designate as B can be further calculated:

$$\begin{aligned}
B = & (k-1) \sum_{m_1=0}^{M-1} \cdots \sum_{m_k=0}^{M-1} \sum_{m_{k+1}=0}^{M-2} \cdots \sum_{m_{k+2n}=0}^{M-2} \sum_{\substack{\{m_2, \dots, m_{k+n}, m_{k+n+1}+1, \dots, m_{k+2n}+1\} \\ \text{Perm}(n_1, n_3, \dots, n_{k+2n})}} C_{m_1 n_1} C_{m_2 m_1} C_{m_3 n_3} \cdots C_{m_k n_k} \\
& C_{(m_{k+1}+1)n_{k+1}} \cdots C_{(m_{k+n}+1)n_{k+n}} C_{m_{k+n+1} n_{k+n+1}} \cdots C_{m_{k+2n} n_{k+2n}} \\
= & (k-1) N \sum_{m_2=0}^{M-1} \cdots \sum_{m_k=0}^{M-1} \sum_{m_{k+1}=0}^{M-2} \cdots \sum_{m_{k+2n}=0}^{M-2} \sum_{\substack{\{m_2, \dots, m_{k+n}, m_{k+n+1}+1, \dots, m_{k+2n}+1\} \\ \text{Perm}(n_1, n_3, \dots, n_{k+2n})}} C_{m_1 n_1} C_{m_3 n_3} \cdots C_{m_k n_k} \\
& C_{(m_{k+1}+1)n_{k+1}} \cdots C_{(m_{k+n}+1)n_{k+n}} C_{m_{k+n+1} n_{k+n+1}} \cdots C_{m_{k+2n} n_{k+2n}} \\
= & (k-1) N M^{k-1} (M-1)^{2n} E \left\{ \hat{P}^{k-1} \left| \hat{R}(T) \right|^{2n} \right\}.
\end{aligned} \tag{H.7}$$

We now go for the optimization of the second term in A which we denote as C:

$$\begin{aligned}
C &= \sum_{m_1=0}^{M-1} \cdots \sum_{m_k=0}^{M-1} \sum_{m_{k+1}=0}^{M-2} \cdots \sum_{m_{k+2n}=0}^{M-2} \sum_{\{m_1, \dots, m_{k+n}, m_{k+n+1}+1, \dots, m_{k+2n}+1\}} \\
&\quad \text{Perm}(n_1, \dots, n_{k+2n}) \wedge n_i \neq m_i, i=1, \dots, k} C_{m_1 n_1} \cdots C_{m_k n_k} C_{(m_{k+1}+1)n_{k+1}} \cdots C_{(m_{k+n}+1)n_{k+n}} \\
&\quad \quad \quad C_{m_{k+n+1} n_{k+n+1}} \cdots C_{m_{k+2n} n_{k+2n}} \\
&= n \sum_{m_1=0}^{M-1} \cdots \sum_{m_k=0}^{M-1} \sum_{m_{k+1}=0}^{M-2} \cdots \sum_{m_{k+2n}=0}^{M-2} \sum_{\{m_2, \dots, m_{k+n}, m_{k+n+1}+1, \dots, m_{k+2n}+1\}} \\
&\quad \text{Perm}(n_1, \dots, n_k, n_{k+2}, \dots, n_{k+2n}) C_{m_1 n_1} \cdots C_{m_k n_k} C_{(m_{k+1}+1)m_1} \cdots C_{(m_{k+n}+1)n_{k+n}} \quad (\text{H.8}) \\
&\quad \quad \quad C_{m_{k+n+1} n_{k+n+1}} \cdots C_{m_{k+2n} n_{k+2n}} + \\
&\quad n \sum_{m_1=0}^{M-1} \cdots \sum_{m_k=0}^{M-1} \sum_{m_{k+1}=0}^{M-2} \cdots \sum_{m_{k+2n}=0}^{M-2} \sum_{\{m_2, \dots, m_{k+n}, m_{k+n+1}+1, \dots, m_{k+2n}+1\}} \\
&\quad \text{Perm}(n_1, \dots, n_{k+2n}) C_{m_1 n_1} \cdots C_{m_k n_k} C_{(m_{k+1}+1)n_{k+1}} \cdots C_{(m_{k+n}+1)n_{k+n}} \\
&\quad \quad \quad C_{m_{k+n+1} n_{k+n+1}} \cdots C_{m_{k+2n} m_1}.
\end{aligned}$$

Using noise feature we write:

$$\begin{aligned}
C &= nN \sum_{m_2=0}^{M-1} \cdots \sum_{m_k=0}^{M-1} \sum_{m_{k+1}=0}^{M-2} \cdots \sum_{m_{k+2n}=0}^{M-2} \sum_{\{m_2, \dots, m_{k+n}, m_{k+n+1}+1, \dots, m_{k+2n}+1\}} \\
&\quad \text{Perm}(n_1, \dots, n_k, n_{k+2}, \dots, n_{k+2n}) C_{m_1 n_1} \cdots C_{m_k n_k} C_{(m_{k+2}+1)n_{k+2}} \cdots \\
&\quad \quad \quad C_{(m_{k+n}+1)n_{k+n}} C_{m_{k+n+1} n_{k+n+1}} \cdots C_{m_{k+2n} n_{k+2n}} + \\
&\quad nN \sum_{m_2=0}^{M-1} \cdots \sum_{m_k=0}^{M-1} \sum_{m_{k+1}=0}^{M-2} \cdots \sum_{m_{k+2n}=0}^{M-2} \sum_{\{m_2, \dots, m_{k+n}, m_{k+n+1}+1, \dots, m_{k+2n}+1\}} \\
&\quad \text{Perm}(n_1, \dots, n_{k+2n-1}) C_{m_1 n_1} \cdots C_{m_k n_k} C_{(m_{k+1}+1)n_{k+1}} \cdots \quad (\text{H.9}) \\
&\quad \quad \quad C_{(m_{k+n}+1)n_{k+n}} C_{m_{k+n+1} n_{k+n+1}} \cdots C_{m_{k+2n} m_1} = \\
&= 2nNM^{k-1} (M-1)^{2n} E \left\{ \hat{P}^{k-1} \left| \hat{R}(T) \right|^{2n} \right\}.
\end{aligned}$$

Finally we get:

$$\begin{aligned}
E \left\{ \hat{P}^k \left| \hat{R}(T) \right|^{2n} \right\} &= \frac{1}{M^k (M-1)^{2n}} \left(M^k (M-1)^{2n} NE \left\{ \hat{P}^k \left| \hat{R}(T) \right|^{2n} \right\} + A \right) \\
&= \frac{1}{M^k (M-1)^{2n}} \left(M^k (M-1)^{2n} NE \left\{ \hat{P}^k \left| \hat{R}(T) \right|^{2n} \right\} + B + C \right) \quad (\text{H.10}) \\
&= \frac{(M+k-1+2n)}{M} E \left\{ \hat{P}^{k-1} \left| \hat{R}(T) \right|^{2n} \right\} N.
\end{aligned}$$

This result is of universal importance because it allows us to express each

$E \left\{ \hat{P}^k \left| \hat{R}(T) \right|^{2n} \right\}$ as a function of $E \left\{ \left| \hat{R}(T) \right|^{2n} \right\}$. That is:

$$E \left\{ \hat{P}^k \left| \hat{R}(T) \right|^{2n} \right\} = \frac{(M+2n) \cdots (M+k-1+2n)}{M^k} E \left\{ \left| \hat{R}(T) \right|^{2n} \right\} N^k. \quad (\text{H.11})$$

This enables us now to calculate the following results which we shall find useful in future derivations. We find first:

$$\begin{aligned}
E \left\{ \hat{P}_h^k \left| \hat{R}_h(T) + \hat{R}_v(T) \right|^2 \right\} &= E \left\{ \hat{P}_h^k \left(\hat{R}_h(T) + \hat{R}_v(T) \right) \left(\hat{R}_h^*(T) + \hat{R}_v^*(T) \right) \right\} \\
&= E \left\{ \hat{P}_h^k \left| \hat{R}_h(T) \right|^2 \right\} + E \left\{ \hat{P}_h^k \right\} E \left\{ \left| \hat{R}_v(T) \right|^2 \right\} \\
&= \left(\frac{\prod_{i=2}^{k+1} (M+i)}{M^k} E \left\{ \left| \hat{R}_h(T) \right|^2 \right\} + \frac{\prod_{i=1}^{k-1} (M+i)}{M^{k-1}} E \left\{ \left| \hat{R}_v(T) \right|^2 \right\} \right) N_h^k.
\end{aligned} \tag{H.12}$$

Using the results from Appendix F:

$$E \left\{ \hat{P}_h^k \left| \hat{R}_h(T) + \hat{R}_v(T) \right|^2 \right\} = \frac{\prod_{i=2}^{k+1} (M+i)}{M^k (M-1)} N_h^{k+2} + \frac{\prod_{i=1}^{k-1} (M+i)}{M^{k-1} (M-1)} N_h^k N_v^2. \tag{H.13}$$

Similarly:

$$\begin{aligned}
E \left\{ \hat{P}_v^{vk} \hat{P}_h^{hk} \left| \hat{R}_h(T) + \hat{R}_v(T) \right|^2 \right\} &= E \left\{ \hat{P}_v^{vk} \hat{P}_h^{hk} \left(\hat{R}_h(T) + \hat{R}_v(T) \right) \left(\hat{R}_h^*(T) + \hat{R}_v^*(T) \right) \right\} \\
&= E \left\{ \hat{P}_v^{vk} \right\} E \left\{ \hat{P}_h^{hk} \left| \hat{R}_h(T) \right|^2 \right\} + E \left\{ \hat{P}_h^{hk} \right\} E \left\{ \hat{P}_v^{vk} \left| \hat{R}_v(T) \right|^2 \right\} \\
&= \frac{\prod_{j=1}^{vk-1} (M+j)}{M^{vk-1}} N_v^{vk} \frac{\prod_{i=2}^{hk+1} (M+i)}{M^{hk}} E \left\{ \left| \hat{R}_h(T) \right|^2 \right\} N_h^{hk} + \\
&\quad \frac{\prod_{j=1}^{hk-1} (M+j)}{M^{hk-1}} N_h^{hk} \frac{\prod_{i=2}^{vk+1} (M+i)}{M^{vk}} E \left\{ \left| \hat{R}_v(T) \right|^2 \right\} N_v^{vk}.
\end{aligned} \tag{H.14}$$

Finally:

$$\begin{aligned}
E \left\{ \hat{P}_v^{vk} \hat{P}_h^{hk} \left| \hat{R}_h(T) + \hat{R}_v(T) \right|^2 \right\} &= \frac{\prod_{j=1}^{vk-1} (M+j)}{M^{vk-1}} \frac{\prod_{i=2}^{hk+1} (M+i)}{M^{hk} (M-1)} N_h^{hk+2} N_v^{vk} + \\
&\quad \frac{\prod_{j=1}^{hk-1} (M+j)}{M^{hk-1}} \frac{\prod_{i=2}^{vk+1} (M+i)}{M^{vk} (M-1)} N_h^{hk} N_v^{vk+2}.
\end{aligned} \tag{H.15}$$

Further:

$$\begin{aligned}
E\left\{\hat{P}_h^k \left|\hat{R}_h(T) + \hat{R}_v(T)\right|^4\right\} &= E\left\{\hat{P}_h^k \left(\hat{R}_h(T) + \hat{R}_v(T)\right)^2 \left(\hat{R}_h^*(T) + \hat{R}_v^*(T)\right)^2\right\} \\
&= E\left\{\hat{P}_h^k \left(\left|\hat{R}_h(T)\right|^4 + 4\left|\hat{R}_h(T)\right|^2 \left|\hat{R}_v(T)\right|^2 + \left|\hat{R}_v(T)\right|^4\right)\right\} \\
&= E\left\{\hat{P}_h^k \left|\hat{R}_h(T)\right|^4\right\} + 4E\left\{\hat{P}_h^k \left|\hat{R}_h(T)\right|^2\right\} E\left\{\left|\hat{R}_v(T)\right|^2\right\} + E\left\{\hat{P}_h^k\right\} E\left\{\left|\hat{R}_v(T)\right|^4\right\} \\
&= \frac{\prod_{i=4}^{k+3} (M+i)}{M^k} E\left\{\left|\hat{R}_h(T)\right|^4\right\} N_h^k + \\
&\quad 4 \frac{\prod_{i=2}^{k+1} (M+i)}{M^k} E\left\{\left|\hat{R}_h(T)\right|^2\right\} N_h^k E\left\{\left|\hat{R}_v(T)\right|^2\right\} + \frac{\prod_{i=1}^{k-1} (M+i)}{M^{k-1}} N_h^k E\left\{\left|\hat{R}_v(T)\right|^4\right\} \\
&= \frac{2M^2 + 2M - 8}{(M-1)^4} \left(\frac{\prod_{i=4}^{k+3} (M+i)}{M^k} N_h^{k+4} + \frac{\prod_{i=1}^{k-1} (M+i)}{M^{k-1}} N_h^k N_v^4 \right) + \\
&\quad 4 \frac{\prod_{i=2}^{k+1} (M+i)}{M^k (M-1)^2} N_h^{k+2} N_v^2.
\end{aligned} \tag{H.16}$$

Similarly:

$$\begin{aligned}
E\left\{\hat{P}_v^{vk} \hat{P}_h^{hk} \left|\hat{R}_h(T) + \hat{R}_v(T)\right|^4\right\} &= E\left\{\hat{P}_v^{vk} \hat{P}_h^{hk} \left(\hat{R}_h(T) + \hat{R}_v(T)\right)^2 \left(\hat{R}_h^*(T) + \hat{R}_v^*(T)\right)^2\right\} \\
&= E\left\{\hat{P}_v^{vk} \hat{P}_h^{hk} \left(\left|\hat{R}_h(T)\right|^4 + 4\left|\hat{R}_h(T)\right|^2 \left|\hat{R}_v(T)\right|^2 + \left|\hat{R}_v(T)\right|^4\right)\right\} \\
&= E\left\{\hat{P}_v^{vk}\right\} E\left\{\hat{P}_h^{hk} \left|\hat{R}_h(T)\right|^4\right\} + 4E\left\{\hat{P}_h^{hk} \left|\hat{R}_h(T)\right|^2\right\} E\left\{\hat{P}_v^{vk} \left|\hat{R}_v(T)\right|^2\right\} + E\left\{\hat{P}_h^{hk}\right\} E\left\{\hat{P}_v^{vk} \left|\hat{R}_v(T)\right|^4\right\} \\
&= \frac{\prod_{i=1}^{vk-1} (M+i)}{M^{vk-1}} N_v^{vk} \frac{\prod_{i=4}^{hk+3} (M+i)}{M^{hk}} E\left\{\left|\hat{R}_h(T)\right|^4\right\} N_h^{hk} + \\
&\quad 4 \frac{\prod_{i=2}^{hk+1} (M+i)}{M^{hk}} E\left\{\left|\hat{R}_h(T)\right|^2\right\} N_h^{hk} \frac{\prod_{i=2}^{vk+1} (M+i)}{M^{vk}} E\left\{\left|\hat{R}_v(T)\right|^2\right\} N_v^{vk} \\
&\quad + \frac{\prod_{i=1}^{hk-1} (M+i)}{M^{hk-1}} N_h^{hk} \frac{\prod_{i=4}^{vk+3} (M+i)}{M^{vk}} E\left\{\left|\hat{R}_v(T)\right|^4\right\} N_v^{vk} \\
&= \frac{2M^2 + 2M - 8}{(M-1)^4} \left(\frac{\prod_{i=1}^{vk-1} (M+i)}{M^{vk-1}} \frac{\prod_{i=4}^{hk+3} (M+i)}{M^{hk}} N_h^{hk+4} N_v^{vk} + \right. \\
&\quad \left. + \frac{\prod_{i=1}^{hk-1} (M+i)}{M^{hk-1}} \frac{\prod_{i=4}^{vk+3} (M+i)}{M^{vk}} N_h^{hk} N_v^{vk+4} \right) + 4 \frac{\prod_{i=2}^{hk+1} (M+i) \prod_{i=2}^{vk+1} (M+i)}{M^{vk+hk} (M-1)^2} N_h^{hk+2} N_v^{vk+2}.
\end{aligned} \tag{H.17}$$

The next moment is:

$$\begin{aligned}
E \left\{ \hat{P}_h^k \left| \hat{R}_h(T) + \hat{R}_v(T) \right|^6 \right\} &= E \left\{ \hat{P}_h^k \left(\hat{R}_h(T) + \hat{R}_v(T) \right)^3 \left(\hat{R}_h^*(T) + \hat{R}_v^*(T) \right)^3 \right\} \\
&= E \left\{ \hat{P}_h^k \left(\left| \hat{R}_h(T) \right|^6 + 9 \left| \hat{R}_h(T) \right|^4 \left| \hat{R}_v(T) \right|^2 + 9 \left| \hat{R}_h(T) \right|^2 \left| \hat{R}_v(T) \right|^4 + \left| \hat{R}_v(T) \right|^6 \right) \right\} \\
&= E \left\{ \hat{P}_h^k \left| \hat{R}_h(T) \right|^6 \right\} + 9E \left\{ \hat{P}_h^k \left| \hat{R}_h(T) \right|^4 \right\} E \left\{ \left| \hat{R}_v(T) \right|^2 \right\} + \\
&\quad 9E \left\{ \hat{P}_h^k \left| \hat{R}_h(T) \right|^2 \right\} E \left\{ \left| \hat{R}_v(T) \right|^4 \right\} + E \left\{ \hat{P}_h^k \right\} E \left\{ \left| \hat{R}_v(T) \right|^4 \right\} \\
&= \frac{\prod_{i=6}^{k+5} (M+i)}{M^k} E \left\{ \left| \hat{R}_h(T) \right|^6 \right\} N_h^k + 9 \frac{\prod_{i=4}^{k+3} (M+i)}{M^k} E \left\{ \left| \hat{R}_h(T) \right|^4 \right\} N_h^k E \left\{ \left| \hat{R}_v(T) \right|^2 \right\} + \\
&\quad 9 \frac{\prod_{i=2}^{k+1} (M+i)}{M^k} E \left\{ \left| \hat{R}_h(T) \right|^2 \right\} N_h^k E \left\{ \left| \hat{R}_v(T) \right|^4 \right\} + \frac{\prod_{i=1}^{k-1} (M+i)}{M^{k-1}} N_h^k E \left\{ \left| \hat{R}_v(T) \right|^6 \right\} \\
&= \frac{6M^3 + 36M^2 - 6M - 180}{(M-1)^6} \left(\frac{\prod_{i=6}^{k+5} (M+i)}{M^k} N_h^6 + \frac{\prod_{i=1}^{k-1} (M+i)}{M^{k-1}} N_v^6 \right) N_h^k + \\
&\quad 9 \frac{2M^2 + 2M - 8}{M^k (M-1)^5} \left(\prod_{i=4}^{k+3} (M+i) N_h^4 N_v^2 + \prod_{i=2}^{k+1} (M+i) N_h^2 N_v^4 \right) N_h^k. \tag{H.18}
\end{aligned}$$

Similarly:

$$\begin{aligned}
& E \left\{ \hat{P}_v^{vk} \hat{P}_h^{hk} \left| \hat{R}_h(T) + \hat{R}_v(T) \right|^6 \right\} = E \left\{ \hat{P}_v^{vk} \hat{P}_h^{hk} \left(\hat{R}_h(T) + \hat{R}_v(T) \right)^3 \left(\hat{R}_h^*(T) + \hat{R}_v^*(T) \right)^3 \right\} \\
& = E \left\{ \hat{P}_v^{vk} \hat{P}_h^{hk} \left(\left| \hat{R}_h(T) \right|^6 + 9 \left| \hat{R}_h(T) \right|^4 \left| \hat{R}_v(T) \right|^2 + 9 \left| \hat{R}_h(T) \right|^2 \left| \hat{R}_v(T) \right|^4 + \left| \hat{R}_v(T) \right|^6 \right) \right\} \\
& = E \left\{ \hat{P}_v^{vk} \right\} E \left\{ \hat{P}_h^{hk} \left| \hat{R}_h(T) \right|^6 \right\} + 9 E \left\{ \hat{P}_h^{hk} \left| \hat{R}_h(T) \right|^4 \right\} E \left\{ \hat{P}_v^{vk} \left| \hat{R}_v(T) \right|^2 \right\} + \\
& \quad 9 E \left\{ \hat{P}_h^{hk} \left| \hat{R}_h(T) \right|^2 \right\} E \left\{ \hat{P}_v^{vk} \left| \hat{R}_v(T) \right|^4 \right\} + E \left\{ \hat{P}_h^{hk} \right\} E \left\{ \hat{P}_v^{vk} \left| \hat{R}_v(T) \right|^4 \right\} \\
& = \frac{\prod_{i=1}^{vk-1} (M+i)}{M^{vk-1}} N_v^{vk} \frac{\prod_{i=6}^{hk+5} (M+i)}{M^{hk}} E \left\{ \left| \hat{R}_h(T) \right|^6 \right\} N_h^{hk} + \\
& \quad 9 \frac{\prod_{i=4}^{hk+3} (M+i)}{M^{hk}} E \left\{ \left| \hat{R}_h(T) \right|^4 \right\} N_h^{hk} \frac{\prod_{i=2}^{vk+1} (M+i)}{M^{vk}} E \left\{ \left| \hat{R}_v(T) \right|^2 \right\} N_h^{vk} + \\
& \quad 9 \frac{\prod_{i=2}^{hk+1} (M+i)}{M^{kk}} E \left\{ \left| \hat{R}_h(T) \right|^2 \right\} N_h^{hk} \frac{\prod_{i=4}^{vk+3} (M+i)}{M^{vk}} E \left\{ \left| \hat{R}_v(T) \right|^4 \right\} N_v^{vk} + \\
& \quad \frac{\prod_{i=1}^{hk-1} (M+i)}{M^{hk-1}} N_h^{hk} \frac{\prod_{i=6}^{vk+5} (M+i)}{M^{vk}} E \left\{ \left| \hat{R}_v(T) \right|^6 \right\} N_v^{vk} \\
& = \frac{6M^3 + 36M^2 - 6M - 180}{(M-1)^6} \left(\frac{\prod_{i=1}^{vk-1} (M+i)}{M^{vk-1}} \frac{\prod_{i=6}^{hk+5} (M+i)}{M^{hk}} N_h^{hk+6} N_v^{vk} + \right. \\
& \quad \left. \frac{\prod_{i=1}^{hk-1} (M+i)}{M^{hk-1}} \frac{\prod_{i=6}^{vk+5} (M+i)}{M^{vk}} N_h^{hk} N_v^{vk+6} \right) + \tag{H.19} \\
& \quad 9 \frac{2M^2 + 2M - 8}{M^{hk+vk} (M-1)^5} \left(\prod_{i=4}^{hk+3} (M+i) \prod_{i=2}^{vk+1} (M+i) N_h^{hk+4} N_v^{vk+2} + \right. \\
& \quad \left. \prod_{i=2}^{hk+1} (M+i) \prod_{i=4}^{vk+3} (M+i) N_h^{hk+2} N_v^{vk+4} \right),
\end{aligned}$$

$$\begin{aligned}
E \left\{ \hat{P}_h^k \left| \hat{R}_h(T) + \hat{R}_v(T) \right|^8 \right\} &= E \left\{ \hat{P}_h^k \left(\hat{R}_h(T) + \hat{R}_v(T) \right)^4 \left(\hat{R}_h^*(T) + \hat{R}_v^*(T) \right)^4 \right\} \\
&= E \left\{ \hat{P}_h^k \left(\left| \hat{R}_h(T) \right|^8 + 16 \left| \hat{R}_h(T) \right|^6 \left| \hat{R}_v(T) \right|^2 + 36 \left| \hat{R}_h(T) \right|^4 \left| \hat{R}_v(T) \right|^4 + \right. \right. \\
&\quad \left. \left. 16 \left| \hat{R}_h(T) \right|^2 \left| \hat{R}_v(T) \right|^6 + \left| \hat{R}_v(T) \right|^8 \right) \right\} \\
&= E \left\{ \hat{P}_h^k \left| \hat{R}_h(T) \right|^8 \right\} + 16E \left\{ \hat{P}_h^k \left| \hat{R}_h(T) \right|^6 \right\} E \left\{ \left| \hat{R}_v(T) \right|^2 \right\} + 36E \left\{ \hat{P}_h^k \left| \hat{R}_h(T) \right|^4 \right\} \times \\
&\quad E \left\{ \left| \hat{R}_v(T) \right|^4 \right\} + 16E \left\{ \hat{P}_h^k \left| \hat{R}_h(T) \right|^2 \right\} E \left\{ \left| \hat{R}_v(T) \right|^6 \right\} + E \left\{ \hat{P}_h^k \right\} E \left\{ \left| \hat{R}_v(T) \right|^8 \right\} \\
&= \frac{\prod_{i=8}^{k+7} (M+i)}{M^k} E \left\{ \left| \hat{R}_h(T) \right|^8 \right\} N_h^k + \\
&\quad 16 \frac{\prod_{i=6}^{k+5} (M+i)}{M^k} E \left\{ \left| \hat{R}_h(T) \right|^6 \right\} N_h^k E \left\{ \left| \hat{R}_v(T) \right|^2 \right\} + \\
&\quad 36 \frac{\prod_{i=4}^{k+3} (M+i)}{M^k} E \left\{ \left| \hat{R}_h(T) \right|^4 \right\} N_h^k E \left\{ \left| \hat{R}_v(T) \right|^4 \right\} + \\
&\quad 16 \frac{\prod_{i=2}^{k+1} (M+i)}{M^k} E \left\{ \left| \hat{R}_h(T) \right|^2 \right\} N_h^k E \left\{ \left| \hat{R}_v(T) \right|^6 \right\} + \frac{\prod_{i=1}^{k-1} (M+i)}{M^{k-1}} N_h^k E \left\{ \left| \hat{R}_v(T) \right|^8 \right\} \\
&= \frac{24M^4 + 336M^3 + 1128M^2 - 1488M - 8064}{(M-1)^8} \times \\
&\quad \left(\frac{\prod_{i=8}^{k+7} (M+i)}{M^k} N_h^8 + \frac{\prod_{i=1}^{k-1} (M+i)}{M^{k-1}} N_v^8 \right) N_h^k + \\
&\quad 36 \frac{\prod_{i=4}^{k+3} (M+i) (2M^2 + 2M - 8)^2}{M^k (M-1)^8} N_h^{k+4} N_v^4 + \\
&\quad 16 \frac{6M^3 + 36M^2 - 6M - 180}{M^k (M-1)^7} \times \\
&\quad \left(\prod_{i=6}^{k+5} (M+i) N_h^6 N_v^2 + \prod_{i=2}^{k+1} (M+i) N_h^2 N_v^6 \right) N_h^k.
\end{aligned} \tag{H.20}$$

Similarly:

$$\begin{aligned}
& E \left\{ \hat{P}_v^{vk} \hat{P}_h^{hk} \left| \hat{R}_h(T) + \hat{R}_v(T) \right|^8 \right\} = E \left\{ \hat{P}_v^{vk} \hat{P}_h^{hk} \left(\hat{R}_h(T) + \hat{R}_v(T) \right)^4 \left(\hat{R}_h^*(T) + \hat{R}_v^*(T) \right)^4 \right\} \\
& = E \left\{ \hat{P}_v^{vk} \hat{P}_h^{hk} \left(\left| \hat{R}_h(T) \right|^8 + 16 \left| \hat{R}_h(T) \right|^6 \left| \hat{R}_v(T) \right|^2 + 36 \left| \hat{R}_h(T) \right|^4 \left| \hat{R}_v(T) \right|^4 + \right. \right. \\
& \quad \left. \left. 16 \left| \hat{R}_h(T) \right|^2 \left| \hat{R}_v(T) \right|^6 + \left| \hat{R}_v(T) \right|^8 \right) \right\} \\
& = E \left\{ \hat{P}_v^{vk} \right\} E \left\{ \hat{P}_h^{hk} \left| \hat{R}_h(T) \right|^8 \right\} + 16 E \left\{ \hat{P}_h^{hk} \left| \hat{R}_h(T) \right|^6 \right\} E \left\{ \hat{P}_v^{vk} \left| \hat{R}_v(T) \right|^2 \right\} + \\
& \quad 36 E \left\{ \hat{P}_h^{hk} \left| \hat{R}_h(T) \right|^4 \right\} E \left\{ \hat{P}_v^{vk} \left| \hat{R}_v(T) \right|^4 \right\} + 16 E \left\{ \hat{P}_h^{hk} \left| \hat{R}_h(T) \right|^2 \right\} E \left\{ \hat{P}_v^{vk} \left| \hat{R}_v(T) \right|^6 \right\} + \\
& \quad E \left\{ \hat{P}_h^{hk} \right\} E \left\{ \hat{P}_v^{vk} \left| \hat{R}_v(T) \right|^8 \right\} \\
& = \frac{\prod_{i=1}^{vk-1} (M+i)}{M^{vk-1}} N_v^{vk} \frac{\prod_{i=8}^{hk+7} (M+i)}{M^{hk}} E \left\{ \left| \hat{R}_h(T) \right|^8 \right\} N_h^{hk} + \\
& \quad 16 \frac{\prod_{i=6}^{hk+5} (M+i)}{M^{hk}} E \left\{ \left| \hat{R}_h(T) \right|^6 \right\} N_h^{hk} \frac{\prod_{i=2}^{vk+1} (M+i)}{M^{vk}} E \left\{ \left| \hat{R}_v(T) \right|^2 \right\} N_v^{vk} + \\
& \quad 36 \frac{\prod_{i=4}^{hk+3} (M+i)}{M^{hk}} E \left\{ \left| \hat{R}_h(T) \right|^4 \right\} N_h^{hk} \frac{\prod_{i=4}^{vk+3} (M+i)}{M^{vk}} E \left\{ \left| \hat{R}_v(T) \right|^4 \right\} N_v^{vk} + \\
& \quad 16 \frac{\prod_{i=2}^{hk+1} (M+i)}{M^{hk}} E \left\{ \left| \hat{R}_h(T) \right|^2 \right\} N_h^{hk} \frac{\prod_{i=6}^{vk+5} (M+i)}{M^{vk}} E \left\{ \left| \hat{R}_v(T) \right|^6 \right\} N_v^{vk} + \\
& \quad \frac{\prod_{i=1}^{hk-1} (M+i)}{M^{hk-1}} N_h^{hk} \frac{\prod_{i=8}^{vk+7} (M+i)}{M^{vk}} E \left\{ \left| \hat{R}_v(T) \right|^8 \right\} N_v^{vk} \\
& = \frac{24M^4 + 336M^3 + 1128M^2 - 1488M - 8064}{(M-1)^8} \times \\
& \quad \left(\frac{\prod_{i=1}^{vk-1} (M+i)}{M^{vk-1}} \frac{\prod_{i=8}^{hk+7} (M+i)}{M^{hk}} N_h^8 + \frac{\prod_{i=1}^{hk-1} (M+i)}{M^{hk-1}} \frac{\prod_{i=8}^{vk+7} (M+i)}{M^{vk}} N_v^8 \right) \times \\
& \quad N_h^{hk} N_v^{vk} + 36 \frac{\prod_{i=4}^{hk+3} (M+i)}{M^{hk}} \frac{\prod_{i=4}^{vk+3} (M+i)}{M^{vk}} \frac{(2M^2 + 2M - 8)^2}{(M-1)^8} N_h^{hk+4} N_v^{vk+4} + \\
& \quad 16 \frac{6M^3 + 36M^2 - 6M - 180}{M^{vk+hk} (M-1)^7} \times \\
& \quad \left(\prod_{i=6}^{hk+5} (M+i) \prod_{i=2}^{vk+1} (M+i) N_h^6 N_v^2 + \prod_{i=2}^{hk+1} (M+i) \prod_{i=6}^{vk+5} (M+i) N_h^2 N_v^6 \right) \times \\
& \quad N_h^{hk} N_v^{vk}
\end{aligned} \tag{H.21}$$

$$\begin{aligned}
& E \left\{ \hat{P}_h^k \left| \hat{R}_h(T) + \hat{R}_v(T) \right|^{10} \right\} = E \left\{ \hat{P}_h^k \left(\hat{R}_h(T) + \hat{R}_v(T) \right)^5 \left(\hat{R}_h^*(T) + \hat{R}_v^*(T) \right)^5 \right\} \\
& = E \left\{ \hat{P}_h^k \left(\left| \hat{R}_h(T) \right|^{10} + 25 \left| \hat{R}_h(T) \right|^8 \left| \hat{R}_v(T) \right|^2 + 100 \left| \hat{R}_h(T) \right|^6 \left| \hat{R}_v(T) \right|^4 + \right. \right. \\
& \quad \left. \left. 100 \left| \hat{R}_h(T) \right|^4 \left| \hat{R}_v(T) \right|^6 + 25 \left| \hat{R}_h(T) \right|^2 \left| \hat{R}_v(T) \right|^8 + \left| \hat{R}_v(T) \right|^{10} \right) \right\} \\
& = E \left\{ \hat{P}_h^k \left| \hat{R}_h(T) \right|^{10} \right\} + 25 E \left\{ \hat{P}_h^k \left| \hat{R}_h(T) \right|^8 \right\} E \left\{ \left| \hat{R}_v(T) \right|^2 \right\} + \\
& \quad 100 E \left\{ \hat{P}_h^k \left| \hat{R}_h(T) \right|^6 \right\} E \left\{ \left| \hat{R}_v(T) \right|^4 \right\} + 100 E \left\{ \hat{P}_h^k \left| \hat{R}_h(T) \right|^4 \right\} E \left\{ \left| \hat{R}_v(T) \right|^6 \right\} + \\
& \quad 25 E \left\{ \hat{P}_h^k \left| \hat{R}_h(T) \right|^2 \right\} E \left\{ \left| \hat{R}_v(T) \right|^8 \right\} + E \left\{ \hat{P}_h^k \right\} E \left\{ \left| \hat{R}_v(T) \right|^{10} \right\} \\
& = \frac{\prod_{i=10}^{k+9} (M+i)}{M^k} E \left\{ \left| \hat{R}_h(T) \right|^{10} \right\} N_h^k + 25 \frac{\prod_{i=8}^{k+7} (M+i)}{M^k} \times \\
& \quad E \left\{ \left| \hat{R}_h(T) \right|^8 \right\} N_h^k E \left\{ \left| \hat{R}_v(T) \right|^2 \right\} + \\
& \quad 100 \frac{\prod_{i=6}^{k+5} (M+i)}{M^k} E \left\{ \left| \hat{R}_h(T) \right|^6 \right\} N_h^k E \left\{ \left| \hat{R}_v(T) \right|^4 \right\} + \\
& \quad 100 \frac{\prod_{i=4}^{k+3} (M+i)}{M^k} E \left\{ \left| \hat{R}_h(T) \right|^4 \right\} N_h^k E \left\{ \left| \hat{R}_v(T) \right|^6 \right\} + \\
& + 25 \frac{\prod_{i=2}^{k+1} (M+i)}{M^k} E \left\{ \left| \hat{R}_h(T) \right|^2 \right\} N_h^k E \left\{ \left| \hat{R}_v(T) \right|^8 \right\} + \frac{\prod_{i=1}^{k-1} (M+i)}{M^{k-1}} N_h^k E \left\{ \left| \hat{R}_v(T) \right|^{10} \right\} \\
& = \frac{120M^5 + 3000M^4 + 24600M^3 + 54600M^2 - 168720M - 604800}{(M-1)^{10}} \times \\
& \quad \left(\frac{\prod_{i=10}^{k+9} (M+i)}{M^k} N_h^{10} + \frac{\prod_{i=1}^{k-1} (M+i)}{M^{k-1}} N_v^{10} \right) N_h^k + \\
& \quad 25 \frac{24M^4 + 336M^3 + 1128M^2 - 1488M - 8064}{(M-1)^9} \times \\
& \quad \left(\frac{\prod_{i=8}^{k+7} (M+i)}{M^k} N_h^8 N_v^2 + \frac{\prod_{i=2}^{k+1} (M+i)}{M^k} N_h^2 N_v^8 \right) N_h^k + \\
& \quad 100 \frac{6M^3 + 36M^2 - 6M - 180}{(M-1)^6} \times \frac{2M^2 + 2M - 8}{(M-1)^4} \times \\
& \quad \left(\frac{\prod_{i=6}^{k+5} (M+i)}{M^k} N_h^6 N_v^4 + \frac{\prod_{i=4}^{k+3} (M+i)}{M^k} N_h^4 N_v^6 \right) N_h^k
\end{aligned} \tag{H.22}$$

$$\begin{aligned}
& E \left\{ \hat{P}_v^{vk} \hat{P}_h^{hk} \left| \hat{R}_h(T) + \hat{R}_v(T) \right|^{10} \right\} = E \left\{ \hat{P}_v^{vk} \hat{P}_h^{hk} \left(\hat{R}_h(T) + \hat{R}_v(T) \right)^5 \left(\hat{R}_h^*(T) + \hat{R}_v^*(T) \right)^5 \right\} \\
& = E \left\{ \hat{P}_v^{vk} \hat{P}_h^{hk} \left(\left| \hat{R}_h(T) \right|^{10} + 25 \left| \hat{R}_h(T) \right|^8 \left| \hat{R}_v(T) \right|^2 + 100 \left| \hat{R}_h(T) \right|^6 \left| \hat{R}_v(T) \right|^4 + \right. \right. \\
& \quad \left. \left. 100 \left| \hat{R}_h(T) \right|^4 \left| \hat{R}_v(T) \right|^6 + 25 \left| \hat{R}_h(T) \right|^2 \left| \hat{R}_v(T) \right|^8 + \left| \hat{R}_v(T) \right|^{10} \right) \right\} \\
& = E \left\{ \hat{P}_v^{vk} \right\} E \left\{ \hat{P}_h^{hk} \left| \hat{R}_h(T) \right|^{10} \right\} + 25 E \left\{ \hat{P}_h^{hk} \left| \hat{R}_h(T) \right|^8 \right\} E \left\{ \hat{P}_v^{vk} \left| \hat{R}_v(T) \right|^2 \right\} + \\
& \quad 100 E \left\{ \hat{P}_h^{hk} \left| \hat{R}_h(T) \right|^6 \right\} E \left\{ \hat{P}_v^{vk} \left| \hat{R}_v(T) \right|^4 \right\} + 100 E \left\{ \hat{P}_h^{hk} \left| \hat{R}_h(T) \right|^4 \right\} E \left\{ \hat{P}_v^{vk} \left| \hat{R}_v(T) \right|^6 \right\} + \\
& \quad 25 E \left\{ \hat{P}_h^{hk} \left| \hat{R}_h(T) \right|^2 \right\} E \left\{ \hat{P}_v^{vk} \left| \hat{R}_v(T) \right|^8 \right\} + E \left\{ \hat{P}_h^{hk} \right\} E \left\{ \hat{P}_v^{vk} \left| \hat{R}_v(T) \right|^{10} \right\} \\
& = \frac{\prod_{i=1}^{vk-1} (M+i)}{M^{vk-1}} N_v^{vk} \frac{\prod_{i=10}^{hk+9} (M+i)}{M^{hk}} E \left\{ \left| \hat{R}_h(T) \right|^{10} \right\} N_h^{hk} + \\
& \quad 25 \frac{\prod_{i=8}^{hk+7} (M+i)}{M^{hk}} E \left\{ \left| \hat{R}_h(T) \right|^8 \right\} N_h^{hk} \frac{\prod_{i=2}^{vk+1} (M+i)}{M^{vk}} E \left\{ \left| \hat{R}_v(T) \right|^2 \right\} N_v^{vk} + \\
& \quad 100 \frac{\prod_{i=6}^{hk+5} (M+i)}{M^{hk}} E \left\{ \left| \hat{R}_h(T) \right|^6 \right\} N_h^{hk} \frac{\prod_{i=4}^{vk+3} (M+i)}{M^{vk}} E \left\{ \left| \hat{R}_v(T) \right|^4 \right\} N_v^{vk} + \\
& \quad 100 \frac{\prod_{i=4}^{hk+3} (M+i)}{M^{hk}} E \left\{ \left| \hat{R}_h(T) \right|^4 \right\} N_h^{hk} \frac{\prod_{i=6}^{vk+5} (M+i)}{M^{vk}} E \left\{ \left| \hat{R}_v(T) \right|^6 \right\} N_v^{vk} + \\
& \quad 25 \frac{\prod_{i=2}^{hk+1} (M+i)}{M^{hk}} E \left\{ \left| \hat{R}_h(T) \right|^2 \right\} N_h^{hk} \frac{\prod_{i=8}^{vk+7} (M+i)}{M^{vk}} E \left\{ \left| \hat{R}_v(T) \right|^8 \right\} N_v^{vk} + \\
& \quad \frac{\prod_{i=1}^{hk-1} (M+i)}{M^{hk-1}} N_h^{hk} \frac{\prod_{i=10}^{vk+9} (M+i)}{M^{vk}} E \left\{ \left| \hat{R}_v(T) \right|^{10} \right\} N_v^{vk}
\end{aligned} \tag{H.23}$$

$$\begin{aligned}
& E \left\{ \hat{P}_v^{vk} \hat{P}_h^{hk} \left| \hat{R}_h(T) + \hat{R}_v(T) \right|^{10} \right\} = \\
& \frac{120M^5 + 3000M^4 + 24600M^3 + 54600M^2 - 168720M - 604800}{(M-1)^{10}} \times \\
& \left(\frac{\prod_{i=10}^{hk+9} (M+i)}{M^{hk}} \frac{\prod_{i=1}^{vk-1} (M+i)}{M^{vk-1}} N_h^{10} + \frac{\prod_{i=1}^{hk-1} (M+i)}{M^{hk-1}} \frac{\prod_{i=10}^{vk+9} (M+i)}{M^{vk}} N_v^{10} \right) N_h^{hk} N_v^{vk} + \\
& 25 \frac{24M^4 + 336M^3 + 1128M^2 - 1488M - 8064}{(M-1)^9} \times \\
& \left(\frac{\prod_{i=8}^{hk+7} (M+i)}{M^{hk}} \frac{\prod_{i=2}^{vk+1} (M+i)}{M^{vk}} N_h^8 N_v^2 + \frac{\prod_{i=2}^{hk+1} (M+i)}{M^{hk}} \frac{\prod_{i=8}^{vk+7} (M+i)}{M^{vk}} N_h^2 N_v^8 \right) N_h^{hk} N_v^{vk} + \\
& 100 \frac{6M^3 + 36M^2 - 6M - 180}{(M-1)^6} \times \frac{2M^2 + 2M - 8}{(M-1)^4} \times \\
& \left(\frac{\prod_{i=6}^{hk+5} (M+i)}{M^{hk}} \frac{\prod_{i=4}^{vk+3} (M+i)}{M^{vk}} N_h^6 N_v^4 + \frac{\prod_{i=4}^{hk+3} (M+i)}{M^{hk}} \frac{\prod_{i=6}^{vk+5} (M+i)}{M^{vk}} N_h^4 N_v^6 \right) N_h^{hk} N_v^{vk} +
\end{aligned} \tag{H.24}$$

Appendix I

Evaluation of Noise Moments for $\left| \hat{R}_{hv}(0) \right|^n \left| \hat{R}_h(T) + \hat{R}_v(T) \right|^n$

To interpolate the odd moments we need to determine the even ones. We shall evaluate the following:

$$\begin{aligned} E \left\{ \left| \hat{R}_{hv}(0) \right|^2 \left| \hat{R}_h(T) + \hat{R}_v(T) \right|^2 \right\} &= E \left\{ \left| \hat{R}_{hv}(0) \right|^2 \left(\hat{R}_h(T) + \hat{R}_v(T) \right) \left(\hat{R}_h^*(T) + \hat{R}_v^*(T) \right) \right\} \\ &= E \left\{ \left| \hat{R}_{hv}(0) \right|^2 \left| \hat{R}_h(T) \right|^2 \right\} + E \left\{ \left| \hat{R}_{hv}(0) \right|^2 \hat{R}_h(T) \hat{R}_v^*(T) \right\} + (I.1) \\ &\quad E \left\{ \left| \hat{R}_{hv}(0) \right|^2 \hat{R}_v(T) \hat{R}_h^*(T) \right\} + E \left\{ \left| \hat{R}_{hv}(0) \right|^2 \left| \hat{R}_v(T) \right|^2 \right\}, \end{aligned}$$

$$\begin{aligned} E \left\{ \left| \hat{R}_{hv}(0) \right|^4 \left| \hat{R}_h(T) + \hat{R}_v(T) \right|^4 \right\} &= E \left\{ \left| \hat{R}_{hv}(0) \right|^4 \left(\hat{R}_h(T) + \hat{R}_v(T) \right)^2 \left(\hat{R}_h^*(T) + \hat{R}_v^*(T) \right)^2 \right\} \\ &= E \left\{ \left| \hat{R}_{hv}(0) \right|^4 \left(\left| \hat{R}_h(T) \right|^4 + 2 \left| \hat{R}_h(T) \right|^2 \hat{R}_h(T) \hat{R}_h^*(T) + \left(\hat{R}_h(T) \hat{R}_h^*(T) \right)^2 + \right. \right. \\ &\quad \left. \left. 2 \left| \hat{R}_h(T) \right|^2 \hat{R}_h^*(T) \hat{R}_v(T) + 4 \left| \hat{R}_h(T) \right|^2 \left| \hat{R}_v(T) \right|^2 + 2 \hat{R}_h(T) \hat{R}_v^*(T) \left| \hat{R}_v(T) \right|^2 + \right. \right. \\ &\quad \left. \left. \left(\hat{R}_v(T) \hat{R}_v^*(T) \right)^2 + 2 \hat{R}_h^*(T) \hat{R}_v(T) \left| \hat{R}_v(T) \right|^2 + \left| \hat{R}_v(T) \right|^4 \right) \right\}. \end{aligned} \quad (I.2)$$

Using the fact that:

$$\begin{aligned} E \left\{ \left| \hat{R}_{hv}(0) \right|^4 \left| \hat{R}_h(T) \right|^2 \hat{R}_h(T) \hat{R}_v^*(T) \right\} &= E \left\{ \left| \hat{R}_{hv}(0) \right|^4 \left| \hat{R}_h(T) \right|^2 \hat{R}_h^*(T) \hat{R}_v(T) \right\} \\ E \left\{ \left| \hat{R}_{hv}(0) \right|^4 \left(\hat{R}_h(T) \hat{R}_v^*(T) \right)^2 \right\} &= E \left\{ \left| \hat{R}_{hv}(0) \right|^4 \left(\hat{R}_v(T) \hat{R}_h^*(T) \right)^2 \right\} \quad (I.3) \\ E \left\{ \left| \hat{R}_{hv}(0) \right|^4 \hat{R}_h(T) \hat{R}_v^*(T) \left| \hat{R}_v(T) \right|^2 \right\} &= E \left\{ \left| \hat{R}_{hv}(0) \right|^4 2 \hat{R}_h^*(T) \hat{R}_v(T) \left| \hat{R}_v(T) \right|^2 \right\}, \end{aligned}$$

we get:

$$\begin{aligned} E \left\{ \left| \hat{R}_{hv}(0) \right|^4 \left| \hat{R}_h(T) + \hat{R}_v(T) \right|^4 \right\} &= E \left\{ \left| \hat{R}_{hv}(0) \right|^4 \left(\left| \hat{R}_h(T) \right|^4 + 4 \left| \hat{R}_h(T) \right|^2 \hat{R}_h(T) \hat{R}_v^*(T) + \right. \right. \\ &\quad \left. \left. + 4 \left| \hat{R}_h(T) \right|^2 \left| \hat{R}_v(T) \right|^2 + 4 \hat{R}_h(T) \hat{R}_v^*(T) \left| \hat{R}_v(T) \right|^2 + 2 \left(\hat{R}_h(T) \hat{R}_v^*(T) \right)^2 + \left| \hat{R}_v(T) \right|^4 \right) \right\}. \end{aligned} \quad (I.4)$$

Similarly:

$$\begin{aligned}
& E \left\{ \left| \hat{R}_{hv}(0) \right|^6 \left| \hat{R}_h(T) + \hat{R}_v(T) \right|^6 \right\} = E \left\{ \left| \hat{R}_{hv}(0) \right|^6 \left(\hat{R}_h(T) + \hat{R}_v(T) \right)^3 \left(\hat{R}_h^*(T) + \hat{R}_v^*(T) \right)^3 \right\} \\
& = E \left\{ \left| \hat{R}_{hv}(0) \right|^6 \left(\left| \hat{R}_h(T) \right|^6 + \left| \hat{R}_v(T) \right|^6 + 9 \left| \hat{R}_h(T) \right|^4 \left| \hat{R}_v(T) \right|^2 + 9 \left| \hat{R}_h(T) \right|^2 \left| \hat{R}_v(T) \right|^4 + \right. \right. \\
& 18 \left| \hat{R}_h(T) \right|^2 \left| \hat{R}_h(T) \right| \left| \hat{R}_v(T) \right|^2 \hat{R}_v^*(T) + 6 \left| \hat{R}_h(T) \right|^4 \hat{R}_h(T) \hat{R}_v^*(T) + 6 \hat{R}_h^*(T) \left| \hat{R}_v(T) \right|^4 \hat{R}_v(T) + \\
& \left. \left. 6 \hat{R}_h^2(T) \left| \hat{R}_v(T) \right|^2 \left(\hat{R}_v^*(T) \right)^2 + 6 \left| \hat{R}_h(T) \right|^2 \hat{R}_h^2(T) \left(\hat{R}_v^*(T) \right)^2 + 2 \left(\hat{R}_h(T) \hat{R}_v^*(T) \right)^3 \right) \right\}. \tag{I.5}
\end{aligned}$$

$$\begin{aligned}
& E \left\{ \left| \hat{R}_{hv}(0) \right|^8 \left| \hat{R}_h(T) + \hat{R}_v(T) \right|^8 \right\} = E \left\{ \left| \hat{R}_{hv}(0) \right|^8 \left(\hat{R}_h(T) + \hat{R}_v(T) \right)^4 \left(\hat{R}_h^*(T) + \hat{R}_v^*(T) \right)^4 \right\} \\
& = E \left\{ \left| \hat{R}_{hv}(0) \right|^8 \left(\left| \hat{R}_h(T) \right|^8 + \left| \hat{R}_v(T) \right|^8 + 2 \hat{R}_h^4(T) \left(\hat{R}_v^*(T) \right)^4 + 8 \left| \hat{R}_h(T) \right|^6 \hat{R}_h(T) \hat{R}_v^*(T) + \right. \right. \\
& 8 \hat{R}_h^*(T) \left| \hat{R}_v(T) \right|^6 \hat{R}_v(T) + 8 \left| \hat{R}_h(T) \right|^2 \hat{R}_h^3(T) \left(\hat{R}_v^*(T) \right)^3 + 8 \left(\hat{R}_h^*(T) \right)^3 \left| \hat{R}_v(T) \right|^2 \hat{R}_v^3(T) + \\
& 12 \left| \hat{R}_h(T) \right|^4 \hat{R}_h^2(T) \left(\hat{R}_v^*(T) \right)^2 + 12 \left(\hat{R}_h^*(T) \right)^2 \left| \hat{R}_v(T) \right|^4 \hat{R}_v^2(T) + 16 \left| \hat{R}_h(T) \right|^6 \left| \hat{R}_v(T) \right|^2 + \\
& 16 \left| \hat{R}_h(T) \right|^2 \left| \hat{R}_v(T) \right|^6 + 32 \left| \hat{R}_h(T) \right|^2 \hat{R}_h^2(T) \left| \hat{R}_v(T) \right|^2 \left(\hat{R}_v^*(T) \right)^2 + 36 \left| \hat{R}_h(T) \right|^4 \left| \hat{R}_v(T) \right|^4 + \\
& \left. \left. 48 \left| \hat{R}_h(T) \right|^4 \hat{R}_h(T) \left| \hat{R}_v(T) \right|^2 \hat{R}_v^*(T) + 48 \left| \hat{R}_h(T) \right|^2 \hat{R}_h^*(T) \left| \hat{R}_v(T) \right|^4 \hat{R}_v(T) \right) \right\}. \tag{I.6}
\end{aligned}$$

To evaluate these we need to determine the intermediate expressions. First we find

$E \left\{ \left| \hat{R}_{hv}(0) \right|^{2k} \left| \hat{R}_h(T) \right|^{2n} \right\}$. This goes as follows:

$$\begin{aligned}
& M^{2k} (M-1)^{2n} E \left\{ \left| \hat{R}_{hv}(0) \right|^{2k} \left| \hat{R}_h(T) \right|^{2n} \right\} = \sum_{m_1=0}^{M-1} \cdots \sum_{m_{2k}=0}^{M-1} \sum_{m_{2k+1}=0}^{M-2} \cdots \sum_{m_{2k+2n}=0}^{M-2} E \left\{ V_v(m_1) V_h^*(m_1) \cdots \right. \\
& V_v(m_k) V_h^*(m_k) V_h(m_{k+1}) V_v^*(m_{k+1}) \cdots V_h(m_{2k}) V_v^*(m_{2k}) \\
& V_h(m_{2k+1}) V_h^*(m_{2k+1}+1) \cdots V_h(m_{2k+n}) V_h^*(m_{2k+n}+1) \\
& V_h(m_{2k+n+1}+1) V_h^*(m_{2k+n+1}) \cdots V_h(m_{2k+2n}+1) V_h^*(m_{2k+2n}) \left. \right\} \\
& = \sum_{m_1=0}^{M-1} \cdots \sum_{m_{2k}=0}^{M-1} \sum_{m_{2k+1}=0}^{M-2} \cdots \sum_{m_{2k+2n}=0}^{M-2} E \left\{ V_h(m_{k+1}) V_h^*(m_1) \cdots V_h(m_{2k}) V_h^*(m_k) \right. \\
& V_h(m_{2k+1}) V_h^*(m_{2k+1}+1) \cdots V_h(m_{2k+n}) V_h^*(m_{2k+n}+1) \\
& V_h(m_{2k+n+1}+1) V_h^*(m_{2k+n+1}) \cdots V_h(m_{2k+2n}+1) V_h^*(m_{2k+2n}) \left. \right\} \\
& E \left\{ V_v(m_1) V_v^*(m_{k+1}) \cdots V_v(m_k) V_v^*(m_{2k}) \right\}. \tag{I.7}
\end{aligned}$$

Let us examine the case when $k = 1$:

$$\begin{aligned}
M^2 (M-1)^{2n} E \left\{ \left| \hat{R}_{hv}(0) \right|^2 \left| \hat{R}_h(T) \right|^{2n} \right\} &= \sum_{m_1=0}^{M-1} \cdots \sum_{m_{2k}=0}^{M-1} \sum_{m_{2k+1}=0}^{M-2} \cdots \sum_{m_{2n}=0}^{M-2} E \left\{ V_h(m_2) V_h^*(m_1) \cdots \right. \\
&V_h(m_{2k+1}) V_h^*(m_{2k+1}+1) \cdots V_h(m_{2k+n}) V_h^*(m_{2k+n}+1) \\
&\left. V_h(m_{2k+n+1}+1) V_h^*(m_{2k+n+1}) \cdots V_h(m_{2k+2n}+1) V_h^*(m_{2k+2n}) \right\} E \left\{ V_v(m_1) V_v^*(m_2) \right\}.
\end{aligned} \tag{I.8}$$

The term $E \left\{ V_v(m_1) V_v^*(m_2) \right\}$ implies that $m_1 = m_2$ so we have:

$$\begin{aligned}
M^2 (M-1)^{2n} E \left\{ \left| \hat{R}_{hv}(0) \right|^2 \left| \hat{R}_h(T) \right|^{2n} \right\} &= \sum_{m_2=0}^{M-1} \sum_{m_3=0}^{M-2} \cdots \sum_{m_{2n}=0}^{M-2} E \left\{ V_h(m_2) V_h^*(m_2) \cdots \right. \\
&V_h(m_3) V_h^*(m_3+1) \cdots V_h(m_{3+n}) V_h^*(m_{3+n}+1) \\
&V_h(m_{3+n+1}+1) V_h^*(m_{3+n+1}) \cdots V_h(m_{3+2n}+1) V_h^*(m_{3+2n}) \left. \right\} N_v \\
&= N_v E \left\{ \hat{P}_h \left| \hat{R}_h(T) \right|^{2n} \right\}.
\end{aligned} \tag{I.9}$$

When $k = 2$ we have:

$$\begin{aligned}
M^4 (M-1)^{2n} E \left\{ \left| \hat{R}_{hv}(0) \right|^4 \left| \hat{R}_h(T) \right|^{2n} \right\} &= \\
&\sum_{m_1=0}^{M-1} \cdots \sum_{m_4=0}^{M-1} \sum_{m_5=0}^{M-2} \cdots \sum_{m_{4+2n}=0}^{M-2} E \left\{ V_h(m_3) V_h^*(m_1) V_h(m_4) V_h^*(m_2) \right. \\
&V_h(m_5) V_h^*(m_5+1) \cdots V_h(m_{4+n}) V_h^*(m_{4+n}+1) \\
&V_h(m_{4+n+1}+1) V_h^*(m_{4+n+1}) \cdots V_h(m_{4+2n}+1) V_h^*(m_{4+2n}) \left. \right\} \\
&\left(E \left\{ V_v(m_1) V_v^*(m_3) \right\} E \left\{ V_v(m_2) V_v^*(m_4) \right\} + E \left\{ V_v(m_2) V_v^*(m_3) \right\} E \left\{ V_v(m_1) V_v^*(m_4) \right\} \right)
\end{aligned} \tag{I.10}$$

The first term in the brackets imposes $m_1 = m_3$, and $m_2 = m_4$, whereas the second one implies $m_2 = m_3$, and $m_1 = m_4$. Using this we have:

$$\begin{aligned}
M^4 (M-1)^{2n} E \left\{ \left| \hat{R}_{hv}(0) \right|^4 \left| \hat{R}_h(T) \right|^{2n} \right\} = \\
\sum_{m_1=0}^{M-1} \sum_{m_2=0}^{M-1} \sum_{m_3=0}^{M-2} \cdots \sum_{m_{4+2n}=0}^{M-2} E \left\{ V_h(m_1) V_h^*(m_1) V_h(m_2) V_h^*(m_2) \right. \\
V_h(m_3) V_h^*(m_3+1) \cdots V_h(m_{4+n}) V_h^*(m_{4+n}+1) \\
\left. V_h(m_{4+n+1}+1) V_h^*(m_{4+n+1}) \cdots V_h(m_{4+2n}+1) V_h^*(m_{4+2n}) \right\} N_v^2 + \\
\sum_{m_1=0}^{M-1} \sum_{m_2=0}^{M-1} \sum_{m_3=0}^{M-2} \cdots \sum_{m_{4+2n}=0}^{M-2} E \left\{ V_h(m_2) V_h^*(m_1) V_h(m_1) V_h^*(m_2) \right. \\
V_h(m_3) V_h^*(m_3+1) \cdots V_h(m_{4+n}) V_h^*(m_{4+n}+1) \\
\left. V_h(m_{4+n+1}+1) V_h^*(m_{4+n+1}) \cdots V_h(m_{4+2n}+1) V_h^*(m_{4+2n}) \right\} N_v^2 \\
= 2N_v^2 M^2 (M-1)^{2n} E \left\{ \hat{P}_h^2 \left| \hat{R}_h(T) \right|^{2n} \right\}
\end{aligned} \tag{I.11}$$

Thus for general case we can write:

$$\begin{aligned}
M^{2k} (M-1)^{2n} E \left\{ \left| \hat{R}_{hv}(0) \right|^{2k} \left| \hat{R}_h(T) \right|^{2n} \right\} = \\
\sum_{m_1=0}^{M-1} \cdots \sum_{m_{2k}=0}^{M-1} \sum_{m_{2k+1}=0}^{M-2} \cdots \sum_{m_{2n}=0}^{M-2} \sum_{\text{Perm}(n_1, \dots, n_{k+2n})}^{\{m_1, \dots, m_k, m_{2k+1}+1, \dots, m_{2k+n}+1, m_{2k+n+1}, \dots, m_{2k+2n}\}} C_{m_1 n_1} \cdots C_{m_{2k+n} n_{k+n}} \\
C_{(m_{2k+n+1}+1) n_{k+n+1}} \cdots C_{(m_{2k+2n}+1) n_{k+2n}} \sum_{\text{Perm}(l_1, \dots, l_k)}^{\{m_{k+1}, \dots, m_{2k}\}} C_{m_1 l_1} \cdots C_{m_k l_k} \\
= k! \sum_{m_1=0}^{M-1} \cdots \sum_{m_k=0}^{M-1} \sum_{m_{2k+1}=0}^{M-2} \cdots \sum_{m_{2n}=0}^{M-2} \sum_{\text{Perm}(n_1, \dots, n_{k+2n})}^{\{m_1, \dots, m_k, m_{2k+1}+1, \dots, m_{2k+n}+1, m_{2k+n+1}, \dots, m_{2k+2n}\}} C_{m_1 n_1} \cdots C_{m_k n_k} C_{m_{2k+n} n_{k+n}} \\
C_{(m_{2k+n+1}+1) n_{k+n+1}} \cdots C_{(m_{2k+2n}+1) n_{k+2n}} N_v^k \\
= k! N_v^k M^k (M-1)^{2n} E \left\{ \hat{P}_h^k \left| \hat{R}_h(T) \right|^{2n} \right\}
\end{aligned} \tag{I.12}$$

Using the result (H.1)

$$E \left\{ \left| \hat{R}_{hv}(0) \right|^{2k} \left| \hat{R}_h(T) \right|^{2n} \right\} = k! \frac{(M+2n) \cdots (M+k-1+2n)}{M^{2k}} E \left\{ \left| \hat{R}_h(T) \right|^{2n} \right\} N_h^k N_v^k. \tag{I.13}$$

Similarly:

$$E \left\{ \left| \hat{R}_{hv}(0) \right|^{2k} \left| \hat{R}_v(T) \right|^{2n} \right\} = k! \frac{(M+2n) \cdots (M+k-1+2n)}{M^{2k}} E \left\{ \left| \hat{R}_v(T) \right|^{2n} \right\} N_h^k N_v^k. \tag{I.14}$$

We shall now evaluate some other intermediate results:

$$\begin{aligned}
E \left\{ \left| \hat{R}_{hv}(0) \right|^2 \hat{R}_h(T) \hat{R}_v^*(T) \right\} &= \frac{1}{M^2 (M-1)^2} \sum_{m_1=0}^{M-1} \sum_{m_2=0}^{M-1} \sum_{m_3=0}^{M-2} \sum_{m_4=0}^{M-2} E \left\{ V_h(m_1) V_h^*(m_2) \right. \\
&\quad \left. V_h(m_3+1) V_h^*(m_3) \right\} E \left\{ V_v^*(m_1) V_v(m_2) V_v^*(m_4+1) V_v(m_4) \right\} \\
&= \frac{N_v^2}{M^2 (M-1)^2} \sum_{m_3=0}^{M-2} \sum_{m_4=0}^{M-2} E \left\{ V_h(m_4) V_h^*(m_4+1) V_h(m_3+1) V_h^*(m_3) \right\} \quad (I.15) \\
&= \frac{N_v^2}{M^2} \left| \hat{R}_h(T) \right|^2 = \frac{N_h^2 N_v^2}{M^2 (M-1)} \\
&= E \left\{ \left| \hat{R}_{hv}(0) \right|^2 \hat{R}_v(T) \hat{R}_h^*(T) \right\},
\end{aligned}$$

$$\begin{aligned}
E \left\{ \left| \hat{R}_{hv}(0) \right|^4 \left| \hat{R}_h(T) \right|^2 \hat{R}_h^*(T) \hat{R}_v(T) \right\} &= \frac{1}{M^4 (M-1)} \sum_{m_1=0}^{M-1} \cdots \sum_{m_4=0}^{M-1} \sum_{m_5=0}^{M-2} E \left\{ V_h(m_1) V_h(m_2) \right. \\
&\quad \left. V_h^*(m_3) V_h^*(m_4) \left| \hat{R}_h(T) \right|^2 \hat{R}_h^*(T) \right\} \quad (I.16) \\
&\quad E \left\{ V_v^*(m_1) V_v^*(m_2) V_v(m_3) V_v(m_4) V_v^*(m_5) V_v(m_5+1) \right\}.
\end{aligned}$$

We observe V channel samples with m_5 index. Obviously, if these two samples are paired together, zero expected value is resulted. Thus, $V_v^*(m_5)$ must be paired with either $V_v(m_3)$ or $V_v(m_4)$, and $V_v(m_5+1)$ with $V_v^*(m_1)$ or $V_v^*(m_2)$. Each pairing imposes either $m_3 = m_5$ or $m_4 = m_5$, and $m_1 = m_5+1$ or $m_2 = m_5+1$, respectively. Regardless of the pairing, the outcome expected value is the same. In total, there are 2^2 such pairings. Then, we have:

$$\begin{aligned}
E \left\{ \left| \hat{R}_{hv}(0) \right|^4 \left| \hat{R}_h(T) \right|^2 \hat{R}_h^*(T) \hat{R}_v(T) \right\} &= \frac{2^2 N_v^2}{M^4 (M-1)} \sum_{m_2=0}^{M-1} \sum_{m_4=0}^{M-1} \sum_{m_5=0}^{M-2} E \left\{ V_v^*(m_2) V_v(m_4) \right\} \\
&\quad E \left\{ V_h(m_5+1) V_h(m_2) V_h^*(m_5) V_h^*(m_4) \left| \hat{R}_h(T) \right|^2 \hat{R}_h^*(T) \right\} \\
&= 2^2 \frac{N_v^2}{M^2} E \left\{ \left| \hat{R}_{hv}(0) \right|^2 \left| \hat{R}_h(T) \right|^4 \right\} \quad (I.17) \\
&= 4(M+4) \frac{2M^2 + 2M - 8}{(M-1)^4 M^4} N_h^5 N_v^3 \\
&= E \left\{ \left| \hat{R}_{hv}(0) \right|^4 \left| \hat{R}_h(T) \right|^2 \hat{R}_h(T) \hat{R}_v^*(T) \right\}.
\end{aligned}$$

Apparently, we can generalize this principle so that each expression:

$$\begin{aligned}
E \left\{ \left| \hat{R}_{hv}(0) \right|^{2k} \left| \hat{R}_h(T) \right|^{2n} \left(\hat{R}_h^*(T) \right)^{2l-1} \hat{R}_v(T) \right\} &= k^2 \frac{N_v^2}{M^2} E \left\{ \left| \hat{R}_{hv}(0) \right|^{2(k-1)} \left| \hat{R}_h(T) \right|^{2n+2l} \right\} \\
&= E \left\{ \left| \hat{R}_{hv}(0) \right|^{2k} \left| \hat{R}_h(T) \right|^{2n} \hat{R}_h^{2l-1}(T) \hat{R}_v^*(T) \right\} \\
&= k^2 (k-1)! \frac{(M+2n+2l) \cdots (M+k-2+2n+2l)}{M^{2k}} E \left\{ \left| \hat{R}_h(T) \right|^{2(n+l)} \right\} N_h^{k-1} N_v^{k+1} \\
E \left\{ \left| \hat{R}_{hv}(0) \right|^{2k} \left| \hat{R}_v(T) \right|^{2n} \left(\hat{R}_v^*(T) \right)^{2l-1} \hat{R}_h(T) \right\} &= k^2 \frac{N_h^2}{M^2} E \left\{ \left| \hat{R}_{hv}(0) \right|^{2(k-1)} \left| \hat{R}_h(T) \right|^{2n+2l} \right\} \\
&= E \left\{ \left| \hat{R}_{hv}(0) \right|^{2k} \left| \hat{R}_v(T) \right|^{2n} \hat{R}_v^{2l-1}(T) \hat{R}_h^*(T) \right\} \\
&= k^2 (k-1)! \frac{(M+2n+2l) \cdots (M+k-2+2n+2l)}{M^{2k}} E \left\{ \left| \hat{R}_v(T) \right|^{2(n+l)} \right\} N_v^{k-1} N_h^{k+1}.
\end{aligned} \tag{I.18}$$

Using this formula we evaluate:

$$\begin{aligned}
E \left\{ \left| \hat{R}_{hv}(0) \right|^6 \left| \hat{R}_h(T) \right|^4 \hat{R}_h(T) \hat{R}_v^*(T) \right\} &= \\
9 * 2 \frac{(M+6)(M+7)}{M^6} \frac{6M^3 + 36M^2 - 6M - 180}{(M-1)^6} (N_h^8 N_v^4 + N_h^4 N_v^8)
\end{aligned} \tag{I.19}$$

As for other expressions, it does not appear possible to arrive at a convenient recursion formula, thus in this case we shall resort to using the computational method. Then we have:

$$E \left\{ \left| \hat{R}_{hv}(0) \right|^4 \left| \hat{R}_h(T) \right|^2 \left| \hat{R}_v(T) \right|^2 \right\} = \frac{2M^4 + 14M^3 + 26M^2 - 22M - 68}{M^4 (M-1)^4} N_h^4 N_v^4, \tag{I.20}$$

$$E \left\{ \left| \hat{R}_{hv}(0) \right|^4 \left(\hat{R}_h^*(T) \hat{R}_v(T) \right)^2 \right\} = \frac{24M^2 + 24M - 128}{M^4 (M-1)^2} N_h^4 N_v^4, \tag{I.21}$$

$$\begin{aligned}
E \left\{ \left| \hat{R}_{hv}(0) \right|^6 \left| \hat{R}_h(T) \right|^4 \left| \hat{R}_v(T) \right|^2 \right\} &= \\
\frac{12M^6 + 252M^5 + 2124M^4 + 8292M^3 + 9096M^2 - 28992M - 63360}{M^6 (M-1)^6} N_h^7 N_v^5,
\end{aligned} \tag{I.22}$$

$$E \left\{ \left| \hat{R}_{hv}(0) \right|^6 \left| \hat{R}_h(T) \right|^2 \left| \hat{R}_v(T) \right|^4 \right\} = \frac{12M^6 + 252M^5 + 2124M^4 + 8292M^3 + 9096M^2 - 28992M - 63360}{M^6(M-1)^6} N_h^5 N_v^7, \quad (\text{I.23})$$

$$E \left\{ \left| \hat{R}_{hv}(0) \right|^6 \left| \hat{R}_h(T) \right|^2 \hat{R}_h^2(T) \left(\hat{R}_v^*(T) \right)^2 \right\} = \frac{432M^4 + 5184M^3 + 14688M^2 - 20304M - 90720}{M^6(M-1)^6} N_h^7 N_v^5, \quad (\text{I.24})$$

$$E \left\{ \left| \hat{R}_{hv}(0) \right|^6 \hat{R}_h^3(T) \left(\hat{R}_v^*(T) \right)^3 \right\} = \frac{2160M^3 + 10368M^2 - 23760M - 109728}{M^6(M-1)^6} N_h^6 N_v^6, \quad (\text{I.25})$$

$$E \left\{ \left| \hat{R}_{hv}(0) \right|^6 \left| \hat{R}_h(T) \right|^2 \hat{R}_h^*(T) \left| \hat{R}_v(T) \right|^2 \hat{R}_v(T) \right\} = \frac{72M^5 + 1152M^4 + 6336M^3 + 97920M^2 - 22104M - 58320}{M^6(M-1)^6} N_h^6 N_v^6. \quad (\text{I.26})$$

Finally:

$$E \left\{ \left| \hat{R}_{hv}(0) \right|^2 \left| \hat{R}_h(T) + \hat{R}_v(T) \right|^2 \right\} = \frac{(M+2)}{M^2(M-1)} (N_h^3 N_v + N_h N_v^3) + \frac{2}{M^2(M-1)} N_h^2 N_v^2, \quad (\text{I.27})$$

$$E \left\{ \left| \hat{R}_{hv}(0) \right|^4 \left| \hat{R}_h(T) + \hat{R}_v(T) \right|^4 \right\} = 2 \frac{(M+4)(M+5)}{M^4} \frac{2M^2 + 2M - 8}{(M-1)^4} (N_h^6 N_v^2 + N_h^2 N_v^6) + 16(M+2) \frac{2M^2 + 2M - 8}{(M-1)^4 M^4} (N_h^5 N_v^3 + N_h^3 N_v^5) + 2 \frac{24M^2 + 24M - 128}{M^4(M-1)^4} N_h^4 N_v^4 \quad (\text{I.28})$$

$$4 \frac{2M^4 + 14M^3 + 26M^2 - 22M - 68}{M^4(M-1)^4} N_h^4 N_v^4,$$

$$\begin{aligned}
E \left\{ \left| \hat{R}_{hv}(0) \right|^6 \left| \hat{R}_h(T) + \hat{R}_v(T) \right|^6 \right\} &= 6 \frac{\prod_{i=6}^8 (M+i)}{M^6} \frac{6M^3 + 36M^2 - 6M - 180}{(M-1)^6} \times \\
&\quad (N_h^9 N_v^3 + N_h^3 N_v^9) + \\
9 \frac{12M^6 + 252M^5 + 2124M^4 + 8292M^3 + 9096M^2 - 28992M - 63360}{M^6 (M-1)^6} \times \\
&\quad (N_h^7 N_v^5 + N_h^5 N_v^7) + \\
6 * 9 * 2 \frac{(M+6)(M+7)}{M^6} \frac{6M^3 + 36M^2 - 6M - 180}{(M-1)^6} (N_h^8 N_v^4 + N_h^4 N_v^8) + \\
6 \frac{432M^4 + 5184M^3 + 14688M^2 - 20304M - 90720}{M^6 (M-1)^6} (N_h^7 N_v^5 + N_h^5 N_v^7) + \\
2 \frac{2160M^3 + 10368M^2 - 23760M - 109728}{M^6 (M-1)^6} N_h^6 N_v^6 + \\
18 \frac{72M^5 + 1152M^4 + 6336M^3 + 97920M^2 - 22104M - 58320}{M^6 (M-1)^6} N_h^6 N_v^6, \quad (I.29)
\end{aligned}$$

or:

$$\begin{aligned}
E \left\{ \left| \hat{R}_{hv}(0) \right|^6 \left| \hat{R}_h(T) + \hat{R}_v(T) \right|^6 \right\} &= 6 \frac{\prod_{i=6}^8 (M+i)}{M^6} \frac{6M^3 + 36M^2 - 6M - 180}{(M-1)^6} \times \\
&\quad (N_h^9 N_v^3 + N_h^3 N_v^9) + \\
\frac{108M^6 + 2268M^5 + 21708M^4 + 105732M^3 + 169992M^2 - 382752M - 1114560}{M^6 (M-1)^6} \times \quad (I.30) \\
&\quad (N_h^7 N_v^5 + N_h^5 N_v^7) + 108 \frac{(M+6)(M+7)}{M^6} \frac{6M^3 + 36M^2 - 6M - 180}{(M-1)^6} (N_h^8 N_v^4 + N_h^4 N_v^8) + \\
\frac{1296M^5 + 20736M^4 + 118368M^3 + 1783296M^2 - 445392M - 1269216}{M^6 (M-1)^6} N_h^6 N_v^6.
\end{aligned}$$

To arrive at the solution for $E \left\{ \left| \hat{R}_{hv}(0) \right|^8 \left| \hat{R}_h(T) \right|^6 \left| \hat{R}_v(T) \right|^2 \right\}$, let us analyze the expression

as:

$$\begin{aligned}
& M^8 (M-1)^8 E \left\{ \left| \hat{R}_{hv}(0) \right|^8 \left| \hat{R}_h(T) \right|^6 \left| \hat{R}_v(T) \right|^2 \right\} = \\
& \sum_{m_1=0}^{M-1} \cdots \sum_{m_8=0}^{M-1} \sum_{m_9=0}^{M-2} \cdots \sum_{m_{16}=0}^{M-2} E \left\{ \prod_{l=1}^4 V_h(m_{l1}) V_v^*(m_{l1}) \prod_{l=5}^8 V_v(m_{l2}) V_h^*(m_{l2}) \right. \\
& \prod_{l=9}^{11} V_h(m_{l3}) V_h^*(m_{l3}+1) \prod_{l=12}^{14} V_h(m_{l4}+1) V_h^*(m_{l4}) V_v(m_{l5}) V_v^*(m_{l5}+1) \\
& \left. V_v(m_{16}+1) V_v^*(m_{16}) \right\} \tag{I.31} \\
& = \sum_{m_1=0}^{M-1} \cdots \sum_{m_8=0}^{M-1} \sum_{m_9=0}^{M-2} \cdots \sum_{m_{16}=0}^{M-2} E \left\{ \prod_{l=1}^4 V_h(m_{l1}) \prod_{l=5}^8 V_h^*(m_{l2}) \right. \\
& \left. \prod_{l=9}^{11} V_h(m_{l3}) V_h^*(m_{l3}+1) \prod_{l=12}^{14} V_h(m_{l4}+1) V_h^*(m_{l4}) \right\} \\
& E \left\{ \prod_{l=1}^4 V_v^*(m_{l1}) \prod_{l=5}^8 V_v(m_{l2}) V_v(m_{15}) V_v^*(m_{15}+1) V_v(m_{16}+1) V_v^*(m_{16}) \right\}.
\end{aligned}$$

By analyzing the above expression, the first expected value requires 10! permutations, while the second one needs 6!. Thus, in total $10! \times 6! = 2.612736 \times 10^9$ permutations are needed. This is a very high number, especially if we take into account that to program the first expected value, 14 nested loops need to be executed. Consequently, optimizations based on the following rationale are introduced. First by looking at the permutation formulae we note that we can break the expression as:

$$M^8 (M-1)^8 E \left\{ \left| \hat{R}_{hv}(0) \right|^8 \left| \hat{R}_h(T) \right|^6 \left| \hat{R}_v(T) \right|^2 \right\} = A + B + C, \tag{I.32}$$

where:

$$\begin{aligned}
A = & \sum_{m_1=0}^{M-1} \cdots \sum_{m_8=0}^{M-1} \sum_{m_9=0}^{M-2} \cdots \sum_{m_{16}=0}^{M-2} \left[\sum_{i=5}^8 E \left\{ V_h(m_1) V_h^*(m_i) \right\} E \left\{ \prod_{l=2}^4 V_h(m_{l1}) \prod_{l=5}^{i-1} V_h^*(m_{l2}) \right. \right. \\
& \left. \left. \prod_{l=2+i}^8 V_h^*(m_{l2}) \prod_{l=9}^{11} V_h(m_{l3}) V_h^*(m_{l3}+1) \prod_{l=12}^{14} V_h(m_{l4}+1) V_h^*(m_{l4}) \right\} \right] \tag{I.33} \\
& E \left\{ \prod_{l=1}^4 V_v^*(m_{l1}) \prod_{l=5}^8 V_v(m_{l2}) V_v(m_{15}) V_v^*(m_{15}+1) V_v(m_{16}+1) V_v^*(m_{16}) \right\},
\end{aligned}$$

$$\begin{aligned}
B = & \sum_{m_1=0}^{M-1} \cdots \sum_{m_8=0}^{M-1} \sum_{m_9=0}^{M-2} \cdots \sum_{m_{16}=0}^{M-2} \left[\sum_{j=9}^{11} E \{ V_h(m_1) V_h^*(m_j+1) \} E \left\{ \prod_{l=2}^4 V_h(m_{l1}) \prod_{l=2}^8 V_h^*(m_{l2}) \right. \right. \\
& \left. \left. \prod_{l=3}^{j-1} V_h^*(m_{l3}) V_h^*(m_{l3}+1) V_h^*(m_j) \prod_{l=3}^{11} V_h(m_{l3}) V_h^*(m_{l3}+1) \prod_{l=4}^{14} V_h(m_{l4}+1) V_h^*(m_{l4}) \right\} \right] \quad (I.34) \\
& E \left\{ \prod_{l=1}^4 V_v^*(m_{l1}) \prod_{l=2}^8 V_v(m_{l2}) V_v(m_{15}) V_v^*(m_{15}+1) V_v(m_{16}+1) V_v^*(m_{16}) \right\},
\end{aligned}$$

$$\begin{aligned}
C = & \sum_{m_1=0}^{M-1} \cdots \sum_{m_8=0}^{M-1} \sum_{m_9=0}^{M-2} \cdots \sum_{m_{16}=0}^{M-2} \left[\sum_{k=12}^{14} E \{ V_h(m_1) V_h^*(m_k) \} E \left\{ \prod_{l=2}^4 V_h(m_{l1}) \prod_{l=2}^8 V_h^*(m_{l2}) \right. \right. \\
& \left. \left. \prod_{l=3}^{11} V_h(m_{l3}) V_h^*(m_{l3}+1) \prod_{l=4}^{k-1} V_h(m_{l4}+1) V_h^*(m_{l4}) V_h(m_k+1) \prod_{l=k+1}^{14} V_h(m_{l4}+1) V_h^*(m_{l4}) \right\} \right] \quad (I.35) \\
& E \left\{ \prod_{l=1}^4 V_v^*(m_{l1}) \prod_{l=2}^8 V_v(m_{l2}) V_v(m_{15}) V_v^*(m_{15}+1) V_v(m_{16}+1) V_v^*(m_{16}) \right\}.
\end{aligned}$$

If we examine closer the expression A for the cases when $i=5$ and $i=i0$ ($i0 \in \{6,7,8\}$) by swapping $m_1=m_{i0}$ and $m_{i0}=m_1$ we realize that these two expressions are equivalent (i.e., their overall sums are the same). Furthermore, by applying the same analysis for expressions B and C we can show the same. Consequently, we write:

$$\begin{aligned}
A = & 4 \sum_{m_1=0}^{M-1} \cdots \sum_{m_8=0}^{M-1} \sum_{m_9=0}^{M-2} \cdots \sum_{m_{16}=0}^{M-2} E \{ V_h(m_1) V_h^*(m_5) \} E \left\{ \prod_{l=2}^4 V_h(m_{l1}) \prod_{l=2}^8 V_h^*(m_{l2}) \right. \\
& \left. \prod_{l=3}^{11} V_h(m_{l3}) V_h^*(m_{l3}+1) \prod_{l=4}^{14} V_h(m_{l4}+1) V_h^*(m_{l4}) \right\} \\
& E \left\{ \prod_{l=1}^4 V_v^*(m_{l1}) \prod_{l=2}^8 V_v(m_{l2}) V_v(m_{15}) V_v^*(m_{15}+1) V_v(m_{16}+1) V_v^*(m_{16}) \right\} \\
= & 4 N_h \sum_{m_2=0}^{M-1} \cdots \sum_{m_8=0}^{M-1} \sum_{m_9=0}^{M-2} \cdots \sum_{m_{16}=0}^{M-2} E \left\{ \prod_{l=2}^4 V_h(m_{l1}) \prod_{l=2}^8 V_h^*(m_{l2}) \right. \quad (I.36) \\
& \left. \prod_{l=3}^{11} V_h(m_{l3}) V_h^*(m_{l3}+1) \prod_{l=4}^{14} V_h(m_{l4}+1) V_h^*(m_{l4}) \right\} \\
& E \left\{ V_v^*(m_5) V_v(m_5) \prod_{l=2}^4 V_v^*(m_{l1}) \prod_{l=2}^8 V_v(m_{l2}) V_v(m_{15}) V_v^*(m_{15}+1) V_v(m_{16}+1) V_v^*(m_{16}) \right\} \\
= & 4 N_h M^7 (M-1)^8 E \left\{ \hat{P}_v \left| \hat{R}_{hv}(0) \right|^6 \left| \hat{R}_h(T) \right|^6 \left| \hat{R}_v(T) \right|^2 \right\}.
\end{aligned}$$

We shall now use result which will be derived later and get:

$$\begin{aligned}
A &= 4N_h N_v M^6 (M-1)^8 (M+5) E \left\{ \left| \hat{R}_{hv}(0) \right|^6 \left| \hat{R}_h(T) \right|^6 \left| \hat{R}_v(T) \right|^2 \right\} \\
&4N_h N_v (M+5) \sum_{m_1=0}^{M-1} \cdots \sum_{m_7=0}^{M-1} \sum_{m_9=0}^{M-2} \cdots \sum_{m_{14}=0}^{M-2} E \left\{ \prod_{l_1=1}^3 V_h(m_{l_1}) \prod_{l_2=4}^6 V_h^*(m_{l_2}) \right. \\
&\quad \left. \prod_{l_3=7}^9 V_h(m_{l_3}) V_h^*(m_{l_3}+1) \prod_{l_4=10}^{12} V_h(m_{l_4}+1) V_h^*(m_{l_4}) \right\} \\
&E \left\{ \prod_{l_1=1}^3 V_v^*(m_{l_1}) \prod_{l_2=4}^6 V_v(m_{l_2}) V_v(m_{l_3}) V_v^*(m_{l_3}+1) V_v(m_{l_4}+1) V_v^*(m_{l_4}) \right\}.
\end{aligned} \tag{I.37}$$

We see that not only the number of permutations evaluated is decreased in the expression for A but even more important the number of nested loops is less by two. Using the computational approach we get:

$$\begin{aligned}
E \left\{ \left| \hat{R}_{hv}(0) \right|^6 \left| \hat{R}_h(T) \right|^6 \left| \hat{R}_v(T) \right|^2 \right\} &= \frac{36M^7 + 1152M^6 + 15264M^5 + 104400M^4 + \dots}{M^6} \\
&\frac{346716M^3 + 175680M^2 - 2022192M - 3846528}{(M-1)^8} N_h^9 N_v^5.
\end{aligned} \tag{I.38}$$

Let us apply the same to B and C :

$$\begin{aligned}
B &= 3N_h \sum_{m_2=0}^{M-1} \cdots \sum_{m_8=0}^{M-1} \sum_{m_9=0}^{M-2} \cdots \sum_{m_{16}=0}^{M-2} E \left\{ \prod_{l_1=2}^4 V_h(m_{l_1}) \prod_{l_2=5}^8 V_h^*(m_{l_2}) \right. \\
&\quad \left. V_h(m_9) \prod_{l_3=10}^{11} V_h(m_{l_3}) V_h^*(m_{l_3}+1) \prod_{l_4=12}^{14} V_h(m_{l_4}+1) V_h^*(m_{l_4}) \right\} \\
&E \left\{ V_v^*(m_9+1) \prod_{l_1=2}^4 V_v^*(m_{l_1}) \prod_{l_2=5}^8 V_v(m_{l_2}) V_v(m_{l_5}) V_v^*(m_{l_5}+1) V_v(m_{l_6}+1) V_v^*(m_{l_6}) \right\},
\end{aligned} \tag{I.39}$$

$$\begin{aligned}
C &= 3N_h \sum_{m_2=0}^{M-1} \cdots \sum_{m_6=0}^{M-1} \sum_{m_9=0}^{M-2} \cdots \sum_{m_{16}=0}^{M-2} E \left\{ \prod_{l_1=2}^4 V_h(m_{l_1}) \prod_{l_2=5}^8 V_h^*(m_{l_2}) \right. \\
&\quad \left. \prod_{l_3=9}^{11} V_h(m_{l_3}) V_h^*(m_{l_3}+1) V_h(m_{l_2}+1) \prod_{l_4=13}^{14} V_h(m_{l_4}+1) V_h^*(m_{l_4}) \right\} \\
&E \left\{ V_v^*(m_{12}) \prod_{l_1=2}^4 V_v^*(m_{l_1}) \prod_{l_2=5}^8 V_v(m_{l_2}) V_v(m_{l_5}) V_v^*(m_{l_5}+1) V_v(m_{l_6}+1) V_v^*(m_{l_6}) \right\}.
\end{aligned} \tag{I.40}$$

Following the similar rationale we shall further optimize the B and C expressions:

$$\begin{aligned}
B = & 3N_h \sum_{m_2=0}^{M-1} \cdots \sum_{m_8=0}^{M-1} \sum_{m_9=0}^{M-2} \cdots \sum_{m_{16}=0}^{M-2} \left[4E \{V_h(m_9)V_h^*(m_5)\} E \left\{ \prod_{l1=2}^4 V_h(m_{l1}) \prod_{l2=6}^8 V_h^*(m_{l2}) \right. \right. \\
& \left. \prod_{l3=10}^{11} V_h(m_{l3}) V_h^*(m_{l3}+1) \prod_{l4=12}^{14} V_h(m_{l4}+1) V_h^*(m_{l4}) \right\} + 2E \{V_h(m_9)V_h^*(m_{10}+1)\} \\
& E \left\{ \prod_{l1=2}^4 V_h(m_{l1}) \prod_{l2=5}^8 V_h^*(m_{l2}) V_h(m_{10}) V_h(m_{11}) V_h^*(m_{11}+1) \prod_{l4=12}^{14} V_h(m_{l4}+1) V_h^*(m_{l4}) \right\} + \\
& 3E \{V_h(m_9)V_h^*(m_{12})\} E \left\{ \prod_{l1=2}^4 V_h(m_{l1}) \prod_{l2=5}^8 V_h^*(m_{l2}) \prod_{l3=10}^{11} V_h(m_{l3}) V_h^*(m_{l3}+1) \right. \\
& \left. V_h(m_{12}+1) \prod_{l4=13}^{14} V_h(m_{l4}+1) V_h^*(m_{l4}) \right\} \\
& E \left\{ V_v^*(m_9+1) \prod_{l1=2}^4 V_v^*(m_{l1}) \prod_{l2=5}^8 V_v(m_{l2}) V_v(m_{15}) V_v^*(m_{15}+1) V_v(m_{16}+1) V_v^*(m_{16}) \right\}, \\
\end{aligned} \tag{I.41}$$

$$\begin{aligned}
C = & 3N_h \sum_{m_2=0}^{M-1} \cdots \sum_{m_6=0}^{M-1} \sum_{m_9=0}^{M-2} \cdots \sum_{m_{16}=0}^{M-2} \left[4E \{V_h(m_{12}+1)V_h^*(m_5)\} E \left\{ \prod_{l1=2}^4 V_h(m_{l1}) \prod_{l2=6}^8 V_h^*(m_{l2}) \right. \right. \\
& \left. \prod_{l3=9}^{11} V_h(m_{l3}) V_h^*(m_{l3}+1) \prod_{l4=13}^{14} V_h(m_{l4}+1) V_h^*(m_{l4}) \right\} + 3E \{V_h(m_{12}+1)V_h^*(m_9+1)\} \\
& E \left\{ \prod_{l1=2}^4 V_h(m_{l1}) \prod_{l2=5}^8 V_h^*(m_{l2}) V_h(m_9) \prod_{l3=10}^{11} V_h(m_{l3}) V_h^*(m_{l3}+1) \prod_{l4=13}^{14} V_h(m_{l4}+1) V_h^*(m_{l4}) \right\} + \\
& 2E \{V_h(m_{12}+1)V_h^*(m_{13})\} E \left\{ \prod_{l1=2}^4 V_h(m_{l1}) \prod_{l2=5}^8 V_h^*(m_{l2}) \prod_{l3=9}^{11} V_h(m_{l3}) V_h^*(m_{l3}+1) \right. \\
& \left. V_h(m_{13}+1) V_h(m_{14}+1) V_h^*(m_{14}) \right\} \\
& E \left\{ V_v^*(m_{12}) \prod_{l1=2}^4 V_v^*(m_{l1}) \prod_{l2=5}^8 V_v(m_{l2}) V_v(m_{15}) V_v^*(m_{15}+1) V_v(m_{16}+1) V_v^*(m_{16}) \right\}. \\
\end{aligned} \tag{I.42}$$

After using the noise feature we can break B and C into:

$$\begin{aligned}
B &= BA + BB + BC \\
C &= CA + CB + CC
\end{aligned} \tag{I.43}$$

where

$$\begin{aligned}
BA &= 12N_h^2 \sum_{m_1=0}^{M-1} \cdots \sum_{m_6=0}^{M-1} \sum_{m_7=0}^{M-2} \cdots \sum_{m_{14}=0}^{M-2} E \left\{ \prod_{l=1}^3 V_h(m_{l1}) \prod_{l=2}^6 V_h^*(m_{l2}) \right. \\
&\quad \left. \prod_{l3=8}^9 V_h(m_{l3}) V_h^*(m_{l3}+1) \prod_{l4=10}^{12} V_h(m_{l4}+1) V_h^*(m_{l4}) \right\} E \left\{ V_v(m_7) V_v^*(m_7+1) \right. \\
&\quad \left. \prod_{l1=1}^3 V_v^*(m_{l1}) \prod_{l2=4}^6 V_v(m_{l2}) V_v(m_{l3}) V_v^*(m_{l3}+1) V_v(m_{l4}+1) V_v^*(m_{l4}) \right\} \\
BB &= 6N_h^2 \sum_{m_1=0}^{M-1} \cdots \sum_{m_7=0}^{M-1} \sum_{m_8=1}^{M-2} \sum_{m_9=0}^{M-2} \cdots \sum_{m_{14}=0}^{M-2} E \left\{ \prod_{l1=1}^3 V_h(m_{l1}) \prod_{l2=4}^7 V_h^*(m_{l2}) \right. \\
&\quad \left. V_h(m_8-1) V_h(m_9) V_h^*(m_9+1) \prod_{l4=10}^{12} V_h(m_{l4}+1) V_h^*(m_{l4}) \right\} E \left\{ V_v^*(m_8+1) \right. \\
&\quad \left. \prod_{l1=1}^3 V_v^*(m_{l1}) \prod_{l2=4}^7 V_v(m_{l2}) V_v(m_{l3}) V_v^*(m_{l3}+1) V_v(m_{l4}+1) V_v^*(m_{l4}) \right\} \\
BC &= 9N_h^2 \sum_{m_1=0}^{M-1} \cdots \sum_{m_7=0}^{M-1} \sum_{m_8=0}^{M-2} \cdots \sum_{m_{14}=0}^{M-2} E \left\{ \prod_{l1=1}^3 V_h(m_{l1}) \prod_{l2=4}^7 V_h^*(m_{l2}) \right. \\
&\quad \left. \prod_{l3=8}^9 V_h(m_{l3}) V_h^*(m_{l3}+1) V_h(m_{10}+1) \prod_{l4=11}^{12} V_h(m_{l4}+1) V_h^*(m_{l4}) \right\} \\
&\quad E \left\{ V_v^*(m_{10}+1) \prod_{l1=1}^3 V_v^*(m_{l1}) \prod_{l2=4}^7 V_v(m_{l2}) V_v(m_{l3}) V_v^*(m_{l3}+1) V_v(m_{l4}+1) V_v^*(m_{l4}) \right\}
\end{aligned} \tag{I.44}$$

$$\begin{aligned}
CA &= 12N_h^2 \sum_{m_1=0}^{M-1} \cdots \sum_{m_6=0}^{M-1} \sum_{m_7=0}^{M-2} \cdots \sum_{m_{14}=0}^{M-2} E \left\{ \prod_{l=1}^3 V_h(m_{l_1}) \prod_{l=2}^6 V_h^*(m_{l_2}) \prod_{l=3}^9 V_h(m_{l_3}) V_h^*(m_{l_3}+1) \right. \\
&\quad \left. \prod_{l=4}^{11} V_h(m_{l_4}+1) V_h^*(m_{l_4}) \right\} E \left\{ \prod_{l=1}^3 V_v^*(m_{l_1}) \right. \\
&\quad \left. \prod_{l=2}^6 V_v(m_{l_2}) V_v(m_{l_2}+1) V_v^*(m_{l_2}) V_v(m_{l_3}) V_v^*(m_{l_3}+1) V_v(m_{l_4}+1) V_v^*(m_{l_4}) \right\} \\
CB &= 9N_h^2 \sum_{m_1=0}^{M-1} \cdots \sum_{m_7=0}^{M-1} \sum_{m_8=0}^{M-2} \cdots \sum_{m_{14}=0}^{M-2} \\
&\quad E \left\{ \prod_{l=1}^3 V_h(m_{l_1}) \prod_{l=2}^7 V_h^*(m_{l_2}) V_h(m_8) \prod_{l=3}^{10} V_h(m_{l_3}) V_h^*(m_{l_3}+1) \prod_{l=4}^{12} V_h(m_{l_4}+1) V_h^*(m_{l_4}) \right\} \\
&\quad E \left\{ V_v^*(m_8) \prod_{l=1}^3 V_v^*(m_{l_1}) \prod_{l=2}^7 V_v(m_{l_2}) V_v(m_{l_3}) V_v^*(m_{l_3}+1) V_v(m_{l_4}+1) V_v^*(m_{l_4}) \right\} \\
CC &= 6N_h^2 \sum_{m_1=0}^{M-1} \cdots \sum_{m_7=0}^{M-1} \sum_{m_8=0}^{M-2} \cdots \sum_{m_{11}=0}^{M-3} \sum_{m_{12}=0}^{M-2} \cdots \sum_{m_{14}=0}^{M-2} E \left\{ \prod_{l=1}^3 V_h(m_{l_1}) \prod_{l=2}^7 V_h^*(m_{l_2}) \right. \\
&\quad \left. \prod_{l=3}^{10} V_h(m_{l_3}) V_h^*(m_{l_3}+1) V_h(m_{l_1}+2) V_h(m_{l_2}+1) V_h^*(m_{l_2}) \right\} \\
&\quad E \left\{ \prod_{l=1}^3 V_v^*(m_{l_1}) \prod_{l=2}^7 V_v(m_{l_2}) V_v^*(m_{l_1}) V_v(m_{l_3}) V_v^*(m_{l_3}+1) V_v(m_{l_4}+1) V_v^*(m_{l_4}) \right\}
\end{aligned} \tag{I.45}$$

If we examine the expressions we notice that $BA = CA$, $BB = CC$, and $BC = CB$, which implies $B = C$. Consequently,

$$M^8 (M-1)^8 E \left\{ \left| \hat{R}_{hv}(0) \right|^8 \left| \hat{R}_h(T) \right|^6 \left| \hat{R}_v(T) \right|^2 \right\} = A + 2B. \tag{I.46}$$

By way of computational approach we get:

$$\begin{aligned}
E \left\{ \left| \hat{R}_{hv}(0) \right|^8 \left| \hat{R}_h(T) \right|^6 \left| \hat{R}_v(T) \right|^2 \right\} &= \frac{144M^8 + 6192M^7 + 116064M^6 + 1212768M^5 +}{M^8} \\
&\quad \frac{7294608M^4 + 21851568M^3 + 5072256M^2 - 139192128M - 244726272}{(M-1)^8} N_h^{10} N_v^6,
\end{aligned} \tag{I.47}$$

$$\begin{aligned}
E \left\{ \left| \hat{R}_{hv}(0) \right|^8 \left| \hat{R}_h(T) \right|^2 \left| \hat{R}_v(T) \right|^6 \right\} &= \frac{144M^8 + 6192M^7 + 116064M^6 + 1212768M^5 +}{M^8} \\
&\quad \frac{7294608M^4 + 21851568M^3 + 5072256M^2 - 139192128M - 244726272}{(M-1)^8} N_h^6 N_v^{10}.
\end{aligned} \tag{I.48}$$

Similarly:

$$E \left\{ \left| \hat{R}_{hv}(0) \right|^8 \left| \hat{R}_h(T) \right|^4 \left| \hat{R}_v(T) \right|^4 \right\} = \frac{96M^8 + 3840M^7 + 69120M^6 + 707520M^5 + 4215456M^4 + 12624192M^3 + 3521280M^2 - 77266944M - 13629344}{(M-1)^8} N_h^8 N_v^8, \quad (\text{I.49})$$

$$E \left\{ \left| \hat{R}_{hv}(0) \right|^8 \left| \hat{R}_h(T) \right|^2 \hat{R}_h^3(T) \left(\hat{R}_v^*(T) \right)^3 \right\} = \frac{69120M^5 + 1520640M^4 + 10824192M^3 + 18220032M^2 - 81727488M - 241532928}{(M-1)^8} N_h^9 N_v^7, \quad (\text{I.50})$$

$$E \left\{ \left| \hat{R}_{hv}(0) \right|^8 \left| \hat{R}_h(T) \right|^4 \hat{R}_h^2(T) \left(\hat{R}_v^*(T) \right)^2 \right\} = \frac{11520M^6 + 357120M^5 + 4103424M^4 + 19825920M^3 + 19883520M^2 - 132433920M - 306561024}{(M-1)^8} N_h^{10} N_v^6, \quad (\text{I.51})$$

$$E \left\{ \left| \hat{R}_{hv}(0) \right|^8 \left| \hat{R}_h(T) \right|^2 \hat{R}_h^2(T) \left| \hat{R}_v(T) \right|^2 \left(\hat{R}_v^*(T) \right)^2 \right\} = \frac{8640M^6 + 241920M^5 + 2567808M^4 + 11632896M^3 + 10342080M^2 - 76902912M - 170843904}{(M-1)^8} N_h^8 N_v^8, \quad (\text{I.52})$$

$$E \left\{ \left| \hat{R}_{hv}(0) \right|^8 \left| \hat{R}_h(T) \right|^4 \hat{R}_h(T) \left| \hat{R}_v(T) \right|^2 \hat{R}_v^*(T) \right\} = \frac{1152M^7 + 40320M^6 + 579456M^5 + 4217472M^4 + 14496768M^3 + 6773760M^2 - 89588736M - 168763392}{(M-1)^8} N_h^9 N_v^7, \quad (\text{I.53})$$

$$E \left\{ \left| \hat{R}_{hv}(0) \right|^8 \hat{R}_h^4(T) \left(\hat{R}_v^*(T) \right)^4 \right\} = \frac{483840M^4 + 6773760M^3 + 20418048M^2 - 60189696M - 260112384}{M^8 (M-1)^8} N_h^8 N_v^8. \quad (\text{I.54})$$

Using we (I.18) get:

$$E \left\{ \left| \hat{R}_{hv}(0) \right|^8 \left| \hat{R}_h(T) \right|^6 \hat{R}_h(T) \hat{R}_v^*(T) \right\} = 16 * 6 \frac{(M+8)(M+9)(M+10)}{M^8} \frac{24M^4 + 336M^3 + 1128M^2 - 1488M - 8064}{(M-1)^8} (N_h^{11} N_v^5 + N_h^5 N_v^{11}). \quad (\text{I.55})$$

Finally:

$$\begin{aligned}
& E \left\{ \left| \hat{R}_{hv}(0) \right|^8 \left| \hat{R}_h(T) + \hat{R}_v(T) \right|^8 \right\} = E \left\{ \left| \hat{R}_{hv}(0) \right|^8 \left(\hat{R}_h(T) + \hat{R}_v(T) \right)^4 \left(\hat{R}_h^*(T) + \hat{R}_v^*(T) \right)^4 \right\} \\
& = 24 \frac{\prod_{i=8}^{11} (M+i)}{M^8} \frac{24M^4 + 336M^3 + 1128M^2 - 1488M - 8064}{(M-1)^8} (N_h^{12} N_v^4 + N_h^4 N_v^{12}) + \\
& 8 * 96 \frac{\prod_{i=8}^{10} (M+i)}{M^8} \frac{24M^4 + 336M^3 + 1128M^2 - 1488M - 8064}{(M-1)^8} (N_h^{11} N_v^5 + N_h^5 N_v^{11}) + \\
& \frac{2304M^8 + 99072M^7 + 1995264M^6 + 23689728M^5 + 165954816M^4 +}{M^8} \\
& \frac{587536128M^3 + 319758336M^2 - 3816281088M - 759435264}{(M-1)^8} (N_h^{10} N_v^6 + N_h^6 N_v^{10}) + \\
& \frac{55296M^7 + 1935360M^6 + 28366848M^5 + 214603776M^4 + 782438400M^3 +}{M^8} \\
& \frac{470900736M^2 - 4954079232M - 10032906240}{(M-1)^8} (N_h^9 N_v^7 + N_h^7 N_v^9) + \\
& \frac{3456M^8 + 138240M^7 + 2764800M^6 + 33212160M^5 + 234893952M^4 +}{M^8} \\
& \frac{840271104M^3 + 498548736M^2 - 5362882560M - 6477886080}{(M-1)^8} N_h^8 N_v^8.
\end{aligned} \tag{I.56}$$

Appendix J

Evaluation of Noise Moments for $\hat{P}_h^{nh} \hat{P}_v^{nv} \left| \hat{R}_h(T) + \hat{R}_v(T) \right|^n \left| \hat{R}_{hv}(0) \right|^n$

We start by finding:

$$\begin{aligned}
 M^{2k} E \left\{ \hat{P}_h^{nh} \left| \hat{R}_{hv}(0) \right|^{2k} \left| \hat{R}_h(T) \right|^{2n} \right\} &= \sum_{m_1=0}^{M-1} \cdots \sum_{m_{2k}=0}^{M-1} E \left\{ \hat{P}_h^{nh} \prod_{l=nh+1}^{nh+k} V_v(m_{l1}) V_h^*(m_{l1}) \right. \\
 &\quad \left. \prod_{l2=nh+k+1}^{nh+2k} V_h(m_{l2}) V_v^*(m_{l2}) \left| \hat{R}_h(T) \right|^{2n} \right\} \\
 &= \sum_{m_1=0}^{M-1} \cdots \sum_{m_{2k}=0}^{M-1} E \left\{ \hat{P}_h^{nh} \prod_{l1=nh+1}^{nh+k} V_h(m_{k+l1}) V_h^*(m_{l1}) \left| \hat{R}_h(T) \right|^{2n} \right\} \\
 &\quad E \left\{ \prod_{l2=nh+1}^{nh+k} V_v(m_{l2}) V_v^*(m_{k+l2}) \right\}.
 \end{aligned} \tag{J.1}$$

Let us consider case when $k = 2$:

$$\begin{aligned}
 M^{2k} E \left\{ \hat{P}_h^{nh} \left| \hat{R}_{hv}(0) \right|^4 \left| \hat{R}_h(T) \right|^{2n} \right\} &= \sum_{m_1=0}^{M-1} \cdots \sum_{m_4=0}^{M-1} E \left\{ \hat{P}_h^{nh} V_h(m_3) V_h^*(m_1) V_h(m_4) \right. \\
 &\quad \left. V_h^*(m_2) \left| \hat{R}_h(T) \right|^{2n} \right\} E \left\{ V_v(m_1) V_v^*(m_3) V_v(m_2) V_v^*(m_4) \right\} \\
 &= \sum_{m_1=0}^{M-1} \cdots \sum_{m_4=0}^{M-1} E \left\{ \hat{P}_h^{nh} V_h(m_3) V_h^*(m_1) V_h(m_4) V_h^*(m_2) \left| \hat{R}_h(T) \right|^{2n} \right\} \\
 &\quad \left[E \left\{ V_v(m_1) V_v^*(m_3) \right\} E \left\{ V_v(m_2) V_v^*(m_4) \right\} + E \left\{ V_v(m_1) V_v^*(m_4) \right\} E \left\{ V_v(m_2) V_v^*(m_3) \right\} \right] \\
 &= 2! N_v^2 E \left\{ \hat{P}_h^{nh+2} \left| \hat{R}_h(T) \right|^{2n} \right\}.
 \end{aligned} \tag{J.2}$$

In general:

$$\begin{aligned}
 M^{2k} E \left\{ \hat{P}_h^{nh} \left| \hat{R}_{hv}(0) \right|^{2k} \left| \hat{R}_h(T) \right|^{2n} \right\} &= \sum_{m_1=0}^{M-1} \cdots \sum_{m_{2k}=0}^{M-1} E \left\{ \hat{P}_h^{nh} \prod_{l1=1}^k V_h(m_{k+l1}) V_h^*(m_{l1}) \left| \hat{R}_h(T) \right|^{2n} \right\} \\
 &\quad \sum_{\text{Perm}\{n_1, \dots, n_k\}}^{\{k+1, \dots, 2k\}} E \left\{ \prod_{l2=1}^k V_v(m_{l2}) V_v^*(m_{n_{l2}}) \right\} \\
 &= k! N_v^k \sum_{m_1=0}^{M-1} \cdots \sum_{m_k=0}^{M-1} E \left\{ \hat{P}_h^{nh} \prod_{l1=1}^k V_h(m_{l1}) V_h^*(m_{l1}) \left| \hat{R}_h(T) \right|^{2n} \right\} \\
 &= k! N_v^k M^k E \left\{ \hat{P}_h^{nh+k} \left| \hat{R}_h(T) \right|^{2n} \right\}.
 \end{aligned} \tag{J.3}$$

Thus:

$$E \left\{ \hat{P}_h^{nh} \left| \hat{R}_{hv}(0) \right|^{2k} \left| \hat{R}_h(T) \right|^{2n} \right\} = k! \frac{(M+2n) \cdots (M+nh+k-1+2n)}{M^{2k}} E \left\{ \left| \hat{R}(T) \right|^{2n} \right\} N_h^k N_v^k, \quad (\text{J.4})$$

$$\begin{aligned} M^{nv+2k} E \left\{ \hat{P}_h^{nh} \hat{P}_v^{nv} \left| \hat{R}_{hv}(0) \right|^{2k} \left| \hat{R}_h(T) \right|^{2n} \right\} &= \sum_{m_1=0}^{M-1} \cdots \sum_{m_{nv+2k}=0}^{M-1} E \left\{ \hat{P}_h^{nh} \prod_{l=1}^{n_v} V_v(m_{l1}) V_v^*(m_{l1}) \right. \\ &\quad \left. \prod_{l_2=nv+1}^{nv+k} V_v(m_{l_2}) V_v^*(m_{l_2}) \prod_{l_3=nv+k+1}^{nv+2k} V_h(m_{l_3}) V_v^*(m_{l_3}) \left| \hat{R}_h(T) \right|^{2n} \right\} \\ &= \sum_{m_1=0}^{M-1} \cdots \sum_{m_{nv+2k}=0}^{M-1} E \left\{ \hat{P}_h^{nh} \prod_{l_1=nv+1}^{nv+k} V_h(m_{k+l_1}) V_h^*(m_{l_1}) \left| \hat{R}_h(T) \right|^{2n} \right\} \\ &\quad E \left\{ \prod_{l_2=1}^{nv} V_v(m_{l_2}) V_v^*(m_{l_2}) \prod_{l_3=nv+1}^{nv+k} V_v(m_{l_3}) V_v^*(m_{k+l_3}) \right\}. \end{aligned} \quad (\text{J.5})$$

Let us consider case when $nv = 1$ and $k = 1$:

$$\begin{aligned} &M^3 E \left\{ \hat{P}_h^{nh} \hat{P}_v \left| \hat{R}_{hv}(0) \right|^2 \left| \hat{R}_h(T) \right|^{2n} \right\} \\ &= \sum_{m_1=0}^{M-1} \sum_{m_2=0}^{M-1} \sum_{m_3=0}^{M-1} E \left\{ \hat{P}_h^{nh} V_h(m_3) V_h^*(m_2) \left| \hat{R}_h(T) \right|^{2n} \right\} \\ &\quad E \left\{ V_v(m_1) V_v^*(m_1) V_v(m_2) V_v^*(m_3) \right\} \\ &= \sum_{m_1=0}^{M-1} \sum_{m_2=0}^{M-1} \sum_{m_3=0}^{M-1} E \left\{ \hat{P}_h^{nh} V_h(m_3) V_h^*(m_2) \left| \hat{R}_h(T) \right|^{2n} \right\} \\ &\quad \left[E \left\{ V_v(m_1) V_v^*(m_1) \right\} E \left\{ V_v(m_2) V_v^*(m_3) \right\} + E \left\{ V_v(m_1) V_v^*(m_3) \right\} E \left\{ V_v(m_2) V_v^*(m_1) \right\} \right] \\ &= MN_v^2 \sum_{m_2=0}^{M-1} E \left\{ \hat{P}_h^{nh} V_h(m_2) V_h^*(m_2) \left| \hat{R}_h(T) \right|^{2n} \right\} + N_v^2 \sum_{m_2=0}^{M-1} E \left\{ \hat{P}_h^{nh} V_h(m_2) V_h^*(m_2) \left| \hat{R}_h(T) \right|^{2n} \right\} \\ &= M(M+1) N_v^2 E \left\{ \hat{P}_h^{nh+1} \left| \hat{R}_h(T) \right|^{2n} \right\}. \end{aligned} \quad (\text{J.6})$$

Let us consider case when $nv = 1$ and $k = 2$:

$$\begin{aligned}
& M^5 E \left\{ \hat{P}_h^{nh} \hat{P}_v \left| \hat{R}_{hv}(0) \right|^4 \left| \hat{R}_h(T) \right|^{2n} \right\} = \\
& = \sum_{m_1=0}^{M-1} \cdots \sum_{m_5=0}^{M-1} E \left\{ \hat{P}_h^{nh} V_h(m_4) V_h^*(m_2) V_h(m_5) V_h^*(m_3) \left| \hat{R}_h(T) \right|^{2n} \right\} \\
& \quad E \left\{ V_v(m_1) V_v^*(m_1) V_v(m_2) V_v^*(m_4) V_v(m_3) V_v^*(m_5) \right\} \\
& = \sum_{m_1=0}^{M-1} \cdots \sum_{m_5=0}^{M-1} E \left\{ \hat{P}_h^{nh} V_h(m_4) V_h^*(m_2) V_h(m_5) V_h^*(m_3) \left| \hat{R}_h(T) \right|^{2n} \right\} \\
& \quad E \left\{ V_v(m_1) V_v^*(m_1) \right\} E \left\{ V_v(m_2) V_v^*(m_4) V_v(m_3) V_v^*(m_5) \right\} + \\
& \quad \sum_{m_1=0}^{M-1} \cdots \sum_{m_5=0}^{M-1} E \left\{ \hat{P}_h^{nh} V_h(m_4) V_h^*(m_2) V_h(m_5) V_h^*(m_3) \left| \hat{R}_h(T) \right|^{2n} \right\} \\
& \quad \left[E \left\{ V_v(m_1) V_v^*(m_4) \right\} E \left\{ V_v(m_2) V_v^*(m_1) V_v(m_3) V_v^*(m_5) \right\} \right. \\
& \quad \left. E \left\{ V_v(m_1) V_v^*(m_5) \right\} E \left\{ V_v(m_2) V_v^*(m_4) V_v(m_3) V_v^*(m_1) \right\} \right] \\
& = MN_v \sum_{m_2=0}^{M-1} \cdots \sum_{m_5=0}^{M-1} E \left\{ \hat{P}_h^{nh} V_h(m_4) V_h^*(m_2) V_h(m_5) V_h^*(m_3) \left| \hat{R}_h(T) \right|^{2n} \right\} \\
& \quad E \left\{ V_v(m_2) V_v^*(m_4) V_v(m_3) V_v^*(m_5) \right\} + \\
& \quad 2N_v \sum_{m_1=0}^{M-1} \cdots \sum_{m_4=0}^{M-1} E \left\{ \hat{P}_h^{nh} V_h(m_4) V_h^*(m_2) V_h(m_1) V_h^*(m_3) \left| \hat{R}_h(T) \right|^{2n} \right\} \\
& \quad E \left\{ V_v(m_2) V_v^*(m_4) V_v(m_3) V_v^*(m_1) \right\} \tag{J.7} \\
& = M^4 (M+2) N_v E \left\{ \hat{P}_h^{nh} \left| \hat{R}_{hv}(0) \right|^4 \left| \hat{R}_h(T) \right|^{2n} \right\} \\
& = 2! M^2 (M+2) N_v^3 E \left\{ \hat{P}_h^{nh+2} \left| \hat{R}_h(T) \right|^{2n} \right\}.
\end{aligned}$$

In general:

$$\begin{aligned}
& M^{nv+2k} E \left\{ \hat{P}_h^{nh} \hat{P}_v^{nv} \left| \hat{R}_{hv}(0) \right|^{2k} \left| \hat{R}_h(T) \right|^{2n} \right\} = \\
& = \sum_{m_1=0}^{M-1} \cdots \sum_{m_{nv+2k}=0}^{M-1} E \left\{ \hat{P}_h^{nh} \prod_{l_4=nv+1}^{nv+k} V_h^*(m_{l_4}) \prod_{l_5=nv+k+1}^{nv+2k} V_h(m_{l_5}) \left| \hat{R}_h(T) \right|^{2n} \right\} \\
& \quad E \left\{ \prod_{l_1=1}^{nv} V_v(m_{l_1}) V_v^*(m_{l_1}) \prod_{l_2=nv+1}^{nv+k} V_v(m_{l_2}) \prod_{l_3=nv+k+1}^{nv+2k} V_v^*(m_{l_3}) \right\} \tag{J.8} \\
& = \sum_{m_1=0}^{M-1} \cdots \sum_{m_{nv+2k}=0}^{M-1} E \left\{ \hat{P}_h^{nh} \prod_{l_4=nv+1}^{nv+k} V_h^*(m_{l_4}) \prod_{l_5=nv+k+1}^{nv+2k} V_h(m_{l_5}) \left| \hat{R}_h(T) \right|^{2n} \right\} \\
& \quad \sum_{\text{Perm}\{n_1, \dots, n_{nv+k}\}}^{\{m_1, \dots, m_{nv}, m_{nv+k+1}, \dots, m_{nv+2k}\}} \prod_{l_1=1}^{nv+k} C_{m_{l_1} n_{l_1}}^v \\
& = (A + B + C),
\end{aligned}$$

where:

$$\begin{aligned}
A &= \sum_{m_1=0}^{M-1} \cdots \sum_{m_{nv+2k}=0}^{M-1} E \left\{ \hat{P}_h^{nh} \prod_{l4=nv+1}^{nv+k} V_h^*(m_{l4}) \prod_{l5=nv+k+1}^{nv+2k} V_h(m_{l5}) \left| \hat{R}_h(T) \right|^{2n} \right\} \\
&\quad \sum_{\text{Perm}\{m_2, \dots, m_{nv}, m_{nv+k+1}, \dots, m_{nv+2k}\}} \prod_{l=1}^{nv+k} C_{m_l n_l} \\
&= \sum_{m_2=0}^{M-1} \cdots \sum_{m_{nv+2k}=0}^{M-1} E \left\{ \hat{P}_h^{nh} \prod_{l4=nv+1}^{nv+k} V_h^*(m_{l4}) \prod_{l5=nv+k+1}^{nv+2k} V_h(m_{l5}) \left| \hat{R}_h(T) \right|^{2n} \right\} \\
&\quad MN_v \sum_{\text{Perm}\{m_2, \dots, m_{nv}, m_{nv+k+1}, \dots, m_{nv+2k}\}} \prod_{l=1}^{nv+k} C_{m_l n_l} \\
&= MN_v M^{nv-1+2k} E \left\{ \hat{P}_h^{nh} \hat{P}_v^{nv-1} \left| \hat{R}_{hv}(0) \right|^{2k} \left| \hat{R}_h(T) \right|^{2n} \right\}
\end{aligned} \tag{J.9}$$

$$\begin{aligned}
B &= \sum_{m_1=0}^{M-1} \cdots \sum_{m_{nv+2k}=0}^{M-1} E \left\{ \hat{P}_h^{nh} \prod_{l4=nv+1}^{nv+k} V_h^*(m_{l4}) \prod_{l5=nv+k+1}^{nv+2k} V_h(m_{l5}) \left| \hat{R}_h(T) \right|^{2n} \right\} \\
&\quad \sum_{\text{Perm}\{m_2, \dots, m_{nv}, m_{nv+k+1}, \dots, m_{nv+2k}\}} C_{m_1 n_1} C_{m_2 n_2} \prod_{l=3}^{nv+k} C_{m_l n_l} + \sum_{\text{Perm}\{m_1, n_1, n_2, n_4, \dots, n_{nv+k}\}} C_{m_1 n_1} C_{m_2 n_2} C_{m_3 n_3} \prod_{l=3}^{nv+k} C_{m_l n_l} + \\
&\quad \dots + \sum_{\text{Perm}\{m_2, \dots, m_{nv}, m_{nv+k+1}, \dots, m_{nv+2k}\}} \prod_{l=1}^{nv+i-1} C_{m_l n_l} C_{m_i n_i} \prod_{l=nv+i+1}^{nv+k} C_{m_l n_l} + \dots \\
&\quad \sum_{\text{Perm}\{m_2, \dots, m_{nv}, m_{nv+k+1}, \dots, m_{nv+2k}\}} C_{m_{nv} n_{nv}} \prod_{l=1}^{nv-1} C_{m_l n_l} \prod_{l=nv+1}^{nv+k} C_{m_l n_l}
\end{aligned} \tag{J.10}$$

Let us calculate the general term in B:

$$\begin{aligned}
\frac{B}{nv-1} &= \sum_{m_1=0}^{M-1} \cdots \sum_{m_{nv+2k}=0}^{M-1} E \left\{ \hat{P}_h^{nh} \prod_{l4=nv+1}^{nv+k} V_h^*(m_{l4}) \prod_{l5=nv+k+1}^{nv+2k} V_h(m_{l5}) \left| \hat{R}_h(T) \right|^{2n} \right\} \\
&\quad \sum_{\text{Perm}\{m_2, \dots, m_{nv}, m_{nv+k+1}, \dots, m_{nv+2k}\}} \prod_{l=1}^{nv+i-1} C_{m_l n_l} C_{m_i n_i} \prod_{l=nv+i+1}^{nv+k} C_{m_l n_l} \\
&= \sum_{m_2=0}^{M-1} \cdots \sum_{m_{nv+2k}=0}^{M-1} E \left\{ \hat{P}_h^{nh} \prod_{l4=nv+1}^{nv+k} V_h^*(m_{l4}) \prod_{l5=nv+k+1}^{nv+2k} V_h(m_{l5}) \left| \hat{R}_h(T) \right|^{2n} \right\} \\
&\quad N_v \sum_{\text{Perm}\{m_2, \dots, m_{nv}, m_{nv+k+1}, \dots, m_{nv+2k}\}} \prod_{l=1}^{nv+i-1} C_{m_l n_l} \prod_{l=nv+i+1}^{nv+k} C_{m_l n_l} \\
&= N_v M^{nv-1+2k} E \left\{ \hat{P}_h^{nh} \hat{P}_v^{nv-1} \left| \hat{R}_{hv}(0) \right|^{2k} \left| \hat{R}_h(T) \right|^{2n} \right\}
\end{aligned} \tag{J.11}$$

$$\begin{aligned}
C &= \sum_{m_1=0}^{M-1} \cdots \sum_{m_{nv+2k}=0}^{M-1} E \left\{ \hat{P}_h^{nh} \prod_{l4=nv+1}^{nv+k} V_h^*(m_{l4}) \prod_{l5=nv+k+1}^{nv+2k} V_h(m_{l5}) \left| \hat{R}_h(T) \right|^{2n} \right\} \\
&\quad \sum_{\{m_2, \dots, m_{nv}, m_{nv+k+1}, \dots, m_{nv+2k}\}} \prod_{l1=1}^{nv} C_{m_{l1}n_{l1}} C_{m_{(nv+1)}m_1} \prod_{l1=nv+2}^{nv+k} C_{m_{l1}n_{l1}} + \\
&\quad \text{Perm}\{n_1, \dots, n_{nv}, n_{nv+2}, \dots, n_{nv+k}\} \\
&\quad \sum_{\{m_2, \dots, m_{nv}, m_{nv+k+1}, \dots, m_{nv+2k}\}} \prod_{l1=1}^{nv+1} C_{m_{l1}n_{l1}} C_{m_{(nv+2)}m_1} \prod_{l1=nv+3}^{nv+k} C_{m_{l1}n_{l1}} + \\
&\quad \text{Perm}\{n_1, \dots, n_{nv+1}, n_{nv+3}, \dots, n_{nv+k}\} \\
&\quad \dots + \sum_{\{m_2, \dots, m_{nv}, m_{nv+k+1}, \dots, m_{nv+2k}\}} \prod_{l1=1}^{nv+i-1} C_{m_{l1}n_{l1}} C_{m_i m_1} \prod_{l1=nv+i+1}^{nv+k} C_{m_{l1}n_{l1}} + \dots \\
&\quad \sum_{\{m_2, \dots, m_{nv+2k}\}} C_{m_{nv+k}m_1} \prod_{l1=1}^{nv+k-1} C_{m_{l1}n_{l1}} \\
&\quad \text{Perm}\{n_1, \dots, n_{nv+k-1}\}
\end{aligned} \tag{J.12}$$

Let us calculate the general term in C:

$$\begin{aligned}
\frac{C}{k} &= \sum_{m_1=0}^{M-1} \cdots \sum_{m_{nv+2k}=0}^{M-1} E \left\{ \hat{P}_h^{nh} \prod_{l4=nv+1}^{nv+k} V_h^*(m_{l4}) \prod_{l5=nv+k+1}^{nv+2k} V_h(m_{l5}) \left| \hat{R}_h(T) \right|^{2n} \right\} \\
&\quad \sum_{\{m_2, \dots, m_{nv}, m_{nv+k+1}, \dots, m_{nv+2k}\}} \prod_{l1=1}^{nv+i-1} C_{m_{l1}n_{l1}} C_{m_i m_1} \prod_{l1=nv+i+1}^{nv+k} C_{m_{l1}n_{l1}} \\
&\quad \text{Perm}\{n_1, \dots, n_{i-1}, n_{i+1}, \dots, n_k\} \\
&= N_v \sum_{m_2=0}^{M-1} \cdots \sum_{m_{nv+2k}=0}^{M-1} E \left\{ \hat{P}_h^{nh} \prod_{l4=nv+1}^{nv+k} V_h^*(m_{l4}) \prod_{l5=nv+k+1}^{nv+2k} V_h(m_{l5}) \left| \hat{R}_h(T) \right|^{2n} \right\} \\
&\quad \sum_{\{m_2, \dots, m_{nv}, m_{nv+k+1}, \dots, m_{nv+2k}\}} \prod_{l1=1}^{nv+i-1} C_{m_{l1}n_{l1}} \prod_{l1=nv+i+1}^{nv+k} C_{m_{l1}n_{l1}} \\
&\quad \text{Perm}\{n_1, \dots, n_{i-1}, n_{i+1}, \dots, n_k\} \\
&= N_v M^{nv-1+2k} E \left\{ \hat{P}_h^{nh} \hat{P}_v^{nv-1} \left| \hat{R}_{hv}(0) \right|^{2k} \left| \hat{R}_h(T) \right|^{2n} \right\}.
\end{aligned} \tag{J.13}$$

Now we can establish the following:

$$\begin{aligned}
E \left\{ \hat{P}_h^{nh} \hat{P}_v^{nv} \left| \hat{R}_{hv}(0) \right|^{2k} \left| \hat{R}_h(T) \right|^{2n} \right\} &= \frac{(M + nv - 1 + k)}{M} N_v E \left\{ \hat{P}_h^{nh} \hat{P}_v^{nv-1} \left| \hat{R}_{hv}(0) \right|^{2k} \left| \hat{R}_h(T) \right|^{2n} \right\} \\
&= \frac{(M + nv - 1 + k) \cdots (M + nv - 1)}{M^{nv}} N_v^{nv} E \left\{ \hat{P}_h^{nh} \left| \hat{R}_{hv}(0) \right|^{2k} \left| \hat{R}_h(T) \right|^{2n} \right\} \\
&= k! \frac{(M + nv - 1 + k) \cdots (M + nv - 1)}{M^{nv+k}} N_v^{nv+k} E \left\{ \hat{P}_h^{nh+k} \left| \hat{R}_h(T) \right|^{2n} \right\}.
\end{aligned} \tag{J.14}$$

Next we find the following:

$$\begin{aligned}
& M^{nh+2k+2n} E \left\{ \hat{P}_h^{nh} \left| \hat{R}_{hv}(0) \right|^{2k} \left| \hat{R}_h(T) \right|^{2n} \left| \hat{R}_v(T) \right|^{2l} \right\} = \\
& \sum_{m_1=0}^{M-1} \cdots \sum_{m_{nh}=0}^{M-1} \sum_{m_{nh+1}=0}^{M-2} \cdots \sum_{m_{nh+2n}=0}^{M-2} \sum_{m_{nh+2n+1}=0}^{M-1} \cdots \sum_{m_{nh+2n+2k}=0}^{M-1} E \left\{ \prod_{l=1}^{nh} V_h(m_{l1}) V_h^*(m_{l1}) \right. \\
& \quad \prod_{l2=nh+1}^{nh+n} V_h(m_{l2}+1) V_h^*(m_{l2}) \prod_{l3=nh+n+1}^{nh+2n} V_h(m_{l3}) V_h^*(m_{l3}+1) \\
& \quad \left. \prod_{l4=nh+2n+1}^{nh+2n} V_h(m_{l4}) V_v^*(m_{l4}) \prod_{l5=nh+2n+k+1}^{nh+2n+2k} V_v(m_{l5}) V_h^*(m_{l5}) \left| \hat{R}_v(T) \right|^{2l} \right\} \\
& = \sum_{m_1=0}^{M-1} \cdots \sum_{m_{nh}=0}^{M-1} \sum_{m_{nh+1}=0}^{M-2} \cdots \sum_{m_{nh+2n}=0}^{M-2} \sum_{m_{nh+2n+1}=0}^{M-1} \cdots \sum_{m_{nh+2n+2k}=0}^{M-1} E \left\{ \prod_{l4=nh+2n+1}^{nh+2n+k} V_v^*(m_{l3}) \right. \\
& \quad \left. \prod_{l5=nh+k+1}^{nh+2n+2k} V_v(m_{l5}) \left| \hat{R}_v(T) \right|^{2l} \right\} E \left\{ \prod_{l1=1}^{nh} V_h(m_{l1}) V_h^*(m_{l1}) \prod_{l2=nh+1}^{nh+n} V_h(m_{l2}+1) V_h^*(m_{l2}) \right. \\
& \quad \left. \prod_{l3=nh+n+1}^{nh+2n} V_h(m_{l3}) V_h^*(m_{l3}+1) \prod_{l4=nh+2n+1}^{nh+2n+k} V_h(m_{l4}) \prod_{l5=nh+2n+k+1}^{nh+2n+2k} V_h^*(m_{l5}) \right\} \\
& = A + B + C + D, \tag{J.15}
\end{aligned}$$

where:

$$\begin{aligned}
A & = \sum_{m_1=0}^{M-1} \cdots \sum_{m_{nh}=0}^{M-1} \sum_{m_{nh+1}=0}^{M-2} \cdots \sum_{m_{nh+2n}=0}^{M-2} \sum_{m_{nh+2n+1}=0}^{M-1} \cdots \sum_{m_{nh+2n+2k}=0}^{M-1} E \left\{ \prod_{l4=nh+2n+1}^{nh+2n+k} V_v^*(m_{l3}) \right. \\
& \quad \left. \prod_{l5=nh+k+1}^{nh+2n+2k} V_v(m_{l5}) \left| \hat{R}_v(T) \right|^{2l} \right\} E \left\{ V_h(m_1) V_h^*(m_1) \right\} E \left\{ \prod_{l1=2}^{nh} V_h(m_{l1}) V_h^*(m_{l1}) \right. \\
& \quad \prod_{l2=nh+1}^{nh+n} V_h(m_{l2}+1) V_h^*(m_{l2}) \prod_{l3=nh+n+1}^{nh+2n} V_h(m_{l3}) V_h^*(m_{l3}+1) \\
& \quad \left. \prod_{l4=nh+2n+1}^{nh+2n+k} V_h(m_{l4}) \prod_{l5=nh+2n+k+1}^{nh+2n+2k} V_h^*(m_{l5}) \right\} \\
& = MN_h M^{nh-1+2k+2n} E \left\{ \hat{P}_h^{nh-1} \left| \hat{R}_{hv}(0) \right|^{2k} \left| \hat{R}_h(T) \right|^{2n} \left| \hat{R}_v(T) \right|^{2l} \right\}. \tag{J.16}
\end{aligned}$$

$$\begin{aligned}
B &= \sum_{m_1=0}^{M-1} \cdots \sum_{m_{nh}=0}^{M-1} \sum_{m_{nh+1}=0}^{M-2} \cdots \sum_{m_{nh+2n}=0}^{M-2} \sum_{m_{nh+2n+1}=0}^{M-1} \cdots \sum_{m_{nh+2n+2k}=0}^{M-1} \\
&E \left\{ \prod_{l4=nh+2n+1}^{nh+2n+k} V_v^*(m_{l3}) \prod_{l5=nh+k+1}^{nh+2n+2k} V_v(m_{l5}) \left| \hat{R}_v(T) \right|^{2l} \right\} \\
&\left[\sum_{\text{Perm}\{n_1, n_3, \dots, n_{nh+2n+k}\}}^{\{m_2, \dots, m_{nh+n}, m_{nh+n+1}+1, \dots, m_{nh+2n}+1, m_{nh+2n+k+1}, \dots, m_{nh+n+2k}\}} C_{m_1 n_1}^h C_{m_2 m_1}^h \prod_{l1=3}^{nh} C_{m_{l1} n_{l1}}^h \prod_{l2=nh+1}^{nh+n} C_{(m_{l2}+1) n_{l2}}^h \right. \\
&\prod_{l3=nh+n+1}^{nh+2n} C_{m_{l3} n_{l3}}^h \prod_{l4=nh+2n+1}^{nh+2n+k} C_{m_{l4} n_{l4}}^h + \dots \\
&\sum_{\text{Perm}\{n_1, \dots, n_{i-1}, n_{i+1}, \dots, n_{nh+2n+k}\}}^{\{m_2, \dots, m_{nh+n}, m_{nh+n+1}+1, \dots, m_{nh+2n}+1, m_{nh+2n+k+1}, \dots, m_{nh+n+2k}\}} \prod_{l1=1}^{nh+i-1} C_{m_{l1} n_{l1}}^h C_{m_i m_1}^h \prod_{l1=nh+i+1}^{nh} C_{m_{l1} n_{l1}}^h \prod_{l2=nh+1}^{nh+n} C_{(m_{l2}+1) n_{l2}}^h \\
&\prod_{l3=nh+n+1}^{nh+2n} C_{m_{l3} n_{l3}}^h \prod_{l4=nh+2n+1}^{nh+2n+k} C_{m_{l4} n_{l4}}^h + \dots \\
&\sum_{\text{Perm}\{n_1, \dots, n_{nh-1}, n_{nh+1}, \dots, n_{nh+2n+k}\}}^{\{m_2, \dots, m_{nh+n}, m_{nh+n+1}+1, \dots, m_{nh+2n}+1, m_{nh+2n+k+1}, \dots, m_{nh+n+2k}\}} \prod_{l1=1}^{nh-1} C_{m_{l1} n_{l1}}^h C_{m_{nh} m_1}^h \prod_{l2=nh+1}^{nh+n} C_{(m_{l2}+1) n_{l2}}^h \\
&\left. \prod_{l3=nh+n+1}^{nh+2n} C_{m_{l3} n_{l3}}^h \prod_{l4=nh+2n+1}^{nh+2n+k} C_{m_{l4} n_{l4}}^h \right]. \tag{J.17}
\end{aligned}$$

Let us calculate the general term in B:

$$\begin{aligned}
\frac{B}{nh-1} &= \sum_{m_1=0}^{M-1} \cdots \sum_{m_{nh}=0}^{M-1} \sum_{m_{nh+1}=0}^{M-2} \cdots \sum_{m_{nh+2n}=0}^{M-2} \sum_{m_{nh+2n+1}=0}^{M-1} \cdots \sum_{m_{nh+2n+2k}=0}^{M-1} \\
&E \left\{ \prod_{l4=nh+2n+1}^{nh+2n+k} V_v^*(m_{l3}) \prod_{l5=nh+k+1}^{nh+2n+2k} V_v(m_{l5}) \left| \hat{R}_v(T) \right|^{2l} \right\} \\
&\sum_{\{m_2, \dots, m_{nh+n}, m_{nh+n+1}+1, \dots, m_{nh+2n}+1, m_{nh+2n+k+1}, \dots, m_{nh+n+2k}\}} \prod_{l1=1}^{nh+i-1} C_{m_{l1}n_{l1}}^h C_{m_i m_i}^h \prod_{l1=nh+i+1}^{nh} C_{m_{l1}n_{l1}}^h \prod_{l2=nh+1}^{nh+n} C_{(m_{l2}+1)n_{l2}}^h \\
&\prod_{l3=nh+n+1}^{nh+2n} C_{m_{l3}n_{l3}}^h \prod_{l4=nh+2n+1}^{nh+2n+k} C_{m_{l4}n_{l4}}^h \\
&= N_h \sum_{m_2=0}^{M-1} \cdots \sum_{m_{nh}=0}^{M-1} \sum_{m_{nh+1}=0}^{M-2} \cdots \sum_{m_{nh+2n}=0}^{M-2} \sum_{m_{nh+2n+1}=0}^{M-1} \cdots \sum_{m_{nh+2n+2k}=0}^{M-1} \\
&E \left\{ \prod_{l4=nh+2n+1}^{nh+2n+k} V_v^*(m_{l3}) \prod_{l5=nh+k+1}^{nh+2n+2k} V_v(m_{l5}) \left| \hat{R}_v(T) \right|^{2l} \right\} \\
&\sum_{\{m_2, \dots, m_{nh+n}, m_{nh+n+1}+1, \dots, m_{nh+2n}+1, m_{nh+2n+k+1}, \dots, m_{nh+n+2k}\}} \prod_{l1=2}^{nh+i-1} C_{m_{l1}n_{l1}}^h C_{m_i n_{l1}}^h \prod_{l1=nh+i+1}^{nh} C_{m_{l1}n_{l1}}^h \prod_{l2=nh+1}^{nh+n} C_{(m_{l2}+1)n_{l2}}^h \\
&\prod_{l3=nh+n+1}^{nh+2n} C_{m_{l3}n_{l3}}^h \prod_{l4=nh+2n+1}^{nh+2n+k} C_{m_{l4}n_{l4}}^h \\
&= N_h M^{nh-1+2k+2n} E \left\{ \hat{P}_h^{nh-1} \left| \hat{R}_{hv}(0) \right|^{2k} \left| \hat{R}_h(T) \right|^{2n} \left| \hat{R}_v(T) \right|^{2l} \right\}.
\end{aligned} \tag{J.18}$$

$$\begin{aligned}
C &= \sum_{m_1=0}^{M-1} \cdots \sum_{m_{nh}=0}^{M-1} \sum_{m_{nh+1}=0}^{M-2} \cdots \sum_{m_{nh+2n}=0}^{M-2} \sum_{m_{nh+2n+1}=0}^{M-1} \cdots \sum_{m_{nh+2n+2k}=0}^{M-1} E \left\{ \prod_{l4=nh+2n+1}^{nh+2n+k} V_v^*(m_{l3}) \right. \\
&\quad \left. \prod_{l5=nh+k+1}^{nh+2n+2k} V_v(m_{l5}) \left| \hat{R}_v(T) \right|^{2l} \right\} E \left\{ \prod_{l1=1}^{nh} V_h(m_{l1}) V_h^*(m_{l1}) \prod_{l2=nh+1}^{nh+n} V_h(m_{l2}+1) V_h^*(m_{l2}) \right. \\
&\quad \left. \prod_{l3=nh+n+1}^{nh+2n} V_h(m_{l3}) V_h^*(m_{l3}+1) \prod_{l4=nh+2n+1}^{nh+2n+k} V_h(m_{l4}) \prod_{l5=nh+2n+k+1}^{nh+2n+2k} V_h^*(m_{l5}) \right\} \\
&\quad \left[\sum_{\text{Perm}\{n_1, \dots, n_{nh}, n_{nh+2}, \dots, n_{nh+2n+k}\}} \left\{ m_2, \dots, m_{nh+n}, m_{nh+n+1}+1, \dots, m_{nh+2n}+1, m_{nh+2n+k+1}, \dots, m_{nh+n+2k} \right\} \prod_{l1=1}^{nh} C_{m_{l1}n_{l1}}^h C_{(m_{nh+1})m_1}^h \prod_{l2=nh+2}^{nh+n} C_{(m_{l2}+1)n_{l2}}^h \right. \\
&\quad \prod_{l3=nh+n+1}^{nh+2n} C_{m_{l3}n_{l3}}^h \prod_{l4=nh+2n+1}^{nh+2n+k} C_{m_{l4}n_{l4}}^h + \dots \\
&\quad \sum_{\text{Perm}\{n_1, \dots, n_{i-1}, n_{i+1}, \dots, n_{nh+2n+k}\}} \left\{ m_2, \dots, m_{nh+n}, m_{nh+n+1}+1, \dots, m_{nh+2n}+1, m_{nh+2n+k+1}, \dots, m_{nh+n+2k} \right\} \prod_{l1=1}^{nh} C_{m_{l1}n_{l1}}^h \prod_{l2=nh+1}^{nh+i-1} C_{(m_{l2}+1)n_{l2}}^h C_{(m_{nh+i}+1)m_1}^h \\
&\quad \prod_{l2=nh+i+1}^{nh+n} C_{(m_{l2}+1)n_{l2}}^h \prod_{l3=nh+n+1}^{nh+2n} C_{m_{l3}n_{l3}}^h \prod_{l4=nh+2n+1}^{nh+2n+k} C_{m_{l4}n_{l4}}^h + \dots \\
&\quad \sum_{\text{Perm}\{n_1, \dots, n_{nh+n-1}, n_{nh+n+1}, \dots, n_{nh+2n+k}\}} \left\{ m_2, \dots, m_{nh+n}, m_{nh+n+1}+1, \dots, m_{nh+2n}+1, m_{nh+2n+k+1}, \dots, m_{nh+n+2k} \right\} \prod_{l1=1}^{nh} C_{m_{l1}n_{l1}}^h \prod_{l2=nh+1}^{nh+n-1} C_{(m_{l2}+1)n_{l2}}^h C_{(m_{nh+n}+1)m_1}^h \\
&\quad \left. \prod_{l3=nh+n+1}^{nh+2n} C_{m_{l3}n_{l3}}^h \prod_{l4=nh+2n+1}^{nh+2n+k} C_{m_{l4}n_{l4}}^h \right] \\
&= M^{nh+2k+2n} E \left\{ \hat{P}_h^{nh} \left| \hat{R}_{hv}(0) \right|^{2k} \left| \hat{R}_h(T) \right|^{2n} \left| \hat{R}_v(T) \right|^{2l} \right\}.
\end{aligned} \tag{J.19}$$

Let us calculate the general term in C:

$$\begin{aligned}
\frac{C}{n} &= \sum_{m_1=0}^{M-1} \cdots \sum_{m_{nh}=0}^{M-1} \sum_{m_{nh+1}=0}^{M-2} \cdots \sum_{m_{nh+2n}=0}^{M-2} \sum_{m_{nh+2n+1}=0}^{M-1} \cdots \sum_{m_{nh+2n+2k}=0}^{M-1} E \left\{ \prod_{l_4=nh+2n+1}^{nh+2n+k} V_v^*(m_{l_3}) \prod_{l_5=nh+k+1}^{nh+2n+2k} V_v(m_{l_5}) \right. \\
&\quad \left. \left| \hat{R}_v(T) \right|^{2l} \right\} \sum_{\text{Perm}\{n_1, \dots, n_{l-1}, n_{l+1}, \dots, n_{nh+2n+k}\}} \prod_{l_1=1}^{nh} C_{m_{l_1} n_{l_1}}^h \prod_{l_2=nh+1}^{nh+i-1} C_{(m_{l_2+1}) n_{l_2}}^h C_{(m_{nh+i+1}) m_1}^h \\
&\quad \prod_{l_2=nh+i+1}^{nh+n} C_{(m_{l_2+1}) n_{l_2}}^h \prod_{l_3=nh+n+1}^{nh+2n} C_{m_{l_3} n_{l_3}}^h \prod_{l_4=nh+2n+1}^{nh+2n+k} C_{m_{l_4} n_{l_4}}^h \\
&= N_h \sum_{m_2=0}^{M-1} \cdots \sum_{m_{nh}=0}^{M-1} \sum_{m_{nh+1}=0}^{M-2} \cdots \sum_{m_{nh+2n}=0}^{M-2} \sum_{m_{nh+2n+1}=0}^{M-1} \cdots \sum_{m_{nh+2n+2k}=0}^{M-1} E \left\{ \prod_{l_4=nh+2n+1}^{nh+2n+k} V_v^*(m_{l_3}) \prod_{l_5=nh+k+1}^{nh+2n+2k} V_v(m_{l_5}) \right. \quad (J.20) \\
&\quad \left. \left| \hat{R}_v(T) \right|^{2l} \right\} \sum_{\text{Perm}\{n_1, \dots, n_{l-1}, n_{l+1}, \dots, n_{nh+2n+k}\}} \prod_{l_1=2}^{nh} C_{m_{l_1} n_{l_1}}^h \prod_{l_2=nh+1}^{nh+i-1} C_{(m_{l_2+1}) n_{l_2}}^h C_{(m_{l_2+i}) n_{l_1}}^h \\
&\quad \prod_{l_2=nh+i+1}^{nh+n} C_{(m_{l_2+1}) n_{l_2}}^h \prod_{l_3=nh+n+1}^{nh+2n} C_{m_{l_3} n_{l_3}}^h \prod_{l_4=nh+2n+1}^{nh+2n+k} C_{m_{l_4} n_{l_4}}^h \\
&= N_h M^{nh-1+2k+2n} E \left\{ \hat{P}_h^{nh-1} \left| \hat{R}_{hv}(0) \right|^{2k} \left| \hat{R}_h(T) \right|^{2n} \left| \hat{R}_v(T) \right|^{2l} \right\} \\
D &= \sum_{m_1=0}^{M-1} \cdots \sum_{m_{nh}=0}^{M-1} \sum_{m_{nh+1}=0}^{M-2} \cdots \sum_{m_{nh+2n}=0}^{M-2} \sum_{m_{nh+2n+1}=0}^{M-1} \cdots \sum_{m_{nh+2n+2k}=0}^{M-1} E \left\{ \prod_{l_4=nh+2n+1}^{nh+2n+k} V_v^*(m_{l_3}) \right. \\
&\quad \left. \prod_{l_5=nh+k+1}^{nh+2n+2k} V_v(m_{l_5}) \left| \hat{R}_v(T) \right|^{2l} \right\} E \left\{ \prod_{l_1=1}^{nh} V_h(m_{l_1}) V_h^*(m_{l_1}) \prod_{l_2=nh+1}^{nh+n} V_h(m_{l_2+1}) V_h^*(m_{l_2}) \right. \\
&\quad \left. \prod_{l_3=nh+n+1}^{nh+2n} V_h(m_{l_3}) V_h^*(m_{l_3+1}) \prod_{l_4=nh+2n+1}^{nh+2n+k} V_h(m_{l_4}) \prod_{l_5=nh+2n+k+1}^{nh+2n+2k} V_h^*(m_{l_5}) \right\} \\
&\quad \left[\sum_{\text{Perm}\{n_1, \dots, n_{nh}, n_{nh+2}, \dots, n_{nh+2n+k}\}} \prod_{l_1=1}^{nh} C_{m_{l_1} n_{l_1}}^h \prod_{l_2=nh+1}^{nh+n} C_{(m_{l_2+1}) n_{l_2}}^h \right. \\
&\quad C_{(m_{nh+n+1}) m_1}^h \prod_{l_3=nh+n+2}^{nh+2n} C_{m_{l_3} n_{l_3}}^h \prod_{l_4=nh+2n+1}^{nh+2n+k} C_{m_{l_4} n_{l_4}}^h + \dots \\
&\quad \left. \sum_{\text{Perm}\{n_1, \dots, n_{nh+n-1}, n_{nh+n+1}, \dots, n_{nh+2n+k}\}} \prod_{l_1=1}^{nh} C_{m_{l_1} n_{l_1}}^h \prod_{l_2=nh+1}^{nh+n} C_{(m_{l_2+1}) n_{l_2}}^h \right. \\
&\quad \prod_{l_3=nh+n+1}^{nh+n+i-1} C_{(m_{l_2+1}) n_{l_2}}^h C_{(m_{nh+n+i+1}) m_1}^h \prod_{l_3=nh+n+i-1}^{nh+2n} C_{m_{l_3} n_{l_3}}^h \prod_{l_4=nh+2n+1}^{nh+2n+k} C_{m_{l_4} n_{l_4}}^h + \dots \\
&\quad \left. \sum_{\text{Perm}\{n_1, \dots, n_{nh+2n-1}, n_{nh+2n+1}, \dots, n_{nh+2n+k}\}} \prod_{l_1=1}^{nh} C_{m_{l_1} n_{l_1}}^h \prod_{l_2=nh+1}^{nh+n} C_{(m_{l_2+1}) n_{l_2}}^h \right. \\
&\quad \left. \prod_{l_3=nh+n+1}^{nh+2n-1} C_{m_{l_3} n_{l_3}}^h C_{(m_{nh+2n+1}) m_1}^h \prod_{l_4=nh+2n+1}^{nh+2n+k} C_{m_{l_4} n_{l_4}}^h \right] \quad (J.21) \\
&= M^{nh+2k+2n} E \left\{ \hat{P}_h^{nh} \left| \hat{R}_{hv}(0) \right|^{2k} \left| \hat{R}_h(T) \right|^{2n} \left| \hat{R}_v(T) \right|^{2l} \right\}
\end{aligned}$$

Let us find general term in D:

$$\begin{aligned}
\frac{D}{n} &= \sum_{m_1=0}^{M-1} \cdots \sum_{m_{nh}=0}^{M-1} \sum_{m_{nh+1}=0}^{M-2} \cdots \sum_{m_{nh+2n}=0}^{M-2} \sum_{m_{nh+2n+1}=0}^{M-1} \cdots \sum_{m_{nh+2n+2k}=0}^{M-1} E \left\{ \prod_{l4=nh+2n+1}^{nh+2n+k} V_v^*(m_{l3}) \prod_{l5=nh+k+1}^{nh+2n+2k} V_v(m_{l5}) \right. \\
&\quad \left. \left| \hat{R}_v(T) \right|^{2l} \right\} \sum_{Perm\{n_1, \dots, n_{nh+n+i-1}, n_{nh+n+i+1}, \dots, n_{nh+2n+k}\}} \prod_{l1=1}^{nh} C_{m_{l1}n_{l1}}^h \prod_{l2=nh+1}^{nh} C_{(m_{l2}+1)n_{l2}}^h \\
&\quad \prod_{l3=nh+n+1}^{nh+n+i-1} C_{m_{l3}n_{l3}}^h C_{m_{nh+n+i}m_{l1}}^h \prod_{l3=nh+n+i-1}^{nh+2n} C_{m_{l3}n_{l3}}^h \prod_{l4=nh+2n+1}^{nh+2n+k} C_{m_{l4}n_{l4}}^h \\
&= N_h \sum_{m_2=0}^{M-1} \cdots \sum_{m_{nh}=0}^{M-1} \sum_{m_{nh+1}=0}^{M-2} \cdots \sum_{m_{nh+2n}=0}^{M-2} \sum_{m_{nh+2n+1}=0}^{M-1} \cdots \sum_{m_{nh+2n+2k}=0}^{M-1} E \left\{ \prod_{l4=nh+2n+1}^{nh+2n+k} V_v^*(m_{l3}) \prod_{l5=nh+k+1}^{nh+2n+2k} V_v(m_{l5}) \right. \quad (J.22) \\
&\quad \left. \left| \hat{R}_v(T) \right|^{2l} \right\} \sum_{Perm\{n_1, \dots, n_{nh+n+i-1}, n_{nh+n+i+1}, \dots, n_{nh+2n+k}\}} \prod_{l1=2}^{nh} C_{m_{l1}n_{l1}}^h \prod_{l2=nh+1}^{nh} C_{(m_{l2}+1)n_{l2}}^h \\
&\quad \prod_{l3=nh+n+1}^{nh+n+i-1} C_{m_{l3}n_{l3}}^h C_{m_{nh+n+i}n_{l1}}^h \prod_{l3=nh+n+i-1}^{nh+2n} C_{m_{l3}n_{l3}}^h \prod_{l4=nh+2n+1}^{nh+2n+k} C_{m_{l4}n_{l4}}^h \\
&= N_h M^{nh-1+2k+2n} E \left\{ \hat{P}_h^{nh-1} \left| \hat{R}_{hv}(0) \right|^{2k} \left| \hat{R}_h(T) \right|^{2n} \left| \hat{R}_v(T) \right|^{2l} \right\} \\
E &= \sum_{m_1=0}^{M-1} \cdots \sum_{m_{nh}=0}^{M-1} \sum_{m_{nh+1}=0}^{M-2} \cdots \sum_{m_{nh+2n}=0}^{M-2} \sum_{m_{nh+2n+1}=0}^{M-1} \cdots \sum_{m_{nh+2n+2k}=0}^{M-1} E \left\{ \prod_{l4=nh+2n+1}^{nh+2n+k} V_v^*(m_{l3}) \right. \\
&\quad \left. \prod_{l5=nh+k+1}^{nh+2n+2k} V_v(m_{l5}) \left| \hat{R}_v(T) \right|^{2l} \right\} \sum_{Perm\{n_1, \dots, n_{nh+2n}, n_{nh+2n+2}, \dots, n_{nh+2n+k}\}} \prod_{l1=1}^{nh} C_{m_{l1}n_{l1}}^h \\
&\quad \prod_{l2=nh+1}^{nh+n} C_{(m_{l2}+1)n_{l2}}^h \prod_{l3=nh+n+1}^{nh+2n} C_{m_{l3}n_{l3}}^h C_{(m_{nh+2n+1})m_{l1}}^h \prod_{l4=nh+2n+2}^{nh+2n+k} C_{m_{l4}n_{l4}}^h + \dots \\
&\quad \sum_{Perm\{n_1, \dots, n_{nh+2n+i-1}, n_{nh+2n+i+1}, \dots, n_{nh+2n+k}\}} \prod_{l1=1}^{nh} C_{m_{l1}n_{l1}}^h \prod_{l2=nh+1}^{nh} C_{(m_{l2}+1)n_{l2}}^h \\
&\quad \prod_{l3=nh+n+1}^{nh+n} C_{(m_{l2}+1)n_{l2}}^h \prod_{l4=nh+n+i-1}^{nh+2n+i-1} C_{m_{l3}n_{l3}}^h C_{(m_{nh+2n+i+1})m_{l1}}^h \prod_{l4=nh+2n+i-1}^{nh+2n+k} C_{m_{l4}n_{l4}}^h + \dots \\
&\quad \sum_{Perm\{n_1, \dots, n_{nh+2n+k-1}\}} \prod_{l1=1}^{nh} C_{m_{l1}n_{l1}}^h \prod_{l2=nh+1}^{nh+n} C_{(m_{l2}+1)n_{l2}}^h \\
&\quad \left. \prod_{l3=nh+n+1}^{nh+2n} C_{m_{l3}n_{l3}}^h \prod_{l4=nh+2n+1}^{nh+2n+k-1} C_{m_{l4}n_{l4}}^h C_{m_{nh+2n+k-1}m_{l1}}^h \right] \\
&= M^{nh+2k+2n} E \left\{ \hat{P}_h^{nh} \left| \hat{R}_{hv}(0) \right|^{2k} \left| \hat{R}_h(T) \right|^{2n} \left| \hat{R}_v(T) \right|^{2l} \right\} \quad (J.23)
\end{aligned}$$

Let us find general term in E:

$$\begin{aligned}
\frac{E}{k} &= \sum_{m_1=0}^{M-1} \cdots \sum_{m_{nh}=0}^{M-1} \sum_{m_{nh+1}=0}^{M-2} \cdots \sum_{m_{nh+2n}=0}^{M-2} \sum_{m_{nh+2n+1}=0}^{M-1} \cdots \sum_{m_{nh+2n+2k}=0}^{M-1} E \left\{ \prod_{l_4=nh+2n+1}^{nh+2n+k} V_v^*(m_{l_3}) \prod_{l_5=nh+k+1}^{nh+2n+2k} V_v(m_{l_5}) \right. \\
&\quad \left. \left| \hat{R}_v(T) \right|^{2l} \right\} \sum_{\text{Perm}\{n_1, \dots, n_{nh+2n+i-1}, n_{nh+2n+i+1}, \dots, n_{nh+2n+k}\}} \prod_{l_1=1}^{nh} C_{m_{l_1} n_{l_1}}^h \prod_{l_2=nh+1}^{nh} C_{(m_{l_2+1}) n_{l_2}}^h \\
&\quad \prod_{l_3=nh+n+1}^{nh+n} C_{(m_{l_2+1}) n_{l_2}}^h \prod_{l_4=nh+n+i-1}^{nh+2n+i-1} C_{m_{l_3} n_{l_3}}^h C_{(m_{nh+2n+i+1}) m_1}^h \prod_{l_4=nh+2n+i-1}^{nh+2n+k} C_{m_{l_4} n_{l_4}}^h \\
&= N_h \sum_{m_2=0}^{M-1} \cdots \sum_{m_{nh}=0}^{M-1} \sum_{m_{nh+1}=0}^{M-2} \cdots \sum_{m_{nh+2n}=0}^{M-2} \sum_{m_{nh+2n+1}=0}^{M-1} \cdots \sum_{m_{nh+2n+2k}=0}^{M-1} E \left\{ \prod_{l_4=nh+2n+1}^{nh+2n+k} V_v^*(m_{l_3}) \prod_{l_5=nh+k+1}^{nh+2n+2k} V_v(m_{l_5}) \right. \quad (\text{J.24}) \\
&\quad \left. \left| \hat{R}_v(T) \right|^{2l} \right\} \sum_{\text{Perm}\{n_1, \dots, n_{nh+2n+i-1}, n_{nh+2n+i+1}, \dots, n_{nh+2n+k}\}} \prod_{l_1=2}^{nh} C_{m_{l_1} n_{l_1}}^h \prod_{l_2=nh+1}^{nh} C_{(m_{l_2+1}) n_{l_2}}^h \\
&\quad \prod_{l_3=nh+n+1}^{nh+n} C_{(m_{l_2+1}) n_{l_2}}^h \prod_{l_4=nh+n+i-1}^{nh+2n+i-1} C_{m_{l_3} n_{l_3}}^h C_{m_{nh+2n+i} n_{l_1}}^h \prod_{l_4=nh+2n+i-1}^{nh+2n+k} C_{m_{l_4} n_{l_4}}^h \\
&= N_h M^{nh-1+2k+2n} E \left\{ \hat{P}_h^{nh-1} \left| \hat{R}_{hv}(0) \right|^{2k} \left| \hat{R}_h(T) \right|^{2n} \left| \hat{R}_v(T) \right|^{2l} \right\}.
\end{aligned}$$

When we put them all together we get:

$$\begin{aligned}
E \left\{ \hat{P}_h^{nh} \left| \hat{R}_{hv}(0) \right|^{2k} \left| \hat{R}_h(T) \right|^{2n} \left| \hat{R}_v(T) \right|^{2l} \right\} &= \\
&= \frac{M + nh - 1 + 2n + k}{M} N_h E \left\{ \hat{P}_h^{nh-1} \left| \hat{R}_{hv}(0) \right|^{2k} \left| \hat{R}_h(T) \right|^{2n} \left| \hat{R}_v(T) \right|^{2l} \right\} \quad (\text{J.25}) \\
&= \frac{(M + 2n + k) \cdots (M + nh - 1 + 2n + k)}{M^{nh}} N_h^{nh} E \left\{ \left| \hat{R}_{hv}(0) \right|^{2k} \left| \hat{R}_h(T) \right|^{2n} \left| \hat{R}_v(T) \right|^{2l} \right\}.
\end{aligned}$$

Or by the same rationale:

$$\begin{aligned}
E \left\{ \hat{P}_h^{nh} \left| \hat{R}_{hv}(0) \right|^{2k} \left(\hat{R}_h(T) \right)^{n_1} \left(\hat{R}_h^*(T) \right)^{n_2} \left(\hat{R}_v(T) \right)^{l_1} \left(\hat{R}_v^*(T) \right)^{l_2} \right\} &= \\
&= \frac{M + nh - 1 + n_1 + n_2 + k}{M} N_h \\
&= \frac{(M + n_1 + n_2 + k) \cdots (M + nh - 1 + n_1 + n_2 + k)}{M^{nh}} N_h^{nh} \times \\
&= E \left\{ \left| \hat{R}_{hv}(0) \right|^{2k} \left(\hat{R}_h(T) \right)^{n_1} \left(\hat{R}_h^*(T) \right)^{n_2} \left(\hat{R}_v(T) \right)^{l_1} \left(\hat{R}_v^*(T) \right)^{l_2} \right\}. \quad (\text{J.26})
\end{aligned}$$

Similarly:

$$\begin{aligned}
E \left\{ \hat{P}_v^{nv} \left| \hat{R}_{hv}(0) \right|^{2k} \left| \hat{R}_h(T) \right|^{2n} \left| \hat{R}_v(T) \right|^{2l} \right\} &= \\
& \frac{M + nv - 1 + 2l + k}{M} N_v E \left\{ \hat{P}_v^{nv-1} \left| \hat{R}_{hv}(0) \right|^{2k} \left| \hat{R}_h(T) \right|^{2n} \left| \hat{R}_v(T) \right|^{2l} \right\} \\
& = \frac{(M + 2l + k) \cdots (M + nv - 1 + 2l + k)}{M^{nv}} N_v^{nv} E \left\{ \left| \hat{R}_{hv}(0) \right|^{2k} \left| \hat{R}_h(T) \right|^{2n} \left| \hat{R}_v(T) \right|^{2l} \right\}.
\end{aligned} \tag{J.27}$$

Now we can calculate some useful expressions:

$$\begin{aligned}
E \left\{ \hat{P}_h^{nh} \left| \hat{R}_{hv}(0) \right|^2 \left| \hat{R}_h(T) + \hat{R}_v(T) \right|^2 \right\} &= \\
& E \left\{ \hat{P}_h^{nh} \left| \hat{R}_{hv}(0) \right|^2 \left(\hat{R}_h(T) + \hat{R}_v(T) \right) \left(\hat{R}_h^*(T) + \hat{R}_v^*(T) \right) \right\} \\
& = E \left\{ \hat{P}_h^{nh} \left| \hat{R}_{hv}(0) \right|^2 \left| \hat{R}_h(T) \right|^2 \right\} + E \left\{ \hat{P}_h^{nh} \left| \hat{R}_{hv}(0) \right|^2 \hat{R}_h(T) \hat{R}_v^*(T) \right\} + \\
& E \left\{ \hat{P}_h^{nh} \left| \hat{R}_{hv}(0) \right|^2 \hat{R}_v(T) \hat{R}_h^*(T) \right\} + E \left\{ \hat{P}_h^{nh} \left| \hat{R}_{hv}(0) \right|^2 \left| \hat{R}_v(T) \right|^2 \right\} \\
& = \frac{\prod_{i=3}^{nh+2} (M+i)}{M^{nh}} N_h^{nh} E \left\{ \left| \hat{R}_{hv}(0) \right|^2 \left| \hat{R}_h(T) \right|^2 \right\} + \\
& \frac{\prod_{i=2}^{nh+1} (M+i)}{M^{nh}} N_h^{nh} E \left\{ \left| \hat{R}_{hv}(0) \right|^2 \hat{R}_h(T) \hat{R}_v^*(T) \right\} + \\
& \frac{\prod_{i=2}^{nh+1} (M+i)}{M^{nh}} N_h^{nh} E \left\{ \left| \hat{R}_{hv}(0) \right|^2 \hat{R}_v(T) \hat{R}_h^*(T) \right\} + \\
& \frac{\prod_{i=1}^{nh} (M+i)}{M^{nh}} N_h^{nh} E \left\{ \hat{P}_h^{nh} \left| \hat{R}_{hv}(0) \right|^2 \left| \hat{R}_v(T) \right|^2 \right\} \\
& = \frac{(M+2) \prod_{i=3}^{nh+2} (M+i)}{M^{nh+2} (M-1)} N_h^{nh+3} N_v + 2 \frac{\prod_{i=2}^{nh+1} (M+i)}{M^{nh+2} (M-1)} N_h^{nh+2} N_v^2 + \\
& \frac{(M+2) \prod_{i=1}^{nh} (M+i)}{M^{nh+2} (M-1)} N_h^{nh+1} N_v^3
\end{aligned} \tag{J.28}$$

$$\begin{aligned}
& E \left\{ \hat{P}_h^{nh} \left| \hat{R}_{hv}(0) \right|^4 \left| \hat{R}_h(T) + \hat{R}_v(T) \right|^4 \right\} = \\
& E \left\{ \hat{P}_h^{nh} \left| \hat{R}_{hv}(0) \right|^4 \left(\left| \hat{R}_h(T) \right|^4 + 4 \left| \hat{R}_h(T) \right|^2 \hat{R}_h(T) \hat{R}_v^*(T) + \right. \right. \\
& \left. \left. + 4 \left| \hat{R}_h(T) \right|^2 \left| \hat{R}_v(T) \right|^2 + 4 \hat{R}_h(T) \hat{R}_v^*(T) \left| \hat{R}_v(T) \right|^2 + 2 \left(\hat{R}_h(T) \hat{R}_v^*(T) \right)^2 + \left| \hat{R}_v(T) \right|^4 \right) \right\} \\
& = \frac{\prod_{i=6}^{nh+5} (M+i)}{M^{nh}} N_h^{nh} E \left\{ \left| \hat{R}_{hv}(0) \right|^4 \left| \hat{R}_h(T) \right|^4 \right\} + 4 \frac{\prod_{i=5}^{nh+4} (M+i)}{M^{nh}} N_h^{nh} \times \\
& E \left\{ \left| \hat{R}_{hv}(0) \right|^4 \left| \hat{R}_h(T) \right|^2 \hat{R}_h(T) \hat{R}_v^*(T) \right\} + \\
& 4 \frac{\prod_{i=4}^{nh+3} (M+i)}{M^{nh}} N_h^{nh} E \left\{ \left| \hat{R}_{hv}(0) \right|^4 \left| \hat{R}_h(T) \right|^2 \left| \hat{R}_v(T) \right|^2 \right\} + \\
& 4 \frac{\prod_{i=3}^{nh+2} (M+i)}{M^{nh}} N_h^{nh} E \left\{ \left| \hat{R}_{hv}(0) \right|^4 \hat{R}_h(T) \hat{R}_v^*(T) \left| \hat{R}_v(T) \right|^2 \right\} + 2 \frac{\prod_{i=4}^{nh+3} (M+i)}{M^{nh}} N_h^{nh} \times \\
& E \left\{ \left| \hat{R}_{hv}(0) \right|^4 \left(\hat{R}_h(T) \hat{R}_v^*(T) \right)^2 \right\} + \frac{\prod_{i=2}^{nh+1} (M+i)}{M^{nh}} N_h^{nh} E \left\{ \left| \hat{R}_{hv}(0) \right|^4 \left| \hat{R}_v(T) \right|^4 \right\} \\
& = 2 \frac{(M+4)(M+5)}{M^{nh+4}} \frac{2M^2 + 2M - 8}{(M-1)^4} \times \\
& \left(\prod_{i=6}^{nh+5} (M+i) N_h^6 N_v^2 + \prod_{i=2}^{nh+1} (M+i) N_h^2 N_v^6 \right) N_h^{nh} + \\
& 16(M+2) \frac{2M^2 + 2M - 8}{(M-1)^4} \frac{1}{M^{nh+4}} \left(\prod_{i=5}^{nh+4} (M+i) N_h^5 N_v^3 + \prod_{i=3}^{nh+2} (M+i) N_h^3 N_v^5 \right) N_h^{nh} + \\
& 2 \frac{24M^2 + 24M - 128}{M^{nh+4} (M-1)^4} \prod_{i=4}^{nh+3} (M+i) N_h^{nh+4} N_v^4 + \\
& 4 \frac{2M^4 + 14M^3 + 26M^2 - 22M - 68}{M^{nh+4} (M-1)^4} \prod_{i=4}^{nh+3} (M+i) N_h^{nh+4} N_v^4
\end{aligned} \tag{J.29}$$

$$\begin{aligned}
& E \left\{ \hat{P}_h^{nh} \left| \hat{R}_{hv}(0) \right|^6 \left| \hat{R}_h(T) + \hat{R}_v(T) \right|^6 \right\} = \\
& E \left\{ \hat{P}_h^{nh} \left| \hat{R}_{hv}(0) \right|^6 \left(\hat{R}_h(T) + \hat{R}_v(T) \right)^3 \left(\hat{R}_h^*(T) + \hat{R}_v^*(T) \right)^3 \right\} \\
& = E \left\{ \hat{P}_h^{nh} \left| \hat{R}_{hv}(0) \right|^6 \left(\left| \hat{R}_h(T) \right|^6 + \left| \hat{R}_v(T) \right|^6 + 9 \left| \hat{R}_h(T) \right|^4 \left| \hat{R}_v(T) \right|^2 + \right. \right. \\
& \quad 9 \left| \hat{R}_h(T) \right|^2 \left| \hat{R}_v(T) \right|^4 + 18 \left| \hat{R}_h(T) \right|^2 \hat{R}_h(T) \left| \hat{R}_v(T) \right|^2 \hat{R}_v^*(T) + \\
& \quad 6 \left| \hat{R}_h(T) \right|^4 \hat{R}_h(T) \hat{R}_v^*(T) + 6 \hat{R}_h^*(T) \left| \hat{R}_v(T) \right|^4 \hat{R}_v(T) + \\
& \quad \left. \left. 6 \hat{R}_h^2(T) \left| \hat{R}_v(T) \right|^2 \left(\hat{R}_v^*(T) \right)^2 + 6 \left| \hat{R}_h(T) \right|^2 \hat{R}_h^2(T) \left(\hat{R}_v^*(T) \right)^2 + 2 \left(\hat{R}_h(T) \hat{R}_v^*(T) \right)^3 \right) \right\} \\
& = 6 \frac{\prod_{i=6}^8 (M+i)}{M^{nh+6}} \frac{6M^3 + 36M^2 - 6M - 180}{(M-1)^6} \times \\
& \quad \left(\prod_{i=9}^{nh+8} (M+i) N_h^9 N_v^3 + \prod_{i=3}^{nh+2} (M+i) N_h^3 N_v^9 \right) N_h^{nh} + \\
& \quad 9 \frac{12M^6 + 252M^5 + 2124M^4 + 8292M^3 + 9096M^2 - 28992M - 63360}{M^{nh+6} (M-1)^6} \times \\
& \quad \left(\prod_{i=7}^{nh+6} (M+i) N_h^7 N_v^5 + \prod_{i=5}^{nh+4} (M+i) N_h^5 N_v^7 \right) N_h^{nh} + \\
& \quad 6 * 9 * 2 \frac{(M+6)(M+7)}{M^{nh+6}} \frac{6M^3 + 36M^2 - 6M - 180}{(M-1)^6} \times \\
& \quad \left(\prod_{i=8}^{nh+7} (M+i) N_h^8 N_v^4 + \prod_{i=4}^{nh+3} (M+i) N_h^4 N_v^8 \right) N_h^{nh} + \\
& \quad 6 \frac{432M^4 + 5184M^3 + 14688M^2 - 20304M - 90720}{M^{nh+6} (M-1)^6} \times \\
& \quad \left(\prod_{i=7}^{nh+6} (M+i) N_h^7 N_v^5 + \prod_{i=5}^{nh+4} (M+i) N_h^5 N_v^7 \right) N_h^{nh} + \\
& \quad 2 \frac{2160M^3 + 10368M^2 - 23760M - 109728}{M^{nh+6} (M-1)^6} \prod_{i=6}^{nh+5} (M+i) N_h^{nh+6} N_v^6 + \\
& \quad 18 \frac{72M^5 + 1152M^4 + 6336M^3 + 97920M^2 - 22104M - 58320}{M^{nh+6} (M-1)^6} \prod_{i=6}^{nh+5} (M+i) N_h^{nh+6} N_v^6 \tag{J.30}
\end{aligned}$$

$$\begin{aligned}
& E \left\{ \hat{P}_h^{nh} \left| \hat{R}_{hv}(0) \right|^8 \left| \hat{R}_h(T) + \hat{R}_v(T) \right|^8 \right\} = \\
& E \left\{ \hat{P}_h^{nh} \left| \hat{R}_{hv}(0) \right|^8 \left(\hat{R}_h(T) + \hat{R}_v(T) \right)^4 \left(\hat{R}_h^*(T) + \hat{R}_v^*(T) \right)^4 \right\} \\
& = E \left\{ \hat{P}_h^{nh} \left| \hat{R}_{hv}(0) \right|^8 \left(\left| \hat{R}_h(T) \right|^8 + \left| \hat{R}_v(T) \right|^8 + 2\hat{R}_h^4(T) \left(\hat{R}_v^*(T) \right)^4 + 8 \left| \hat{R}_h(T) \right|^6 \hat{R}_h(T) \hat{R}_v^*(T) + \right. \right. \\
& 8\hat{R}_h^*(T) \left| \hat{R}_v(T) \right|^6 \hat{R}_v(T) + 8 \left| \hat{R}_h(T) \right|^2 \hat{R}_h^3(T) \left(\hat{R}_v^*(T) \right)^3 + 8 \left(\hat{R}_h^*(T) \right)^3 \left| \hat{R}_v(T) \right|^2 \hat{R}_v^3(T) + \\
& 12 \left| \hat{R}_h(T) \right|^4 \hat{R}_h^2(T) \left(\hat{R}_v^*(T) \right)^2 + 12 \left(\hat{R}_h^*(T) \right)^2 \left| \hat{R}_v(T) \right|^4 \hat{R}_v^2(T) + 16 \left| \hat{R}_h(T) \right|^6 \left| \hat{R}_v(T) \right|^2 + \\
& 16 \left| \hat{R}_h(T) \right|^2 \left| \hat{R}_v(T) \right|^6 + 32 \left| \hat{R}_h(T) \right|^2 \hat{R}_h^2(T) \left| \hat{R}_v(T) \right|^2 \left(\hat{R}_v^*(T) \right)^2 + 36 \left| \hat{R}_h(T) \right|^4 \left| \hat{R}_v(T) \right|^4 + \\
& \left. \left. 48 \left| \hat{R}_h(T) \right|^4 \hat{R}_h(T) \left| \hat{R}_v(T) \right|^2 \hat{R}_v^*(T) + 48 \left| \hat{R}_h(T) \right|^2 \hat{R}_h^*(T) \left| \hat{R}_v(T) \right|^4 \hat{R}_v(T) \right) \right\} \\
& = 24 \frac{\prod_{i=8}^{11} (M+i) 24M^4 + 336M^3 + 1128M^2 - 1488M - 8064}{M^{nh+8} (M-1)^8} \times \\
& \left(\prod_{i=12}^{nh+11} (M+i) N_h^{12} N_v^4 + \prod_{i=4}^{nh+3} (M+i) N_h^4 N_v^{12} \right) N_h^{nh} + \\
& 8 * 96 \frac{\prod_{i=8}^{10} (M+i) 24M^4 + 336M^3 + 1128M^2 - 1488M - 8064}{M^{nh+8} (M-1)^8} \times \\
& \left(\prod_{i=11}^{nh+10} (M+i) N_h^{11} N_v^5 + \prod_{i=5}^{nh+4} (M+i) N_h^5 N_v^{11} \right) N_h^{nh} + \\
& \frac{2304M^8 + 99072M^7 + 1995264M^6 + 23689728M^5 + 165954816M^4 +}{M^{nh+8}} \\
& \frac{587536128M^3 + 319758336M^2 - 3816281088M - 759435264}{(M-1)^8} \times \\
& \left(\prod_{i=10}^{nh+9} (M+i) N_h^{10} N_v^6 + \prod_{i=6}^{nh+5} (M+i) N_h^6 N_v^{10} \right) N_h^{nh} + \\
& \frac{55296M^7 + 1935360M^6 + 28366848M^5 + 214603776M^4 + 782438400M^3 +}{M^{nh+8}} \\
& \frac{470900736M^2 - 4954079232M - 10032906240}{(M-1)^8} \times \\
& \left(\prod_{i=9}^{nh+8} (M+i) N_h^9 N_v^7 + \prod_{i=7}^{nh+6} (M+i) N_h^7 N_v^9 \right) N_h^{nh} + \\
& \frac{3456M^8 + 138240M^7 + 2764800M^6 + 33212160M^5 + 234893952M^4 +}{M^{nh+8}} \tag{J.31} \\
& \frac{840271104M^3 + 498548736M^2 - 5362882560M - 6477886080}{(M-1)^8} \prod_{i=8}^{nh+7} (M+i) N_h^{nh+8} N_v^8
\end{aligned}$$

Following the same procedure we derive:

$$\begin{aligned}
& E \left\{ \hat{P}_h^{nh} \hat{P}_v^{nv} \left| \hat{R}_{hv}(0) \right|^{2k} \left| \hat{R}_h(T) \right|^{2n} \left| \hat{R}_v(T) \right|^{2l} \right\} = \\
& \quad \frac{M + nv - 1 + 2l + k}{M} N_v E \left\{ \hat{P}_h^{nh} \hat{P}_v^{nv-1} \left| \hat{R}_{hv}(0) \right|^{2k} \left| \hat{R}_h(T) \right|^{2n} \left| \hat{R}_v(T) \right|^{2l} \right\} \\
& = \frac{(M + 2l + k) \cdots (M + nv - 1 + 2l + k)}{M^{nv}} N_v^{nv} E \left\{ \hat{P}_h^{nh} \left| \hat{R}_{hv}(0) \right|^{2k} \left| \hat{R}_h(T) \right|^{2n} \left| \hat{R}_v(T) \right|^{2l} \right\} \quad (\text{J.32}) \\
& = \frac{\prod_{i=0}^{nv-1} (M + i + 2n + k) \prod_{j=0}^{nh-1} (M + j + 2n + k)}{M^{nh+nv}} N_h^{nh} N_v^{nv} E \left\{ \left| \hat{R}_{hv}(0) \right|^{2k} \left| \hat{R}_h(T) \right|^{2n} \left| \hat{R}_v(T) \right|^{2l} \right\}
\end{aligned}$$

Appendix K

Assessment of the Accuracy of the Weighted Sum *pdf* Approximation

Usage of general gamma distribution for the approximation of a weighted sum *pdf* inevitably raises the question: what is the accuracy of such approximation? Here the approximation assessment is done for the following PFA values 10^{-2} , 10^{-3} , 10^{-4} , 10^{-5} , and for the range of weight values. The error assessment was performed by first calculating the thresholds using the generalized gamma *pdf* approximation for the desired PFA, and subsequently evaluating the true PFA through Monte Carlo simulations. The results are presented in Figs. K.1, K.2, and K.3 for M of 17, 25, and 32, respectively. The max. errors obtained are 3.7%, 17.4%, 38.3%, and 59.2% for PFA's of 10^{-2} , 10^{-3} , 10^{-4} , 10^{-5} , respectively. Notice that errors gradually increase with the number of samples M . In addition, approximation errors appear to be significantly smaller in the area where the weight α is of greater value than β .

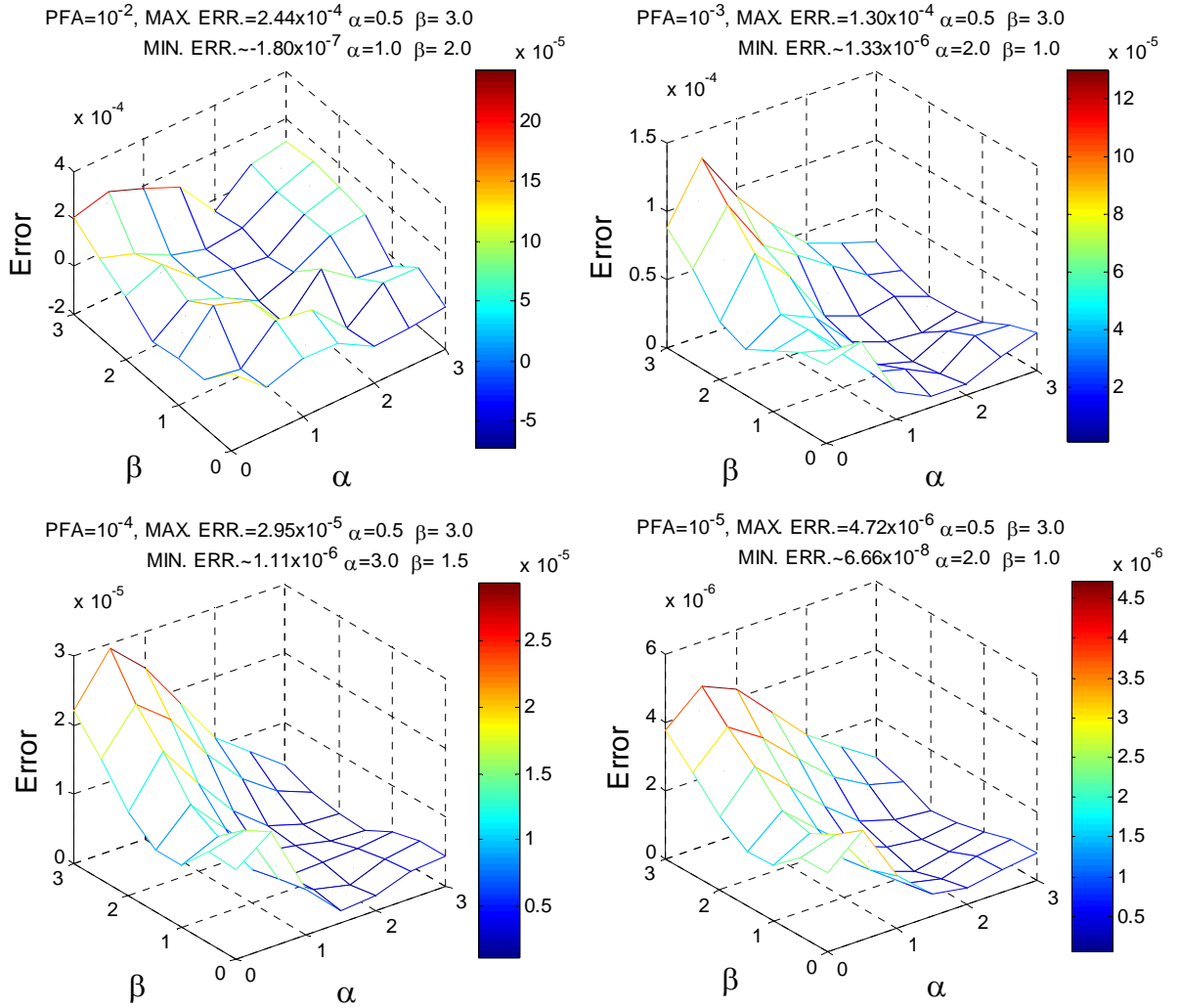


Figure K.1 3-D plot of a weighted sum approximation errors using generalized gamma distribution for $M = 17$, and $\gamma = 2$.

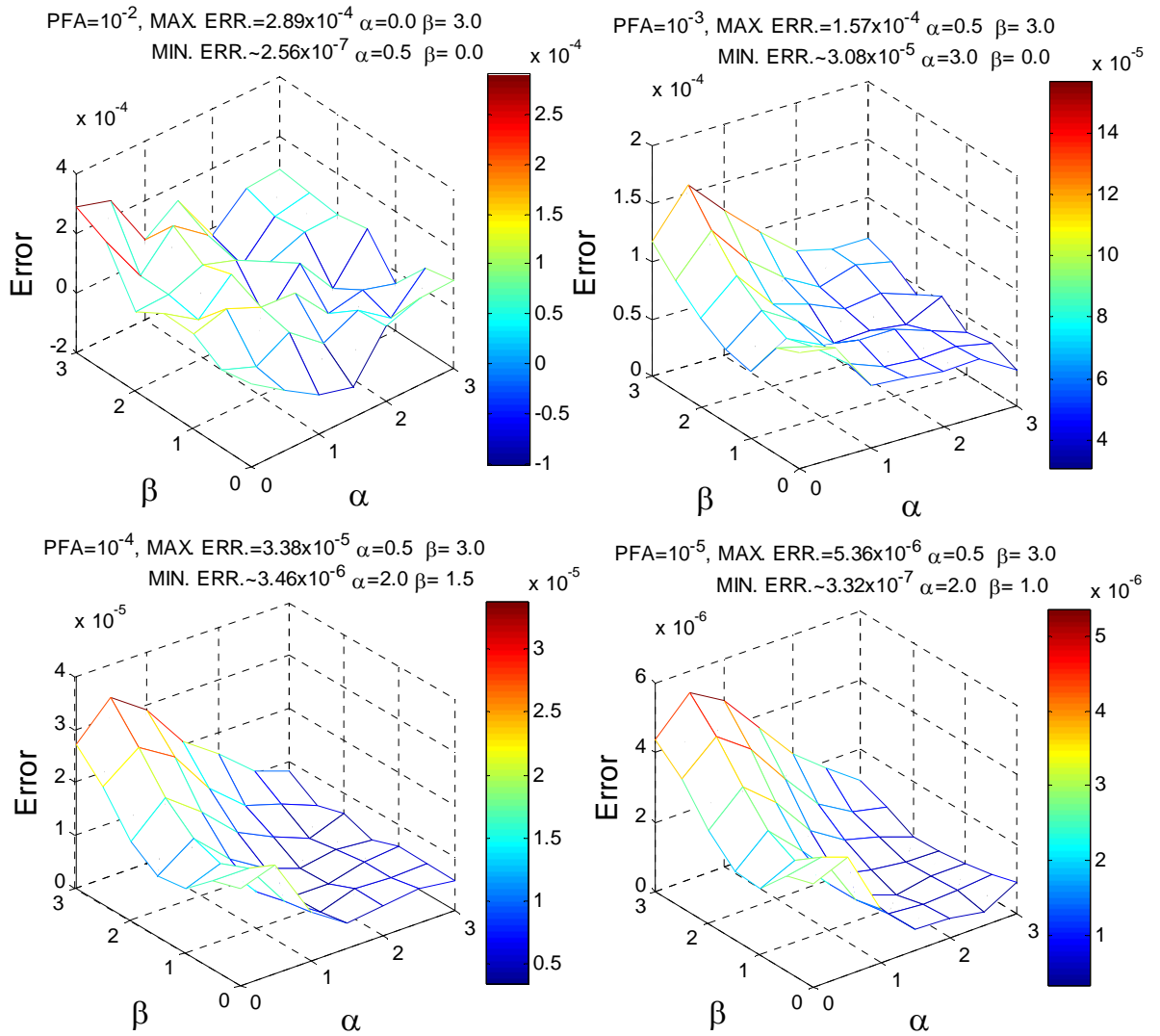


Figure K.2 3-D plot of a weighted sum approximation errors using generalized gamma distribution for $M = 25$, and $\gamma = 2$.

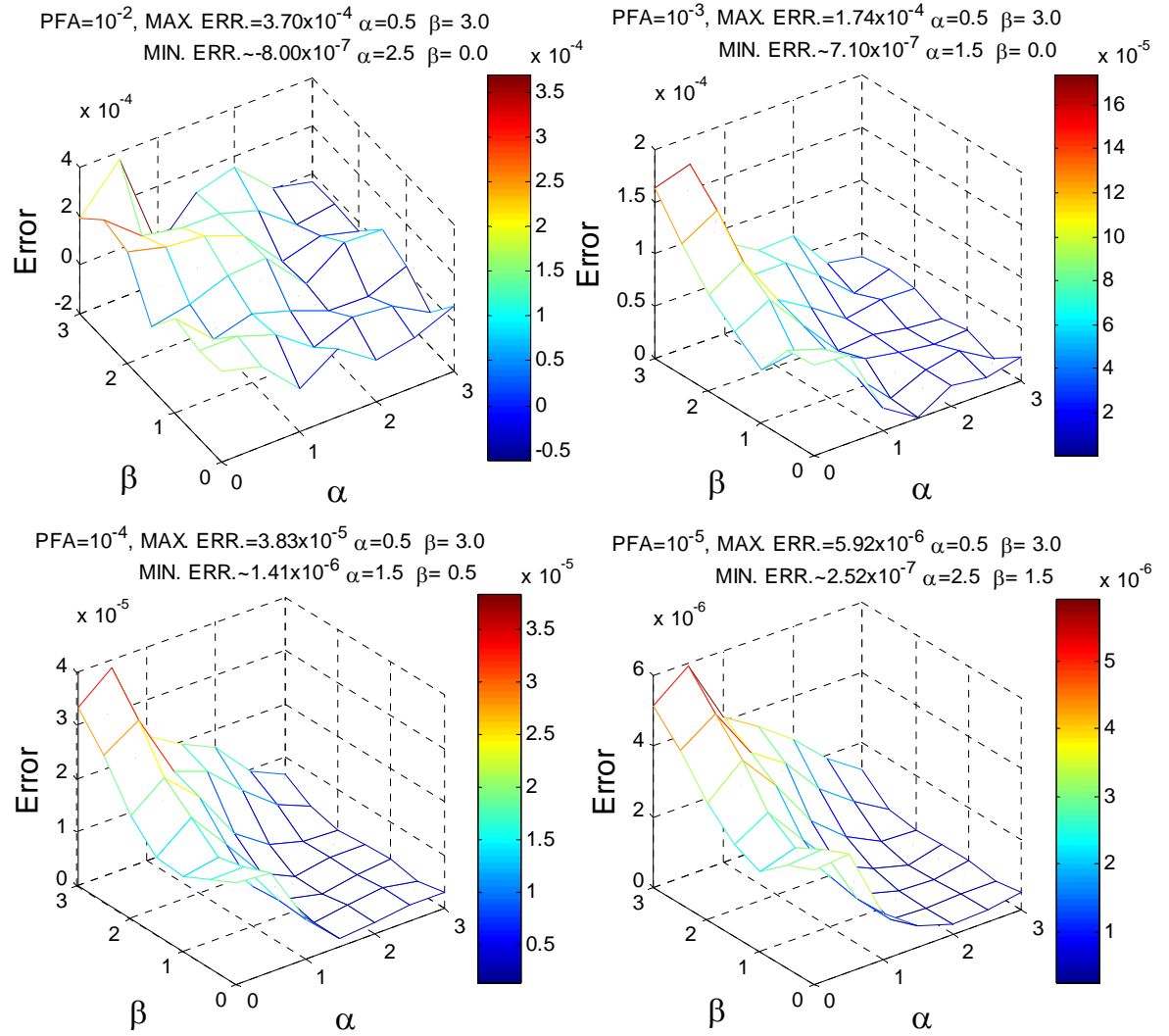


Figure K.3 3-D plot of a weighted sum approximation errors using generalized gamma distribution for $M = 32$, and $\gamma = 2$.

Appendix L

Calculation of Fitting Function Coefficient

To perform least squares fitting with function

$$f(y_i) \approx x^B e^{A+Cx_i}. \quad (\text{L.1})$$

We define the minimization function as

$$R = \sum_{i=0}^{N-1} (\ln y_i - A - B \ln x_i - Cx_i)^2. \quad (\text{L.2})$$

The derivatives are:

$$\begin{aligned} \frac{\partial R}{\partial A} &= -2 \sum_{i=0}^{N-1} (\ln y_i - A - B \ln x_i - Cx_i) \\ \frac{\partial R}{\partial B} &= -2 \sum_{i=0}^{N-1} (\ln y_i - A - B \ln x_i - Cx_i) \ln x_i \\ \frac{\partial R}{\partial C} &= -2 \sum_{i=0}^{N-1} (\ln y_i - A - B \ln x_i - Cx_i) x_i. \end{aligned} \quad (\text{L.3})$$

By setting these to zero we get

$$\begin{aligned} \sum_{i=0}^{N-1} \ln y_i &= AN + B \sum_{i=0}^{N-1} \ln x_i + C \sum_{i=0}^{N-1} x_i \\ \sum_{i=0}^{N-1} \ln x_i \ln y_i &= A \sum_{i=0}^{N-1} \ln x_i + B \sum_{i=0}^{N-1} (\ln x_i)^2 + C \sum_{i=0}^{N-1} x_i \ln x_i \\ \sum_{i=0}^{N-1} x_i \ln y_i &= A \sum_{i=0}^{N-1} x_i + B \sum_{i=0}^{N-1} x_i \ln x_i + C \sum_{i=0}^{N-1} (x_i)^2. \end{aligned} \quad (\text{L.4})$$

This can be represented in a matrix form

$$\begin{bmatrix} N & \sum_{i=0}^{N-1} \ln x_i & \sum_{i=0}^{N-1} x_i \\ \sum_{i=0}^{N-1} \ln x_i & \sum_{i=0}^{N-1} (\ln x_i)^2 & \sum_{i=0}^{N-1} x_i \ln x_i \\ \sum_{i=0}^{N-1} x_i & \sum_{i=0}^{N-1} x_i \ln x_i & \sum_{i=0}^{N-1} (x_i)^2 \end{bmatrix} \begin{bmatrix} A \\ B \\ C \end{bmatrix} = \begin{bmatrix} \sum_{i=0}^{N-1} \ln y_i \\ \sum_{i=0}^{N-1} \ln x_i \ln y_i \\ \sum_{i=0}^{N-1} x_i \ln y_i \end{bmatrix}. \quad (\text{L.5})$$

Then coefficients can be obtained by solving the system of linear equations.

Appendix M

Censoring Algorithm Using Uniform Sum for the Operational Dual-pol WSR-88D

The main motivation for this work is the upgrade of the WSR-88D network to dual-polarization; and the goal is to devise an improved censoring algorithm that mitigates the degradation of radar sensitivity to minimize its impact on the radar products with minimal impact on radar operation. In the legacy WSR-88D system, the operator is allowed to vary the SNR thresholds in the range of ± 20 dB with respect to the noise power in the H channel. Thus, the proposed censoring algorithm sensitivity needs to be manually adjustable. At the same time, it is desirable that the algorithm can be easily implemented.

Given the threshold (THR_{dB}) specified in dB the SNR threshold (THR_{SNR}) is computed as

$$THR_{SNR} = 10^{\frac{THR_{dB}}{10}}. \quad (M.1)$$

At each range gate the SNR in the H channel is estimated as,

$$SNR_h = \frac{\frac{1}{M} \sum_{i=0}^{M-1} |H_i|^2}{N_h} - 1, \quad (M.2)$$

and compared to (M.1). If $SNR_h \geq THR_{SNR}$ it is classified as a “significant return”, otherwise it represents a “non-significant return”. After the dual-polarization upgrade, the power of the returned echoes in the H channel is halved and the portion of the SNR estimates, which would be classified as “significant returns” in the single-pol system, will inevitably fall below the censoring threshold (i.e., THR_{SNR}). This results in the loss of the low SNR features as shown in Chapter 6. Clearly, if this loss is to be mitigated, the

missed estimates need to be recovered, but with an acceptable false alarm rate. One possibility is to simply lower the SNR threshold to $THR_{SNR}/2$. Unfortunately, this has the potential to increase the false alarm rate to unacceptable level (as shown in Chapter 6). The PFA increase depends on the number of samples M (Figure M.1) for the cases when the default thresholds of 2 and 3.5 dB are cut by half (i.e., to -1 and 0.5 dB).

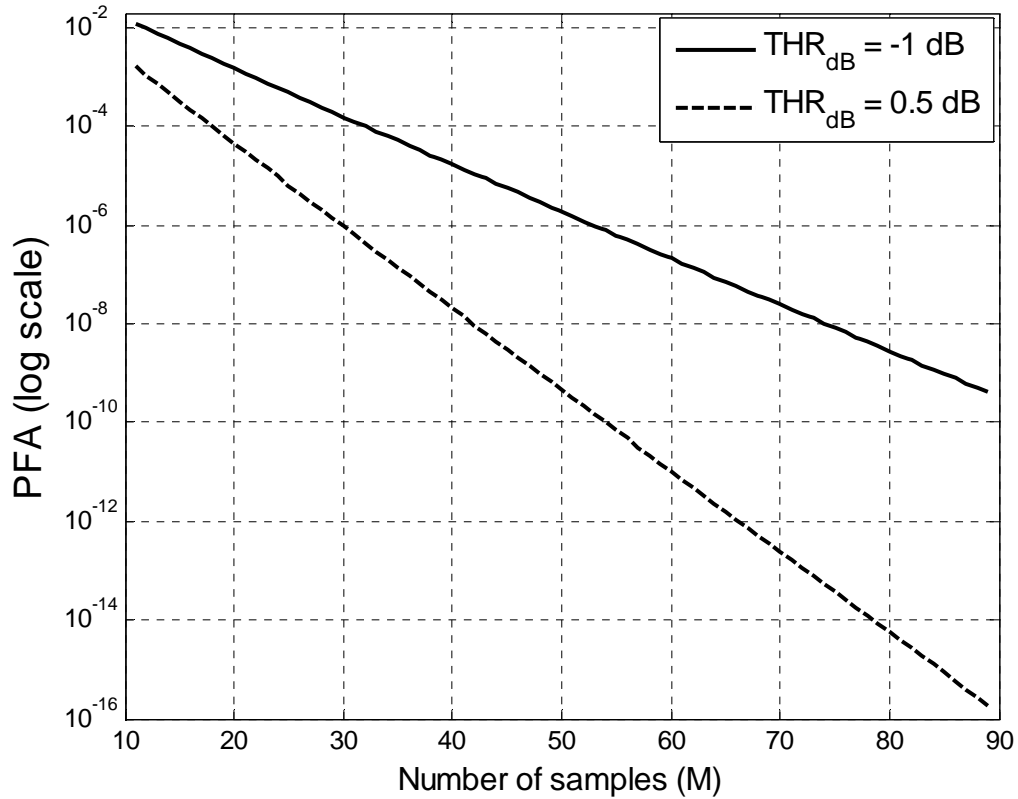


Figure M.1 False alarm rate dependency on the number of samples M .

The solid line obtained using the formula (A.11) shows that, if M is greater than 52, the default threshold of 2 dB can be reduced by half while still maintaining the PFA below 1.2×10^{-6} . Similarly, the dashed line obtained using the formula (A.11) shows that, if M is greater than 29, the default threshold of 3.5 dB can be reduced by half while still maintaining the PFA below 1.2×10^{-6} . The default threshold of 2 dB is used for censoring in surveillance scans whereas the number of samples M is, in most cases, less than 52.

Thus, lowering the threshold by half is unacceptable in such situations; clearly, a more sophisticated approach is required.

Because of its improved detection rate, the uniform sum can be used to detect signals whose SNR estimate falls below the THR_{SNR} . Thus, one possible arrangement would be to estimate the uniform sum, for all range gates where the SNR_h estimate is less than the THR_{SNR} , and compare these estimates to some threshold (e.g., THR_{US}) for classification. This, however, contradicts the concept of adjustable thresholds because comparing the uniform sum estimate (US) to THR_{US} inevitably leads to classification of some of SNR estimates, which are smaller than THR_{SNR} in single-pol, as “significant returns”. Consequently, an additional condition that the SNR_h estimate must be larger than $THR_{SNR}/2$ ought to be applied at each range gate (and before the classification using the uniform sum). Therefore, the proposed signal censoring algorithm that applies to each range gate is:

```
if  $M > 89$ 
  if  $SNR_h \geq THR_{SNR}/2$ 
    accept as “significant return”
  else
    reject as “non-significant return”
  end
else
  if  $(SNR_h \geq THR_{SNR})$  or  $(SNR_h \geq THR_{SNR}/2$  and  $US \geq THR_{US})$ 
    accept as “significant return”
  else
    reject as “non-significant return”
  end
end
```

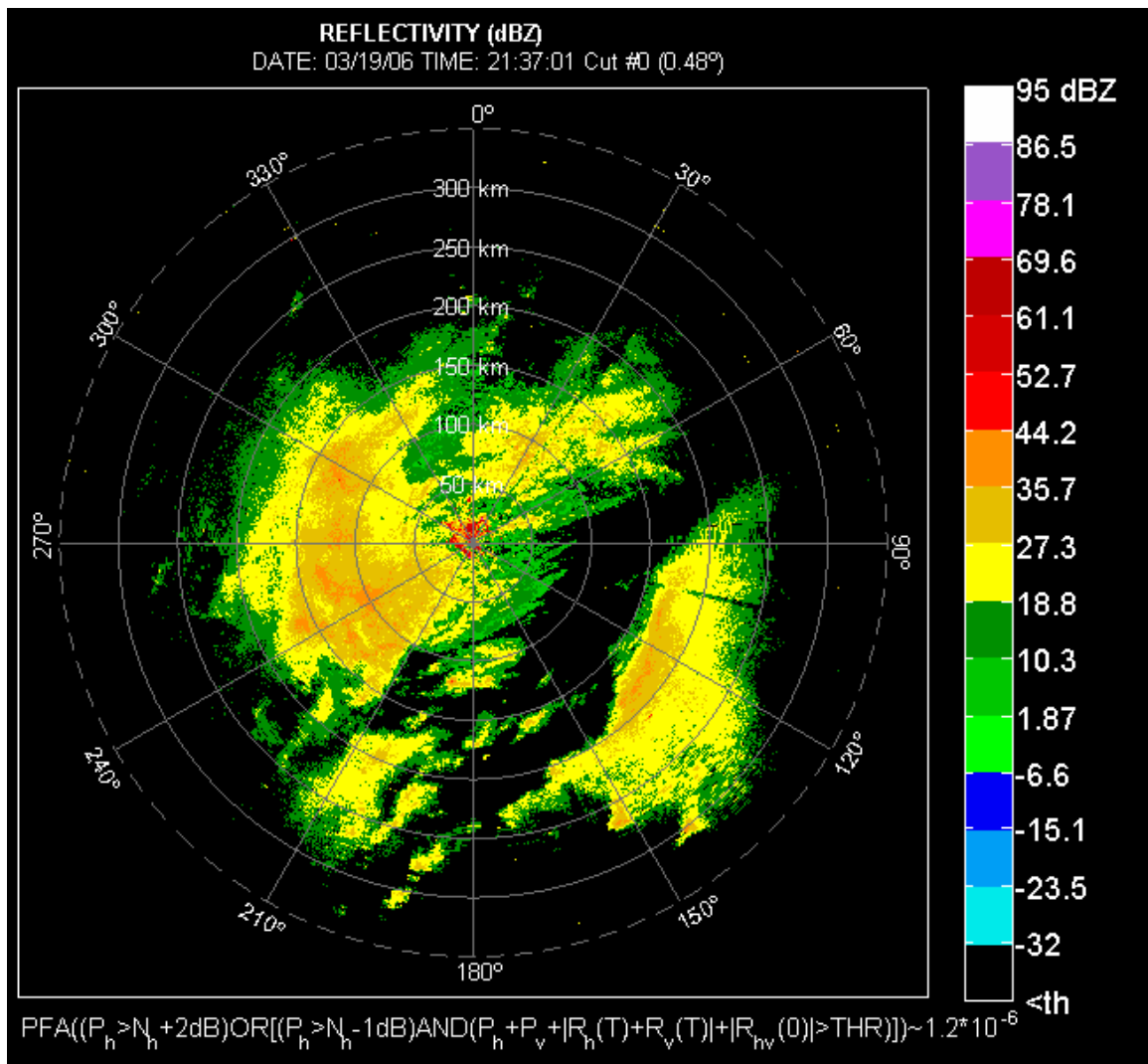
Note that if M is greater than 89 the algorithm proposes that the square law detector is used for detection after the legacy SNR threshold is lowered by half. The reason for this is twofold. First is that the majority of operational modes use the number of samples that is less than 90. Second, the curves in Figure M.1 show that, if M is greater than 89, lowering the default thresholds by half yields the false alarm rates that are well below the acceptable ones. The threshold for the “uniform sum” (i.e., THR_{US}) is computed using (7.2). The coefficients are chosen so that the uniform sum produces the PFA of 1.2×10^{-6} in all cases where the legacy square law detector, with the default SNR threshold (i.e., 2 dB for reflectivity, and 3.5 dB for velocity estimates), yields the false alarm rate that is less than or equal to 1.2×10^{-6} . If this is not the case, the coefficients are set so the uniform sum matches the PFA of the legacy detector with the default threshold. This occurs when M is 6, 7, 8, or 9, for which the SNR based detector with the threshold of 3.5 dB produces the PFAs of 1.1×10^{-4} , 3.6×10^{-5} , 1.2×10^{-5} , and 3.8×10^{-6} . In case when $M = 16$ and the halved default threshold is -1 dB, the resulting PFA is 2.28×10^{-6} . The coefficients are given in Table M.1.

M	6	7	8	9	10	11	12
A	1.4424	1.4367	1.417	1.4044	1.3975	1.3615	1.3298
B	-9.911e-2	-8.97e-2	-9.307e-2	-9.361e-2	-9.394e-2	-8.032e-2	-6.791e-2
C	0.61055	0.59579	0.59827	0.59864	0.59725	0.58165	0.56929
M	13	14	15	16	17	18	19
A	1.3024	1.2576	1.239	1.1946	1.2039	1.1552	1.1511
B	-5.574e-2	-6.159e-2	-4.879e-2	-3.914e-2	-2.933e-2	-4.542e-2	-2.944e-2
C	0.55685	0.56567	0.55126	0.54377	0.52846	0.55309	0.53341
M	20	21	22	23	24	25	26
A	1.1223	1.1026	1.0953	1.0798	1.0691	1.0622	1.0454
B	-3.266e-2	-3.1927e-2	-2.1782e-2	-1.8855e-2	-1.3561e-2	-6.174e-3	-6.1895e-3
C	0.54113	0.53956	0.52826	0.52593	0.51962	0.50996	0.51269

<i>M</i>	27	28	29	30	31	32	33
<i>A</i>	1.0313	1.028	1.0098	0.99348	0.99406	0.98481	0.98154
<i>B</i>	-5.154e-3	2.1922e-3	-2.6402e-4	-2.9082e-3	6.8651e-3	9.0159e-3	1.5671e-2
<i>C</i>	0.51222	0.50091	0.50718	0.51114	0.49914	0.49704	0.4895
<i>M</i>	34	35	36	37	38	39	40
<i>A</i>	0.96288	0.95693	0.94897	9.3505	0.93681	0.92138	0.9188
<i>B</i>	9.7531e-3	1.3140e-2	1.5368e-2	1.2681e-2	2.0367e-2	1.5745e-2	2.0107e-2
<i>C</i>	0.49788	0.49382	0.49269	0.49756	0.48692	0.49384	0.48811
<i>M</i>	41	42	43	44	45	46	47
<i>A</i>	0.93523	0.90515	0.91548	0.89475	0.89016	0.89692	0.8842
<i>B</i>	3.9809e-2	2.2990e-2	3.5888e-2	2.6591e-2	2.8431e-2	3.9408e-2	3.5303e-2
<i>C</i>	0.46344	0.48666	0.46772	0.48242	0.47995	0.46646	0.4728
<i>M</i>	48	49	50	51	52	53	54
<i>A</i>	0.87752	0.87178	0.86942	0.85894	0.85721	0.85255	0.83821
<i>B</i>	3.5153e-2	3.4939e-2	3.8871e-2	3.5241e-2	3.9386e-2	3.9818e-2	3.3166e-2
<i>C</i>	0.47314	0.47245	0.46917	0.47388	0.47038	0.46945	0.47848
<i>M</i>	55	56	57	58	59	60	61
<i>A</i>	0.84241	0.83417	0.8987	0.84118	0.8275	0.82514	0.82332
<i>B</i>	4.0473e-2	3.8784e-2	9.0213e-2	5.14e-2	4.5207e-2	4.6739e-2	4.8742e-2
<i>C</i>	0.46883	0.4722	0.40202	0.45508	0.46448	0.46184	0.45937
<i>M</i>	62	63	64	65	66	67	68
<i>A</i>	0.81501	0.82465	0.80524	0.81076	0.81984	0.80407	0.79094
<i>B</i>	4.6716e-2	5.7596e-2	4.6096e-2	5.3856e-2	6.2571e-2	5.4979e-2	4.7713e-2
<i>C</i>	0.46332	0.44921	0.46461	0.45511	0.44152	0.45374	0.4629
<i>M</i>	69	70	71	72	73	74	75
<i>A</i>	0.79447	0.79848	0.79574	0.77834	0.78912	0.7843	0.78488
<i>B</i>	5.3431e-2	6.0617e-2	6.1305e-2	5.0397e-2	6.1416e-2	6.0368e-2	6.3499e-2
<i>C</i>	0.4557	0.44867	0.44756	0.46121	0.44682	0.4483	0.44447
<i>M</i>	76	77	78	79	80	81	82
<i>A</i>	0.77636	0.77323	0.77593	0.77078	0.7684	0.75642	0.75893
<i>B</i>	5.9776e-2	6.021e-2	6.4660e-2	6.3186e-2	6.3552e-2	5.823e-2	6.2054e-2
<i>C</i>	0.44982	0.44968	0.44393	0.4458	0.44489	0.45462	0.44882
<i>M</i>	83	84	85	86	87	88	89
<i>A</i>	0.77053	0.75412	0.75366	0.75373	0.77179	0.74069	0.74232
<i>B</i>	7.2384e-2	6.2609e-2	6.4402e-2	6.659e-2	8.2723e-2	6.1024e-2	6.4296e-2
<i>C</i>	0.43402	0.44794	0.44572	0.44276	0.42155	0.45054	0.44636

Table M.1 Coefficients for the “uniform sum” threshold (THR_{US}) calculation as a function of the number of samples M .

The algorithm is tested on the same data sets as those used in Chapter 6. The results are given in Figure M.2 and Figure M.3, and statistics in Table M.2 and Table M.3.



(a)

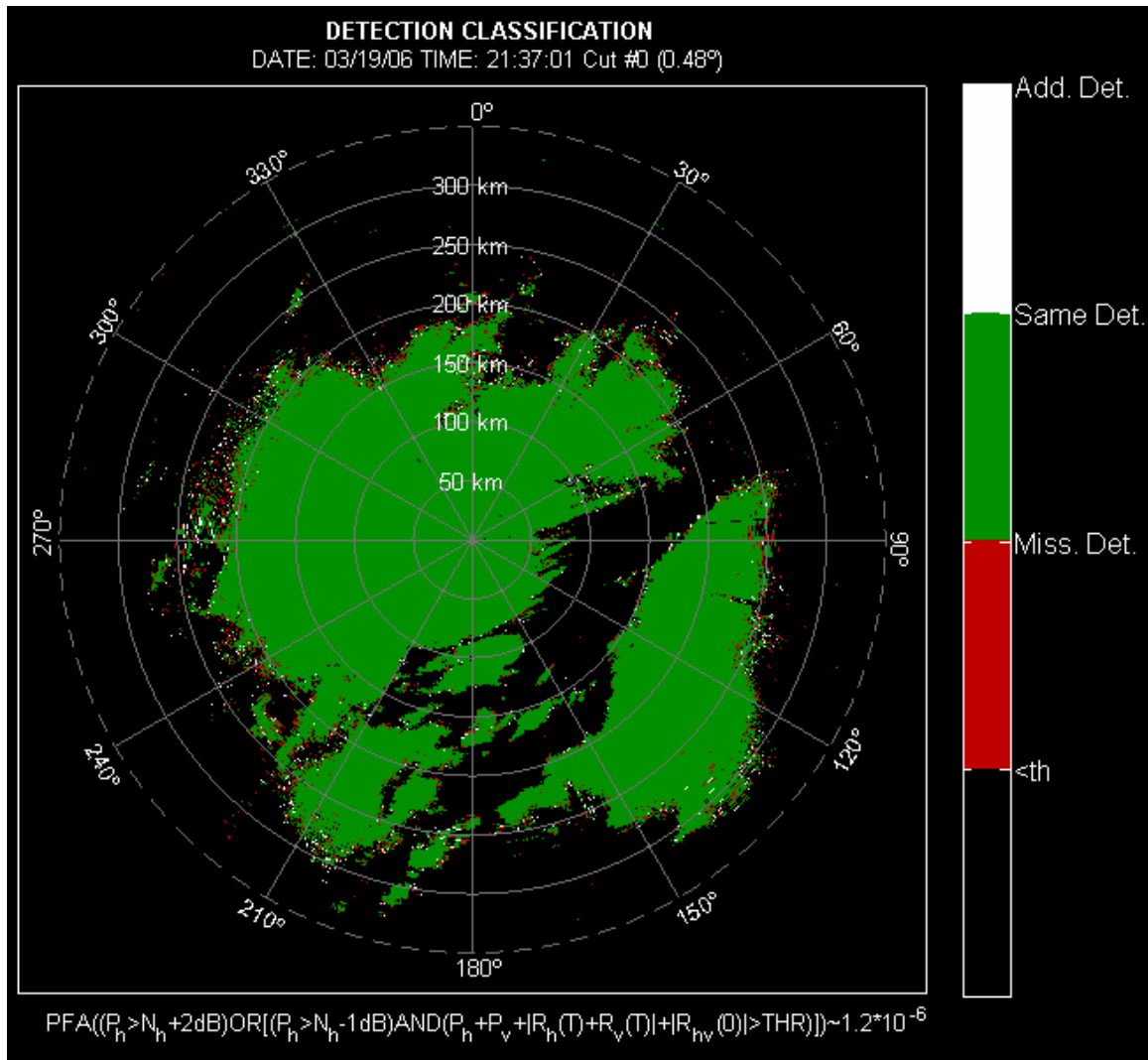


Figure M.2 Reflectivity field (a) and the classification of detections (b) obtained after doubling the noise power, and using the proposed algorithm for detection.

D	$P \geq N_h - 1\text{dB}$	UNIFORM SUM	P&UNIFORM SUM
<i>Ratio of total detections</i>	0.982318	0.984358	0.975147
<i>The Ratio of bounded detections</i>	0.801132	0.820519	0.718047
<i>Ratio of additional detections</i>	0.026012	0.018693	0.008848

Table M.2 Real data statistics for surveillance scan collected on 03/19/06.

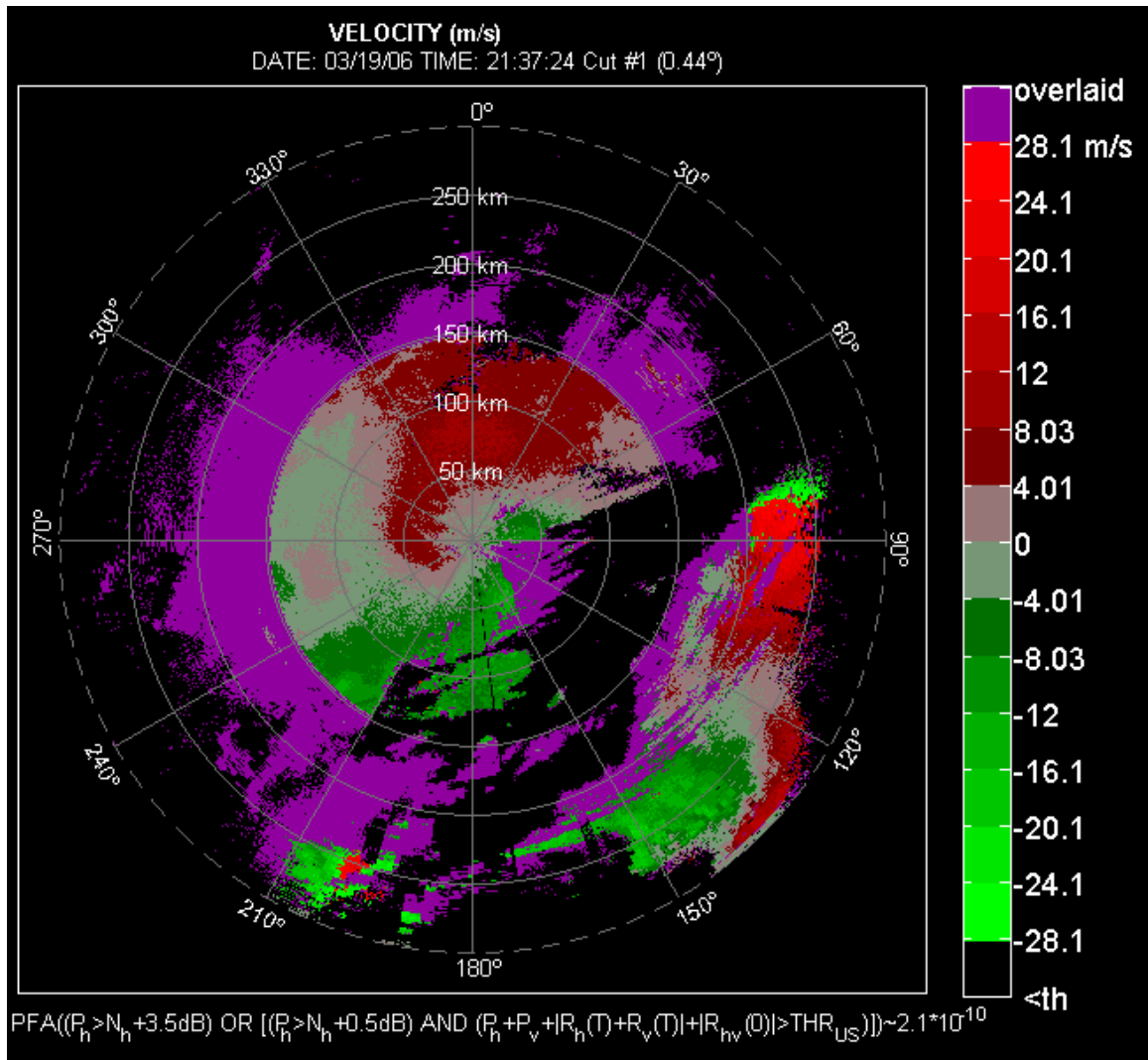


Figure M.3 Unfolded velocity field obtained after doubling the noise power, and using the proposed algorithm for detection.

D	$P \geq N_h + 0.5dB$	$UNIFORM\ SUM$	$P \& UNIFORM\ SUM$
PFA	2.14×10^{-10}	$1.2 * 10^{-6}$	$1.2 * 10^{-6}$
Ratio of total detections	0.989575	0.995178	0.986660
The Ratio of bounded detections	0.637883	0.724477	0.685400
Ratio of additional detections	0.007643	0.033545	0.014736

Table M.3 Statistics for range unfolded Doppler scan collected on 03/19/06.

The comparison between statistics obtained using the uniform sum exclusively and the proposed algorithm (i.e., columns 3 and 4 in Table M.2 and M.3) reveals that combining

the square law detector and the uniform sum, as proposed by the novel detection algorithm, produces the detection rates that are somewhat smaller than what would be obtained if the uniform sum were used solely. This is expected because the added condition, discards some data with SNR estimates smaller than $THR_{SNR}/2$, which according to the uniform sum detection rule contain “significant returns”. In view of the description given in Chapter 5, the added condition reduces the region, in $2M$ dimensional space, which contains all possible values of the observation vector \mathbf{V} that meet the detection requirement as given by the proposed algorithm. Moreover, the proposed detection algorithm, when used in the Doppler scan, yields practically the same results as if the SNR threshold has been lowered by half (i.e., $SNR_h \geq THR_{SNR}/2$), for the given case. This is because for the given case of $M = 52$ and $THR_{SNR}/2 = 0.5$ dB the $PFA(SNR_h \geq THR_{SNR}/2) = 2.1 \times 10^{-10}$, which is much smaller than the PFA of the uniform sum. Consequently, the use of the uniform sum could be omitted whenever $PFA(SNR_h \geq THR_{SNR}/2) \ll PFA(US)$. Adding additional logic, that determines when to use the uniform sum, has the potential to decrease the amount of real-time computations, but it imposes additional implementation requirement, whereas the false alarm rate of the SNR based detector has to be evaluated using (A.11). This in turn requires calculation of the incomplete gamma function which is not a part of the standard C language mathematical library. Nonetheless, the open source C++ code, working at double precision, that computes the incomplete gamma function can be obtained via Internet. Another interesting thing is that the proposed algorithm still does significantly better when compared to simple lowering SNR by half in both surveillance and Doppler scans (i.e., second column in Table M.3). This is because for $M = 17$, the $PFA(SNR_h \geq -1$ dB) =

0.003 and the $PFA(US) = 1.2 \times 10^{-6}$; hence, the uniform sum sifts through the SNR detections discarding those that are noise. This results in an improved range unfolding using the surveillance scan.